

The DUNE Far Detector Interim Design Report  
**Volume 3: Dual-Phase Module**  
Deep Underground Neutrino Experiment (DUNE)

arXiv:1807.10340v1 [physics.ins-det] 26 Jul 2018

This document was prepared by Deep Underground Neutrino Experiment (DUNE) using the resources of the Fermi National Accelerator Laboratory (Fermilab), a U.S. Department of Energy, Office of Science, HEP User Facility. Fermilab is managed by Fermi Research Alliance, LLC (FRA), acting under Contract No. DE-AC02-07CH11359. Fermilab-Design-2018-04

**DUNE**  
DEEP UNDERGROUND  
NEUTRINO EXPERIMENT

FERMILAB-DESIGN-2018-02

Cover design: Diana Brandonisio, Fermilab Creative Services, July 2018

Cover photo: "Inside ProtoDUNE" by Maximilien Brice, ©CERN, November 2017

## Authors

B. Abi,<sup>125</sup> R. Acciarri,<sup>54</sup> M. A. Acero,<sup>8</sup> M. Adamowski,<sup>54</sup> C. Adams,<sup>62</sup> D. Adams,<sup>15</sup> P. Adamson,<sup>54</sup> M. Adinolfi,<sup>14</sup>  
Z. Ahmad,<sup>165</sup> C. H. Albright,<sup>54</sup> L. Aliaga Soplin,<sup>54</sup> T. Alion,<sup>152</sup> S. Alonso Monsalve,<sup>20</sup> M. Alrashed,<sup>89</sup> C. Alt,<sup>47</sup>  
J. Anderson,<sup>5</sup> K. Anderson,<sup>54</sup> C. Andreopoulos,<sup>99</sup> M. P. Andrews,<sup>54</sup> R. A. Andrews,<sup>54</sup> A. Ankowski,<sup>140</sup>  
J. Anthony,<sup>27</sup> M. Antonello,<sup>58</sup> M. Antonova,<sup>68</sup> S. Antusch,<sup>10</sup> A. Aranda Fernandez,<sup>34</sup> A. Ariga,<sup>11</sup> T. Ariga,<sup>11</sup>  
D. Aristizabal Sierra,<sup>154</sup> E. Arrieta Diaz,<sup>150</sup> J. Asaadi,<sup>157</sup> M. Ascencio,<sup>135</sup> D. Asner,<sup>15</sup> M. S. Athar,<sup>1</sup> M. Auger,<sup>11</sup>  
A. Aurisano,<sup>32</sup> V. Aushev,<sup>94</sup> D. Autiero,<sup>79</sup> F. Azfar,<sup>125</sup> A. Back,<sup>82</sup> H. Back,<sup>126</sup> J. Back,<sup>170</sup> C. Backhouse,<sup>100</sup>  
P. Baesso,<sup>14</sup> L. Bagby,<sup>54</sup> X. Bai,<sup>147</sup> M. Baird,<sup>167</sup> B. Balantekin,<sup>173</sup> S. Balasubramanian,<sup>175</sup> B. Baller,<sup>54</sup> P. Ballett,<sup>46</sup>  
L. Balleyguier,<sup>79</sup> B. Bambah,<sup>66</sup> H. Band,<sup>175</sup> M. Bansal,<sup>129</sup> S. Bansal,<sup>129</sup> G. Barenboim,<sup>68</sup> G. J. Barker,<sup>170</sup>  
C. Barnes,<sup>108</sup> G. Barr,<sup>125</sup> J. Barranco Monarca,<sup>60</sup> N. Barros,<sup>132</sup> J. Barrow,<sup>155</sup> A. Bashyal,<sup>123</sup> V. Basque,<sup>105</sup>  
M. Bass,<sup>15</sup> F. Bay,<sup>160</sup> K. Bays,<sup>26</sup> J. L. Bazo,<sup>135</sup> J. F. Beacom,<sup>122</sup> E. Bechetoille,<sup>79</sup> B. R. Behera,<sup>129</sup> L. Bellantoni,<sup>54</sup>  
G. Bellettini,<sup>133</sup> V. Bellini,<sup>28</sup> O. Beltramello,<sup>20</sup> D. Belver,<sup>21</sup> N. Benekos,<sup>20</sup> P. A. Benetti,<sup>130</sup> A. Bercellie,<sup>139</sup>  
E. Berman,<sup>54</sup> P. Bernardini,<sup>164</sup> R. Berner,<sup>11</sup> H.-G. Berns,<sup>23</sup> R. H. Bernstein,<sup>54</sup> S. Bertolucci,<sup>74</sup> M. Betancourt,<sup>54</sup>  
V. Bhatnagar,<sup>129</sup> M. Bhattacharjee,<sup>71</sup> B. Bhuyan,<sup>71</sup> S. Biagi,<sup>96</sup> J. Bian,<sup>24</sup> K. Biery,<sup>54</sup> B. Bilki,<sup>81</sup> M. Bishai,<sup>15</sup>  
A. Bitadze,<sup>105</sup> T. Blackburn,<sup>152</sup> A. Blake,<sup>97</sup> B. Blanco Siffert,<sup>51</sup> F. Blaszczyk,<sup>13</sup> E. Blaufuss,<sup>106</sup> G. C. Blazey,<sup>113</sup>  
M. Blennow,<sup>88</sup> E. Blucher,<sup>30</sup> V. Bocean,<sup>54</sup> F. Boffelli,<sup>130</sup> J. Boissevain,<sup>101</sup> S. Bolognesi,<sup>19</sup> T. Bolton,<sup>89</sup>  
M. Bonesini,<sup>73</sup> T. Boone,<sup>36</sup> A. Booth,<sup>152</sup> C. Booth,<sup>143</sup> S. Bordini,<sup>20</sup> A. Borkum,<sup>152</sup> T. Boschi,<sup>46</sup> P. Bour,<sup>39</sup>  
B. Bourguille,<sup>67</sup> S. B. Boyd,<sup>170</sup> D. Boyden,<sup>113</sup> J. Bracinik,<sup>12</sup> D. Brailsford,<sup>97</sup> A. Brandt,<sup>157</sup> J. Bremer,<sup>20</sup>  
S. J. Brice,<sup>54</sup> C. Bromberg,<sup>109</sup> G. Brooijmans,<sup>37</sup> J. Brooke,<sup>14</sup> G. Brown,<sup>157</sup> N. Buchanan,<sup>36</sup> H. Budd,<sup>139</sup>  
P. C. de Holanda,<sup>49</sup> T. Cai,<sup>139</sup> D. Caiulo,<sup>79</sup> P. Calafiura,<sup>98</sup> A. Calatayud,<sup>135</sup> J. Calcutt,<sup>109</sup> C. Callahan,<sup>132</sup>  
E. Calligarich,<sup>130</sup> E. Calvo,<sup>21</sup> L. Camilleri,<sup>37</sup> A. Caminata,<sup>56</sup> M. Campanelli,<sup>100</sup> G. Cancelo,<sup>54</sup> K. Cankocak,<sup>81</sup>  
C. Cantini,<sup>47</sup> D. Caratelli,<sup>54</sup> B. Carlus,<sup>79</sup> M. Carneiro,<sup>123</sup> I. Caro Terrazas,<sup>36</sup> T. J. Carroll,<sup>158</sup> M. P. Carvalho,<sup>151</sup>  
M. Cascella,<sup>100</sup> C. Castromonte,<sup>114</sup> E. Catano-Mur,<sup>82</sup> M. Cavalli-Sforza,<sup>67</sup> F. Cavanna,<sup>54</sup> E. Cazzato,<sup>10</sup>  
S. Centro,<sup>128</sup> G. Cerati,<sup>54</sup> A. Cervelli,<sup>74</sup> A. Cervera Villanueva,<sup>68</sup> T. Cervi,<sup>130</sup> M. Chalifour,<sup>20</sup> A. Chappuis,<sup>95</sup>  
A. Chatterjee,<sup>157</sup> S. Chattopadhyay,<sup>54</sup> S. Chattopadhyay,<sup>165</sup> J. Chaves,<sup>132</sup> H. Chen,<sup>15</sup> M.-C. Chen,<sup>24</sup>  
S. Chen,<sup>159</sup> D. Cherdack,<sup>36</sup> C.-Y. Chi,<sup>37</sup> S. Childress,<sup>54</sup> K. Cho,<sup>92</sup> S. Choubey,<sup>61</sup> B. C. Choudhary,<sup>43</sup>  
A. Christensen,<sup>36</sup> D. Christian,<sup>54</sup> G. Christodoulou,<sup>99</sup> C.-A. Christofferson,<sup>147</sup> E. Church,<sup>126</sup> P. Clarke,<sup>48</sup>  
T. E. Coan,<sup>150</sup> A. Cocco,<sup>115</sup> G. H. Collin,<sup>107</sup> E. Conley,<sup>45</sup> J. M. Conrad,<sup>107</sup> M. Convery,<sup>140</sup> R. Corey,<sup>147</sup>  
L. Corwin,<sup>147</sup> P. Cotte,<sup>19</sup> L. Cremonesi,<sup>100</sup> J. I. Crespo-Anadón,<sup>37</sup> J. Creus Prats,<sup>20</sup> E. Cristaldo,<sup>163</sup> P. Crivelli,<sup>47</sup>  
D. Cronin-Hennessy,<sup>112</sup> C. Crowley,<sup>54</sup> C. Cuesta,<sup>21</sup> A. Curioni,<sup>73</sup> D. Cussans,<sup>14</sup> M. Dabrowski,<sup>15</sup> D. Dale,<sup>76</sup>  
H. Da Motta,<sup>18</sup> T. Davenne,<sup>141</sup> E. Davenport,<sup>157</sup> G. S. Davies,<sup>78</sup> J. Davies,<sup>152</sup> S. Davini,<sup>56</sup> J. Dawson,<sup>4</sup> K. De,<sup>157</sup>  
M. P. Decowski,<sup>119</sup> P. Dedin Neto,<sup>49</sup> I. de Icaza Astiz,<sup>152</sup> A. Delbart,<sup>19</sup> D. Delepine,<sup>60</sup> M. Delgado,<sup>3</sup> A. Dell,<sup>20</sup>  
J. de Mello Neto,<sup>51</sup> D. DeMuth,<sup>166</sup> Z. Deng,<sup>159</sup> S. Dennis,<sup>99</sup> C. Densham,<sup>141</sup> I. De Bonis,<sup>95</sup> A. De Gouvêa,<sup>120</sup>  
P. De Jong,<sup>119</sup> P. De Lurgio,<sup>5</sup> S. De Rijck,<sup>158</sup> A. De Roeck,<sup>20</sup> J. J. de Vries,<sup>27</sup> R. Dharmapalan,<sup>5</sup> N. Dhirra,<sup>129</sup>  
M. Diamantopoulou,<sup>7</sup> F. Diaz,<sup>135</sup> J. S. Díaz,<sup>78</sup> G. Diaz Bautista,<sup>139</sup> P. Ding,<sup>54</sup> C. Distefano,<sup>96</sup> M. Diwan,<sup>15</sup>  
S. Di Domizio,<sup>56</sup> L. Di Giulio,<sup>20</sup> S. Di Luise,<sup>67</sup> Z. Djurcic,<sup>5</sup> F. Doizon,<sup>79</sup> N. Dokania,<sup>151</sup> M. J. Dolinski,<sup>44</sup>  
R. Dong,<sup>81</sup> J. dos Anjos,<sup>18</sup> D. Douglas,<sup>109</sup> G. Drake,<sup>5</sup> D. Duchesneau,<sup>95</sup> K. Duffy,<sup>54</sup> B. Dung,<sup>158</sup> D. Dutta,<sup>61</sup>  
M. Duvernois,<sup>173</sup> H. Duyang,<sup>145</sup> O. Dvornikov,<sup>63</sup> D. A. Dwyer,<sup>98</sup> S. Dye,<sup>63</sup> A. S. Dyshkant,<sup>113</sup> S. Dytman,<sup>134</sup>  
M. Eads,<sup>113</sup> B. Eberly,<sup>140</sup> D. Edmunds,<sup>109</sup> J. Eisch,<sup>82</sup> A. Elagin,<sup>30</sup> S. Elliott,<sup>101</sup> W. Ellsworth,<sup>64</sup> M. Elnimr,<sup>24</sup>  
S. Emery,<sup>19</sup> S. Eno,<sup>106</sup> A. Ereditato,<sup>11</sup> C. O. Escobar,<sup>54</sup> L. Escudero Sanchez,<sup>27</sup> J. J. Evans,<sup>105</sup> A. Ezeribe,<sup>143</sup>  
K. Fahey,<sup>54</sup> A. Falcone,<sup>157</sup> L. Falk,<sup>152</sup> A. Farbin,<sup>157</sup> C. Farnese,<sup>128</sup> Y. Farzan,<sup>75</sup> M. Fasoli,<sup>73</sup> A. Fava,<sup>54</sup> J. Felix,<sup>60</sup>  
E. Fernandez-Martinez,<sup>104</sup> P. Fernandez Menendez,<sup>68</sup> F. Ferraro,<sup>56</sup> F. Feyzi,<sup>54</sup> L. Fields,<sup>54</sup> A. Filkins,<sup>172</sup>  
F. Filthaut,<sup>119</sup> A. Finch,<sup>97</sup> O. Fischer,<sup>10</sup> M. Fitton,<sup>141</sup> R. Fitzpatrick,<sup>108</sup> W. Flanagan,<sup>41</sup> B. T. Fleming,<sup>175</sup>  
R. Flight,<sup>139</sup> T. Forest,<sup>76</sup> J. Fowler,<sup>45</sup> W. Fox,<sup>78</sup> J. Franc,<sup>39</sup> K. Francis,<sup>113</sup> P. Franchini,<sup>170</sup> D. Franco,<sup>175</sup>  
J. Freeman,<sup>54</sup> J. Freestone,<sup>105</sup> J. Fried,<sup>15</sup> A. Friedland,<sup>140</sup> S. Fuess,<sup>54</sup> I. Furic,<sup>55</sup> A. Furmanski,<sup>105</sup> A. M. Gago,<sup>135</sup>  
H. Gallagher,<sup>161</sup> A. Gallego-Ros,<sup>21</sup> V. Galymov,<sup>79</sup> E. Gamberini,<sup>20</sup> S. Gambetta,<sup>20</sup> T. Gamble,<sup>143</sup> R. Gandhi,<sup>61</sup>  
R. Gandrajula,<sup>109</sup> S. Gao,<sup>15</sup> D. Garcia-Gamez,<sup>105</sup> S. Gardiner,<sup>23</sup> D. Gastler,<sup>13</sup> J. Gehrlein,<sup>104</sup> B. Gelli,<sup>49</sup>  
A. Gendotti,<sup>47</sup> Z. Ghorbani-Moghaddam,<sup>23</sup> A. Ghosh,<sup>154</sup> D. Gibin,<sup>128</sup> I. Gil-Botella,<sup>21</sup> C. Girerd,<sup>79</sup> A. K. Giri,<sup>72</sup>  
S. Glavin,<sup>132</sup> D. Goeldi,<sup>11</sup> O. Gogota,<sup>94</sup> M. Gold,<sup>117</sup> S. Gollapinni,<sup>155</sup> K. Gollwitzer,<sup>54</sup> R. A. Gomes,<sup>57</sup> L. Gomez,<sup>142</sup>  
L. V. Gomez Bermeo,<sup>142</sup> J. J. Gomez Cadenas,<sup>68</sup> H. Gong,<sup>159</sup> F. Gonnella,<sup>12</sup> J. A. Gonzalez-Cuevas,<sup>163</sup>  
M. Goodman,<sup>5</sup> O. Goodwin,<sup>105</sup> D. Gorbunov,<sup>80</sup> S. Goswami,<sup>127</sup> E. Goudzovski,<sup>12</sup> C. Grace,<sup>98</sup> N. Graf,<sup>134</sup>  
N. Graf,<sup>140</sup> M. Graham,<sup>140</sup> E. Gramellini,<sup>175</sup> R. Gran,<sup>111</sup> A. Grant,<sup>42</sup> C. Grant,<sup>13</sup> N. Grant,<sup>170</sup> V. Greco,<sup>28</sup>  
S. Green,<sup>27</sup> H. Greenlee,<sup>54</sup> L. Greenler,<sup>173</sup> M. Greenwood,<sup>123</sup> J. Greer,<sup>14</sup> W. C. Griffith,<sup>152</sup> M. Groh,<sup>78</sup>

J. Grudzinski,<sup>5</sup> K. Grzelak,<sup>168</sup> G. Guanghua,<sup>159</sup> E. Guardincerri,<sup>101</sup> V. Guarino,<sup>5</sup> G. P. Guedes,<sup>53</sup> R. Guenette,<sup>62</sup>  
A. Guglielmi,<sup>128</sup> B. Guo,<sup>145</sup> S. Gupta,<sup>84</sup> V. Gupta,<sup>71</sup> K. K. Guthikonda,<sup>91</sup> R. Gutierrez,<sup>3</sup> P. Guzowski,<sup>105</sup>  
M. M. Guzzo,<sup>49</sup> A. Habig,<sup>111</sup> R. W. Hackenburg,<sup>15</sup> A. Hackenburg,<sup>175</sup> B. Hackett,<sup>63</sup> H. Hadavand,<sup>157</sup>  
R. Haenni,<sup>11</sup> A. Hahn,<sup>54</sup> J. Haigh,<sup>170</sup> T. Haines,<sup>101</sup> J. Haiston,<sup>147</sup> T. Hamernik,<sup>54</sup> P. Hamilton,<sup>153</sup> J. Han,<sup>134</sup>  
T. Handler,<sup>155</sup> S. Hans,<sup>15</sup> D. A. Harris,<sup>54</sup> J. Hartnell,<sup>152</sup> T. Hasegawa,<sup>87</sup> R. Hatcher,<sup>54</sup> A. Hatzikoutelis,<sup>155</sup>  
S. Hays,<sup>54</sup> E. Hazen,<sup>13</sup> M. Headley,<sup>148</sup> A. Heavey,<sup>54</sup> K. Heegerv,<sup>175</sup> J. Heise,<sup>148</sup> K. Hennessy,<sup>99</sup> S. Henry,<sup>139</sup>  
A. Hernandez,<sup>3</sup> J. Hernandez-Garcia,<sup>104</sup> K. Herner,<sup>54</sup> V. Hewes,<sup>32</sup> J. Hignight,<sup>109</sup> A. Higuera,<sup>64</sup> T. Hill,<sup>76</sup>  
S. Hillier,<sup>12</sup> A. Himmel,<sup>54</sup> C. Hohl,<sup>10</sup> A. Holin,<sup>100</sup> E. Hoppe,<sup>126</sup> S. Horikawa,<sup>47</sup> G. Horton-Smith,<sup>89</sup> M. Hostert,<sup>46</sup>  
A. Hourlier,<sup>107</sup> B. Howard,<sup>78</sup> R. Howell,<sup>139</sup> J. Huang,<sup>158</sup> J. Hugon,<sup>102</sup> P. Hurh,<sup>54</sup> J. Huyen,<sup>54</sup> R. Illingworth,<sup>54</sup>  
J. Insler,<sup>44</sup> G. Introzzi,<sup>130</sup> A. Ioannisian,<sup>176</sup> A. Izmaylov,<sup>68</sup> D. E. Jaffe,<sup>15</sup> C. James,<sup>54</sup> E. James,<sup>54</sup> C.-H. Jang,<sup>31</sup>  
F. Jediny,<sup>39</sup> Y. S. Jeong,<sup>6</sup> A. Jhingan,<sup>129</sup> W. Ji,<sup>15</sup> A. Jipa,<sup>16</sup> S. Jiménez,<sup>21</sup> C. Johnson,<sup>36</sup> M. Johnson,<sup>54</sup>  
R. Johnson,<sup>32</sup> J. Johnstone,<sup>54</sup> B. Jones,<sup>157</sup> S. Jones,<sup>100</sup> J. Joshi,<sup>15</sup> H. Jostlein,<sup>54</sup> C. K. Jung,<sup>151</sup> T. Junk,<sup>54</sup>  
A. Kaboth,<sup>141</sup> I. Kadenko,<sup>94</sup> F. Kamiya,<sup>52</sup> Y. Kamyshev,<sup>155</sup> G. Karagiorgi,<sup>37</sup> D. Karasavvas,<sup>7</sup> Y. Karyotakis,<sup>95</sup>  
S. Kasai,<sup>93</sup> S. Kasetti,<sup>102</sup> K. Kaur,<sup>129</sup> B. Kayser,<sup>54</sup> N. Kazaryan,<sup>176</sup> E. Kearns,<sup>13</sup> P. Keener,<sup>132</sup> E. Kemp,<sup>49</sup>  
C. Kendziora,<sup>54</sup> W. Ketchum,<sup>54</sup> S. H. Kettell,<sup>15</sup> M. Khabibullin,<sup>80</sup> A. Khotjantsev,<sup>80</sup> D. Kim,<sup>20</sup> B. Kirby,<sup>15</sup>  
M. Kirby,<sup>54</sup> J. Klein,<sup>132</sup> Y.-J. Ko,<sup>31</sup> T. Kobilarcik,<sup>54</sup> B. Kocaman,<sup>160</sup> L. W. Koerner,<sup>64</sup> S. Kohn,<sup>22</sup> G. Koizumi,<sup>54</sup>  
P. Koller,<sup>11</sup> A. Kopylov,<sup>80</sup> M. Kordosky,<sup>172</sup> L. Kormos,<sup>97</sup> T. Kosc,<sup>79</sup> U. Kose,<sup>20</sup> V. A. Kostecký,<sup>78</sup> K. Kotheke,<sup>14</sup>  
M. Kramer,<sup>22</sup> F. Krennrich,<sup>82</sup> I. Kreslo,<sup>11</sup> K. Kriesel,<sup>173</sup> W. Kropp,<sup>24</sup> Y. Kudenko,<sup>80</sup> V. A. Kudryavtsev,<sup>143</sup>  
S. Kulagin,<sup>80</sup> J. Kumar,<sup>63</sup> L. Kumar,<sup>129</sup> A. Kumar,<sup>129</sup> S. Kumbhare,<sup>157</sup> C. Kuruppu,<sup>145</sup> V. Kus,<sup>39</sup> T. Kutter,<sup>102</sup>  
R. LaZur,<sup>36</sup> K. Lande,<sup>132</sup> C. Lane,<sup>44</sup> K. Lang,<sup>158</sup> T. Langford,<sup>175</sup> F. Lanni,<sup>15</sup> P. Lasorak,<sup>152</sup> D. Last,<sup>132</sup>  
C. Lastoria,<sup>21</sup> A. Laudrie,<sup>173</sup> I. Lazanu,<sup>16</sup> T. Le,<sup>161</sup> J. Learned,<sup>63</sup> P. Lebrun,<sup>54</sup> D. Lee,<sup>101</sup> G. Lehmann Miotto,<sup>20</sup>  
M. A. Leigui de Oliveira,<sup>52</sup> Q. Li,<sup>54</sup> S. Li,<sup>15</sup> S. W. Li,<sup>140</sup> X. Li,<sup>151</sup> Y. Li,<sup>15</sup> Z. Li,<sup>45</sup> H.-Y. Liao,<sup>89</sup> S.-K. Lin,<sup>36</sup>  
C.-J. S. Lin,<sup>98</sup> R. Linehan,<sup>140</sup> V. Linhart,<sup>39</sup> J. Link,<sup>167</sup> Z. Liptak,<sup>35</sup> D. Lissauer,<sup>15</sup> L. Littenberg,<sup>15</sup> B. Littlejohn,<sup>69</sup>  
J. Liu,<sup>146</sup> T. Liu,<sup>150</sup> L. LoMonaco,<sup>28</sup> J. M. LoSecco,<sup>121</sup> S. Lockwitz,<sup>54</sup> N. Lockyer,<sup>54</sup> T. Loew,<sup>98</sup> M. Lokajicek,<sup>17</sup>  
K. Long,<sup>77</sup> K. Loo,<sup>86</sup> J. P. Lopez,<sup>35</sup> D. Lorca,<sup>11</sup> T. Lord,<sup>170</sup> M. Losada,<sup>3</sup> W. C. Louis,<sup>101</sup> M. Luethi,<sup>11</sup> K.-B. Luk,<sup>22</sup>  
T. Lundin,<sup>54</sup> X. Luo,<sup>175</sup> N. Lurkin,<sup>12</sup> T. Lux,<sup>67</sup> V. P. Luzio,<sup>52</sup> J. Lykken,<sup>54</sup> J. Maalampi,<sup>86</sup> R. MacLellan,<sup>146</sup>  
A. A. Machado,<sup>52</sup> P. Machado,<sup>54</sup> C. T. Macias,<sup>78</sup> J. Macier,<sup>54</sup> P. Madigan,<sup>22</sup> S. Magill,<sup>5</sup> G. Mahler,<sup>15</sup> K. Mahn,<sup>109</sup>  
M. Malek,<sup>143</sup> J. A. Maloney,<sup>40</sup> F. Mammoliti,<sup>62</sup> S. K. Mandal,<sup>43</sup> G. Mandrioli,<sup>74</sup> L. Manenti,<sup>100</sup> S. Manly,<sup>139</sup>  
A. Mann,<sup>161</sup> A. Marchionni,<sup>54</sup> W. Marciano,<sup>15</sup> S. Marocci,<sup>54</sup> D. Marfatia,<sup>63</sup> C. Mariani,<sup>167</sup> J. Maricic,<sup>63</sup>  
F. Marinho,<sup>162</sup> A. D. Marino,<sup>35</sup> M. Marshak,<sup>112</sup> C. Marshall,<sup>98</sup> J. Marshall,<sup>27</sup> J. Marteau,<sup>79</sup> J. Martin-Albo,<sup>125</sup>  
D. Martinez,<sup>69</sup> N. Martinez,<sup>137</sup> H. Martinez,<sup>142</sup> K. Mason,<sup>161</sup> A. Mastbaum,<sup>30</sup> M. Masud,<sup>68</sup> H. Mathez,<sup>79</sup>  
S. Matsumo,<sup>63</sup> J. Matthews,<sup>102</sup> C. Mauger,<sup>132</sup> N. Mauri,<sup>74</sup> K. Mavrokoridis,<sup>99</sup> R. Mazza,<sup>73</sup> A. Mazzacane,<sup>54</sup>  
E. Mazzucato,<sup>19</sup> N. McCauley,<sup>99</sup> E. McCluskey,<sup>54</sup> N. McConkey,<sup>143</sup> K. McDonald,<sup>136</sup> K. S. McFarland,<sup>139</sup>  
C. McGivern,<sup>54</sup> A. McGowan,<sup>139</sup> C. McGrew,<sup>151</sup> R. McKeown,<sup>172</sup> A. McNab,<sup>105</sup> D. McNulty,<sup>76</sup> R. McTaggart,<sup>149</sup>  
V. Meddage,<sup>89</sup> A. Mefodiev,<sup>80</sup> P. Mehta,<sup>85</sup> D. Mei,<sup>146</sup> O. Mena,<sup>68</sup> S. Menary,<sup>177</sup> H. Mendez,<sup>137</sup> D. P. Mendez,<sup>152</sup>  
A. Menegolli,<sup>130</sup> G. Meng,<sup>128</sup> M. Messier,<sup>78</sup> W. Metcalf,<sup>102</sup> M. Mewes,<sup>78</sup> H. Meyer,<sup>171</sup> T. Miao,<sup>54</sup> J. Migenda,<sup>143</sup>  
R. Milincic,<sup>63</sup> J. Miller,<sup>154</sup> W. Miller,<sup>112</sup> J. Mills,<sup>161</sup> C. Milne,<sup>76</sup> O. Mineev,<sup>80</sup> O. Miranda,<sup>33</sup> C. S. Mishra,<sup>54</sup>  
S. R. Mishra,<sup>145</sup> A. Mislivec,<sup>112</sup> B. Mitrica,<sup>65</sup> D. Mladenov,<sup>20</sup> I. Mocioiu,<sup>131</sup> K. Moffat,<sup>46</sup> N. Moggi,<sup>74</sup> R. Mohanta,<sup>66</sup>  
N. Mokhov,<sup>54</sup> J. Molina,<sup>163</sup> L. Molina Bueno,<sup>47</sup> A. Montanari,<sup>74</sup> C. Montanari,<sup>130</sup> D. Montanari,<sup>54</sup>  
L. Montano Zetina,<sup>33</sup> J. Moon,<sup>107</sup> M. Mooney,<sup>36</sup> C. Moore,<sup>54</sup> D. Moreno,<sup>3</sup> B. Morgan,<sup>170</sup> G. F. Moroni,<sup>54</sup>  
C. Morris,<sup>64</sup> W. Morse,<sup>15</sup> C. Mossey,<sup>54</sup> C. A. Moura,<sup>52</sup> J. Mousseau,<sup>108</sup> L. Mualem,<sup>26</sup> M. Muether,<sup>171</sup> S. Mufson,<sup>78</sup>  
F. Muheim,<sup>48</sup> H. Muramatsu,<sup>112</sup> S. Murphy,<sup>47</sup> J. Musser,<sup>78</sup> J. Nachtman,<sup>81</sup> M. Nalbandyan,<sup>176</sup> R. Nandakumar,<sup>141</sup>  
D. Naples,<sup>134</sup> S. Narita,<sup>83</sup> G. Navarro,<sup>3</sup> J. Navarro,<sup>8</sup> D. Navas-Nicolás,<sup>21</sup> N. Nayak,<sup>24</sup> M. Nebot-Guinot,<sup>48</sup>  
M. Needham,<sup>48</sup> K. Negishi,<sup>83</sup> J. Nelson,<sup>172</sup> M. Nessi,<sup>20</sup> D. Newbold,<sup>14</sup> M. Newcomer,<sup>132</sup> R. Nichol,<sup>100</sup>  
T. C. Nicholls,<sup>141</sup> E. Niner,<sup>54</sup> A. Norman,<sup>54</sup> B. Norris,<sup>54</sup> J. Norris,<sup>76</sup> P. Novella,<sup>68</sup> E. Nowak,<sup>20</sup> J. Nowak,<sup>97</sup>  
M. S. Nunes,<sup>49</sup> H. O'Keefe,<sup>97</sup> M. Oberling,<sup>5</sup> A. Olivares Del Campo,<sup>46</sup> A. Olivier,<sup>139</sup> Y. Onel,<sup>81</sup> Y. Onishchuk,<sup>94</sup>  
T. Ovsjannikova,<sup>80</sup> S. Ozturk,<sup>20</sup> L. Pagani,<sup>23</sup> S. Pakvasa,<sup>63</sup> O. Palamara,<sup>54</sup> J. Paley,<sup>54</sup> M. Pallavicini,<sup>56</sup>  
C. Palomares,<sup>21</sup> J. Palomino,<sup>151</sup> E. Pantic,<sup>23</sup> A. Paolo,<sup>64</sup> V. Paolone,<sup>134</sup> V. Papadimitriou,<sup>54</sup> R. Papaleo,<sup>96</sup>  
S. Paramesvaran,<sup>14</sup> J. Park,<sup>167</sup> S. Parke,<sup>54</sup> Z. Parsa,<sup>15</sup> S. Pascoli,<sup>46</sup> J. Pasternak,<sup>77</sup> J. Pater,<sup>105</sup> L. Patrizii,<sup>74</sup>  
R. B. Patterson,<sup>26</sup> S. J. Patton,<sup>98</sup> T. Patzak,<sup>4</sup> A. Paudel,<sup>89</sup> B. Paulos,<sup>173</sup> L. Paulucci,<sup>52</sup> Z. Pavlovic,<sup>54</sup>  
G. Pawloski,<sup>112</sup> P. Payam,<sup>75</sup> D. Payne,<sup>99</sup> V. Pec,<sup>143</sup> S. J. M. Peeters,<sup>152</sup> E. Pennacchio,<sup>79</sup> A. Penzo,<sup>81</sup>  
G. N. Perdue,<sup>54</sup> O. I. G. Peres,<sup>49</sup> L. Periale,<sup>47</sup> K. Petridis,<sup>14</sup> G. Petrillo,<sup>140</sup> R. Petti,<sup>145</sup> P. Picchi,<sup>130</sup> L. Pickering,<sup>109</sup>  
F. Pietropaolo,<sup>128</sup> J. Pillow,<sup>170</sup> P. Plonski,<sup>169</sup> R. Plunkett,<sup>54</sup> R. Poling,<sup>112</sup> X. Pons,<sup>20</sup> N. Poonthottathil,<sup>82</sup>

M. Popovic,<sup>54</sup> R. Pordes,<sup>54</sup> S. Pordes,<sup>54</sup> M. Potekhin,<sup>15</sup> R. Potenza,<sup>28</sup> B. Potukuchi,<sup>84</sup> S. Poudel,<sup>64</sup> J. Pozimski,<sup>77</sup> M. Pozzato,<sup>74</sup> T. Prakash,<sup>98</sup> R. Preece,<sup>141</sup> O. Prokofiev,<sup>54</sup> N. Pruthi,<sup>129</sup> P. Przewlocki,<sup>116</sup> F. Psihas,<sup>78</sup> D. Pugnre,<sup>79</sup> D. Pushka,<sup>54</sup> K. Qi,<sup>151</sup> X. Qian,<sup>15</sup> J. L. Raaf,<sup>54</sup> R. Raboanary,<sup>2</sup> V. Radeka,<sup>15</sup> J. Rademacker,<sup>14</sup> V. Radescu,<sup>20</sup> B. Radics,<sup>47</sup> A. Radovic,<sup>172</sup> A. Rafique,<sup>89</sup> M. Rajaoalisoa,<sup>2</sup> I. Rakhno,<sup>54</sup> H. T. Rakotondramanana,<sup>2</sup> L. Rakotondravohitra,<sup>2</sup> Y. A. Ramachers,<sup>170</sup> R. A. Rameika,<sup>54</sup> M. A. Ramirez Delgado,<sup>60</sup> J. Ramsey,<sup>101</sup> B. J. Ramson,<sup>54</sup> A. Rappoldi,<sup>130</sup> G. L. Raselli,<sup>130</sup> P. Ratoff,<sup>97</sup> S. Ravat,<sup>20</sup> O. Ravinez,<sup>114</sup> H. Razafinime,<sup>2</sup> B. Rebel,<sup>54</sup> D. Redondo,<sup>21</sup> C. Regenfus,<sup>47</sup> M. Reggiani-Guzzo,<sup>49</sup> T. Rehak,<sup>44</sup> J. Reichenbacher,<sup>147</sup> D. Reitzner,<sup>54</sup> M. H. Reno,<sup>81</sup> A. Renshaw,<sup>64</sup> S. Rescia,<sup>15</sup> F. Resnati,<sup>20</sup> A. Reynolds,<sup>125</sup> G. Riccobene,<sup>96</sup> L. C. J. Rice,<sup>113</sup> K. Rielage,<sup>101</sup> K. Riesselmann,<sup>54</sup> Y. - A. Rigaut,<sup>47</sup> D. Rivera,<sup>132</sup> L. Rochester,<sup>140</sup> M. Roda,<sup>99</sup> P. Rodrigues,<sup>125</sup> M. J. Rodriguez Alonso,<sup>20</sup> B. Roe,<sup>108</sup> A. J. Roeth,<sup>45</sup> R. M. Roser,<sup>54</sup> M. Ross-Lonergan,<sup>46</sup> M. Rossella,<sup>130</sup> J. Rout,<sup>85</sup> S. Roy,<sup>61</sup> A. Rubbia,<sup>47</sup> C. Rubbia,<sup>59</sup> R. Rucinski,<sup>54</sup> B. Russell,<sup>175</sup> J. Russell,<sup>140</sup> D. Ruterbories,<sup>139</sup> M. R. Vagins,<sup>90</sup> R. Saakyan,<sup>100</sup> N. Sahu,<sup>72</sup> P. Sala,<sup>110</sup> G. Salukvadze,<sup>20</sup> N. Samios,<sup>15</sup> F. Sanchez,<sup>67</sup> M. C. Sanchez,<sup>82</sup> C. Sandoval,<sup>3</sup> B. Sands,<sup>136</sup> S. U. Sankar,<sup>70</sup> S. Santana,<sup>137</sup> L. M. Santos,<sup>49</sup> G. Santucci,<sup>151</sup> N. Saoulidou,<sup>7</sup> P. Sapienza,<sup>96</sup> C. Sarasty,<sup>32</sup> I. Sarcevic,<sup>6</sup> G. Savage,<sup>54</sup> A. Scaramelli,<sup>130</sup> A. Scarpelli,<sup>4</sup> T. Schaffer,<sup>111</sup> H. Schellman,<sup>123</sup> P. Schlabach,<sup>54</sup> C. M. Schloesser,<sup>47</sup> D. W. Schmitz,<sup>30</sup> J. Schneps,<sup>161</sup> K. Scholberg,<sup>45</sup> A. Schukraft,<sup>54</sup> E. Segreto,<sup>49</sup> S. Sehrawat,<sup>61</sup> J. Sensenig,<sup>132</sup> I. Seong,<sup>24</sup> J. A. Sepulveda-Quiroz,<sup>82</sup> A. Sergi,<sup>12</sup> F. Sergiampietri,<sup>151</sup> D. Sessumes,<sup>157</sup> K. Sexton,<sup>15</sup> L. Sexton-Kennedy,<sup>54</sup> D. Sgalaberna,<sup>20</sup> M. H. Shaevitz,<sup>37</sup> S. Shafaq,<sup>85</sup> J. S. Shahi,<sup>129</sup> S. Shahsavarani,<sup>157</sup> P. Shanahan,<sup>54</sup> H. R. Sharma,<sup>84</sup> R. Sharma,<sup>15</sup> R. K. Sharma,<sup>138</sup> T. Shaw,<sup>54</sup> S. Shin,<sup>30</sup> I. Shoemaker,<sup>146</sup> D. Shooltz,<sup>109</sup> R. Shrock,<sup>151</sup> N. Simos,<sup>15</sup> J. Sinclair,<sup>11</sup> G. Sinev,<sup>45</sup> V. Singh,<sup>9</sup> J. Singh,<sup>103</sup> J. Singh,<sup>103</sup> I. Singh,<sup>129</sup> J. Singh,<sup>129</sup> R. Sipos,<sup>20</sup> F. W. Sippach,<sup>37</sup> G. Sirri,<sup>74</sup> K. Siyeon,<sup>31</sup> D. Smargianaki,<sup>151</sup> A. Smith,<sup>27</sup> A. Smith,<sup>45</sup> E. Smith,<sup>78</sup> P. Smith,<sup>78</sup> J. Smolik,<sup>39</sup> M. Smy,<sup>24</sup> E. L. Snider,<sup>54</sup> P. Snopok,<sup>69</sup> J. Sobczyk,<sup>174</sup> H. Sobel,<sup>24</sup> M. Soderberg,<sup>153</sup> C. J. Solano Salinas,<sup>114</sup> N. Solomey,<sup>171</sup> W. Sondheim,<sup>101</sup> M. Sorel,<sup>68</sup> J. A. Soto-Oton,<sup>21</sup> A. Sousa,<sup>32</sup> K. Soustruznik,<sup>29</sup> F. Spaggiardi,<sup>125</sup> M. Spanu,<sup>130</sup> J. Spitz,<sup>108</sup> N. J. C. Spooner,<sup>143</sup> R. Staley,<sup>12</sup> M. Stancari,<sup>54</sup> L. Stanco,<sup>128</sup> A. Stefanik,<sup>54</sup> H. M. Steiner,<sup>98</sup> J. Stewart,<sup>15</sup> J. Stock,<sup>147</sup> F. Stocker,<sup>20</sup> S. Stoica,<sup>65</sup> J. Stone,<sup>13</sup> J. Strait,<sup>54</sup> M. Strait,<sup>112</sup> T. Strauss,<sup>54</sup> S. Striganov,<sup>54</sup> A. Stuart,<sup>34</sup> G. Sullivan,<sup>106</sup> M. Sultana,<sup>139</sup> Y. Sun,<sup>63</sup> A. Surdo,<sup>164</sup> V. Susic,<sup>10</sup> L. Suter,<sup>54</sup> C. M. Suter, <sup>28</sup> R. Svoboda,<sup>23</sup> B. Szczerbinska,<sup>156</sup> A. M. Szcl, <sup>105</sup> S. Söldner-Rembold,<sup>105</sup> N. Tagg,<sup>124</sup> R. Talaga,<sup>5</sup> H. Tanaka,<sup>140</sup> B. Tapia Oregui,<sup>158</sup> S. Tariq,<sup>54</sup> E. Tatar,<sup>76</sup> R. Tayloe,<sup>78</sup> M. Tenti,<sup>74</sup> K. Terao,<sup>140</sup> C. A. Ternes,<sup>68</sup> F. Terranova,<sup>73</sup> G. Testera,<sup>56</sup> A. Thea,<sup>141</sup> L. F. Thompson,<sup>143</sup> J. Thompson,<sup>143</sup> C. Thorn,<sup>15</sup> A. Timilsina,<sup>15</sup> S. C. Timm,<sup>54</sup> J. Todd,<sup>32</sup> A. Tonazzo,<sup>4</sup> T. Tope,<sup>54</sup> D. Torbunov,<sup>112</sup> M. Torti,<sup>73</sup> M. Tórtola,<sup>68</sup> F. Tortorici,<sup>28</sup> M. Touns,<sup>54</sup> C. Touramanis,<sup>99</sup> J. Trevor,<sup>26</sup> M. Tripathi,<sup>23</sup> W. Tromeur,<sup>79</sup> I. Tropin,<sup>54</sup> W. H. Trzaska,<sup>86</sup> Y.-T. Tsai,<sup>140</sup> K. V. Tsang,<sup>140</sup> A. Tsaris,<sup>54</sup> S. Tufanli,<sup>175</sup> C. Tull,<sup>98</sup> J. Turner,<sup>46</sup> M. Tzanov,<sup>102</sup> E. Tziaferi,<sup>7</sup> Y. Uchida,<sup>77</sup> J. Urheim,<sup>78</sup> T. Usher,<sup>140</sup> G. A. Valdivieso,<sup>50</sup> E. Valencia,<sup>172</sup> L. Valerio,<sup>54</sup> Z. Vallari,<sup>151</sup> J. W. F. Valle,<sup>68</sup> R. Van Berg,<sup>132</sup> R. Van de Water,<sup>101</sup> F. Varanini,<sup>128</sup> G. Varner,<sup>63</sup> J. Vassel,<sup>78</sup> G. Vasseur,<sup>19</sup> K. Vaziri,<sup>54</sup> G. Velev,<sup>54</sup> S. Ventura,<sup>128</sup> A. Verdugo,<sup>21</sup> M. Vermeulen,<sup>119</sup> E. Vernon,<sup>15</sup> M. Verzocchi,<sup>54</sup> T. Viant,<sup>47</sup> C. Vignoli,<sup>58</sup> S. Vihonen,<sup>86</sup> C. Vilela,<sup>151</sup> B. Viren,<sup>15</sup> P. Vokac,<sup>39</sup> T. Vrba,<sup>39</sup> T. Wachala,<sup>118</sup> D. Wahl,<sup>173</sup> M. Wallbank,<sup>32</sup> H. Wang,<sup>25</sup> J. Wang,<sup>23</sup> T.-C. Wang,<sup>46</sup> B. Wang,<sup>150</sup> Y. Wang,<sup>151</sup> Z. Wang,<sup>159</sup> K. Warburton,<sup>82</sup> D. Warner,<sup>36</sup> M. O. Wascko,<sup>77</sup> D. Waters,<sup>100</sup> A. Watson,<sup>12</sup> A. Weber,<sup>125,141</sup> M. Weber,<sup>11</sup> H. Wei,<sup>15</sup> W. Wei,<sup>146</sup> A. Weinstein,<sup>82</sup> D. Wenman,<sup>173</sup> M. Wetstein,<sup>82</sup> M. While,<sup>147</sup> A. White,<sup>157</sup> L. H. Whitehead,<sup>20</sup> D. Whittington,<sup>153</sup> K. Wierman,<sup>126</sup> M. Wilking,<sup>151</sup> C. Wilkinson,<sup>11</sup> J. Willhite,<sup>54</sup> Z. Williams,<sup>157</sup> R. J. Wilson,<sup>36</sup> P. Wilson,<sup>54</sup> P. Wittich,<sup>38</sup> J. Wolcott,<sup>161</sup> T. Wongjirad,<sup>161</sup> K. Wood,<sup>151</sup> L. Wood,<sup>126</sup> E. Worcester,<sup>15</sup> M. Worcester,<sup>15</sup> S. Wu,<sup>47</sup> W. Wu,<sup>54</sup> W. Xu,<sup>146</sup> C. Yanagisawa,<sup>151</sup> S. Yang,<sup>32</sup> T. Yang,<sup>54</sup> G. Yang,<sup>151</sup> J. Ye,<sup>150</sup> M. Yeh,<sup>15</sup> N. Yershov,<sup>80</sup> K. Yonehara,<sup>54</sup> L. Yoshimura,<sup>163</sup> B. Yu,<sup>15</sup> J. Yu,<sup>157</sup> J. Zalesak,<sup>17</sup> L. Zambelli,<sup>95</sup> B. Zamorano,<sup>152</sup> A. Zani,<sup>20</sup> K. Zarembo,<sup>169</sup> L. Zazueta,<sup>172</sup> G. P. Zeller,<sup>54</sup> J. Zennamo,<sup>54</sup> C. Zhang,<sup>15</sup> C. Zhang,<sup>146</sup> M. Zhao,<sup>15</sup> Y.-L. Zhou,<sup>46</sup> G. Zhu,<sup>122</sup> E. D. Zimmerman,<sup>35</sup> M. Zito,<sup>19</sup> S. Zucchelli,<sup>74</sup> J. Zuklin,<sup>17</sup> V. Zutshi,<sup>113</sup> and R. Zwaska<sup>54</sup>

(The DUNE Collaboration)

<sup>1</sup>Aligarh Muslim University, Department of Physics, Aligarh-202002, India

<sup>2</sup>University of Antananarivo, BP 566, Antananarivo 101, Madagascar

<sup>3</sup>Universidad Antonio Nariño, Cra 3 Este No 47A-15, Bogota, Colombia

<sup>4</sup>APC, AstroParticule et Cosmologie, Universit Paris Diderot, CNRS/IN2P3, CEA/Irfu, Observatoire de Paris, Sorbonne Paris Cit, 10, rue Alice Domon et Lonie Duquet, 75205 Paris Cedex 13, France

<sup>5</sup>Argonne National Laboratory, Argonne, IL 60439, USA

<sup>6</sup>University of Arizona, 1118 E. Fourth Street Tucson, AZ 85721, USA

<sup>7</sup>University of Athens, University Campus, Zografou GR 157 84, Greece

<sup>8</sup>Universidad del Atlantico, Carrera 30 Nmero 8- 49 Puerto Colombia - Atlntico, Colombia

<sup>9</sup>Banaras Hindu University, Department of Physics, Varanasi - 221 005, India

- <sup>10</sup> University of Basel, Klingelbergstrasse 82, CH-4056 Basel, Switzerland
- <sup>11</sup> University of Bern, Sidlerstrasse 5, CH-3012 Bern, Switzerland
- <sup>12</sup> University of Birmingham, Edgbaston, Birmingham B15 2TT, United Kingdom
- <sup>13</sup> Boston University, Boston, MA 02215, USA
- <sup>14</sup> University of Bristol, H. H. Wills Physics Laboratory, Tyndall Avenue Bristol BS8 1TL, United Kingdom
- <sup>15</sup> Brookhaven National Laboratory, Upton, NY 11973, USA
- <sup>16</sup> University of Bucharest, Faculty of Physics, Bucharest, Romania
- <sup>17</sup> Institute of Physics, Czech Academy of Sciences, Na Slovance 2, 182 21 Praha 8, Czech Republic
- <sup>18</sup> Centro Brasileiro de Pesquisas Físicas, Rio de Janeiro, RJ 22290-180, Brazil
- <sup>19</sup> CEA/Saclay, IRFU (Institut de Recherche sur les Lois Fondamentales de l'Univers), F-91191 Gif-sur-Yvette CEDEX, France
- <sup>20</sup> CERN, European Organization for Nuclear Research 1211 Geneve 23, Switzerland, CERN
- <sup>21</sup> CIEMAT, Centro de Investigaciones Energéticas, Medioambientales y Tecnológicas, Av. Complutense, 40, E-28040 Madrid, Spain
- <sup>22</sup> University of California (Berkeley), Berkeley, CA 94720, USA
- <sup>23</sup> University of California (Davis), Davis, CA 95616, USA
- <sup>24</sup> University of California (Irvine), Irvine, CA 92697, USA
- <sup>25</sup> University of California (Los Angeles), Los Angeles, CA 90095, USA
- <sup>26</sup> California Institute of Technology, Pasadena, CA 91125, USA
- <sup>27</sup> University of Cambridge, JJ Thomson Avenue, Cambridge CB3 0HE, United Kingdom
- <sup>28</sup> University of Catania, INFN Sezione di Catania, Via Santa Sofia 64, I-95123 Catania, Italy
- <sup>29</sup> Institute of Particle and Nuclear Physics of the Faculty of Mathematics and Physics of the Charles University in Prague, V Holešovičkách 747/2, 180 00 Praha 8-Libeň, Czech Republic
- <sup>30</sup> University of Chicago, Chicago, IL 60637, USA
- <sup>31</sup> Chung-Ang University, Dongjak-Gu, Seoul 06974, South Korea
- <sup>32</sup> University of Cincinnati, Cincinnati, OH 45221, USA
- <sup>33</sup> Cinvestav, Apdo. Postal 14-740, 07000 Ciudad de Mexico, Mexico
- <sup>34</sup> Universidad de Colima, 340 Colonia Villa San Sebastian Colima, Colima, Mexico
- <sup>35</sup> University of Colorado (Boulder), Boulder, CO 80309, USA
- <sup>36</sup> Colorado State University, Fort Collins, CO 80523, USA
- <sup>37</sup> Columbia University, New York, NY 10027, USA
- <sup>38</sup> Cornell University, Ithaca, NY 14853, USA
- <sup>39</sup> Czech Technical University in Prague, Břehová 78/7, 115 19 Prague 1, Czech Republic
- <sup>40</sup> Dakota State University, Madison, SD 57042, USA
- <sup>41</sup> University of Dallas, Irving, TX 75062-4736, USA
- <sup>42</sup> Daresbury Laboratory, Daresbury Warrington, Cheshire WA4 4AD, United Kingdom
- <sup>43</sup> University of Delhi, Department of Physics and Astrophysics, Delhi 110007, India
- <sup>44</sup> Drexel University, Philadelphia, PA 19104, USA
- <sup>45</sup> Duke University, Durham, NC 27708, USA
- <sup>46</sup> University of Durham, South Road, Durham DH1 3LE, United Kingdom
- <sup>47</sup> ETH Zurich, Institute for Particle Physics, Zurich, Switzerland
- <sup>48</sup> University of Edinburgh, Edinburgh EH8 9YL, UK, United Kingdom
- <sup>49</sup> Universidade Estadual de Campinas, Campinas - SP, 13083-970, Brazil
- <sup>50</sup> Universidade Federal de Alfenas, Poços de Caldas - MG, 37715-400, Brazil
- <sup>51</sup> Universidade Federal do Rio de Janeiro, Rio de Janeiro - RJ, 21941-901, Brazil
- <sup>52</sup> Universidade Federal do ABC, Santo André, SP 09210-580, Brazil
- <sup>53</sup> UEFS/DFIS - State University of Feira de Santana, Feira de Santana - BA, 44036-900, Brazil
- <sup>54</sup> Fermi National Accelerator Laboratory, Batavia, IL 60510, USA
- <sup>55</sup> University of Florida, PO Box 118440 Gainesville, FL 32611-8440, USA
- <sup>56</sup> University of Genova, 16126 Genova GE, Italy
- <sup>57</sup> Universidade Federal de Goias, Goiania, GO 74690-900, Brazil
- <sup>58</sup> Laboratori Nazionali del Gran Sasso, I-67010 Assergi, AQ, Italy
- <sup>59</sup> Gran Sasso Science Institute, Viale Francesco Crispi 7, L'Aquila, Italy
- <sup>60</sup> Universidad de Guanajuato, Gto., C.P. 37000, Mexico
- <sup>61</sup> Harish-Chandra Research Institute, Jhansi, Allahabad 211 019, India
- <sup>62</sup> Harvard University, 17 Oxford St. Cambridge, MA 02138, USA
- <sup>63</sup> University of Hawaii, Honolulu, HI 96822, USA
- <sup>64</sup> University of Houston, Houston, TX 77204, USA
- <sup>65</sup> Horia Hulubei National Institute of Physics and Nuclear Engineering, Strada Reactorului 30, Măgurele, Romania
- <sup>66</sup> University of Hyderabad, Gachibowli, Hyderabad - 500 046, India
- <sup>67</sup> Institut de Física d'Altes Energies (IFAE), Campus UAB, Facultat Ciències Nord, 08193 Bellaterra, Barcelona, Spain
- <sup>68</sup> Instituto de Física Corpuscular, Catedrático Jose Beltrán, 2 E-46980 Paterna (Valencia), Spain
- <sup>69</sup> Illinois Institute of Technology, Chicago, IL 60616, USA
- <sup>70</sup> Indian Institute of Technology Bombay, Department of Physics Mumbai 400 076, India
- <sup>71</sup> Indian Institute of Technology Guwahati, Guwahati, 781 039, India

- <sup>72</sup>Indian Institute of Technology Hyderabad, Hyderabad, 502285, India
- <sup>73</sup>Sezione INFN Milano Bicocca and University of Milano Bicocca, Milano, Italy
- <sup>74</sup>INFN Universit degli Studi di Bologna, 40127 Bologna BO, Italy
- <sup>75</sup>Institute for Research in Fundamental Sciences (IPM), Farmanieh St. Tehran, 19538-33511, Iran
- <sup>76</sup>Idaho State University, Department of Physics, Pocatello, ID 83209, USA
- <sup>77</sup>Imperial College of Science Technology & Medicine, Blackett Laboratory Prince Consort Road, London SW7 2BZ, United Kingdom
- <sup>78</sup>Indiana University, Bloomington, IN 47405, USA
- <sup>79</sup>Institut de Physique Nucleaire de Lyon (IPNL), Rue E. Fermi 4 69622 Villeurbanne, France
- <sup>80</sup>Institute for Nuclear Research of the Russian Academy of Sciences (INR RAS), 60th October Anniversary Prosp. 7a Moscow, 117312, Russia
- <sup>81</sup>University of Iowa, Department of Physics and Astronomy 203 Van Allen Hall Iowa City, IA 52242, USA
- <sup>82</sup>Iowa State University, Ames, Iowa 50011, USA
- <sup>83</sup>Iwate University, Morioka, Iwate 020-8551, Japan
- <sup>84</sup>University of Jammu, Physics Department, JAMMU-180006, India
- <sup>85</sup>Jawaharlal Nehru University, Jawaharlal Nehru University, New Delhi 110067, India
- <sup>86</sup>University of Jyvaskyla, P.O. Box 35, FI-40014, Finland
- <sup>87</sup>High Energy Accelerator Research Organization (KEK), Ibaraki, 305-0801, Japan
- <sup>88</sup>KTH Royal Institute of Technology, Roslagstullsbacken 21, SE-106 91 Stockholm, Sweden
- <sup>89</sup>Kansas State University, Manhattan, KS 66506, USA
- <sup>90</sup>Kavli Institute for the Physics and Mathematics of the Universe (WPI), Kashiwa, Chiba 277-8583, Japan
- <sup>91</sup>Department of Physics, K L E F, Green Fields, Guntur - 522 502, AP, India
- <sup>92</sup>Korea Institute for Science and Technology Information, Daejeon, 34141, South Korea
- <sup>93</sup>National Institute of Technology, Kure College, Hiroshima, 737-8506, Japan
- <sup>94</sup>Kyiv National University, 64, 01601 Kyiv, Ukraine
- <sup>95</sup>Laboratoire d'Annecy-le-Vieux de Physique des Particules, CNRS/IN2P3 and Université Savoie Mont Blanc, 74941 Annecy-le-Vieux, France
- <sup>96</sup>INFN - Laboratori Nazionali del Sud (LNS), Via S. Sofia 62, 95123 Catania, Italy
- <sup>97</sup>Lancaster University, Bailrigg, Lancaster LA1 4YB, United Kingdom
- <sup>98</sup>Lawrence Berkeley National Laboratory, Berkeley, CA 94720, USA
- <sup>99</sup>University of Liverpool, L69 7ZE, Liverpool, United Kingdom
- <sup>100</sup>University College London, London, WC1E 6BT, United Kingdom
- <sup>101</sup>Los Alamos National Laboratory, Los Alamos, NM 87545, USA
- <sup>102</sup>Louisiana State University, Baton Rouge, LA 70803, USA
- <sup>103</sup>University of Lucknow, Lucknow 226007, Uttar Pradesh, India
- <sup>104</sup>Madrid Autonoma University, Ciudad Universitaria de Cantoblanco 28049 Madrid, Spain
- <sup>105</sup>University of Manchester, Oxford Road, Manchester M13 9PL, United Kingdom
- <sup>106</sup>University of Maryland, College Park, MD 20742, USA
- <sup>107</sup>Massachusetts Institute of Technology, Cambridge, MA 02139, USA
- <sup>108</sup>University of Michigan, Ann Arbor, MI 48109, USA
- <sup>109</sup>Michigan State University, East Lansing, MI 48824, USA
- <sup>110</sup>INFN Milano, INFN Sezione di Milano, I-20133 Milano, Italy
- <sup>111</sup>University of Minnesota (Duluth), Duluth, MN 55812, USA
- <sup>112</sup>University of Minnesota (Twin Cities), Minneapolis, MN 55455, USA
- <sup>113</sup>Northern Illinois University, Department of Physics, DeKalb, Illinois 60115, USA
- <sup>114</sup>Universidad Nacional de Ingeniería, Av. Tupac Amaru 210, Lima 25, Peru
- <sup>115</sup>Istituto Nazionale di Fisica Nucleare - Sezione di Napoli, Complesso Universitario di Monte S. Angelo, I-80126 Napoli, Italy
- <sup>116</sup>National Centre for Nuclear Research, A. Soltana 7, 05 400 Otwock, Poland
- <sup>117</sup>University of New Mexico, 1919 Lomas Blvd. N.E. Albuquerque, NM 87131, USA
- <sup>118</sup>H. Niewodniczanski Institute of Nuclear Physics, Polish Academy of Sciences, Cracow, Poland
- <sup>119</sup>Nikhef National Institute of Subatomic Physics, Science Park, Amsterdam, Netherlands
- <sup>120</sup>Northwestern University, Evanston, IL 60208, USA
- <sup>121</sup>University of Notre Dame, Notre Dame, IN 46556, USA
- <sup>122</sup>Ohio State University, 191 W. Woodruff Ave. Columbus, OH 43210, USA
- <sup>123</sup>Oregon State University, Corvallis, OR 97331, USA
- <sup>124</sup>Otterbein University, One South Grove Street Westerville, OH 43081, USA
- <sup>125</sup>University of Oxford, Oxford, OX1 3RH, United Kingdom
- <sup>126</sup>Pacific Northwest National Laboratory, Richland, WA 99352, USA
- <sup>127</sup>Physical Research Laboratory, Ahmedabad 380 009, India
- <sup>128</sup>University of Padova, Dip. Fisica e Astronomia G. Galilei and INFN Sezione di Padova, I-35131 Padova, Italy
- <sup>129</sup>Panjab University, Chandigarh, 160014 U.T., India
- <sup>130</sup>University of Pavia, INFN Sezione di Pavia, I-27100 Pavia, Italy
- <sup>131</sup>Pennsylvania State University, University Park, PA 16802, USA
- <sup>132</sup>University of Pennsylvania, Philadelphia, PA 19104, USA

- <sup>133</sup> *University di Pisa, Theor. Division; Largo B. Pontecorvo 3, Ed. B-C, I-56127 Pisa, Italy*
- <sup>134</sup> *University of Pittsburgh, Pittsburgh, PA 15260, USA*
- <sup>135</sup> *Pontificia Universidad Católica del Perú, Apartado 1761, Lima, Peru*
- <sup>136</sup> *Princeton University, Princeton, New Jersey 08544, USA*
- <sup>137</sup> *University of Puerto Rico, Mayaguez, 00681, USA*
- <sup>138</sup> *Punjab Agricultural University, Department of Math. Stat. & Physics, Ludhiana 141004, India*
- <sup>139</sup> *University of Rochester, Rochester, NY 14627, USA*
- <sup>140</sup> *SLAC National Acceleratory Laboratory, Menlo Park, CA 94025, USA*
- <sup>141</sup> *STFC Rutherford Appleton Laboratory, OX11 0QX Harwell Campus, Didcot, United Kingdom*
- <sup>142</sup> *University Sergio Arboleda, Cll 74 -14 -14, 11022 Bogotá, Colombia*
- <sup>143</sup> *University of Sheffield, Department of Physics and Astronomy, Sheffield S3 7RH, United Kingdom*
- <sup>144</sup> *University of Sofia, 5 James Bourchier Blvd., Sofia, Bulgaria*
- <sup>145</sup> *University of South Carolina, Columbia, SC 29208, USA*
- <sup>146</sup> *University of South Dakota, Vermillion, SD 57069, USA*
- <sup>147</sup> *South Dakota School of Mines and Technology, Rapid City, SD 57701, USA*
- <sup>148</sup> *South Dakota Science And Technology Authority, Lead, SD 57754, USA*
- <sup>149</sup> *South Dakota State University, Brookings, SD 57007, USA*
- <sup>150</sup> *Southern Methodist University, Dallas, TX 75275, USA*
- <sup>151</sup> *Stony Brook University, Stony Brook, New York 11794, USA*
- <sup>152</sup> *University of Sussex, Brighton, BN1 9RH, United Kingdom*
- <sup>153</sup> *Syracuse University, Syracuse, NY 13244, USA*
- <sup>154</sup> *Universidad Tecnica Federico Santa Maria, Department de Fisica, Casino 110-V, Valparaiso, Chile*
- <sup>155</sup> *University of Tennessee at Knoxville, TN, 37996, USA*
- <sup>156</sup> *Texas A&M University (Corpus Christi), Corpus Christi, TX 78412, USA*
- <sup>157</sup> *University of Texas (Arlington), Arlington, TX 76019, USA*
- <sup>158</sup> *University of Texas (Austin), Austin, TX 78712, USA*
- <sup>159</sup> *Tsinghua University, Haidian District, Beijing 100084, China*
- <sup>160</sup> *TUBITAK Space Technologies Research Institute, TR-06800, Ankara, Turkey*
- <sup>161</sup> *Tufts University, Medford, MA 02155, USA*
- <sup>162</sup> *Universidade Federal de São Carlos, Araras - SP, 13604-900, Brazil*
- <sup>163</sup> *Universidade Nacional de Asuncion, 585540/2 Interno 1068 CC: 910, Asunción, Paraguay*
- <sup>164</sup> *Università del Salento - INFN, Via Provinciale per Arnesano, 73100 - Lecce , Italy*
- <sup>165</sup> *Variable Energy Cyclotron Centre, 1/AF, Bidhanagar Kolkata - 700 064 West Bengal, India*
- <sup>166</sup> *Valley City State University, Valley City, ND 58072, USA*
- <sup>167</sup> *Virginia Tech, Blacksburg, VA 24060, USA*
- <sup>168</sup> *University of Warsaw, Faculty of Physics ul. Pasteura 5 02-093 Warsaw, Poland*
- <sup>169</sup> *Warsaw University of Technology, Nowowiejska 15/19, 00-665 Warszawa Poland, Poland*
- <sup>170</sup> *University of Warwick, Coventry CV4 7AL, United Kingdom*
- <sup>171</sup> *Wichita State University, Physics Division, Wichita, KS 67260, USA*
- <sup>172</sup> *William and Mary, Williamsburg, VA 23187, USA*
- <sup>173</sup> *University of Wisconsin (Madison), Madison, WI 53706, USA*
- <sup>174</sup> *Wroclaw University, Plac Maxa Borny 9, 50-204 Wroclaw, Poland*
- <sup>175</sup> *Yale University, New Haven, CT 06520, USA*
- <sup>176</sup> *Yerevan Institute for Theoretical Physics and Modeling, Halabian Str. 34, Yerevan 0036, Armenia*
- <sup>177</sup> *York University, Physics and Astronomy Department, 4700 Keele St. Toronto M3J 1P3, Canada*





# Contents

|  |            |
|--|------------|
| <b>Contents</b>  | <b>i</b>   |
| <b>List of Figures</b>   | <b>vii</b> |
| <b>List of Tables</b>  | <b>1</b>   |
| <b>1 Design Motivation</b>   | <b>3</b>   |
| 1.1 Introduction to the DUNE Dual-Phase Far Detector Module Design . . . . . | 3          |
| 1.2 Dual-Phase (DP) LArTPC Operational Principle . . . . .                   | 3          |
| 1.3 Motivation for the DP Design . . . . .                                   | 4          |
| 1.4 Overview of Dual-Phase Design . . . . .                                  | 6          |
| 1.5 Detector systems . . . . .   | 9          |
| 1.5.1 Charge Readout Planes . . . . .  | 9          |
| 1.5.2 Readout Electronics and Chimneys . . . . .                             | 11         |
| 1.5.3 Cathode, Field Cage and HV System . . . . .                            | 12         |
| 1.5.4 Photon Detection System . . . . .                                      | 13         |
| 1.5.5 Data Acquisition . . . . .   | 13         |
| 1.5.6 Cryogenics Instrumentation and Slow Controls . . . . .                 | 14         |
| <b>2 Charge Readout Planes</b>   | <b>16</b>  |
| 2.1 Charge Readout Planes (CRP) Overview . . . . .                           | 16         |
| 2.1.1 Introduction . . . . .   | 16         |
| 2.1.2 Design Considerations . . . . .  | 18         |
| 2.1.3 Scope . . . . .  | 19         |
| 2.2 CRP Design . . . . .   | 20         |
| 2.2.1 Mechanical structure . . . . .   | 21         |
| 2.2.2 Extraction Grid . . . . .  | 22         |
| 2.2.3 Large Electron Multiplier (LEM) . . . . .                              | 23         |
| 2.2.4 Anode . . . . .  | 24         |
| 2.2.5 Instrumentation . . . . .  | 25         |
| 2.2.6 Suspension System and Drive . . . . .                                  | 26         |
| 2.3 Production and Assembly . . . . .  | 28         |
| 2.3.1 G10 and Invar Frame Production . . . . .                               | 28         |
| 2.3.2 LEM and Anode Production . . . . .                                     | 29         |
| 2.3.3 Tooling . . . . .  | 33         |
| 2.3.4 Assembly Procedures . . . . .  | 34         |

|          |   |           |
|----------|---|-----------|
| 2.4      | Interfaces . . . . .  | 36        |
| 2.4.1    | TPC Electronics . . . . .   | 37        |
| 2.4.2    | Instrumentation and HV Feedthrough Flanges . . . . .                                    | 37        |
| 2.4.3    | Cryostat and Detector Support Structure . . . . .                                       | 37        |
| 2.4.4    | HV and Slow Controls . . . . .  | 39        |
| 2.5      | Installation, Integration and Commissioning . . . . .                                   | 39        |
| 2.5.1    | Transport and Handling . . . . .  | 40        |
| 2.5.2    | Calibration . . . . .   | 41        |
| 2.6      | Quality Control . . . . .   | 41        |
| 2.7      | Safety . . . . .  | 41        |
| <b>3</b> | <b>TPC Electronics</b>  | <b>43</b> |
| 3.1      | TPC Electronics System Overview . . . . .   | 43        |
| 3.1.1    | Introduction . . . . .  | 43        |
| 3.1.2    | Design Considerations . . . . .   | 45        |
| 3.1.3    | Scope . . . . .   | 47        |
| 3.2      | TPC Electronics System Design . . . . .   | 48        |
| 3.2.1    | Cryogenic Analog Front-end Electronics . . . . .  | 50        |
| 3.2.2    | Signal Feedthrough Chimneys . . . . .   | 53        |
| 3.2.3    | Digital Advanced Mezzanine Card Electronics for Charge Readout . . . . .                | 55        |
| 3.2.4    | Electronics for Light Readout . . . . .   | 57        |
| 3.2.5    | Network-based $\mu$ TCA Architecture . . . . .  | 60        |
| 3.2.6    | Timing Distribution . . . . .   | 62        |
| 3.3      | Production and Quality Assurance . . . . .  | 64        |
| 3.3.1    | Cryogenic Analog FE Electronics . . . . .   | 64        |
| 3.3.2    | Signal Feedthrough Chimneys . . . . .   | 64        |
| 3.3.3    | The Timing System and $\mu$ TCA . . . . .   | 65        |
| 3.3.4    | Charge Readout Electronics . . . . .  | 65        |
| 3.3.5    | Light Readout Electronics . . . . .   | 65        |
| 3.4      | Interfaces . . . . .  | 66        |
| 3.4.1    | Electronics System to charge-readout plane (CRP) and Photon Detection Systems . . . . . | 66        |
| 3.4.2    | Electronics System to DAQ System . . . . .  | 67        |
| 3.4.3    | Electronics System to Cryostat and Cryogenics . . . . .                                 | 68        |
| 3.4.4    | Electronics System to Slow Control System . . . . .                                     | 69        |
| 3.5      | Transport and Handling . . . . .  | 70        |
| 3.6      | Installation, Integration and Commissioning . . . . .                                   | 70        |
| 3.6.1    | SFT Chimneys . . . . .  | 70        |
| 3.6.2    | Digital $\mu$ TCA Crates . . . . .  | 71        |
| 3.6.3    | Integration within the DAQ . . . . .  | 71        |
| 3.6.4    | Integration with the Photon Detection System . . . . .                                  | 71        |
| 3.6.5    | Commissioning . . . . .   | 71        |
| 3.7      | Risks and Vulnerabilities . . . . .   | 72        |
| 3.8      | Organization and Management . . . . .   | 73        |
| 3.8.1    | Dual-Phase TPC Electronics Consortium Organization . . . . .                            | 73        |
| 3.8.2    | Planning Assumptions . . . . .  | 73        |
| 3.8.3    | WBS and Responsibilities . . . . .  | 73        |
| 3.8.4    | High-level Cost and Schedule . . . . .  | 73        |

|          |   |           |
|----------|---|-----------|
| <b>4</b> | <b>High Voltage System</b>                              | <b>75</b> |
| 4.1      | High Voltage System (HV) Overview . . . . .             | 75        |
| 4.1.1    | Introduction . . . . .                                  | 75        |
| 4.1.2    | Design Considerations . . . . .                         | 76        |
| 4.1.3    | Scope . . . . .   | 76        |
| 4.1.4    | System Overview . . . . .                               | 78        |
| 4.2      | HV System Design . . . . .                              | 78        |
| 4.2.1    | High Voltage Power Supply and Feedthroughs . . . . .    | 78        |
| 4.2.2    | High Voltage Extender and Voltage Degradation . . . . . | 81        |
| 4.2.3    | Cathode Plane . . . . .                                 | 81        |
| 4.2.4    | Ground Grid . . . . .                                   | 84        |
| 4.2.5    | Field Cage . . . . .                                    | 84        |
| 4.2.6    | HV Return and Monitoring Devices . . . . .              | 88        |
| 4.3      | Quality Assurance . . . . .                             | 90        |
| 4.4      | Production and Assembly . . . . .                       | 91        |
| 4.4.1    | Field Cage Submodule Frames . . . . .                   | 91        |
| 4.4.2    | Cathode Plane . . . . .                                 | 92        |
| 4.4.3    | Ground Plane . . . . .                                  | 92        |
| 4.4.4    | Electrical Interconnections . . . . .                   | 93        |
| 4.5      | Interfaces to the HV System . . . . .                   | 93        |
| 4.5.1    | Cryostat . . . . .                                      | 93        |
| 4.5.2    | Charge Readout Plane . . . . .                          | 93        |
| 4.5.3    | Photon Detection System . . . . .                       | 93        |
| 4.6      | Transport, Handling and Integration . . . . .           | 94        |
| 4.7      | Quality Control . . . . .                               | 94        |
| 4.8      | Safety . . . . .  | 95        |
| 4.9      | Organization and Management . . . . .                   | 96        |
| 4.9.1    | HV Consortium Organization . . . . .                    | 96        |
| 4.9.2    | Planning Assumptions . . . . .                          | 97        |
| <b>5</b> | <b>Photon Detection System</b>                          | <b>99</b> |
| 5.1      | Overview . . . . .                                      | 99        |
| 5.1.1    | Introduction . . . . .                                  | 99        |
| 5.1.2    | Physics and the Role of Photodetection . . . . .        | 100       |
| 5.1.3    | Technical Requirements . . . . .                        | 101       |
| 5.1.4    | Detector Layout . . . . .                               | 101       |
| 5.1.5    | Operation Principles . . . . .                          | 103       |
| 5.2      | Photosensor System . . . . .                            | 104       |
| 5.2.1    | Photodetector Selection and Procurement . . . . .       | 104       |
| 5.2.2    | Photodetector Characterization . . . . .                | 105       |
| 5.2.3    | High Voltage System . . . . .                           | 106       |
| 5.2.4    | Wavelength Shifters . . . . .                           | 107       |
| 5.2.5    | Light Collectors . . . . .                              | 107       |
| 5.3      | Mechanics . . . . .                                     | 108       |
| 5.4      | Readout Electronics . . . . .                           | 109       |
| 5.4.1    | Photomultiplier High Voltage Dividers . . . . .         | 109       |
| 5.4.2    | High Voltage and Signal Splitters . . . . .             | 110       |

|        |   |     |
|--------|---|-----|
| 5.4.3  | Signal Readout Requirements . . . . .                 | 111 |
| 5.5    | Photon Calibration System . . . . .                   | 113 |
| 5.5.1  | System Design and Procurement . . . . .               | 113 |
| 5.5.2  | Validation Tests . . . . .                            | 114 |
| 5.6    | Photon Detector Performance . . . . .                 | 115 |
| 5.6.1  | Simulations . . . . .                                 | 117 |
| 5.6.2  | Light Data in DP Prototypes . . . . .                 | 122 |
| 5.6.3  | Simulation of Physics Events . . . . .                | 122 |
| 5.7    | Photon Detector Operations . . . . .                  | 124 |
| 5.7.1  | Trigger Strategy . . . . .                            | 124 |
| 5.7.2  | Data Quality Monitoring . . . . .                     | 125 |
| 5.8    | Interfaces . . . . .                                  | 125 |
| 5.9    | Installation, Integration and Commissioning . . . . . | 127 |
| 5.9.1  | Transport and Handling . . . . .                      | 127 |
| 5.9.2  | Integration and Testing Facility Operations . . . . . | 127 |
| 5.9.3  | Underground Installation and Integration . . . . .    | 128 |
| 5.9.4  | Commissioning . . . . .                               | 128 |
| 5.10   | Quality Control . . . . .                             | 128 |
| 5.10.1 | Production and Assembly . . . . .                     | 128 |
| 5.10.2 | Post-Factory Installation . . . . .                   | 129 |
| 5.11   | Safety . . . . .                                      | 130 |
| 5.12   | Management and Organization . . . . .                 | 130 |
| 5.12.1 | Consortium Organization . . . . .                     | 130 |
| 5.12.2 | Planning Assumptions . . . . .                        | 131 |
| 5.12.3 | WBS and Responsibilities . . . . .                    | 132 |
| 5.12.4 | High-Level Cost and Schedule . . . . .                | 132 |

**6 Data Acquisition System 134**

|       |  |     |
|-------|--|-----|
| 6.1   | Data Acquisition (DAQ) System Overview . . . . . | 134 |
| 6.1.1 | Introduction . . . . .                           | 134 |
| 6.1.2 | Design Considerations . . . . .                  | 136 |
| 6.1.3 | Scope . . . . .                                  | 143 |
| 6.2   | DAQ Design . . . . .                             | 144 |
| 6.2.1 | Overview . . . . .                               | 144 |
| 6.2.2 | Front-end Readout and Buffering . . . . .        | 146 |
| 6.2.3 | Front-end Trigger Primitive Generation . . . . . | 148 |
| 6.2.4 | Dataflow, Trigger and Event Builder . . . . .    | 148 |
| 6.2.5 | Data Selection Algorithms . . . . .              | 151 |
| 6.2.6 | Timing and Synchronization . . . . .             | 154 |
| 6.2.7 | Computing and Network Infrastructure . . . . .   | 155 |
| 6.2.8 | Run Control and Monitoring . . . . .             | 156 |
| 6.3   | Interfaces . . . . .                             | 157 |
| 6.3.1 | TPC Electronics . . . . .                        | 157 |
| 6.3.2 | PD Electronics . . . . .                         | 157 |
| 6.3.3 | Offline Computing . . . . .                      | 158 |
| 6.3.4 | Slow Control . . . . .                           | 158 |
| 6.3.5 | External Systems . . . . .                       | 159 |

|          |   |            |
|----------|---|------------|
| 6.4      | Production and Assembly . . . . .                               | 160        |
| 6.4.1    | DAQ Components . . . . .  | 160        |
| 6.4.2    | Quality Assurance and Quality Control . . . . .                 | 161        |
| 6.4.3    | Integration testing . . . . .                                   | 162        |
| 6.5      | Installation, Integration and Commissioning . . . . .           | 162        |
| 6.5.1    | Installation . . . . .  | 162        |
| 6.5.2    | Integration with Detector Electronics . . . . .                 | 164        |
| 6.5.3    | Commissioning . . . . .   | 164        |
| 6.6      | Safety . . . . .  | 165        |
| 6.7      | Organization and Management . . . . .                           | 165        |
| 6.7.1    | DAQ Consortium Organization . . . . .                           | 165        |
| 6.7.2    | Planning Assumptions . . . . .                                  | 166        |
| 6.7.3    | High-level Cost and Schedule . . . . .                          | 166        |
| <b>7</b> | <b>Slow Controls and Cryogenics Instrumentation</b>             | <b>168</b> |
| 7.1      | Slow Controls and Cryogenics Instrumentation Overview . . . . . | 168        |
| 7.1.1    | Introduction . . . . .  | 168        |
| 7.1.2    | Design Considerations . . . . .                                 | 169        |
| 7.1.3    | Scope . . . . .   | 171        |
| 7.2      | Cryogenics Instrumentation . . . . .                            | 173        |
| 7.2.1    | Fluid Dynamics Simulations . . . . .                            | 175        |
| 7.2.2    | Purity Monitors . . . . .                                       | 177        |
| 7.2.3    | Thermometers . . . . .  | 181        |
| 7.2.4    | Liquid Level Monitoring . . . . .                               | 187        |
| 7.2.5    | Gas Analyzers . . . . .   | 189        |
| 7.2.6    | Cameras . . . . .   | 190        |
| 7.2.7    | Cryogenics Test Facility . . . . .                              | 196        |
| 7.2.8    | Cryogenic Internal Piping . . . . .                             | 196        |
| 7.3      | Slow Controls . . . . .   | 197        |
| 7.3.1    | Slow Controls Hardware . . . . .                                | 198        |
| 7.3.2    | Slow Controls Infrastructure . . . . .                          | 199        |
| 7.3.3    | Slow Controls Software . . . . .                                | 200        |
| 7.3.4    | Slow Controls Quantities . . . . .                              | 200        |
| 7.3.5    | Local Integration . . . . .                                     | 202        |
| 7.4      | Interfaces . . . . .  | 202        |
| 7.5      | Installation, Integration and Commissioning . . . . .           | 204        |
| 7.5.1    | Cryogenics Internal Piping . . . . .                            | 204        |
| 7.5.2    | Purity Monitors . . . . .                                       | 204        |
| 7.5.3    | Thermometers . . . . .  | 205        |
| 7.5.4    | Gas Analyzers . . . . .   | 206        |
| 7.5.5    | Liquid Level Monitoring . . . . .                               | 207        |
| 7.5.6    | Cameras and Light-Emitting System . . . . .                     | 207        |
| 7.5.7    | Slow Controls Hardware . . . . .                                | 208        |
| 7.5.8    | Transport, Handling and Storage . . . . .                       | 208        |
| 7.6      | Quality Control . . . . .                                       | 208        |
| 7.6.1    | Purity Monitors . . . . .                                       | 209        |
| 7.6.2    | Thermometers . . . . .  | 209        |

|          |  |            |
|----------|--|------------|
| 7.6.3    | Gas Analyzers . . . . .  | 211        |
| 7.6.4    | Liquid Level Monitoring . . . . .  | 211        |
| 7.6.5    | Cameras . . . . .  | 211        |
| 7.6.6    | Light-emitting System . . . . .  | 212        |
| 7.6.7    | Slow Controls Hardware . . . . .   | 212        |
| 7.7      | Safety . . . . .   | 212        |
| 7.8      | Organization and Management . . . . .  | 213        |
| 7.8.1    | Slow Controls and Cryogenics Instrumentation Consortium Organization . . . . . | 213        |
| 7.8.2    | Planning Assumptions . . . . .   | 214        |
| 7.8.3    | High-level Schedule . . . . .  | 215        |
| <b>8</b> | <b>Technical Coordination</b>  | <b>216</b> |
| 8.1      | Project Support . . . . .  | 220        |
| 8.1.1    | Schedule . . . . .   | 222        |
| 8.1.2    | Risk . . . . .   | 224        |
| 8.1.3    | Reviews . . . . .  | 225        |
| 8.1.4    | Quality Assurance . . . . .  | 225        |
| 8.1.5    | ESH . . . . .  | 227        |
| 8.2      | Integration Engineering . . . . .  | 228        |
| 8.2.1    | Configuration Management . . . . .   | 228        |
| 8.2.2    | Engineering Process and Support . . . . .                                      | 230        |
| 8.3      | Detector Infrastructure . . . . .  | 232        |
| 8.4      | The Integration and Test Facility . . . . .                                    | 233        |
| 8.4.1    | Requirements . . . . .   | 235        |
| 8.4.2    | Management . . . . .   | 236        |
| 8.4.3    | Inventory System . . . . .   | 236        |
| 8.4.4    | ITF Infrastructure . . . . .   | 236        |
| 8.5      | Installation Coordination and Support . . . . .                                | 236        |
| 8.5.1    | UIT Infrastructure . . . . .   | 237        |
| 8.5.2    | Underground Detector Installation . . . . .                                    | 237        |
| 8.5.3    | Preparation for Operations . . . . .   | 246        |
|          | <b>Glossary</b>  | <b>247</b> |
|          | <b>References</b>  | <b>258</b> |

# List of Figures

|      |  |    |
|------|--|----|
| 1.1  | Principle of the DP readout . . . . .  | 5  |
| 1.2  | Diagram of the DP module . . . . .   | 7  |
| 1.3  | Thicknesses and HV values for electron extraction from liquid to gaseous Ar . . . . .  | 10 |
| 2.1  | Dual-phase readout . . . . .   | 17 |
| 2.2  | View of a complete 9 m <sup>2</sup> charge-readout plane (CRP) module . . . . .        | 18 |
| 2.3  | Main components of a CRP module of 9 m <sup>2</sup> . . . . .                          | 20 |
| 2.4  | First CRP Invar frame under construction for ProtoDUNE-DP . . . . .                    | 21 |
| 2.5  | G10 elements of a full CRP module . . . . .  | 22 |
| 2.6  | Decoupling system attached to the Invar frame . . . . .                                | 22 |
| 2.7  | Extraction grid components on the CRP structure . . . . .                              | 23 |
| 2.8  | Picture of a large electron multiplier (LEM) module used for ProtoDUNE-DP . . . . .    | 24 |
| 2.9  | Picture of the anode symmetric 2D strip design. . . . .                                | 25 |
| 2.10 | View of the distance meter plates on the sides of a CRP . . . . .                      | 26 |
| 2.11 | View of the thermometer board . . . . .  | 27 |
| 2.12 | Suspension feedthrough and various assembly details . . . . .                          | 27 |
| 2.13 | Anchoring system of the suspension cable on the CRP frame . . . . .                    | 28 |
| 2.14 | High-pressure vessel for the characterization of the ProtoDUNE-DP LEM modules. . . . . | 32 |
| 2.15 | Event display of a 5.5 MeV alpha track in argon gas at 1 bar. . . . .                  | 33 |
| 2.16 | Test of anode strip continuity . . . . .   | 34 |
| 2.17 | Extraction grid construction bench details . . . . .                                   | 35 |
| 2.18 | LEM and anode connection and extraction grid module installation. . . . .              | 36 |
| 2.19 | Elements for assembly of ProtoDUNE-DP CRP at CERN . . . . .                            | 36 |
| 2.20 | LEM high voltage (HV) distribution boxes mounted on a CRP . . . . .                    | 38 |
| 2.21 | HV distribution box for LEM top electrodes before filling . . . . .                    | 38 |
| 3.1  | Schematic layout of the dual-phase (DP) charge readout (CRO) sub-system . . . . .      | 44 |
| 3.2  | Schematic layout of the DP light readout (LRO) sub-system . . . . .                    | 45 |
| 3.3  | Top corner view of DP module . . . . .   | 49 |
| 3.4  | Cryogenic front-end (FE) ASIC properties . . . . .                                     | 51 |
| 3.5  | Image of an analog FE card mounted on the extraction blade . . . . .                   | 51 |
| 3.6  | Noise measurements in the WA105 DP demonstrator in different conditions . . . . .      | 52 |
| 3.7  | Details of the signal feedthrough chimney (SFT chimney) design . . . . .               | 54 |
| 3.8  | Signal feedthrough chimney cold flange . . . . .                                       | 54 |
| 3.9  | Block diagram of advanced mezzanine card (AMC) . . . . .                               | 56 |
| 3.10 | Block diagram of LRO . . . . .   | 58 |



|      |  |     |
|------|--|-----|
| 3.11 | Photo of prototype LRO card . . . . .  | 58  |
| 3.12 | CATIROC ASIC . . . . .   | 60  |
| 3.13 | Instrumented $\mu$ TCA crate from the WA105 DP demonstrator . . . . .                                  | 62  |
| 3.14 | Picture of White Rabbit (WR) slave node card . . . . .   | 63  |
| 3.15 | Architecture of WR network . . . . .   | 64  |
| 3.16 | Images of the WA105 DP demonstrator signal feedthrough (SFT) cold feedthrough . . . . .                | 67  |
| 3.17 | Details of SFT chimney interface to the cryostat structure . . . . .                                   | 69  |
|      |  |     |
| 4.1  | DP module overview . . . . .   | 76  |
| 4.2  | HV system for a DP detector module . . . . .   | 79  |
| 4.3  | HV powersupply and feedthrough for a DP detector module . . . . .                                      | 80  |
| 4.4  | DP HVFT and extender . . . . .   | 82  |
| 4.5  | Cutaway view of ProtoDUNE-DP cathode . . . . .   | 83  |
| 4.6  | ProtoDUNE-DP cathode E field . . . . .   | 83  |
| 4.7  | DP field cage (FC) parts . . . . .   | 85  |
| 4.8  | E field map and equipotential contours of an array of roll-formed profiles . . . . .                   | 87  |
| 4.9  | DP HVDB . . . . .  | 88  |
| 4.10 | DP FC installation process and inter-module connection . . . . .                                       | 89  |
|      |  |     |
| 5.1  | The DP module (partially open) . . . . .   | 103 |
| 5.2  | Picture of the Hamamatsu R5912-MOD20 photomultiplier tube (PMT). . . . .                               | 104 |
| 5.3  | Picture of the PMTs being installed in the testing vessel . . . . .                                    | 105 |
| 5.4  | Sketch of the setup for PMT characterization tests. . . . .  | 106 |
| 5.5  | Cryogenic Hamamatsu R5912-MOD20 PMT fixed on the membrane floor. . . . .                               | 109 |
| 5.6  | Positive power supply and cathode grounding scheme. . . . .  | 109 |
| 5.7  | Generic splitter circuit diagram. . . . .  | 111 |
| 5.8  | SPE waveforms and amplitudes from the WA105 at different voltages. . . . .                             | 112 |
| 5.9  | Event rates for different trigger thresholds observed in the WA105 DP demonstrator. . . . .            | 113 |
| 5.10 | Diagram of the photon calibration system to be implemented in ProtoDUNE-DP. . . . .                    | 114 |
| 5.11 | A sketch depicting the mechanism of light production in argon. . . . .                                 | 115 |
| 5.12 | Landau fits of the travel time distributions for a sources close to and far from the PMT. . . . .      | 118 |
| 5.13 | Evolution of the visibility seen by a central PMT . . . . .  | 119 |
| 5.14 | Evolution of the visibility and peak time as a function of source-PMT distance (preliminary) . . . . . | 120 |
| 5.15 | Light yield in terms of photoelectron/MeV summed over all PMTs . . . . .                               | 121 |
| 5.16 | Averaged waveform of the S1 light signal from the WA105 DP demonstrator . . . . .                      | 122 |
| 5.17 | Response for simulated SNB neutrino interactions (ProtoDUNE-DP geometry) . . . . .                     | 123 |
| 5.18 | Response for simulated nucleon decays (ProtoDUNE-DP geometry) . . . . .                                | 124 |
|      |  |     |
| 6.1  | DAQ overview . . . . .   | 137 |
| 6.2  | data acquisition (DAQ) overview . . . . .  | 138 |
| 6.3  | DP FE DAQ fragment . . . . .   | 146 |
| 6.4  | CUC control room layout . . . . .  | 163 |
| 6.5  | DAQ high-level schedule . . . . .  | 167 |
|      |  |     |
| 7.1  | CISC subsystems . . . . .  | 169 |
| 7.2  | Cryostat ports . . . . .   | 174 |
| 7.3  | CFD example . . . . .  | 176 |
| 7.4  | CFD example geometry . . . . .   | 176 |

|      |  |     |
|------|--|-----|
| 7.5  | Electron lifetimes measured in the purity monitors in the 35 ton prototype . . . . . | 179 |
| 7.6  | Purity monitor diagram . . . . .   | 179 |
| 7.7  | Purity monitor block diagram . . . . .   | 180 |
| 7.8  | Purity monitor string . . . . .  | 181 |
| 7.9  | Cryostat bolts and temperature sensor support . . . . .                              | 183 |
| 7.10 | Temperature sensor resolution and reproducibility . . . . .                          | 184 |
| 7.11 | Dynamic T-gradient monitor overview . . . . .  | 185 |
| 7.12 | Sensor-cable assembly for dynamic T-gradient monitor . . . . .                       | 186 |
| 7.13 | Cable supports for individual temperature sensors . . . . .                          | 186 |
| 7.14 | Gas Analyzer switchyard . . . . .  | 189 |
| 7.15 | Gas analyzer purge . . . . .   | 190 |
| 7.16 | Gas analyzer $O_2$ level after liquid argon (LAr) filling . . . . .                  | 191 |
| 7.17 | A camera enclosure . . . . .   | 193 |
| 7.18 | Inspection camera design . . . . .   | 194 |
| 7.19 | LED chain for illumination . . . . .   | 195 |
| 7.20 | CryTest Blanche Test . . . . .   | 196 |
| 7.21 | Cryogenic internal piping . . . . .  | 197 |
| 7.22 | Slow Controls connections and data . . . . .   | 198 |
| 7.23 | cryogenic instrumentation and slow controls (CISC) consortium organization . . . . . | 214 |
| 8.1  | Organization of technical coordination (TC) . . . . .                                | 217 |
| 8.2  | Flow of components from the consortia to the far detector (FD). . . . .              | 218 |
| 8.3  | LBNF/DUNE systems engineering organizational structure. . . . .                      | 219 |
| 8.4  | DUNE Technical Board. . . . .  | 220 |
| 8.5  | DUNE management organizational structure. . . . .                                    | 221 |
| 8.6  | APA and CPA installation steps . . . . .   | 239 |
| 8.7  | cathode plane assembly (CPA) and FC unpacking and assembly . . . . .                 | 240 |
| 8.8  | 3D model of underground area showing installation infrastructure . . . . .           | 241 |
| 8.9  | Section view of the 3D model showing layout . . . . .                                | 242 |
| 8.10 | End view of SP module with endwall field cage (endwall FC) in place . . . . .        | 243 |
| 8.11 | High-level installation schedule . . . . .   | 244 |
| 8.12 | Image of the DP CRPs being installed in the DP module . . . . .                      | 245 |

# List of Tables

|      |  |     |
|------|--|-----|
| 1.1  | Dual-phase module parameters . . . . .   | 7   |
| 1.2  | Quantities of items or parameters for the DP module . . . . .                          | 8   |
| 2.1  | Interstage distances and E field settings of the DP readout components . . . . .       | 17  |
| 2.2  | Important parameters for the charge-readout plane (CRP) system design . . . . .        | 19  |
| 2.3  | Tolerance values on various large electron multiplier (LEM) parameters . . . . .       | 31  |
| 2.4  | Specifications for the anode dimensions . . . . .                                      | 33  |
| 3.1  | Parameters for the TPC electronics system design . . . . .                             | 47  |
| 3.2  | Numbers for DP electronics components to procure . . . . .                             | 48  |
| 3.3  | Summary of some of the principal parameters of the TPC electronics system. . . . .     | 50  |
| 3.4  | Main characteristics of analog-to-digital converter (ADC) AD9257 . . . . .             | 56  |
| 3.5  | Main characteristics of ADC AD9249 . . . . .   | 59  |
| 3.6  | Main characteristics of CATIROC. . . . .   | 61  |
| 3.7  | Bandwidth requirements per $\mu$ TCA crate. . . . .                                    | 61  |
| 3.8  | Interface documents relevant to DP TPC electronics system . . . . .                    | 66  |
| 3.9  | DP TPC electronics consortium key milestones . . . . .                                 | 74  |
| 3.10 | DP TPC electronics consortium schedule . . . . .                                       | 74  |
| 4.1  | HIGH VOLTAGE (HV) system requirements . . . . .  | 77  |
| 4.2  | HV consortium participants . . . . .   | 97  |
| 5.1  | Summary of tentative requirements for the DP module photon detection system (PDS) .    | 102 |
| 5.2  | Default optical parameters chosen for the light simulation methods . . . . .           | 116 |
| 5.3  | DP photon detector (PD) interface documents . . . . .                                  | 126 |
| 5.4  | Pre-technical design report (TDR) key milestones . . . . .                             | 133 |
| 5.5  | Post-TDR key milestones . . . . .  | 133 |
| 6.1  | Important requirements on the data acquisition (DAQ) system design . . . . .           | 140 |
| 6.2  | Pre-trigger data rates from the far detector (FD) TPCs and into DAQ front end. . . . . | 141 |
| 6.3  | Uncompressed data rates for one SP module. . . . .                                     | 142 |
| 7.1  | Important design requirements on the DP CISC system design . . . . .                   | 172 |
| 7.2  | Liquid level monitor requirements . . . . .  | 188 |
| 7.3  | Camera system requirements . . . . .   | 192 |
| 7.4  | Slow controls quantities . . . . .   | 201 |
| 7.5  | Key cryogenic instrumentation and slow controls (CISC) milestones . . . . .            | 215 |

---

8.1 Overall DUNE Project Tier-1 milestones. . . . . 223

# Chapter 1

## Design Motivation

### 1.1 Introduction to the DUNE Dual-Phase Far Detector Module Design

The DUNE dual-phase (DP) detector module aims to open new windows of opportunity in the study of neutrinos, a goal it shares with the SP module. DUNE's rich physics program, with discovery potential for charge parity (CP) in the neutrino sector, and its capability to make significant observations of nucleon decay and astrophysical events, is enabled by the exquisite resolution of the LArTPC detector technique, which the DP design further augments. This design improves the S/N ratio in the charge readout, lowering the threshold for the smallest observable signals while also achieving a finer readout granularity. The DP technology enables the construction of larger drift volumes, thereby reducing the quantity of nonactive materials in the LAr. Although the physics requirements are identical for both the SP and DP designs, some aspects of the DP design offer augmented performance.

### 1.2 Dual-Phase (DP) LArTPC Operational Principle

The basic operational principle is very similar to that of the SP design. Charged particles that traverse the active volume of the LArTPC ionize the medium, while also producing scintillation light. The ionization electrons drift along an E field towards a segmented anode where they deposit their charge, and photon detectors (PDs) pick up the scintillation light. The precision tracking and calorimetry offered by the DP technology provides excellent capabilities for identifying interactions of interest while mitigating sources of background. Whereas the SP design has multiple drift volumes, the DP module design allows for a single, fully homogeneous LAr volume with a much longer drift length. This volume is surrounded by a field cage (FC) on the sides and a cathode at the bottom, which together define the drift field.

The key differentiating concept of the DP design is the amplification of the ionization signal in an avalanche process. In the SP design, charges drift horizontally to the anode, which consists of a set of induction and collection wire layers immersed in the LAr. In the DP design, electrons drift vertically upward towards an extraction grid just below the liquid-vapor interface. After reaching the grid, an E field stronger than the drift field extracts the electrons from the liquid up into the gas phase. Once in the gas, electrons encounter micro-pattern gas detectors with high-field regions, called large electron multipliers (LEMs). The LEMs amplify the electrons in avalanches that occur in these high-field regions. The amplified charge is then collected and recorded on a 2D anode consisting of two sets of 3.125 mm-pitch gold-plated copper strips that provide the  $x$  and  $y$  coordinates (and thus two views) of an event.

The extraction grid, LEM and anode are assembled into three-layered *sandwiches* with precisely defined inter-stage distances and inter-alignment, which are then connected together horizontally into modular units of area  $9 \text{ m}^2$ . These units are called charge-readout planes (CRPs). The CRPs integrate the LEMs and anodes, and support the extraction grid. These units can be individually positioned in a horizontal plane a few millimeters beneath the liquid-gas interface, ensuring complete immersion of the extraction grid.

The argon scintillation light, which at a wavelength of 127 nm is deep in the UV spectrum and it is recorded by an array of photomultiplier tubes (PMTs) located below the cathode. The PMTs, coated with a wavelength-shifting material, shifts the light closer to the visible spectrum and records the time and pulse characteristics of the incident light.

Two key factors affect the performance of the LArTPC. First, the LAr purity must be extremely high in order to achieve minimum charge attenuation over the longest drift lengths in the LArTPC. This requires that the levels of electronegative contaminants (e.g., oxygen, water), be reduced and maintained at  $\sim$ ppt levels. The DP and SP designs are subject to the same purity requirements. Second, the electronic readout of the LArTPC requires very low noise levels in order that the signal from the drifting electrons be clearly discernible over the baseline of the electronics. This requires use of low-noise cryogenic electronics.

The amplification of the electron signal in the gas phase mitigates the potential impact of these factors on the performance of the DP design. On the other hand this design requires higher voltages on the cathode, relative to the SP, due to the longer drift field.

### 1.3 Motivation for the DP Design

The innovative DP design is similar in many ways to the SP design, but implements some unique features and offers several advantages over it, providing an appealing and complementary approach, as summarized below:

- Gain on the ionization signal obtained in the gas phase:
  - leading to a robust and tunable S/N and a lower detection threshold, and

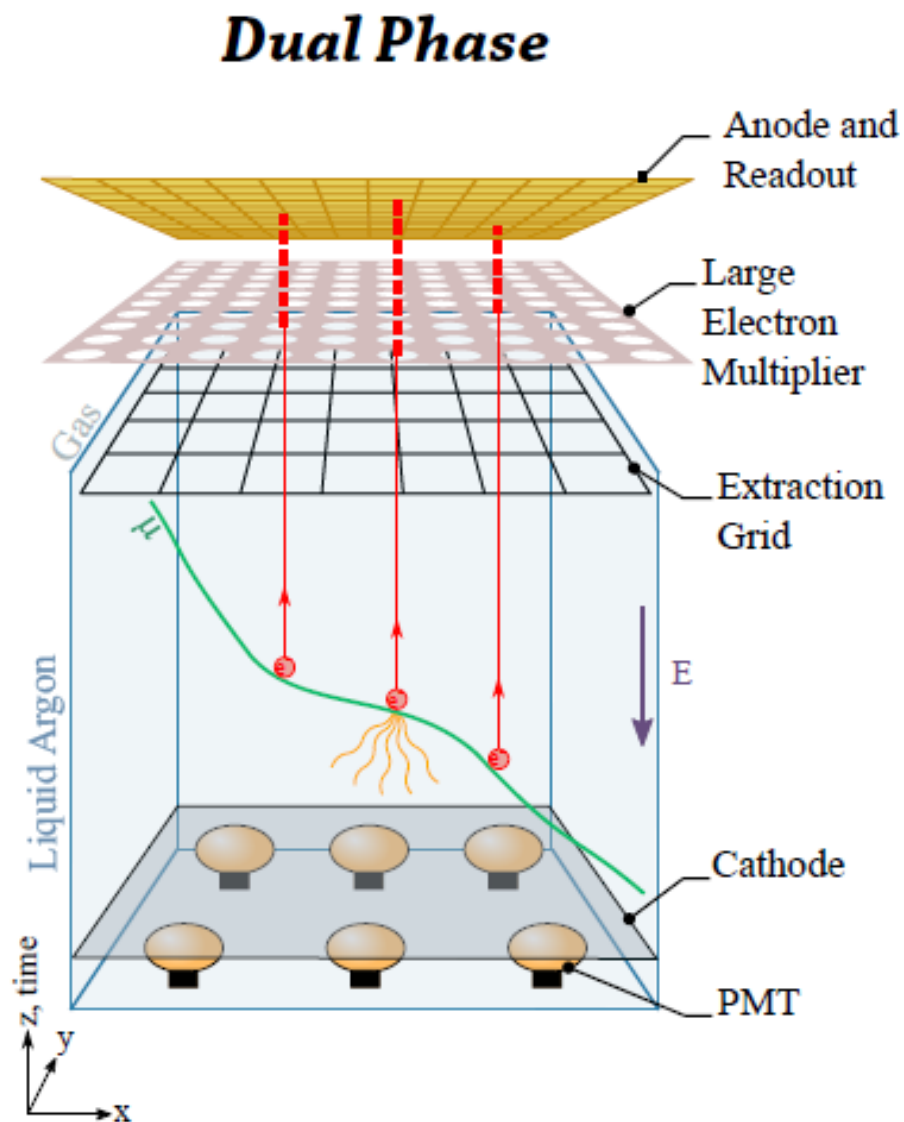


Figure 1.1: Principle of the DP readout

- compensating for potential charge attenuation due to long drift paths;
- Larger fiducial volume, enabling very long drift paths;
- Absence of dead material in the LAr drift volume;
- Finer readout pitch (3 mm), implemented in two identical collection views,  $x$  and  $y$ ;
- Fewer readout channels (153,600 for DP versus 384,000 for SP for a 10 kt module);
- Fewer construction modules;
- Full accessibility and replaceability of the front-end (FE) electronics during the detector operation.

The DP design features maximize the capability of the experiment and are motivated to cope with the unprecedented scale of the detector modules and the deep underground location where construction will occur.

Among the features driven by the underground location of the experiment, all detector components are sized to fit within the constraints of the SURF shafts and access pathways. The CRP modules are essentially planar objects with a surface of  $3 \times 3 \text{ m}^2$ . All the other detector components (FC and cathode modules) are designed in order to stay within this envelope. The relatively small number of detector elements makes the underground installation easier.

A drift time of several milliseconds is typical for ionization charge to arrive at the anode wires after drifting several meters. This lengthy duration, as well as aspects of the DUNE physics program looking for rare and low-energy processes, makes the deep underground location essential for the DP module. The 1.5 km overburden of earth will vastly reduce the rate of cosmic rays reaching the active volume of the DP module, greatly enhancing the ability to search for rare and low-energy signatures without the influence of cosmic-induced backgrounds.

## 1.4 Overview of Dual-Phase Design

This DP design implements a DP liquid argon time projection chamber (LArTPC) augmented with a light-readout system. *DP* refers to the extraction of ionization electrons at the interface between the liquid and gas argon and their amplification and collection in the gas phase.

The DP module features a 12.096 kt active mass LArTPC, with all associated cryogenics, electronic readout, computing, and safety systems. The DP module is designed to maximize the active volume within the confines of the membrane cryostat while minimizing dead regions and the presence of dead materials in the drift region. The detector is built as a single active volume 60 m long, 12 m wide and 12 m high, with the anode at the top, the cathode near the bottom, and an array of PMTs located at the bottom underneath the cathode. The active volume (see Figure 1.2) is surrounded



by the FC. The ionization electrons in the liquid phase drift in a uniform E field towards the anode plane at the top of the active volume. This is made by an array of 80 independent CRP modules,  $3 \times 3 \text{ m}^2$  each. The cryogenic FE electronics is installed in the signal feedthrough chimneys (SFT chimneys) on the roof of the cryostat. There are no active electronics elements in the cryostat volume besides the PMT bases. The proposed design optimally exploits the cryostat volume of  $14.0 \text{ m(w)} \times 14.1 \text{ m(h)} \times 62.0 \text{ m(l)}$  with an anode active area of  $12 \text{ m} \times 62.0 \text{ m}$  and a maximum drift length of 12 m, corresponding to an active LAr mass of 12.096 kt (10.643 kt fiducial).

The detector elements (CRPs, FC and cathode) have been modularized such that their production can proceed in parallel with the construction of the DUNE caverns and cryostats, and sized so that they conform to the access restrictions for transport underground. Table 1.1 summarizes the high-level parameters of the DP module while Figure 1.2 shows the DP module's main components.

Table 1.1: DP module parameters

| Parameter              | Value     | Note |
|------------------------|-----------|------|
| Cryostat LAr Mass      | 17.5 kt   |      |
| Active LAr Mass        | 12.096 kt |      |
| Active height          | 12 m      |      |
| Active length          | 60 m      |      |
| Maximum drift          | 12 m      |      |
| Number of CRPs         | 80        |      |
| Number of CRP channels | 153,600   |      |
| Number of PMT channels | 720       |      |

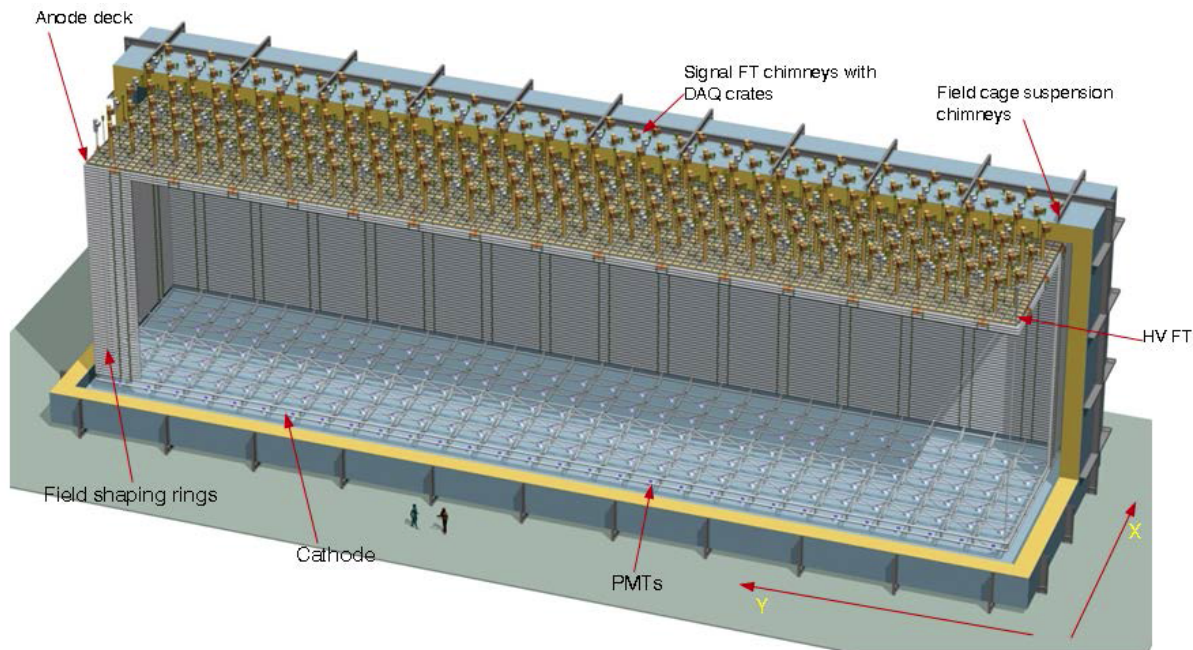


Figure 1.2: The DP module with cathode, PMTs, FC and anode plane with SFT chimneys.

The extraction of the electrons from the liquid to vapor phase is performed thanks to the submerged horizontal extraction grid, integrated in each CRP structure. A CRP unit includes 36

(0.5 m×0.5 m) LEM/anode sandwiches, providing tunable amplification and charge collection on two independent views organized in strips of 3 m length and 3.125 mm pitch. There are 1920 readout channels for each CRP. Signals in each CRP unit are collected via three SFT chimneys hosting the FE cards with the cryogenic ASIC amplifiers (6400 channels/chimney) which are accessible and replaceable without contaminating the pure LAr volume. Each SFT chimney is coupled to a microTCA crate to provide for the signals' digitization and data acquisition (DAQ). These crates are connected via optical fiber links to the DAQ back-end. The total number of readout channels per 10 kt module is 153,600.

Each CRP unit is independently suspended by three stainless steel ropes. The vertical level of each CRP unit can be automatically adjusted with respect to the LAr level via three suspension feedthroughs. The stainless steel ropes are operated by step motors located outside the suspension feedthroughs. Slow-control feedthroughs, one per CRP unit, are used for level meters and temperature probes readout, for pulsing the calibration signals, and to apply the high voltage (HV) bias on the two sides of the LEMs and on the extraction grid. The FC and the anode are constructed of modules of similar dimensions as those in ProtoDUNE-DP.

The number of components and corresponding parameters for the 12.096 kt DP module are summarized in Table 1.2.

Table 1.2: Quantities of items or parameters for the 12.096 kt DP module

| Item                                   | Number or Parameter     |
|--|-------------------------|
| Anode plane size                       | W = 12 m, L = 60 m      |
| CRP unit size                          | W = 3 m, L = 3 m        |
| CRP units                              | 4 × 20 = 80             |
| LEM-anode sandwiches per CRP unit      | 36                      |
| LEM-anode sandwiches (total)           | 2880                    |
| SFT chimney per CRP unit               | 3                       |
| SFT chimney (total)                    | 240                     |
| Charge readout channels / SFT chimney  | 640                     |
| Charge readout channels (total)        | 153,600                 |
| Suspension feedthrough per CRP unit    | 3                       |
| Suspension feedthroughs (total)        | 240                     |
| Slow Control feedthrough per sub-anode | 1                       |
| Slow Control feedthroughs (total)      | 80                      |
| HV feedthrough                         | 1                       |
| HV for vertical drift                  | 600 kV                  |
| Voltage degrader resistive chains      | 12                      |
| Cathode modules                        | 80                      |
| Field cage rings                       | 197                     |
| Field cage modules (3 m×12 m)          | 48                      |
| PMTs (total)                           | 720 (1/m <sup>2</sup> ) |

A number of factors make the DP TPC concept, as described in this chapter, well suited to

large detector sizes like the DP module. In this design, the charge amplification in the CRPs compensates for the charge attenuation on the long drift paths. This configuration also simplifies construction by optimally exploiting the long vertical dimensions of the cryostat, providing a large homogeneous fiducial volume free of embedded passive materials (effectively increasing the detector size), reducing the number of readout channels, and ultimately lowering costs.

The CRPs collect the charge in a projective way, with practically no dead region, and read the signals out in two collection views, eliminating the need for induction views, which simplifies the reconstruction of complicated topologies. The tunable high S/N provides operative margins with respect to the noise and electron lifetime conditions, and lowers the threshold on the minimal detectable energy depositions .

The scope of a DP module includes the design, procurement, fabrication, testing, delivery, installation and commissioning of the detector components, which is organized in detector consortia, specific to DP or joint with SP.

- CRP, including extraction grid, LEM and anode and readout planes (DP consortium);
- Analog and digital electronics and SFT chimney (DP consortium);
- photon detection system (PDS) (DP Consortium);
- Cathode, FC and HV system (joint SP-DP consortium);
- Slow-control (joint SP-DP consortium);
- Back-end DAQ system (joint SP-DP consortium).

## 1.5 Detector systems

### 1.5.1 Charge Readout Planes

An extraction efficiency of 100 % of the electrons from the liquid to the gas phase is achieved with an E field of the order of 2kV/cm across the liquid-gas interface, applied between an extraction grid submersed in the liquid and charge amplification devices situated in the ultra-pure argon gas.

These amplification devices, called LEMs, are horizontally oriented 1mm-thick printed circuit boards with electrodes on the top and bottom surfaces. They are drilled through with many holes that collectively form a micro-pattern structure; when a 3kV potential difference is applied across the electrodes the ionization electrons are amplified by avalanches (Townsend multiplication) occurring in the pure argon gas in this micro-pattern structure due to the high E field (30 kV/cm).

The use of avalanches to amplify the charges in the gas phase increases the S/N ratio by at

least one order of magnitude with a gain between 20 to 100, significantly improving the event reconstruction quality. It also lowers the threshold for small energy depositions and provides a better resolution per volumetric pixel (voxel) compared to a SP LArTPC. The charge is collected in a finely segmented 2D ( $x$  and  $y$ ) readout anode plane at the top of the gas volume and fed to the FE electronics.

The collection, amplification and readout components are combined in an array of independent (layered) modules called CRPs. A CRP is composed of several  $0.5 \times 0.5 \text{ m}^2$  units, each of which is composed of a LEM-anode *sandwich*. These units are embedded in a mechanically reinforced frame of FR-4 and iron-nickel invar alloy. This design guarantees the planarity requirements over the CRP span although the temperature gradient present in the gas phase and possible sagging effects with respect to the three suspension points. The CRP structure also integrates the submersed extraction grid, which is an array of  $x$  and  $y$  oriented stainless steel wires, 0.1 mm in diameter, with 3.125 mm pitch. Thicknesses and possible biasing voltages for the different layers are indicated in Figure 1.3.

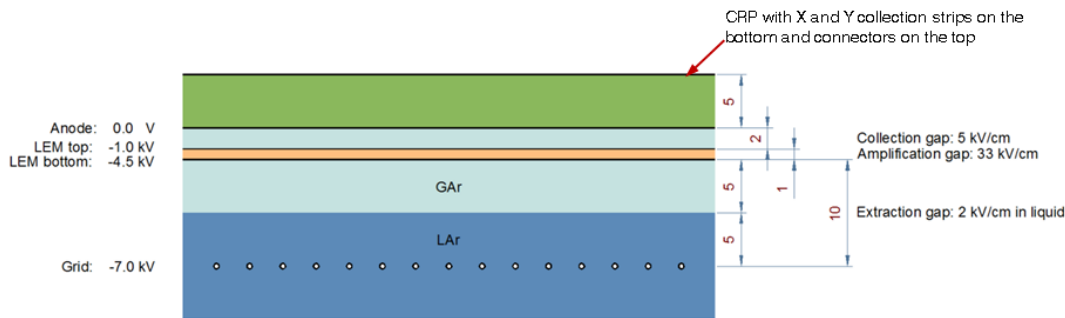


Figure 1.3: Thicknesses and HV values for electron extraction from liquid to gaseous argon, their multiplication by LEMs and their collection on the  $x$  and  $y$  readout anode plane. The HV values are indicated for a drift field of  $0.5 \text{ kV/cm}$  in LAr.

Each CRP is independently suspended by three stainless-steel ropes linked to the top deck of the cryostat. This suspension system allows adjustment of the CRP distance and parallelism with respect to the LAr surface, and keeps the extraction grid immersed. A CRP provides an adjustable charge gain (with a minimal required gain of 20) and two independent, orthogonal readout views, each with a pitch of 3.125 mm. The LEM/anode sandwiches in the same CRP unit are interconnected with short flat cables so that each readout channel corresponds to a total strip length of 3 m. Combined with the time information coming from the LAr scintillation readout by the PMT arrays ( $t_0$ ), a CRP provides 3D track imaging with  $dE/dx$  information. The CRPs and their components are described in Chapter 2.

The typical amplification achieved by this design, between 20 to 100, improves the S/N ratio and thus compensates for the charge losses that occur along the very long drift paths due to the presence of electronegative impurities. Therefore, despite the longer drift length, this design requires no higher purity of the LAr than does the reference design, around 0.1 ppb (or 100 ppt) of oxygen equivalent, and yields a 3 ms electron lifetime. The required level of purity can be reached by starting from commercially available ppm-level bulk argon and filling a non-evacuated vessel [2].

For instance, given an electron lifetime of 3 ms corresponding to the minimal requirement, a drift

field of 0.5 kV/cm and a LEM gain of 20, S/N ratio would be larger than 40:1 for tracks up to 6 m from the anode, while reaching 11:1 for minimum ionizing particle (MIP) tracks that are 12 m from the anode.

Other feedthroughs than the signal chimney connected to the CRPs and the CRP slow control and feedthroughs are planned for the cathode HV connection, the CRPs' suspension and level adjustment, the HV and signal readout of the PMTs, and the monitoring instrumentation (level meters, temperature probes, strain gauges, etc.).

## 1.5.2 Readout Electronics and Chimneys

The electrical signals from the collected charges are passed to the outside of the tank via a set of dedicated SFT chimney. The chimney are pipes passing through the top layer of the cryostat insulation and closed at the top and at the bottom by ultra-high-vacuum flanges (warm and cold). The volume inside each SFT chimney is tight with respect to the cryostat inner volume and it is filled with nitrogen gas. The bottom (cold) flange of each SFT chimney is a short distance from the CRPs in the cryostat gas volume.

The cryogenic FE electronics cards, housed at the bottom of the chimney are plugged to the top side of the cold flange. The FE cards are based on analog cryogenic preamplifiers implemented in CMOS ASIC circuits for high integration and large-scale affordable production. The ASIC circuits have been especially designed, following an R&D process started in 2006, to match the signal dynamics of a DP module. Within the chimney, the cards are actively cooled to a temperature of about 110 K and isolated with respect to the LAr vessel by the cold flange feedthrough. The bottom side of the cold flange is connected to the CRP via short flat cables (of length 0.5 m) in order to minimize the input capacitance to the preamplifiers. Each SFT chimney collects 640 readout channels.

The FE cards are mounted on 2 m long blades that slide on lateral guides that are integrated into the mechanical structure of the chimney, allowing access to and replacement of the analog FE electronics from the outside without contaminating the LAr volume. Swapping the FE electronics requires opening a flange at the top of the SFT chimney and feeding the SFT chimney with nitrogen in slight over-pressure with respect to the atmospheric pressure. This operation quite rapid and straightforward, and can be performed while the detector module is taking data. The chimney act also as Faraday cages, thereby entirely decoupling the analog FE electronics from possible noise pickup from the digital electronics.

The digital electronics for the charge digitization system, also resulting from a long R&D process started in 2006, is located on the roof the cryostat at room temperature. This makes it possible to use the low-cost, high-speed networking technologies used in the telecommunication industries, such as Micro Telecommunications Computing Architecture ( $\mu$ TCA). Digitization cards in the advanced mezzanine card (AMC) format read 64 channels per card. Each AMC card can digitize all 64 channels at 2.5 MHz and compress and transmit this continuous data stream, without zero skipping, over a network link operating at 10 Gbit/s. Lossless data compression is particularly effective thanks to the high S/N ratio of DP, which limits noise contributions at the level of one

analog-to-digital converter (ADC) count. Each SFT chimney is coupled to a  $\mu$ TCA crate housing in 10 AMC digitization cards in order to read 640 channels and transmit the data via the MicroTCA Carrier Hub (MCH) switch via a 10 Gbit/s optical link connected to the DAQ back-end. It requires 240  $\mu$ TCA crates to read the entire detector module. The SFT chimney warm flange is used to connect the analog differential signals, via shielded VHDCI cables, to the AMC digitization cards and also to distribute the LV and slow control signals to the analog FE electronics.

The light-readout digitization system is also based on  $\mu$ TCA AMC cards derived from the design of the charge readout and hosting a specific circuitry, based on the CATIROC ASIC for the light-readout triggering. By assuming a PMT channel density similar to that in ProtoDUNE-DP, five  $\mu$ TCA crates are sufficient to read 720 PMTs.

The timing synchronization is based on the White Rabbit (WR) standard. Specifically developed timing MCH connected to a WR network ensure the distribution of clock, absolute timing, and trigger information on the backplane of the  $\mu$ TCA crates. The White Rabbit  $\mu$ TCA Carrier Hub (WR-MCH) are connected via 1 Gbit/s optical fibers to a system of WR switches which interconnect the WR network. This ensures that the digitization performed by the various AMC cards is completely aligned and it also refers to the absolute UTC time. The WR grandmaster switch is connected to a GPS disciplined oscillator unit providing absolute time and the clock frequency reference to the system. The timing system includes 16 WR switches and 240 (charge readout) + 5 (light readout) MCH units.

The entire readout electronics system has been optimized to support the DP features including: charge signal dynamics, readout organization via the chimney, the number of readout channels, the high S/N ratio, and the possibility of performing continuous data streaming with zero losses to the DAQ back-end.

Employing cost-effective technologies and performing the corresponding R&D needed to fully exploit these technologies are strategies that are in place since the beginning of the R&D period in order reduce and optimize costs. This optimization adds to the fact that the number of readout channels is naturally lower for a DP module thanks to the long projective geometry: 153,600 channels for a DP module with 3 mm readout pitch to be compared to 384,000 channels for a SP module with 5 mm readout pitch.

### 1.5.3 Cathode, Field Cage and HV System

The HV system is designed by a common SP-DP consortium. The drift field ( $E \simeq 0.5$  kV/cm) inside the fully active LAr volume is produced by applying HV to the cathode plane at the bottom of the cryostat and is kept uniform by the FC, a stack of 60 equally spaced field-shaping electrodes, polarized at linearly decreasing voltages from the cathode voltage to almost ground potential, reached at the level of the CRP. The electrodes are rectangles made of extruded aluminum profiles (vertical pitch 60.6 mm) with rounded corners running horizontally (and stacked vertically) around the active volume. The aluminum profiles are supported and insulated by FRP supporting beams with a pattern of slots where the aluminum profiles can be mounted. Similarly as in ProtoDUNE-DP the profiles are arranged in modules of 3 m width including two FRP supporting columns.

These modules are chained together and are hanging from the cryostat roof. A chain of 6 modules covers the 12 m drift. The aluminum profiles of the different modules are joined together with short clipping profiles in order to ensure the electrical continuity over the 60 m long horizontal rings.

The drift cage design shares common structure elements (aluminum profiles and FRP supporting beams) as the SP FC design but with a different arrangement (vertically hung structure) in order to cope with the DP module geometry.

The cathode structure, constructed of a reinforced frame to guarantee its planarity, is suspended from the FC and hangs near the bottom of the cryostat. It is a segmented structure of tubes of different sizes arranged in a grid to minimize weight, limit sagging and avoid high E field regions in its proximity. The segmented structure allows scintillation light to pass through and be detected by uniform arrays of PMTs mounted 1 m below it at the bottom of the tank. As in ProtoDUNE-DP, the cathode is made out of modules 3 m in size in order to allow for transportation and underground installation.

## 1.5.4 Photon Detection System

The PDS is based on an array of PMTs uniformly distributed below the cathode. Assuming a similar channel density as in ProtoDUNE-DP, this translates to 720 channels. The PMTs have a tetra-phenyl butadiene (TPB) coating on the photocathode's external glass surface that shifts the scintillation light from deep UV to visible light. The PMTs sit on the corrugated membrane cryostat floor, on mechanical supports that do not interfere with the membrane thermal contraction. A single cable provides both HV and signal transmission by way of a positively biased base circuitry, thus reducing the required number of feedthrough channels. Optical fibers provide the calibration system.

## 1.5.5 Data Acquisition

The Ethernet-based DAQ back-end system is designed by a joint SP-DP consortium. It connects to 10 Gbits/s optical links that provide continuous, lossless, compressed data streaming from the  $\mu$ TCA crates, and it has the task of determining the trigger conditions for *interesting* events (beam, cosmics, supernova neutrino burst (SNB) neutrino interactions). This system also manages the recording of data to disk. The system can exploit the high S/N ratio peculiar to the DP design, the availability of the entire data stream without losses, and the possibility of going to lower detection thresholds for SNB events.

It is assumed that this DAQ back-end system will be composed of a set of event-building and trigger machines, high-performance network elements, and a high-bandwidth distributed storage system based on an array of storage servers operating in parallel. In particular, the DAQ system is expected to:

- Collect the high-bandwidth data volume coming from the data links of the FE digitization crates;
- Put together the data streams from different crates in Regions Of Interest (ROI) or over the entire detector volume (A ROI is typically the size of a ProtoDUNE-DP four-CRP surface, since events are contained in such a region.);
- Process this data flow by an online trigger farm as a prelude to selecting relevant events to be recorded on disk (both neutrino beam and off-beam events);
- Produce charge-readout triggers independently of the light-readout triggers and beam-spill information (In particular for SNB events, the trigger farm would issue triggers over a sliding timing window of about 10s based on the presence of low-energy depositions; the entire content would be dumped to disk.).

The DP readout architecture can be organized into 20 ROIs, each similar to the ProtoDUNE-DP back-end architecture. Triggers are searched on the level-1 event builder machines, interconnecting multiple  $\mu$ TCA crates, on a sliding windows of 10s contained in the event builder RAM.

The event builders combine the continuous lossless, compressed data (streaming from the charge readout) with beam data and light data in order to define the window  $t_0$  and select disk streams from beam events, cosmics and SNB events. The data decompression is necessary on the event builders in order to perform the charge data analysis for the triggers definition. Compressed data are kept in memory, while the trigger definition analysis is performed, for further writing on disk from level-2 machines from the output streams: beam, cosmics and proton decay, and SNB. The level-1 event builders exchange trigger primitive data on the network with a global supervisor machine, which then decides what data to write onto disk. The supervisor can order the dump onto disk of the event builder's memory windows if a certain number of candidate energy depositions is found from the charge data. This scheme makes it possible to put selected portions of different detector modules in communication with one another. Typically for beam data and cosmic events, the amount of data written to disk can be limited to one or two ROIs; there are cases in which in case events occur at the border between two ROIs rather than in a single one.

## 1.5.6 Cryogenics Instrumentation and Slow Controls

The cryogenic instrumentation and slow controls (CISC) system is designed by a joint SP-DP consortium. This system controls the following items:

- Cryogenic instrumentation: measurements of temperatures (gas and liquid), pressure (gas), liquid level, purity monitors;
- CRP instrumentation: temperatures, pulsing system, precision level meters, readout of CRP stepping motors;
- Generation and control of HV biasing of LEM and grid;



- Generation and control of HV biasing for the PMTs and calibration (via optical pulsing);
- Slow control of the  $\mu$ TCA crates, analog FELV control, charge injection control to preamplifiers;
- Control of the cathode HV biasing system;
- Alignment survey of CRP position (via external reference points);
- Control of the laser system;
- Analysis of LAr purity and LEM gain calibration.

# Chapter 2

## Charge Readout Planes

### 2.1 Charge Readout Planes (CRP) Overview

#### 2.1.1 Introduction

In the DP LArTPC concept, the ionization electrons are multiplied in avalanches occurring inside micro-pattern detectors, the large electron multipliers (LEMs), located in the argon gas phase above the LAr surface. The drift field of the TPC brings the electrons up to the LAr surface where they can be extracted into the gas using a 2 kV/cm E field defined across the liquid-gas interface.

This extraction field is defined by the potentials applied to submersed extraction grid (stainless steel wires tensioned in both  $x$  and  $y$  directions) and to the bottom side of the large electron multipliers (LEMs). The LEMs are printed circuit boards oriented horizontally, with conductive layers (electrodes) on the top and bottom surfaces, and many holes drilled through. The holes form a micro-pattern structure within which the amplification occurs given the presence of a strong E field.

By applying voltages across the two electrodes of the LEM, an E field region (up to 35 kV/cm) is defined in the holes, which produces an electronic signal gain exceeding 20 after the initial phase of charging-up the LEM dielectric material. Electrons transiting these high E field regions in the holes trigger Townsend multiplication in the pure argon gas.

The amplified charge is then collected and recorded on a 2D anode consisting of two sets of 3.125 mm-pitch gold-plated copper strips that provide the  $x$  and  $y$  coordinates (and thus two orthogonal views) of the event. The strips are defined by a pattern of tracks on the bottom face of the anode printed circuit board. It is possible to define two electrically insulated views of strips crossing each other orthogonally by ensuring continuity of the tracks with a set of vias and tracks extending to the top face of the anode printed circuit board.

Typical E fields between each stage of the readout are illustrated in Figure 2.1. Table 2.1 shows the inter-stage distance and the tolerances required to obtain uniformity of gain to within  $\sim 5\%$ .

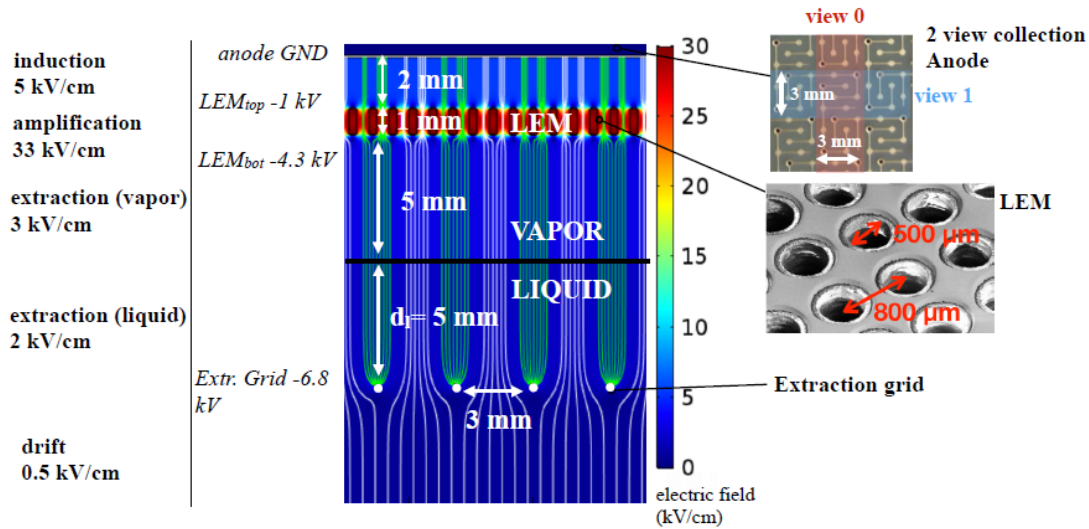


Figure 2.1: Illustration of the E fields in the amplification region of a DP LArTPC. The simulated field lines in dark blue indicate the paths followed by the drifting charges (without diffusion).

Table 2.1: Interstage distances and E field settings of the DP readout components.

| Component                 | Distance [mm] | Tolerance [mm] | E field [kV/cm]                     |
|---------------------------|---------------|----------------|-------------------------------------|
| Anode-LEM top electrode   | 2             | 0.1            | 5                                   |
| LEM top-bottom electrode  | 1             | 0.01           | 30 to 35                            |
| LEM bottom electrode-grid | 10            | 1              | 2 (in LAr) and 3 (in gaseous argon) |

The extraction grid, LEM and anode are assembled into a three-layered unit, called a LEM-anode Sandwich (LAS), with precisely defined inter-stage distances and inter-alignment. The LASs are then connected together horizontally into modular units of area  $9\text{ m}^2$ . These units are called charge-readout planes (CRPs). Figure 2.2 shows an engineering view of one CRP fully assembled.

The CRP mechanical structure provides the integration of the LASs over a large area by minimizing the dead spaces. The planarity of the active surface must be guaranteed despite possible sagging effects with respect to the three hanging points, differential thermal contraction effects on the various components and the presence of a temperature gradient in the gas phase, which could induce different thermal contractions as a function of the distance from the liquid surface. In order to ensure the planarity, the design incorporates a supporting frame in Invar, which can provide a stiff supporting structure, extending vertically into the gas phase, with little sagging and very minor contraction effects. The LEM and anodes, which would be affected by a significant thermal contraction, are integrated into a G10 planar structure with similar contraction properties. The G10 structure is mechanically decoupled on the horizontal plane with respect to the Invar structure and it is free to slide during thermal contraction.

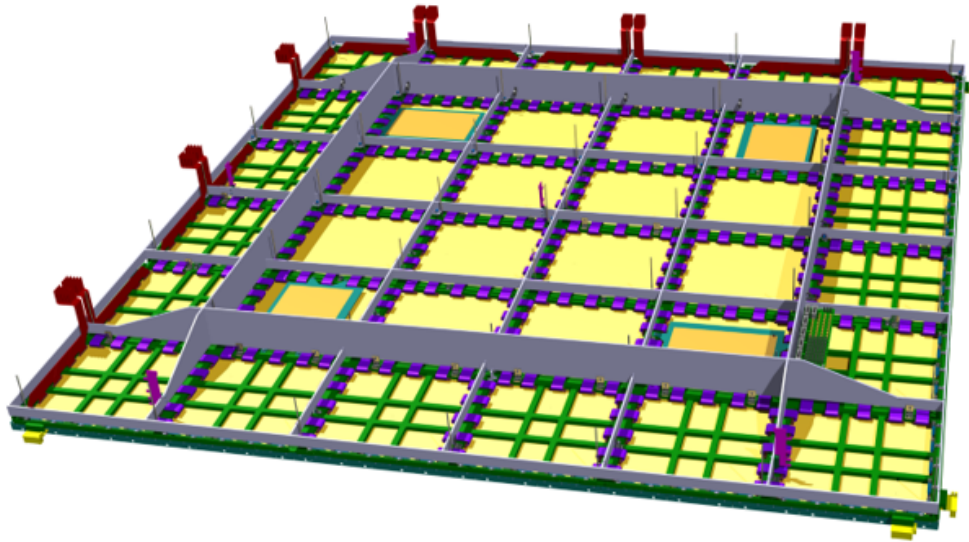


Figure 2.2: View of a complete 9 m<sup>2</sup> CRP module.

### 2.1.2 Design Considerations

Each CRP is an independent detector element that performs charge extraction, multiplication and collection, and has its own high voltage (HV) system and independent signal feedthroughs. The entire area of the LEM and anode in a CRP is active. The position and the parallelism with respect to the LAr surface can be individually adjusted for each CRP.

The LEM and corresponding anode are mounted into 50×50 cm<sup>2</sup> LASs before being assembled with an extraction grid into a CRP. Each anode in a LAS is segmented in 50 cm long  $x$  and  $y$  strips. Adjacent LAS anodes are bridged together to form readout strips of the required length by connecting short flat cables to KEL<sup>1</sup> connectors soldered onto the top sides of the anodes. The signals from the last anode in each strip chain are brought to feedthroughs mounted on the other side of the front-end electronics embedded inside dedicated signal-feedthrough chimneys using 50 cm-long flat cables.

Each CRP is independently hung from the vessel deck through its three suspension feedthroughs. It has its own HV system and independent signal and slow-control feedthroughs.

Table 2.2 summarizes the set of requirements and parameters that drive the CRPs design.

The CRP design foreseen for the DP module is based on the one developed for ProtoDUNE-DP.

<sup>1</sup>KEL 8925E-068-1795 .27mm Pitch, 2 piece, IDC for 0.635mm FC Connector, Low profile type, KEL Corporation™, <https://www.kel.jp/english/product/>.

Table 2.2: Important parameters for the CRP system design

| Parameter  | Value                |
|--|----------------------|
| Planarity tolerance on the detection plane over $3 \times 3 \text{ m}^2$ | $\pm 0.5 \text{ mm}$ |
| CRP vertical positioning precision                                       | $\pm 0.5 \text{ mm}$ |
| Range of vertical displacement   | $\pm 20 \text{ mm}$  |
| Lateral inter-CRP dead space   | $< 10 \text{ mm}$    |
| Distance between the extraction grid wires and the LEM plane             | 10mm                 |
| HV of the extraction grid wires in LAr                                   | 6.8 kV               |
| HV of the LEM down surface in gas argon                                  | 4.5 kV               |
| HV of the LEM up surface in gas argon                                    | 1 kV                 |

### 2.1.3 Scope

The scope of the CRPs includes the continued procurement of materials for, and the fabrication, testing, delivery and installation of the following systems:

- Production and quality assurance (QA) of the LEM and anodes;
- Production of the G10 and Invar frames;
- Production of the suspension feedthroughs and motorization;
- Production of the extraction grid elements;
- Production of the HV distribution system associated with the CRP for applying voltages to the LEM and anodes;
- Production of the temperature probe system associated with the CRP;
- Production of the level meter system associated with the CRP;
- Production of the strip-pulsing system associated with the CRPs;
- Production of the transportation and storage boxes for the CRPs;
- Assembly of the LASs;
- Assembly of the CRP structures, LAS grid elements, HV, slow controls and cabling for each CRP;
- Testing of the assembled CRPs;
- Installation of the produced CRPs into the storage boxes;

- Installation of the CRPs into the transportation boxes and delivery to SURF;
- Installation, cabling and test of the CRPs in the cryostat.

## 2.2 CRP Design

The complete CRP system includes, as illustrated in Figure 2.3:

- mechanical frames,
- the detection plane made of LEMs and anodes,
- the extraction grid,
- instrumentation devices: level meters, distance meters, and temperature probes,
- internal cabling: to patch panels (LEM HV, slow control instruments),
- suspension and control system.

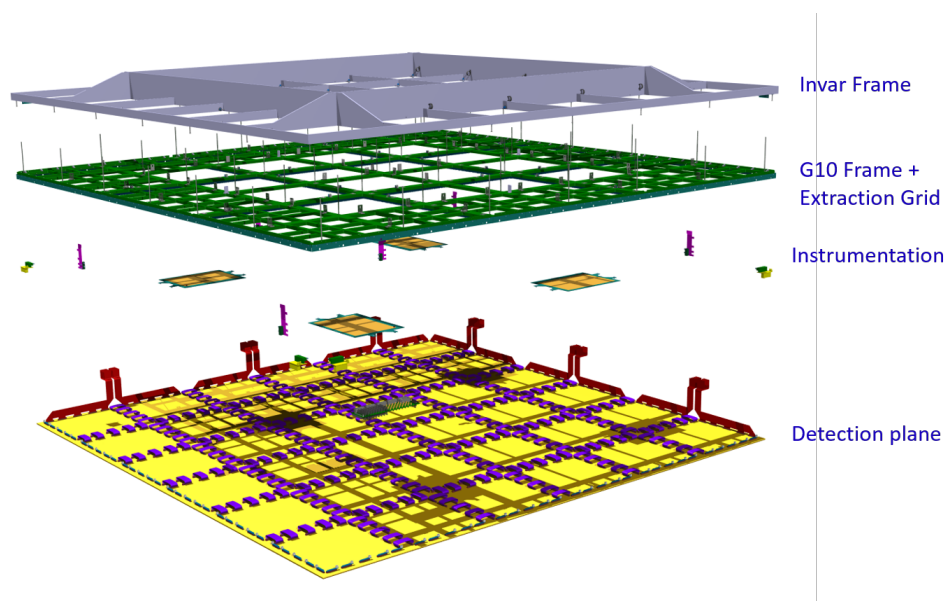


Figure 2.3: Main components of a CRP module of 9 m<sup>2</sup>

## 2.2.1 Mechanical structure

### 2.2.1.1 Invar Frame

The main mechanical supporting structure of the CRP is made of Invar nickel-iron alloy. This material is chosen for its low coefficient of thermal expansion leading to a very small deformation at cold temperatures, especially in the gas argon where the temperature gradient in the cryostat may be of the order of a few K/cm. The structure is made of a grid of soldered Invar beams 3000 mm long and 6.5 mm wide. The four main ones have a height of 150 mm while the internal ones are 40 mm high, as are the four surrounding plates. The heights have been optimized to keep the stiffness as needed and to reduce the total frame weight to about 112 kg. Figure 2.4 shows the soldering of one of the first CRP frame for ProtoDUNE-DP.

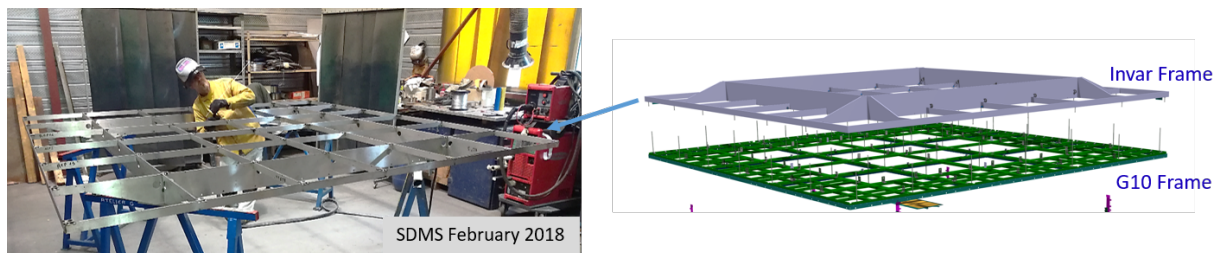


Figure 2.4: First CRP Invar frame under construction for ProtoDUNE-DP

### 2.2.1.2 G10 Frames and Modules

The  $3 \times 3 \text{ m}^2$  G10 fiberglass structure used to attach the 36 LEMs and anodes, the extraction grid and the level meters is composed of an assembly of nine  $1 \times 1 \text{ m}^2$  subframes. The choice of G10 is driven by the need to match the LEM and anode thermo-mechanical behavior and avoid over-stress due to differential thermal contraction. Figure 2.5 shows the pattern of the nine G10 parts composing a full CRP frame as well as the supporting comb positioned at every meter, and the extraction grid support plates along the side of the CRP.

Since G10 is a composite material created by stacking multiple layers of glass fibers, the orientation of the stacking has to be taken into account prior to assembly. At the construction level, the fiber directions are matched between the different subframes to ensure harmony in thermal shrinkage. Three different patterns have to be produced, one for the four angles, one for the four face centers and one for the central subframe. Two versions of each pattern for the supporting extraction grid bars and the combs follow same rule.

The subframes have been designed to guarantee adequate stiffness in the regions subject to larger tension while minimizing material in order to reduce the weight. The G10 structure is 15 mm thick and weights about 68 kg.

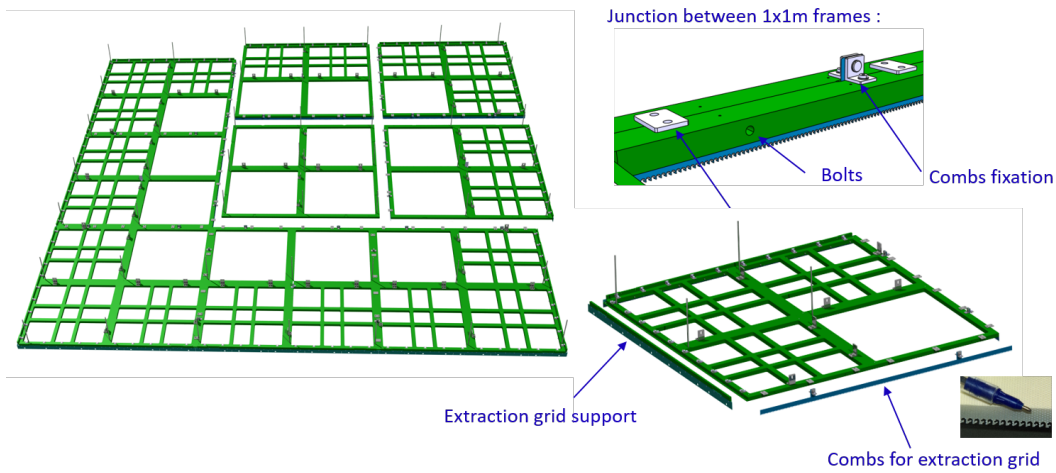


Figure 2.5: G10 elements of a full CRP module

### 2.2.1.3 Decoupling system

During cooling, Invar's dimensions remain nearly unchanged whereas the G10 frame and LEMs-anodes contract in similar ways. Thermal decoupling allows a lateral sliding of the G10 frame, without changing the level. Dedicated decoupling systems are installed at each corner of the Invar frame (50 systems by  $3 \times 3 \text{ m}^2$  module). One decoupling system that allows the G10 and LEM-anode elements to slide is shown in Figure 2.6.

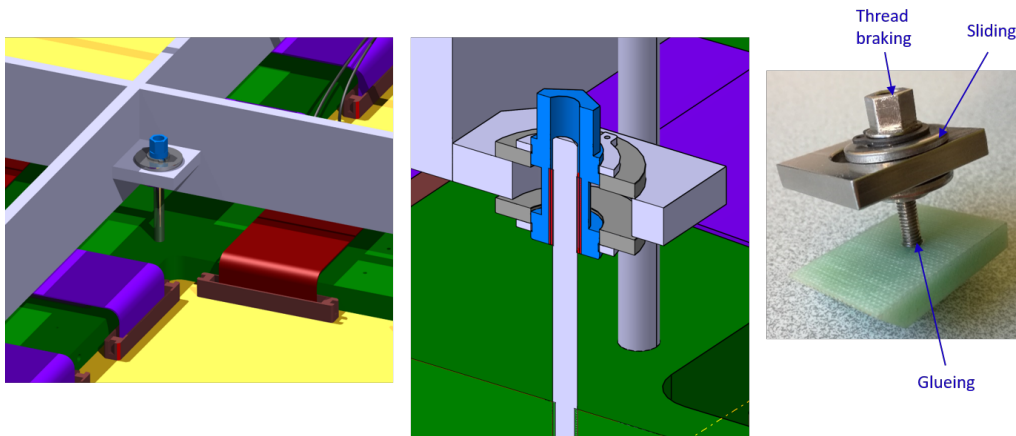


Figure 2.6: Decoupling system attached to the Invar frame, with detailed view. Example of one of the systems built for ProtoDUNE-DP.

The full weight of a CRP including the mass of LEMs and anodes is about 330 kg.

## 2.2.2 Extraction Grid

The extraction grid consists of  $100 \mu\text{m}$ -diameter stainless steel wires tensioned in both  $x$  and  $y$  directions over the entire 3 m length and width of the CRP with 3.125 mm pitch. They are



soldered into groups of 64 on independent wire-tensioning pads oriented perpendicularly to the side of the CRP frame. Each wire-tensioning pad consists of a printed circuit board (PCB) that is fixed very precisely to mechanical support beams screwed to the G10 frame of the CRP, as shown in Figure 2.7.

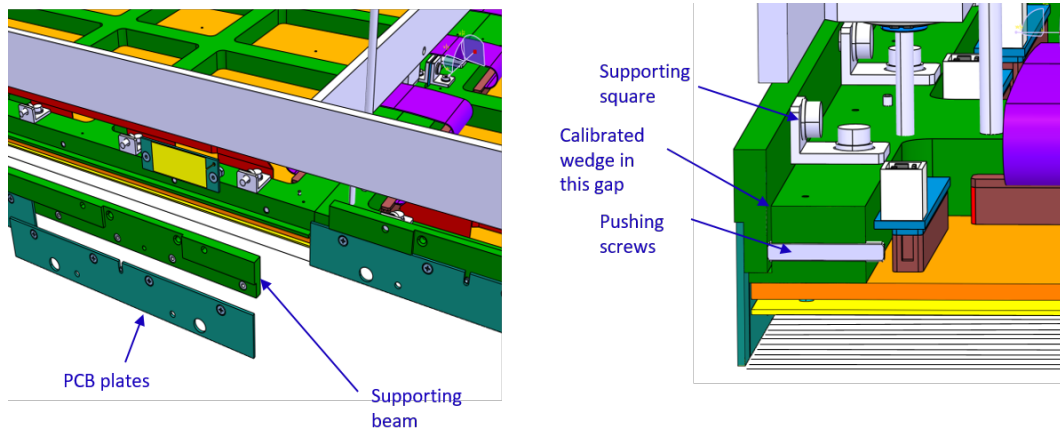


Figure 2.7: Extraction grid components on the CRP structure. On the left are the PCB plates and their supporting bars. On the right is the wire tensioning system with the pushing screws and calibrated wedges to keep the right distance.

The PCB has 64 soldering pads with  $200\ \mu\text{m}$  grooves for precise positioning of the wires. During the soldering process each wire is tensioned and positioned in a groove. The PCB is then mounted on the G10 supporting bars and the tension of the group of 64 wires can be precisely adjusted by pushing the supporting bars against the CRPs G10 frame with screws. The tensioning is performed by tightening *pushing screws*, adding a calibrated wedge, and locking the supporting square. Supporting comb-teeth blades that are inserted between the  $1\ \text{m}^2$  G10 subframes in both  $x$  and  $y$  restrict the sag to  $0.1\ \text{mm}$  in the wires, which are  $3\ \text{m}$  long in both directions. The array of blades penetrates the liquid surface and has the additional benefit of acting as a baffle against potential surface waves in the LAr.

The grid-HV connection for a CRP is made through a varnished copper track into two of the CRP's 60 PCB plates; a special isolated connection is made inside the CRP structure.

### 2.2.3 Large Electron Multiplier (LEM)

Each LEM consists of a  $1\ \text{mm}$ -thick,  $50 \times 50\ \text{cm}^2$  copper-clad standard PCB epoxy plate. Holes of  $500\ \mu\text{m}$  diameter, through which electrons undergo amplification, are mechanically drilled in a hexagonal pattern with a pitch of  $800\ \mu\text{m}$ , yielding about 180 holes per  $\text{cm}^2$ . In addition, each hole has a  $40\ \mu\text{m}$  dielectric rim, obtained by a chemical process, to prevent electrical discharges from occurring near the holes. The holes provide confinement for the UV photons produced during the avalanche process and thus act as a mechanical quencher to prevent photon feedback. This property makes the LEM suitable for operation in ultra-pure argon vapor without the addition of a quenching gas. The final gold-plated copper thickness of each LEM electrode is about  $60\ \mu\text{m}$ . Twenty peripheral and nine central  $2.2\ \text{mm}$ -diameter holes are used for assembling the LEM module

together with its anode on the G10 frame. Figure 2.8 shows a picture of a LEM module used for ProtoDUNE-DP. To prevent HV discharges near or across the edges, the LEM module has a 10 mm border free from metallization and another 5 mm copper guard ring. Similar copper guard rings are located around the 2.2 mm diameter holes and the HV connectors. The latter are made with 1.2 mm diameter male pins (Deutsch<sup>2</sup> 6860-201-22278.) that are soldered onto specifically designed pads imprinted on the LEM electrodes. The pins are insulated with circular tubes made in MACOR and a 10 mm circular clearance around each pin.

The total active area of a LEM module used for ProtoDUNE-DP represents about 86% of the  $50 \times 50 \text{ cm}^2$  area. The choice of the LEM design for ProtoDUNE-DP was made in order to achieve stable operation conditions up to 3.5 kV in DP LAr (DLAr) mode, corresponding to amplification gains larger than 30 (100) after (before) charging-up of the LEM dielectric material. For the DP module, a further optimization of the current LEM design will be performed in order to find the best compromise between the detector active area and the operation stability.



Figure 2.8: Picture of a LEM module used for ProtoDUNE-DP

## 2.2.4 Anode

The anode is a four-layer PCB having a set of orthogonal strips with a 3.125 mm pitch that provide the two views of the collected charge. The area of the anode is the same as that of the LEM,  $50 \times 50 \text{ cm}^2$ . Twenty nine holes of 2.2 mm diameter matching the LEM holes are used for

<sup>2</sup>Deutsch™ <http://www.deutsch.net/>.

the LEM and anode assembly on their G10 frame. The 2 mm distance between the anode and the LEM is ensured by 29 precisely machined spacers made of polyetheretherketone (PEEK).

The pattern of readout strips, printed on the bottom PCB layer and used for charge collection, is optimized such that the charge is evenly split between both views (Figure 2.9). Electrical insulation in the locations where orthogonal tracks would superimpose is achieved by using a system of vias between the top and bottom layers of the PCB to allow the tracks to cross over and under one another. Each strip, made of thin gold-plated copper tracks, has a capacitance per unit length to ground of about 160 pF/m. The readout strips are routed to the top layer towards 68-pin female connectors (KEL 8925E-068-179-F) soldered on the anode periphery. Each connector reads 32 strips; its 36 remaining pins are connected to the detector ground via a copper strip that runs around the periphery of the top layer of the anode (see Figure 2.16).

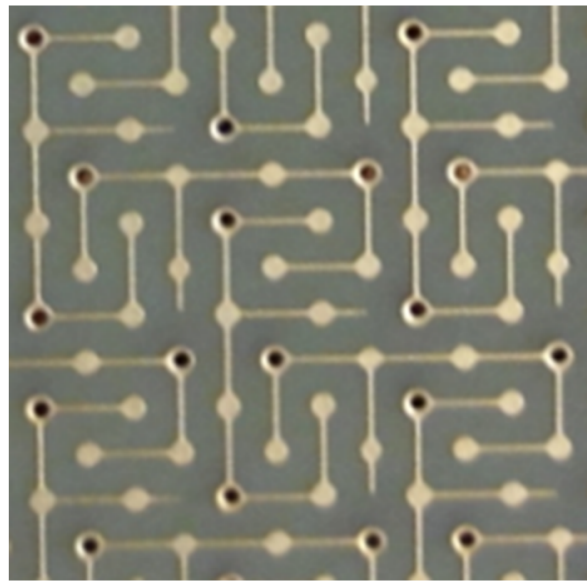


Figure 2.9: Picture of the anode symmetric 2D strip design.

## 2.2.5 Instrumentation

### 2.2.5.1 Distance meters and level meters

The vertical and lateral positions of the CRPs are measured by different means. It is possible to know the vertical position of the CRP both from the suspension system and from dedicated capacitive measurements. The suspension system and its motorization on three points provides an accurate measurement for each CRP of order 0.1 mm due to the accuracy of the steps motors and encoders. In order to exploit the information from the encoders, the anchor points on the CRP must be surveyed during construction and the absolute positions of the suspensions must be surveyed from the roof of the cryostat during the installation of the feedthrough.

There will be also the possibility to get relative measurements of the CRP position with respect to

the LAr level using capacitive level meters put on the sides of the CRPs located at the periphery of the detection plane. The measurements of the capacitance between the LEM and the extraction grid, which depends on the height of the liquid above the grid, can also provide a relative measurement of the CRP's vertical position with respect to the liquid surface. This method is used for the CRPs which are not located at the periphery, while the ones at the periphery can exploit both the LEM-grid capacitance measurements and the capacitive level meters.

The measurement of the distance between each CRP pair is performed by using capacitive devices called *distance meters* made of two parallel plates. This measurement enables positioning of the CRPs with the correct inter-CRP distance all along the detection plane. These devices do not require any contact among CRPs and give an accuracy of the order of 0.1 mm on the inter-CRP distance. Four devices per CRP side are embedded in the G10 frame side as can be seen on Figure 2.10.

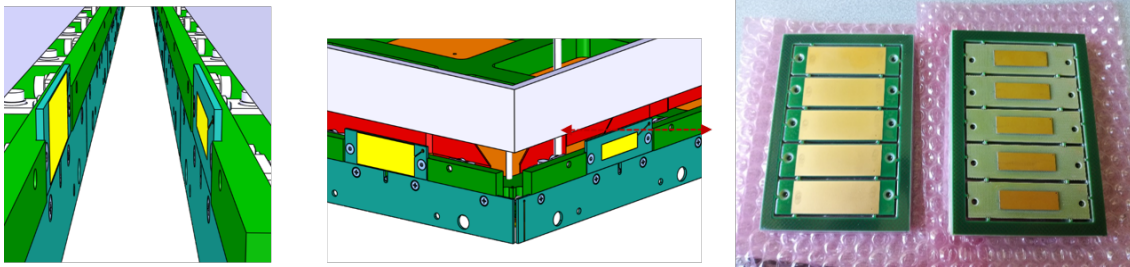


Figure 2.10: CAD views (left, center) of the distance meter plates, represented by the yellow rectangles, on the sides of a CRP. Two different plate sizes are used in pairs, installed on facing sides of neighboring CRPs, to increase the measurement accuracy of the overlapping surface which translates in the capacitance to be measured. A set of five distance meter plates of the two sizes (right) received from the production factory

### 2.2.5.2 Thermometers

The temperature in the gas above the anode plane is monitored at different heights with resistance thermometers (Pt sensors) soldered on six PCB boards distributed over the full surface of the CRP, six sensors per PCB. The configuration and the Pt positions are shown in Figure 2.11.

## 2.2.6 Suspension System and Drive

Three suspension feedthroughs are arranged in an equilateral triangle whose barycenter coincides with that of the CRP; an automated system is used to suspend the CRP at the required position and precisely adjust the CRP level with respect to the LAr surface.

Figure 2.12 shows the design of the suspension feedthrough including the bellows and the motors. There are three feedthroughs per CRP.

At the level of the flanges on the cryostat roof the adjusting table on which the suspension

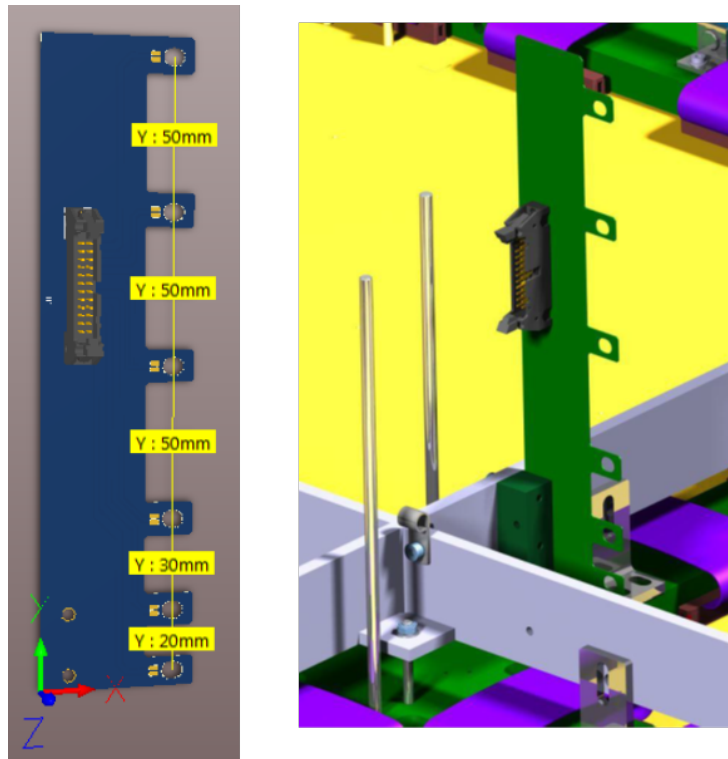


Figure 2.11: View of the thermometer board and the positions of the Pt sensors along the PCB plate.

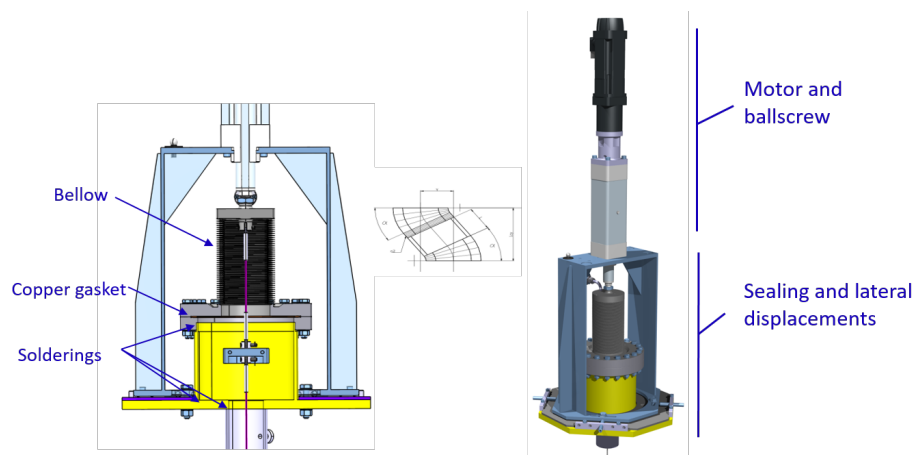


Figure 2.12: Suspension feedthrough and various assembly details.

feedthrough is screwed allows a lateral stroke of 26 mm. Any tranverse movement is absorbed by lateral deformation of the bellows. The vertical stroke available with the bellows size is  $\pm 20$  mm. The system incorporates a mechanical stop and a simple obstruction of the chimney for maintenance purpose or bellows replacement. At the top pf the suspension feedthrough there is a special slot to position a laser tracker target such that the feedthrough position can be precisely surveyed during installation.

The suspension cables anchoring system on the CRP is shown in Figure 2.13. In case of variation of the cryostat pipes' verticality, this system allows to change an anchoring point on a module, in warm conditions. In cold conditions, the transverse movement is done with the suspension feedthrough position adjustment.

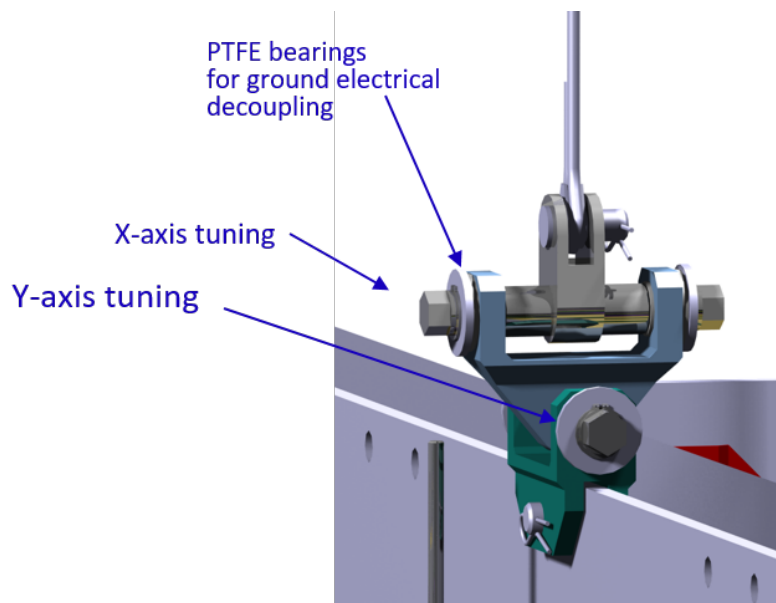


Figure 2.13: Anchoring system of the suspension cable on the CRP frame.

Each motor has independent controls for tuning the horizontality of the plane using the level information output from the sensors. In standard, stable running conditions several CRP modules are associated together as a global system and controlled via an automatic process.

## 2.3 Production and Assembly

### 2.3.1 G10 and Invar Frame Production

The G10 and Invar frames are both produced by industry. For the DP module, 80 Invar frames and 720 G10 subframes of  $1\text{ m}^2$  are required. For ProtoDUNE-DP, the process and quality control (QC) procedures have been defined. For the Invar structure, SDMS<sup>3</sup>, the company chosen for ProtoDUNE-DP's four CRPs, has produced them within the specifications without identified

<sup>3</sup>SDMS<sup>TM</sup>, [www.sdms.fr/en](http://www.sdms.fr/en).

problems. They had to organize the procurement of raw Invar plates, which depends on the available world stock. For the DP module it is important to plan ahead, for this procurement. The manufacturing process followed by the manufacturer (SDMS) included eight steps:

- plate rectification,
- laser cutting,
- assembly,
- welding,
- geometrical controls,
- washing,
- packing, and
- shipping.

During the process a special validation step was included for a full-size test frame to verify all the technical aspects and conformity to the requirements. The acceptance tests are performed on the geometry, the welding quality and the proper position of the different holes made in the Invar beams.

For ProtoDUNE-DP, fabrication of the G10 frames for the four CRPs was done by a company with expertise in composite materials. The manufacturing process includes the production of frames with fiber layers in different orientations as explained in Section 2.2.1.2, the drilling of more than 100 screw threads per square meter of G10 frames, among them 80 with a 2 mm diameter. The acceptance tests are mostly based on geometrical and dimension criteria, and quality of the threads. The G10 production is longer and more difficult than that for the Invar structure. G10 production would require a minimum of two production sites, while one company would suffice for the Invar frame production.

### 2.3.2 LEM and Anode Production

The construction of a DP module involves the production of 2880 charge readout modules made of a LEM and its anode. For such a large production, it is desirable to use more than one manufacturer in order to mitigate risks and costs. The ELTOS<sup>4</sup> company in Italy is making the LEM modules and the anodes for ProtoDUNE-DP and as such, has successfully worked out the QA and QC processes based on requirements and specifications agreed with the WA105 DP demonstrator collaboration. So far, the fraction of rejected LEM modules produced by ELTOS, after the final phase of tests, has

---

<sup>4</sup> ELTOS™ [www.eltos.com](http://www.eltos.com).

proven to be small, less than one LEM per CRP. The rejection factor for the anodes is, however, higher and corresponds to about 10 %, due to the very thin and fragile conducting strips forming the anode plane and also to the close proximity of the outer strips to the PCB edges.

Small modifications to the anode design will be necessary for the DP module in order to increase the robustness of the manufacturing process. It is believed that such modifications are possible without significantly affecting the performance of the anode.

A second manufacturer, ELVIA<sup>5</sup> in France, is also known to have the capability for large-scale LEM and anode production with the requested specifications. Recently, several LEM prototypes have indeed been built for CEA/Irfu by ELVIA and extensive tests have demonstrated the same LEM performance as the ELTOS products achieve. One key issue for a very large production, like the one necessary for DUNE, is to establish thorough QA and QC processes that can be applied throughout the whole LEM production. The definition of the LEM manufacturing requirements and specifications is naturally an important part of the tendering process. As far as the anodes are concerned, several prototypes have already been manufactured by ELVIA with satisfactory results. Despite the large size ( $50 \times 50 \text{ cm}^2$ ) of the anode, its fabrication follows a rather standard process mastered by several PCB manufacturers in Europe and around the world.

### 2.3.2.1 LEM production and QA and QC

In the following scheme, an effective production time of 40 weeks per year and a total duration of two years is assumed. This corresponds to an average LEM production rate of one CRP or 36 LEM modules per effective week. The main limitation to the manufacturing speed comes from the LEM drilling process. While it is likely that ELTOS and ELVIA will have the capability each to produce 18 LEM modules per week by assigning dedicated drilling machines, it would still be highly advisable to identify, well before the start of the LEM production phase, additional manufacturers capable of large-scale production.

Based on the experience gained with ProtoDUNE-DP, the QA and QC requirements during the LEM manufacturing process include the selection of the base material for the LEM PCB, thickness measurements of the dielectric material and copper layers before and after the process, a control of the size of the LEM holes, rims and outer dimensions, as well as a measurement of the electrical insulation across the two faces of the PCB. Table 2.3 gives, as an example, the requested tolerance values on the various parameters of the LEM detectors for ProtoDUNE-DP. In addition, pre-series productions of several LEM modules from each manufacturing site will be necessary in order to validate the complete fabrication process prior to the start of the full production.

Once manufactured, the LEM modules are shipped to one or several collaboration sites for their final characterization and validation. Several infrastructures are necessary in order to perform these tasks, e.g., a survey bench, clean rooms and storage rooms, cleaning stations and HV test setups. Here is a list of tasks to be performed, in sequential order:

- **Visual inspection and survey.** Upon receipt of the LEM modules from the manufacturing

---

<sup>5</sup>ELVIA™ <https://www.pcb-elvia.com/>.



Table 2.3: Tolerance values on various LEM parameters

| Parameter               | Value and tolerance  |
|-------------------------|--|
| Dielectric thickness    | $1.00_{-0.05}^{+0.00}$ mm                                      |
| Average total thickness | $1.20_{-0.06}^{+0.00}$ mm                                      |
| Dimensions              | $499.5_{-0.30}^{+0.00}$ mm $\times$ $499.5_{-0.30}^{+0.00}$ mm |
| Final PCB thickness     | $1.10_{-0.05}^{+0.02}$ mm                                      |
| Active hole diameter    | $0.50_{-0.01}^{+0.00}$ mm                                      |
| Rim size                | $40 \pm 4$ $\mu$ m   |
| Electrical insulation   | $>1$ G $\Omega$  |

sites, the first operations to be carried out are the visual inspection to examine the quality of the LEM surfaces, followed by the detector survey. The parameters that determine the LEM amplification gain are the thickness of the PCB and the geometry of the holes. It is therefore important to assess the uniformity of these parameters over the entire area of a LEM module. For ProtoDUNE-DP, this is performed on a sampling basis with the use of a confocal laser scanning microscope (CLSM). Several hundred measurements are done in each of 25 predefined locations, distributed uniformly over the LEM surface. With such an optical system, the total LEM and copper layer thicknesses as well as the rim size can be measured with a precision of a few microns. For the magnitude of production required for a DP module, the development of a fully automated survey system is mandatory.

- **HV connection.** The next step consists of soldering the HV connection pins on the two LEM copper surfaces as well as gluing the MACOR insulators around the connectors.
- **Cleaning and polymerization.** The cleaning operation is an important phase of the LEM preparation. Following a procedure defined by CERN/EP-DT-EF-MP and CEA/Irfu, this is done using an ultrasonic bath at 65 C with a micro-finishing solution (NGL 17.40 Sp ALU III) to clean the gold-plated copper surfaces of the LEM. It is followed by a rinsing phase with water and then with a spray of pressurized deionized water ( $< 30$  bar). The LEM is then dried in an oven at 60 C for several hours and then baked for three hours up to 160 C, a temperature near the glass transition point of the dielectric material. From the cleaning operation on, each LEM is handled via an aluminum frame on which it is mounted in order to avoid any contact with the PCB surfaces. They are also to be handled and operated in a clean environment with the use, for example, of a laminar flux.
- **HV tests.** The final validation of a LEM is obtained after successful and stable operation in pure argon at room temperature and an absolute pressure of about 3.2 to 3.3 bar. A high-pressure vessel is used for this purpose. The argon pressure value is precisely adjusted as a function of the argon temperature inside the vessel in order to reach the same gas density as the one existing in DLAr mode. In such a way, the LEM modules are tested at the same Townsend avalanche operation point as in cold. Figure 2.14 shows the 360 L high-pressure vessel used at CEA/Irfu for the characterization of the ProtoDUNE-DP LEM modules. Up to nine LEM modules can be stacked inside this chamber for the HV tests. The HP vessel is also instrumented with front-end (FE) electronics and a data acquisition (DAQ) system

for gain measurements in pure argon. In this configuration, a single LEM is installed with its 2D charge-collecting anode inside a  $50 \times 50 \times 5 \text{ cm}^3$  TPC together with a collimated  $^{241}\text{Am}$  open alpha source mounted on the cathode. Figure 2.15 shows an event display of a 5.5 MeV alpha track observed in pure argon gas at an absolute pressure of 1 bar. During the LEM validation HV tests, a two-step procedure is followed. After pumping for about 60 hours down to a residual pressure of  $10^{-4}$  mbar, the chamber is filled with dry synthetic air and HV up to 4.5 kV is applied across the LEM in order to burn possible residual dust. Then, the vessel is pumped again and pure argon (graded 5.7) is introduced at an absolute pressure of about 3.2 to 3.3 bar. Each LEM module is tested and validated so see that it can reach the value of 3.5 kV across the two faces, consistent with amplification gains higher than 100 before charging up, with no occurrence of discharges. The amount of time needed to perform the HV tests is typically one week for an entire batch of nine LEM modules. This last figure can probably be increased to 12 with a slightly larger volume vessel.

While the tasks related to the LEM visual inspection, survey and the implementation of the HV connections can be done at a single participating institution site, the subsequent operations could be dispatched among several sites. In that case, it is important that each site have the necessary infrastructure for both the cleaning phase and the HV tests, as iterations are sometimes necessary in order to fully validate the LEM modules. With the assumption of 36 LEM modules produced per effective week, a reasonable number of setups needed for the HV tests, together with their associated instrumentation and infrastructure, could amount to three or four. Finally, based on the experience gained in ProtoDUNE-DP, the processing time needed for the preparation, characterization and tests of a batch of nine to twelve LEM modules is estimated to be about three weeks.

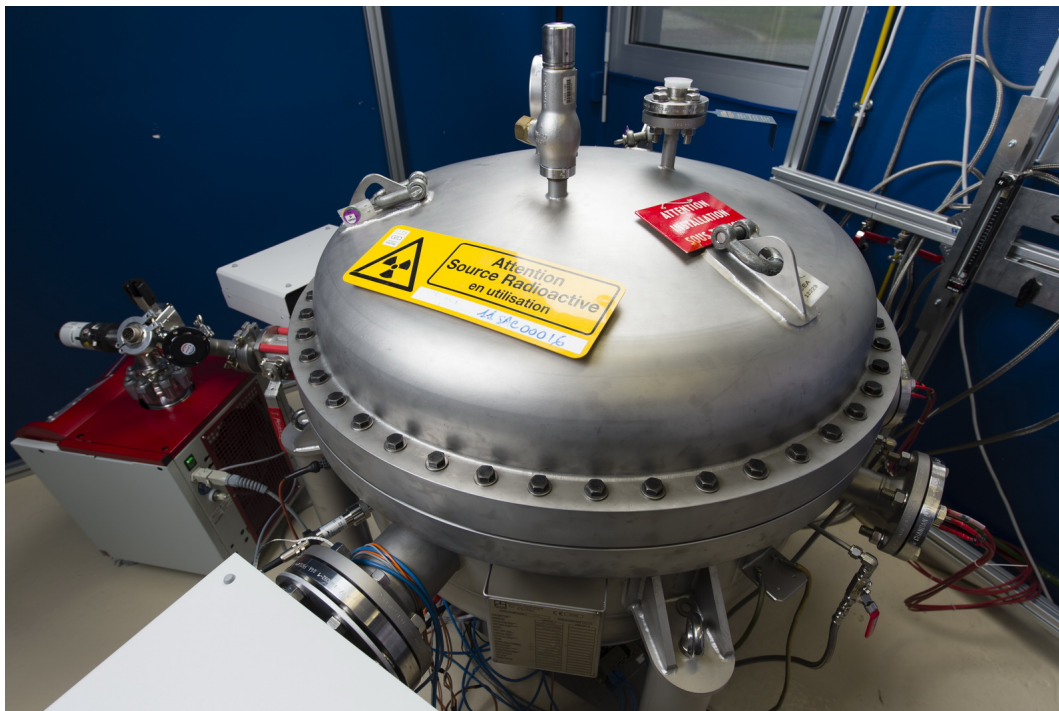


Figure 2.14: High-pressure vessel for the characterization of the ProtoDUNE-DP LEM modules.

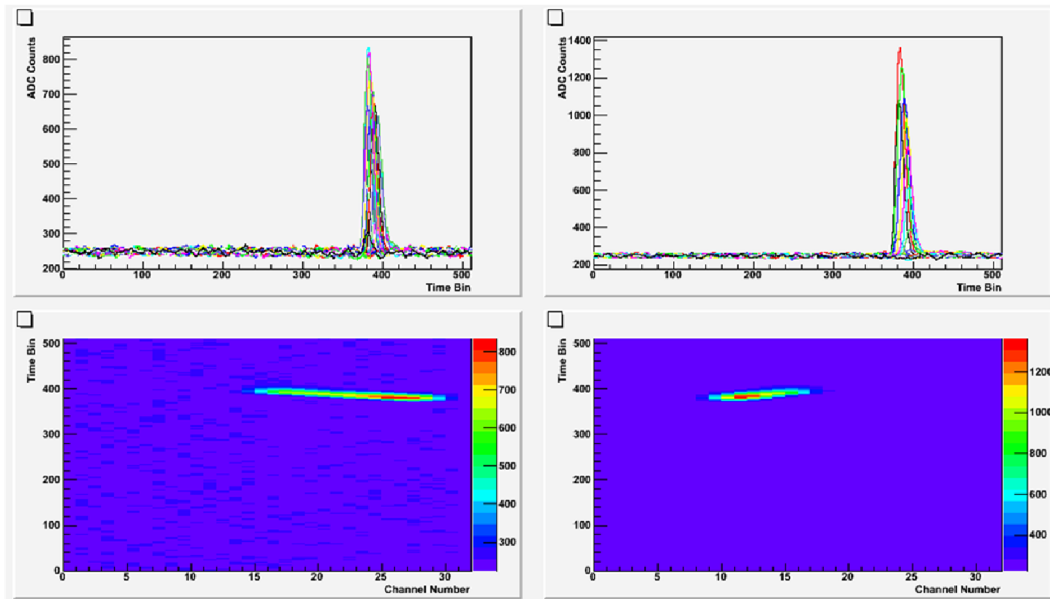


Figure 2.15: Event display of a 5.5 MeV alpha track in argon gas at 1 bar. Left:  $x$ -View. Right:  $y$ -View. Top: Pulse-height distributions of hits in ADC counts. Bottom: Hit time [300 ns bins] vs strip number.

### 2.3.2.2 Anode production and QA/QC

It is realistic to assume that the lead time in the manufacturing of the anodes will be compatible with the production time of the LEM modules. Table 2.4 gives the anode specifications for the dimensions of the PCB. In addition, visual inspection and continuity tests are requested at the manufacturing site after the soldering of the signal connectors. Upon receipt at the collaborating institution site(s) where the CRP assembly will take place, continuity and short circuit tests of the anode strips are performed (see Figure 2.16). This task is rather quick and should not take more than one day per CRP.

Table 2.4: Specifications for the anode dimensions

| Parameter     | Value and tolerance  |
|---------------|--|
| Dimensions    | $499.5^{+0.2}_{-0.0}$ mm $\times$ $499.5^{+0.2}_{-0.0}$ mm |
| PCB thickness | $3.5 \pm 0.05$ mm  |
| PCB sagitta   | $< 1$ mm   |

### 2.3.3 Tooling

Once the anodes, the LEMs, the mechanical Invar and G10 frames are produced and delivered, the CRPs production site should be equipped with several toolings. The CRPs construction activity requires a clean room large enough to accommodate the different work spaces. Separate work areas are required in this clean room for:

- a 10 m<sup>2</sup> table for assembling the G10 subframes and for surveying the whole structure;

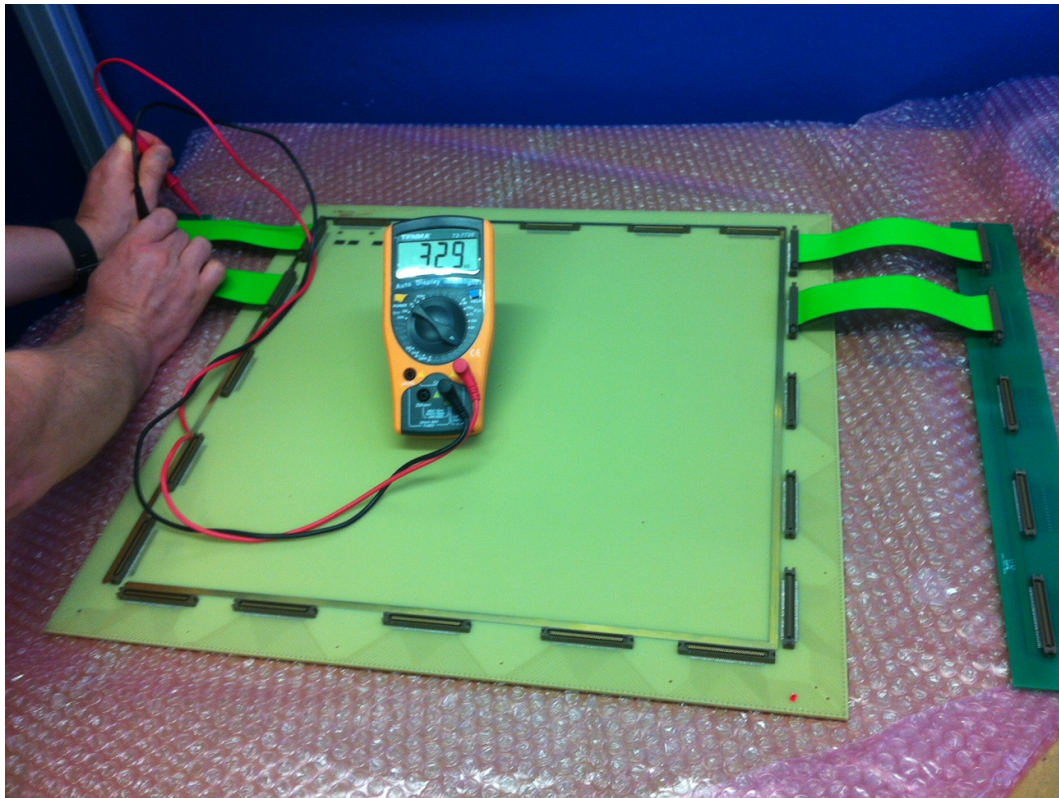


Figure 2.16: Test of anode strip continuity.

- a supporting structure to hang the Invar frame and to allow coupling of the G10 frame and the installation of the anodes, LEM and extraction grid modules;
- storage of the anodes and LEMs on special shelves;
- construction of the extraction grid modules and storage of the modules before mounting on the CRP structure.

The required tooling includes: two mobile cranes (4m span) to manipulate the Invar frame, an aluminum support frame and parts of the transport boxes, a large assembly table, storage shelves for the LEM and anodes and for cables, and a fabrication bench for the extraction grid modules. Figure 2.17 shows the 3m long wiring bench with details and the real tooling at CERN used for the CRP in ProtoDUNE-DP.

### 2.3.4 Assembly Procedures

The CRP assembly production activity will span two years prior to CRP installation underground at SURF. The CRPs will be integrated in at least two different production sites and stored locally in temporary storage boxes before being shipped to the integration and test facility (ITF). The CRP assembly will be pipelined with the LEM and anode production and testing during these two production years with an initial shift of three months. This is intended to constitute a large

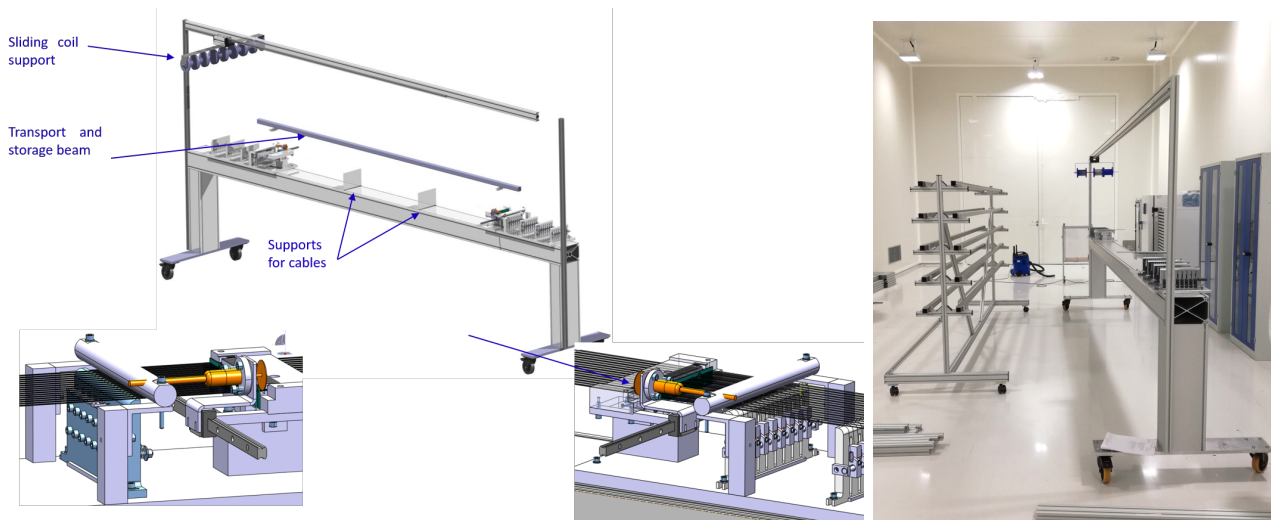


Figure 2.17: Extraction grid construction bench details and picture in the clean room 185 at CERN.

enough buffer between the LEMs and anodes to start the CRP assembly activities.

The assembly of a CRP in the clean room is a process that goes from the reception of the Invar frame to the closing of the transport box. A detailed animation of the assembly steps and procedures for the construction of a ProtoDUNE-DP CRP is available<sup>6</sup>.

This is divided in the following way:

1. Reception of the Invar frame in the clean room;
2. Suspension of the Invar frame below the supporting structure;
3. Adjustment of vertical position of the frame using lifting cranks;
4. Assembly of the G10 frame on the optical table (proceeds in parallel);
5. Positioning of the Invar frame above the G10 frame, and connection through 50 decoupling systems;
6. Assembly of LEM and anodes (done from below);
7. Connection of anodes with jumpers;
8. Weaving and soldering of the extraction grid on the special tooling (done in parallel), then storage on shelves, or direct installation on the CRP.

Some of the steps are illustrated in Figure 2.18 and real components and tooling for ProtoDUNE-DP are shown in Figure 2.19.

<sup>6</sup><https://www.youtube.com/watch?v=jcnJj1U-Cyc&feature=youtu.be>.

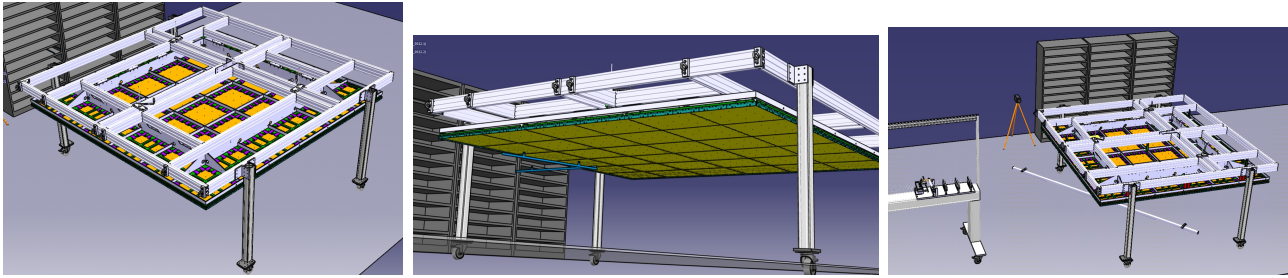


Figure 2.18: Some assembly steps: LEM and anode connection and extraction grid module installation.



Figure 2.19: Elements for assembly of ProtoDUNE-DP CRP in clean room 185 at CERN: assembly structure and G10 subframes being prepared.

Once ready, the planarity of the CRP is checked and adjusted using metrology and the decoupling systems. All the components and instrumentation of the CRP are carefully checked, and the assembly is then packed in the transport box.

## 2.4 Interfaces

The main CRP interfaces are with the elements connected directly to them. The documents that describe the interfaces are referenced.

- The readout electronics (DocDB 6751), concerning the cabling of the signal cables on the bottom part of the cold flange of the signal chimneys;
- The cryogenic instrumentation and slow controls (CISC) (DocDB 6760), concerning the power supplies for the LEM and extraction grid, the cameras, LED ribbons, temperature sensors, and distance meters; all these devices go to the CRP instrumentation feedthroughs;
- Drift HV (DocDB 6754), at the level of design requirements; this includes the system for maintaining the proper distance between the top-most field shaping profile to the extraction grid in order to maintain the proper extraction field and to protect the contact between the two systems.

## 2.4.1 TPC Electronics

The interface with the DP TPC electronics is at the level of the bottom flanges of the signal feedthrough chimneys (SFT chimneys) where the flat cables bringing the signals from the anodes are plugged in during the CRP installation in the cryostat. The system for pulsing the anode strips is installed by the CRP consortium concurrently with the CRP installations. Calibration of the strips is then performed jointly by the two consortia.

## 2.4.2 Instrumentation and HV Feedthrough Flanges

The 36 LEM modules of a CRP are supplied with HV by 42 coaxial cables connecting the feedthrough flange from the top of the cryostat to distribution boxes located on the CRP (Figure 2.20). Each cable (20 AWG, 50  $\Omega$  Kapton<sup>7</sup> insulated coaxial cable from ACCU-GLASS<sup>8</sup>) can sustain 30 kV in air and has SHV plugs on each end in order to facilitate connections during the CRP installation.

Six coaxial cables are used for the top LEM electrodes and 36 cables for the bottom ones. Each of the cables for the top LEM electrodes is connected to a single distribution box that contains a PCB for distributing HV individually to the six LEM modules through a 500 M $\Omega$  resistor in series (see Figure 2.21). The 36 coaxial cables for the bottom LEM electrodes are connected in groups of four to nine distribution boxes. For these, each HV cable is directly linked to an individual bottom LEM electrode. In total, 72 output coaxial cables rated for 10 kV (26 AWG, 50  $\Omega$  Kapton insulated coaxial cable from ACCU-GLASS) are used to supply HV to both electrodes of all LEM modules of a CRP. The grounding of each coaxial line is ensured by the feedthrough flange down to about 5 cm from the LEM final connection point via the PCB located inside each of the 15 distribution boxes. In this way, contributions from the HV lines to the electronic noise is limited as much as possible. In order to avoid electrical discharges inside the distribution boxes, the latter are filled with Arathane<sup>9</sup> epoxy glue. Finally, the connections to the HV contacts of the LEM modules are done via Deutsch 6862-201-22278 female connectors and each of them is covered by a heat-shrink sleeve.

## 2.4.3 Cryostat and Detector Support Structure

The cryostat includes the dedicated penetrations for the hanging system of each CRP. Each penetration has a diameter of 60 mm. The layout of the cryostat penetrations matches the position of the hanging points on the CRP supporting structure. The penetration flanges and CRP suspension step motors are provided by the CRP consortium.

<sup>7</sup>DuPont™ Kapton, polyimide film, E. I. du Pont de Nemours and Company, <http://www.dupont.com/>.

<sup>8</sup>ACCU-GLASS™, <http://www.accu-glass.com/>.

<sup>9</sup>Arathane™ advanced polyurethane based adhesives, Huntsman Advanced Materials, [http://www.huntsman.com/advanced\\_materials/a/Home](http://www.huntsman.com/advanced_materials/a/Home).

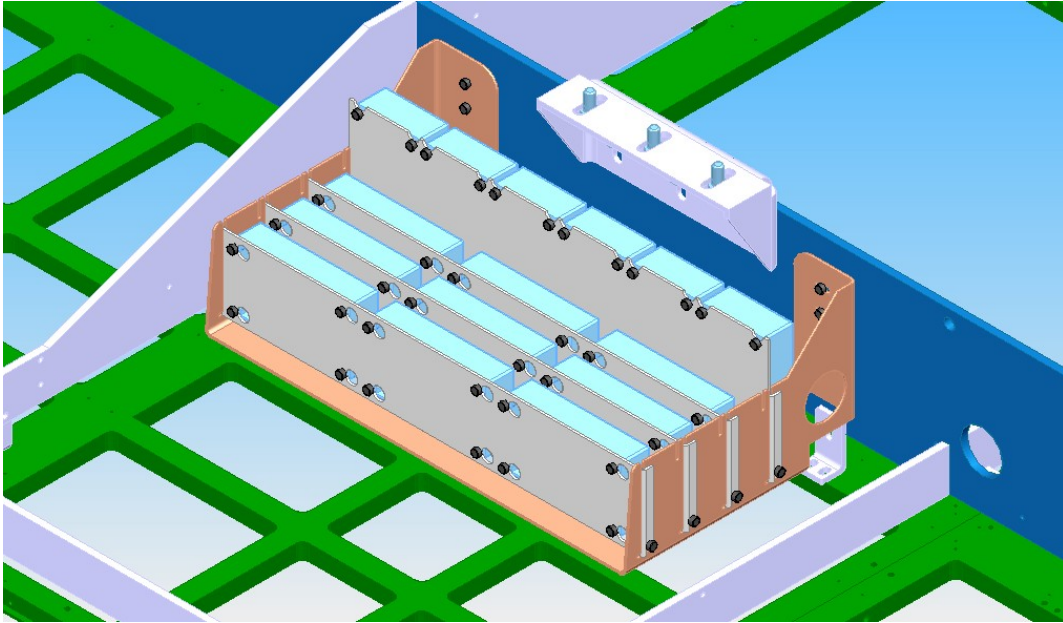


Figure 2.20: LEM HV distribution boxes mounted on a CRP.

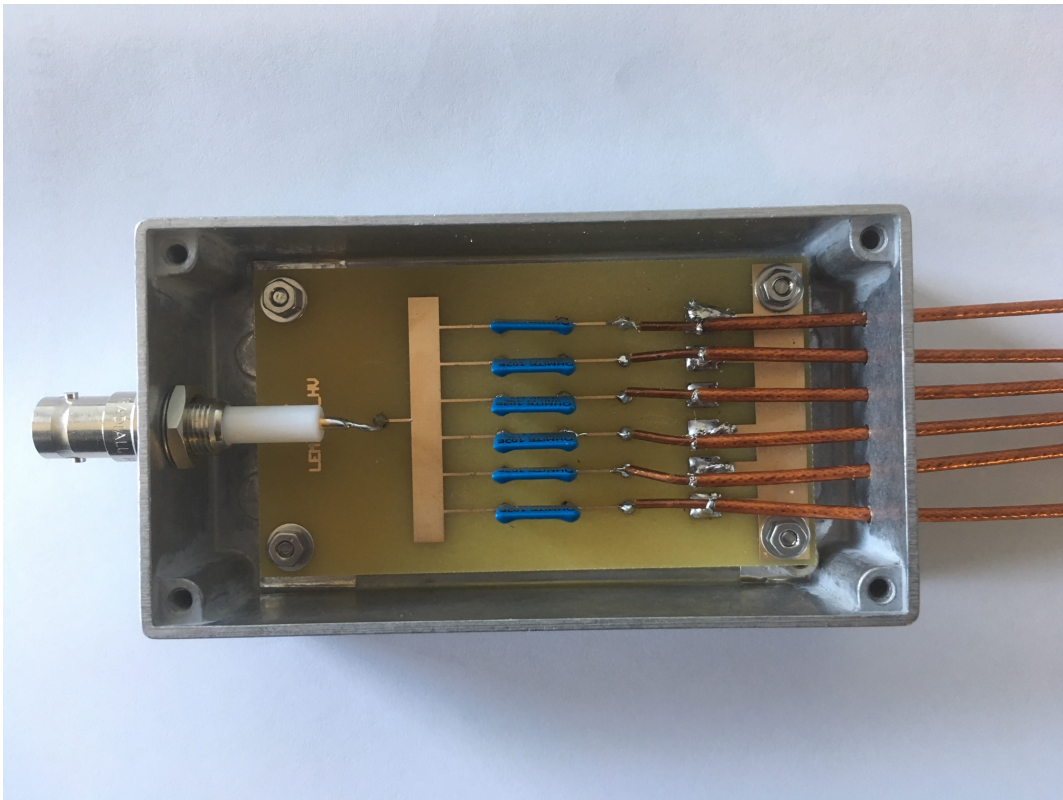


Figure 2.21: HV distribution box for LEM top electrodes before filling with ARATHANE glue.



## 2.4.4 HV and Slow Controls

The interface with the slow controls includes:

- The procurement and control of the power supplies for the HV and grid LEM biasing;
- The control of the CRP temperature probes and level meters;
- The procurement and control of the CRP pulsing system (external to the cryostat);
- The procurement of the instrumentation and HV feedthrough flanges;
- The control of the CRP suspension step motors.

## 2.5 Installation, Integration and Commissioning

The installation of the CRPs in the cryostat will be performed on a time span of nine months, following the installation of the signal chimneys, which will take three months. The signal chimneys must be present in order to connect the CRP signal flat cables. The suspension, instrumentation and HV flanges must also be installed prior to CRP installation. The installation of these flanges can be performed in parallel with the installation of the signal chimneys.

The production of the CRPs will be performed before the installation, and the CRPs will be stored in temporary storage boxes at the production centers. During installation the already produced CRPs will be moved to the transportation boxes in order to be shipped to the ITF, which is used as a delivery destination buffer, and then immediately moved underground for installation. Given the installation rate of eight CRPs/month a set of 30 transportation boxes will ensure a sufficient turnover among the production sites and the installation site.

The installation procedure plans for three two-person teams working in parallel inside the cryostat to install three CRPs at a time. It is assumed that approximately 1.3 weeks is needed for a team to prepare, survey, tune and cable a CRP in the cryostat, and 35 working weeks for the overall installation of the 80 CRPs.

Once the three CRPs are ready to be lifted, three people are needed to manipulate the manual winches on the top of the cryostat for a few hours. This activity is expected to occur during the 1.3 week period just before the cabling activity for the connection to the flanges.

The sequence of operations needed underground per CRP is similar to the one foreseen for ProtoDUNE-DP and is the following:

1. A CRP module in its transport box is brought to the entrance of the cryostat.

2. The box is hung from the side of the insertion rail, and guided through the temporary construction opening (TCO).
3. Inside the cryostat the CRP is laid down horizontally, and rolled below the SFT chimneys.
4. The structure is suspended from temporary cables coming down from the chimney.
5. The transport box is dismantled and removed.
6. The CRP planarity is measured and tuned based on metrology survey.
7. The CRP is raised up with the manual winches, then the mechanical stop is assembled.
8. The CRP is lowered down on the mechanical stop.
9. The cabling of the CRP patch panels to HV, signal and slow control feedthroughs is done.
10. The winch cable is disconnected and the winch removed.
11. The bellows is compressed using special tooling.
12. The cable from the bellows is connected with a pin.
13. The compression tool is removed and the bellows attached.
14. The motor is inserted and screwed from the top.

The assembly is then complete and operational. The lateral and vertical alignment of the CRP is performed from the top of the cryostat with a SPFT translation mechanism, distance meter measurements and metrology.

The cabling activity is done working at the nominal height position using elevating platforms. The access between two adjacent CRPs is done by staggering the altitude of the two modules by about 20 cm allowing enough space to do the electrical connection.

### 2.5.1 Transport and Handling

The transportation boxes are sized (3.5×3.5×0.8 m) for the shafts and underground handling at SURF. They are protected by a plastic layer that should be removed once the transportation box arrives at the clean area underground so that the box can be introduced into the cryostat in a clean state via the TCO. The transportation box is also essential for manipulating the CRP from the vertical orientation (i.e., for insertion in the TCO) to the horizontal orientation, required prior to hanging it from the suspension system. Once the installation is complete the transportation boxes are wrapped again with a protective layer and shipped back to the production centers.

## 2.5.2 Calibration

The CRP calibration relies on a pulsing system that performs charge injection in the strips via 1 pF capacitors. The pulse distribution system and related cabling, and the boards with the charge-injection capacitors are integrated with the CRP during CRP assembly. This system is connected via flat cables to the instrumentation flange. A pulse distribution system external to the cryostat (provided by the CISC consortium) ensures the signals feeding to the charge injection system. The information from the pulse calibration is then combined with that from the FE electronics calibration and the analysis of the reconstructed charged tracks, enabling extraction of the overall calibration constants per channel.

## 2.6 Quality Control

Several quality control procedures are applied at the level of the LEM and anode production, as described in more detail in their corresponding sections. The components of the HV distribution system are also individually tested. Continuity tests are performed at the time of the CRP assembly. The CRP geometry is also systematically surveyed as well as the tensioning of the grid wires. It will also be possible to perform cold-box testing on a small subsample of the CRPs production using the infrastructure set up at CERN for ProtoDUNE-DP.

## 2.7 Safety

Safety must be a central feature of all tasks performed by the CRP consortium. All aspects of CRP construction, installation, and commissioning will adhere to procedures established by the DUNE Technical Coordinator and relevant host institutions.

The CRP installation and operation does not present particular safety issues apart from working at heights for the connection of the CRP cabling to the SFT chimneys and the instrumentation and HV feedthroughs.

@@ -0,0 +1,770 @@

# Chapter 3

## TPC Electronics

### 3.1 TPC Electronics System Overview

#### 3.1.1 Introduction

The aim of the dual-phase (DP) TPC electronics is to collect and digitize the signals from the charge-readout planes (CRPs) (see chapter 2) and photon detection systems (PDSs) (see chapter 5), which implements photomultiplier tubes (PMTs). These two tasks are respectively accomplished by the charge readout (CRO) and light readout (LRO) sub-systems. The design of the system incorporates the components already developed for ProtoDUNE-DP as a result of an R&D activity started in 2006. One of the key objectives of this R&D program has been the design of an electronics system that is easily scalable and cost-effective in order to meet the needs of the large-scale neutrino liquid argon (LAr) detector.

While a single DP module has a factor of 20 more readout (both charge and light) channels than ProtoDUNE-DP, a simple scaling of the number of the components used in the prototype design is sufficient to meet these needs without necessitating any additional R&D. A small-scale version of the TPC electronics system was used in the WA105 DP demonstrator at CERN, a preliminary DP LArTPC prototype with an active volume of  $3 \times 1 \times 1 \text{ m}^3$  (CRP area of  $3 \times 1 \text{ m}^2$ ) that took data in the summer-fall of 2017. Operation of the WA105 DP demonstrator validated the design choices and provided checks on various performance markers, e.g., noise.

The CRO electronics system, illustrated in the Figure 3.1, is designed to provide continuous, non-zero-suppressed, and losslessly compressed digital signals by reading the charge collected on the CRPs' 3 m long strips that are arranged in two collection views, all with a pitch of 3.125 mm. The system consists of the front-end (FE) analog electronics operating at cryogenic temperatures and digital electronics working in the warm environment outside of the cryostat. The cryogenic FE analog electronics is based on an application-specific integrated circuit (ASIC) chip with a large dynamic range (up to 1200 fC) to cope with the charge amplification in the CRPs. The analog

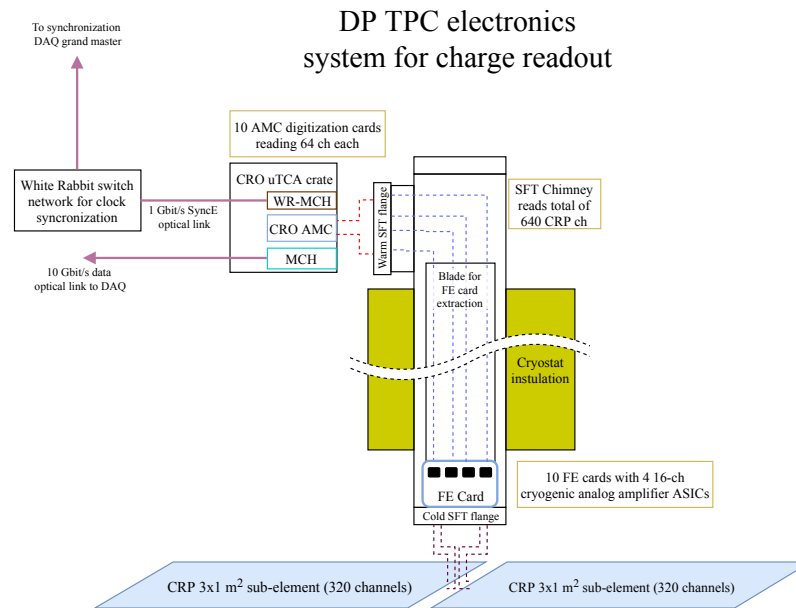


Figure 3.1: Schematic layout of the DP CRO sub-system.

FE cards are housed in dedicated signal feedthrough chimneys (SFT chimneys) and are accessible from the outside even after the DP module is in operation, thus removing any significant risks associated with their long-term survivability. The SFT chimneys are approximately 2.3 m long stainless steel pipes that traverse the entire insulation layer of the cryostat allowing placement of the FE electronics close to the CRPs to minimize cable capacitance (noise). In addition, their metallic structure shields the FE cards from any interference from the warm digital electronics and ambient environment. The analog signals are digitized by advanced mezzanine cards (AMCs), which are housed in the commercial Micro Telecommunications Computing Architecture ( $\mu$ TCA) crates on top of the cryostat near the SFT chimneys.

The CRO data are sampled at the rate of 2.5 MHz with 12 bit resolution. This frequency, traditionally used in LArTPC experiments, is well matched to the 1  $\mu$ s pulse-shaping time of the FE electronics and the detector response times determined by the electron drift velocity in the LAr. The corresponding sampling resolution along the drift coordinate is better than 1 mm.

The LRO electronics system, illustrated in the Figure 3.2, collects and digitizes the signals from the PDS, which consists of tetra-phenyl butadiene (TPB)-coated 8 in PMTs (Hamamatsu<sup>1</sup> R5912-02-mod) located beneath the TPC cathode. The LRO electronics facilitates the detection of the primary scintillation signals, which provide the absolute time reference for the interaction events. It also enables recording the light signals generated by photons from the so-called *proportional scintillation component*, the light created by the electrons extracted and amplified in the gaseous phase. A fraction of this light can reach the PMTs after traversing the entire detector volume. The LRO electronics, consisting of analog and digital stages, is housed in the  $\mu$ TCA crates on top of the cryostat structure (similar to the CRO electronics). The LRO AMC card design shares a similar architecture with the AMCs for the charge readout. The LRO  $\mu$ TCA crates are connected to specific LRO signal feedthrough flanges on top of the cryostat (see chapter 5).

<sup>1</sup>Hamamatsu™R5912-02-mod, <http://www.hamamatsu.com/>.

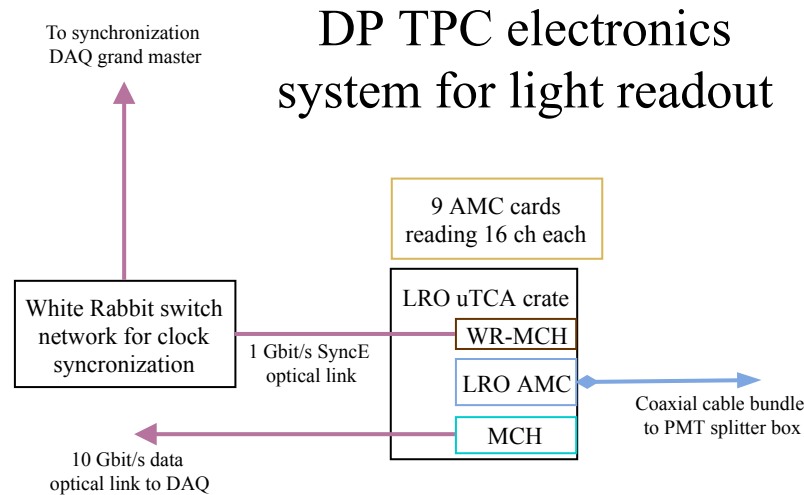


Figure 3.2: Schematic layout of the DP LRO sub-system.

Each  $\mu$ TCA crate for either charge or light readout is connected to the data acquisition (DAQ) system via an optical fiber link that supports at least 10 Gbit/s. Every crate also contains a White Rabbit  $\mu$ TCA Carrier Hub (WR-MCH) for the time synchronization of the digital electronics. This timing slave unit is connected via 1 Gbit/s optical fiber to a master node that serves as a synchronization reference for all the connected slave nodes on the network. This system for the time synchronization is based on the commercially available components developed within the framework of the White Rabbit (WR) project<sup>2</sup> with ad-hoc hardware and firmware development. The system performs automatic and continuous self-calibrations to account for any propagation delays and is able to provide sub-ns accuracy for the timing synchronization.

### 3.1.2 Design Considerations

The CRO electronics design covers the analog FE cards containing pre-amplifier ASICs operating at cryogenic temperatures and digitization cards with the relevant system for their synchronization working in the warm environment outside of the cryostat. The system reads and digitizes signals from a total of 153,600 channels (per one DP module) and is capable of continuously streaming the collected and losslessly compressed data to the DAQ without any zero suppression. The design of the CRO electronics system was developed to fit the following requirements:

- The CRO electronics must measure signals of up to 1200 fC without saturation; this has been optimized following Monte Carlo (MC) studies on the maximal occupancy per channel in shower events [2]. For a nominal CRP gain of 20, a minimum ionizing particle (MIP) signal is expected to be around 30 fC – the lowest limit that assumes a particle travelling horizontally with an azimuthal angle of 0 degrees – giving a maximal operational range of up to 40 MIPs.

<sup>2</sup><https://www.ohwr.org/projects/white-rabbit>.

- The electronic noise in the CRO analog electronics is required to be  $<2500 e^-$ . This condition can be derived from the requirement on the minimal S/N, which should be greater than 5:1 once the charge attenuation is taken into account. Given the maximum drift distance of 12 m, the largest attenuation factor due to electro-negative impurities assuming the 3 ms (minimally required) electron lifetime and the drift field of 0.5 kV/cm is 0.08. The smallest MIP signal with the CRP effective gain of 20 is therefore 2.5 fC ( $15,600 e^-$ ).
- The peaking time of the FE analog amplifiers must be 1  $\mu$ s. This requirement is driven by the need for optimal vertex resolution, determined in turn by the single track resolution and the power to separate two or more tracks that are close to one another.
- The sampling frequency must be 2.5 MHz to match the peaking time of the FE electronics.
- The power dissipated by the FE analog electronics must be below 50 mW/channel in order to minimize the heat input to the cryostat volume.
- The FE analog electronics must be replaceable without the risk of contaminating the main LAr volume in order to guarantee the long-term reliability of the system.
- The analog-to-digital converter (ADC) resolution must be such that the noise is at the level of an ADC given a dynamic range wide enough to match the response of the FE amplifier. This can be achieved with a 12 bit ADC.
- The digital electronics to be placed outside of the cryostat in the warm environment must be capable of adopting standard industrial components and solutions, to keep the costs lower and to benefit from technological evolution, e.g., higher network speeds.

As described in subsequent sections, the achieved performance of the final system is significantly better than many of the listed requirements.

The magnitude of the noise also has an effect on the quality of the lossless compression of the raw data. A compression factor of about 10 is achieved with the RMS noise level below 1 ADC. To give an idea of the compression efficiency dependency on the noise level a compression factor of four is obtained with the noise at around 1.5 ADC counts.

The primary objective of the LRO system is to detect signals, from a minimum of one photoelectron on one PMT, giving a precise timestamp that can be used in conjunction with the charge signals to determine the absolute event time ( $T_0$ ). Precise measurements of LRO signal charge allow the continual monitoring of the PMT gain at the single photoelectron level, and the determination of the number of photons in each scintillation event. In addition, an ADC continuously streams data, downsampled to 400 ns as for the CRO signals, which, amongst other items, allows measurements of the scintillation time profile. The LRO system also reads 20 channels from reference SiPM sensors from the photon detector (PD) calibration system.

The cryogenic analog electronics for the CRO is housed in the dedicated SFT chimneys. Its design enables access to the FE card for possible replacement without risk of contaminating the pure LAr in the main cryostat volume. The chimneys possess a cooling system that can control the



temperature around the FE cards to roughly 110 K to reach their optimal noise level and that compensates for the heat input from the chimneys into the cryostat volume.

The digital electronics for both charge and light readout is located in the warm environment on the top of the cryostat supporting structure and is therefore easily accessible. This fact removes any constraints associated with the accessibility and operation in cryogenic environments allowing for the usage of standard components and industrial solutions in the design. Digital electronics must be continuously and automatically synchronized to better than 400 ns to ensure the correct temporal alignment of the ADC samples from all of the readout channels. This is a minimal requirement dictated by the fact that the sampling rate is 2.5 MHz.

Key parameters for the electronics system design are summarized in Table 3.1.

Table 3.1: Parameters for the TPC electronics system design. The numbers are given for one DP module.

| Parameter                    | Value       |
|------------------------------|-------------|
| CRO channels                 | 153,600     |
| CRO continuous sampling rate | 2.5 MHz     |
| CRO ADC resolution           | 12 bit      |
| CRO data compression factor  | 10          |
| CRO data flow                | 430 Gibit/s |
| LRO channels                 | 720         |
| LRO continuous sampling rate | 2.5 MHz     |
| LRO ADC resolution           | 14 bit      |
| LRO data compression factor  | 1           |
| LRO data flow                | 24 Gibit/s  |

### 3.1.3 Scope

The scope of the TPC electronics system covers the procurement, production, testing, validation, installation, and commissioning of all the components necessary to ensure the complete readout of the charge and light signals from a given DP module. This includes:

- Cryogenic analog FE cards for charge readout;
- AMC cards for charge and light readout;
- The WR-MCH cards for AMC clock synchronization;
- $\mu$ TCA crates;
- Switches for the WR network;

- SFT chimneys;
- Low-voltage power supplies, distribution, and filtering system for the FE cards;
- Flat cables connecting the FE cards to the warm flange interface of the SFT chimneys;
- VHDCI cables connecting the warm flange interface of the SFT chimneys to AMCs.

The total numbers for components to be procured to instrument one DP module are given in Table 3.2

Table 3.2: Numbers for DP electronics components to procure for one DP module.

| Name                                  | Number |
|---------------------------------------|--------|
| CRO cryogenic ASICs (16 ch)           | 9600   |
| CRO cryogenic analog FE cards (64 ch) | 2400   |
| CRO AMCs                              | 2400   |
| SFT chimneys                          | 240    |
| Flat cables for SFT chimney (68 ch)   | 2400   |
| Flat cables for SFT chimney (80 ch)   | 2400   |
| VHDCI cables (32 ch)                  | 4800   |
| LRO AMCs with analog FE               | 45     |
| $\mu$ TCA crates                      | 245    |
| WR-MCH units                          | 245    |
| WR switches (18 ports)                | 16     |

## 3.2 TPC Electronics System Design

The CRO FE analog electronics is based on a cryogenic ASIC chip with a large dynamic range (up to 1200 fC) to accommodate the charge amplification in the CRP. The FE cards read 64 CRP channels each. They are mounted in dedicated SFT chimneys and are located within a short distance (<1 m) from each CRP to minimize the noise caused by long cables (large cable capacitance). The cards remain accessible throughout the DP module operation. Each SFT chimney accommodates 10 FE analog cards, which corresponds to the readout of 640 CRP channels per chimney. There are, therefore, 240 SFT chimneys to be installed for the charge readout in a given DP module.

The differential analog signals from the analog FE cards, carried by the twisted-pair ribbon cables and routed via an interface flange of the SFT chimneys, are digitized by the AMC cards located outside of the cryostat. These cards are installed in  $\mu$ TCA crates placed in the immediate vicinity of the SFT chimneys (one crate per chimney). In the design for ProtoDUNE-DP, each AMC digitizes 64 channels, corresponding to reading one FE analog card. Each  $\mu$ TCA contains 10 AMCs reading a total of 640 channels. However, an implementation with AMCs supporting a higher channel density is being investigated for cost-reduction purposes.

The LRO FE analog and digital electronics is based on a custom-built AMC. The card contains a CATIROC ASIC [3], which is used to determine the charge and start times of signals from each individual PMT to high precision. In addition, a 14 bit 65 MHz ADC digitizes the data for continuous streaming of the PMT signals. Each card reads up to 16 channels. A potential upgrade is to increase the channel density per card to 32 channels. The LRO cards are housed in five dedicated  $\mu$ TCA crates located close to the PMT instrumentation feedthroughs.

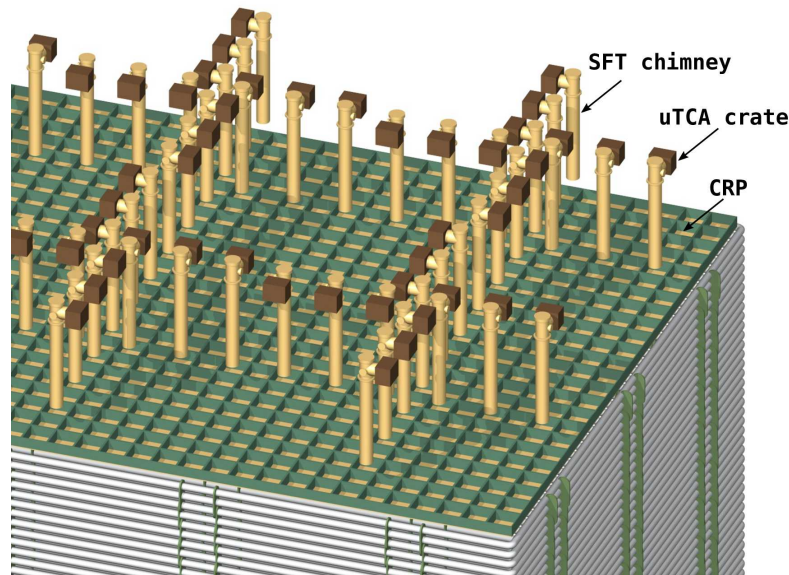


Figure 3.3: Corner view of DP module showing the pattern of the SFT chimneys and  $\mu$ TCA crates for charge readout above CRPs.

Every  $\mu$ TCA crate contains a network switch, MicroTCA Carrier Hub (MCH), via which the data are sent to the DAQ and to a (WR-MCH) for time synchronization and trigger timestamp distribution to the AMCs. Both MCH and WR-MCH require one optical fiber link each.

The MCH switch streams the data from AMCs via a dedicated optical link. Currently ProtoDUNE-DP uses MCH operating at 10 Gbit/s. However, a move to 40 Gbit/s links for the DP module implementation is under consideration because of the technology evolution with associated cost reductions and a possible increase in the channel density of each AMC.

The WR-MCH time synchronization unit is based on the WR system, which provides hardware and protocols for the network-based sub-ns synchronization between a master and different slave nodes. The connection of the WR-MCH to the WR network is done via 1 Gbit/s synchronous Ethernet optical link. WR-MCH distributes the timing information for synchronization of the AMCs via the  $\mu$ TCA backplane. In addition, this unit can be used to transmit triggers to the digitization units within the crate. This is achieved by sending it dedicated data packets containing trigger timestamp information.

Figure 3.3 shows a corner view of the DP module illustrating the pattern of the SFT chimneys and the attached  $\mu$ TCA crates above the CRPs. Each crate/SFT chimney collects signals from 3 m long strips of two  $1 \times 3 \text{ m}^2$  CRP segments. Each chimney completely penetrates the cryostat insulation layers (not shown in the figure).

Table 3.3: Summary of some of the principal parameters of the TPC electronics system for charge and light readout of a DP module.

| Name  | Number |
|---|--------|
| CRO SFT chimneys/ $\mu$ TCA crates            | 240    |
| CRO channels per SFT chimney/ $\mu$ TCA crate | 640    |
| CRO cryogenic analog FE cards per SFT chimney | 10     |
| CRO AMCs per $\mu$ TCA crate                  | 10     |
| LRO FE cards per $\mu$ TCA crate              | 9      |
| LRO channels per $\mu$ TCA crate              | 144    |
| LRO $\mu$ TCA crate                           | 5      |
| WR-MCH per $\mu$ TCA crate                    | 1      |

A short summary of some of the number of principal components and channel granularity in the design of the DP electronics is provided in Table 3.3.

### 3.2.1 Cryogenic Analog Front-end Electronics

The cryogenic amplifier ASIC is the main component of the FE analog cards. Its design is based on the CMOS 0.35  $\mu\text{m}$  technology and is an outcome of an R&D activity started in 2006, which resulted in several versions of the cryogenic amplifier for both SP and DP liquid argon time-projection chamber (LArTPC) detectors. Two principal versions of ASIC chips have been produced for DP LArTPC operation. In the first version the amplifiers have a constant gain in signal inputs of 0 to 1200 fC (0 to 40 MIP). In the second, the amplifiers have a higher linear gain for signals up to 400 fC (roughly 10 MIP signals) and a logarithmic response in the 400 to 1200 fC range. This double-slope behavior is obtained by using a MOSCAP capacitor in the feedback loop of the amplifier that changes its capacitance above a certain signal threshold. The aim of this solution is to optimize the resolution for few-MIP charge depositions while preserving the overall large dynamic range of the amplifier.

The ASIC version with the double-slope gain was selected for ProtoDUNE-DP and has been adopted for the DP TPC electronics design. The left plot in Figure 3.4 illustrates the response of this amplifier for different values of the injected charge, while that on the right shows the measured noise in units of Equivalent Noise Charge (ENC) as a function of the detector capacitance at different temperatures. For the CRP anode (detector) capacitance of 480 pF per 3 m strip, the expected noise is around 2000  $e^-$  at 110 K. Each ASIC contains 16 amplifier channels with differential line buffers and has a power consumption of 11 mW/channel, surpassing the <50 mW/channel requirement.

Each cryogenic FE card, shown in Figure 3.5, holds four ASIC amplifier chips and a few passive discrete components. The input stage of each amplifier channel has a 1 G $\Omega$  resistor to ground followed by a 2.2 nF decoupling capacitor; both are rated for high voltage (HV) operation. The

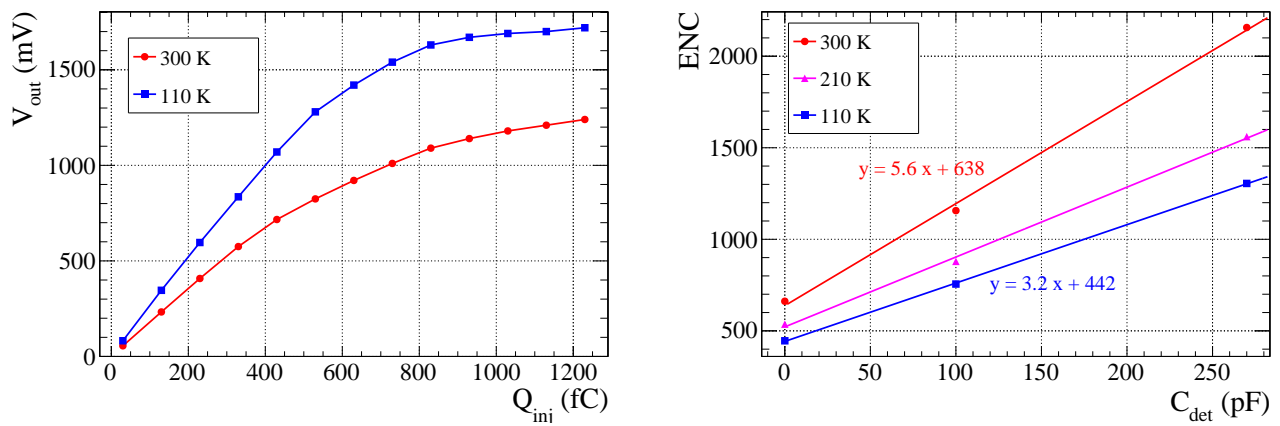


Figure 3.4: Cryogenic FE ASIC properties: amplifier response (left) and noise (right) at different temperatures measured at the output of differential buffer.

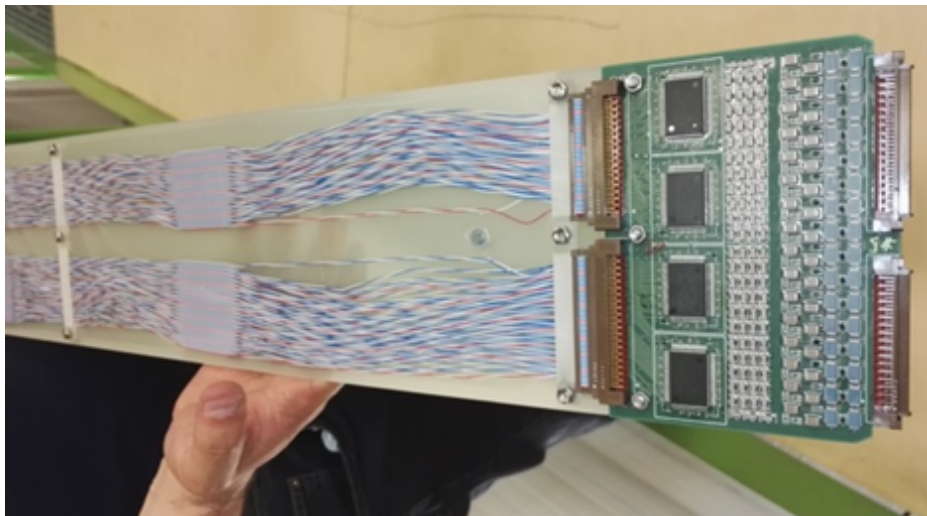


Figure 3.5: Image of an analog cryogenic FE card mounted on the extraction blade, which is a part of the SFT chimney sub-system.

resistor grounds the CRP anode strips. A TVS diode<sup>3</sup> protects each input stage against discharges coming from the DP module. This component was selected after studying the performance of different devices for the electrostatic discharge protection by subjecting them systematically to discharges of a few kV with an energy similar to that of the large electron multipliers (LEMs) in the CRP. The FE cards also house the blocking capacitors for further filtering of the low-voltage power lines. These are first filtered at the power supply and transported via shielded cables.

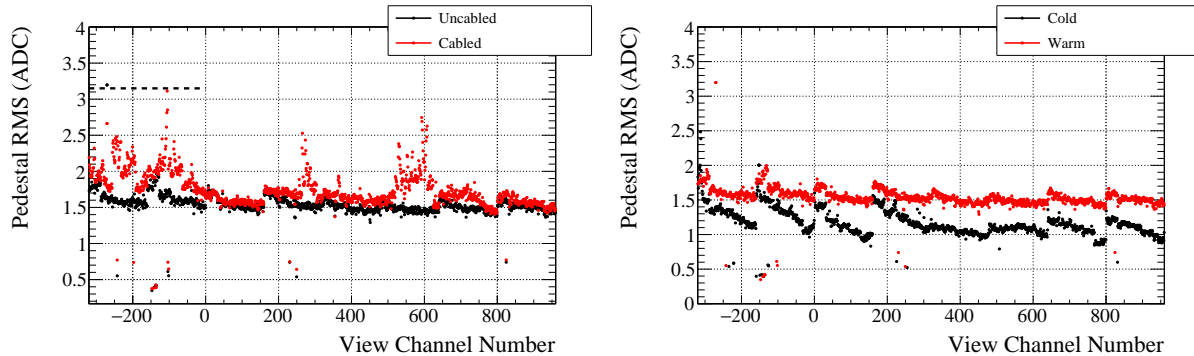


Figure 3.6: Noise of measurements in the WA105 DP demonstrator in different conditions. Left: warm with the slow control cables connected to the cryostat flanges (red points) and disconnected (black points). The horizontal dashed line in this plot indicates the noise level expected for 3 m strips. Right: warm (red points) and cold (black points) with the slow control cables disconnected. The channels with negative (positive) channel number correspond to the strips of 3 m (1 m).

Although the FE amplifier ASICs are in a shielded environment provided by the chimneys, which act as Faraday cages, interference from other equipment (via a noisy ground or ground loops) could significantly worsen the noise performance from the design target. Figure 3.6 shows results of noise measurements performed under different conditions in the WA105 DP demonstrator. The channels reading 3 m (1 m) long strips correspond to negative (positive) channel numbering in the plots and the 1 ADC count is equivalent to about 900 electrons. The left plot of Figure 3.6 shows the noise measurements performed at warm temperature with and without slow control cables (CRP HV, CRP motors, level meters, temperature probes, etc.) connected. The noise is clearly affected by the grounding of the slow controls: the average value of the noise RMS is around 1.7 ADC with slow control cables connected, and decreases to about 1.5 ADC counts when they are removed. The grounding scheme of the WA105 DP demonstrator does not correspond to the one planned for the DP module, where all electrical equipment is referred uniquely to the cryostat ground and is completely insulated from the external environment.

One interesting feature, particularly visible with the cables disconnected, is the similarity of the noise measured for the channels connected to the 1 m and 3 m long strips in the WA105 DP demonstrator. Given that the longer strips have three times the input capacitance of the shorter ones, the expected noise (see Figure 3.4) for these should be larger by about a factor of two as indicated by the dashed line in the plot. In addition, the noise on the short strips is lower than expected (1.5 ADC) for the 160 pF/m strip input capacitance (1.7 ADC). The reason for this behavior in the WA105 DP demonstrator is still under investigation. Measurements have already shown that the capacitance of the CRP anode strips is not purely to ground, but rather it is driven by the inter-strip couplings, which creates a more complicated electrical network.

<sup>3</sup>Bourns™ CDSOD323-T08LC TVS diode.

Figure 3.6 (right) also shows a comparison of the noise measurements in the WA105 DP demonstrator taken with the FE electronics at warm (red points) and cold (black points) at around 150 K. The slow control cables were disconnected in both cases. However, the cold measurements were performed with the recirculation pump active and the cathode HV connected. The RMS noise averaged over all channels decreases by about 25% from roughly 1.5 ADC to 1.1 ADC when the FE analog cards are cold. For comparison, the expected signal for a MIP with the CRP gain of 20 should be around 200 ADC counts.

The overall grounding principle of the WA105 DP demonstrator was based on using the cryostat as the ground reference. The low-voltage power supplies for the FE analog electronics and the  $\mu$ TCA crates were powered using insulating transformers to ensure that no other ground could interfere. In contrast, the design of the slow control system did not include any insulation transformers. This equipment was grounded to the building electrical network, thereby creating an interference with the ground of the cryostat. Stricter treatment of the ground connections, as implemented for ProtoDUNE-DP and planned for the DP module, and a lower SFT chimney operating temperature of around 110 K (from 150 K) should help to further reduce the noise from the levels observed in the WA105 DP demonstrator.

### 3.2.2 Signal Feedthrough Chimneys

The SFT chimneys are designed to enable access to the FE analog electronics for a potential repair or exchange while the DP module is filled and in operation. In addition, their metallic structure acts as a Faraday cage isolating the FE ASICs from environmental interference. Each SFT chimney hosts 10 analog cryogenic FE cards (reading 640 channels in total). Details of the design are illustrated in Figure 3.7.

The chimneys are closed at the bottom and top with vacuum-tight feedthrough flanges whose function is to dispatch the signal and slow control lines. The feedthrough at the bottom, the cold (signal) feedthrough, isolates (ultra-high vacuum tightness standard) the inner volume of the DP module from the chimney volume and interconnects the signals from the CRP to the analog FE cards. The feedthrough at the top, the warm (signal) feedthrough, seals the chimney from the outside environment. It also passes the low voltage and control lines to the FE electronics inside and brings out the differential analog signal lines from the FE amplifiers.

The SFT chimney volume is filled with nitrogen gas at near-atmospheric pressure. The temperature inside the chimney can be adjusted using a heat exchanger copper coil cooled with LAr. It is located at the bottom close to the cold feedthrough around the FE cards. This cooling system mitigates the heat input to the main DP module volume and provides an optimal (lowest noise) operating temperature for the FE electronics of around 110 K. A pressure release valve, indicated in Figure 3.7, protects the structure from an accidental overpressure in the inner volume.

The expected heat input from a given SFT chimney is about 20 W. This number includes the heat through the twisted-pair cables connected to the warm feedthrough, the heat in the SFT outer metallic tube, as well as the heat dissipation by the FE cards. A total heat input from all 240 SFT chimneys is at the level of 5 kW.

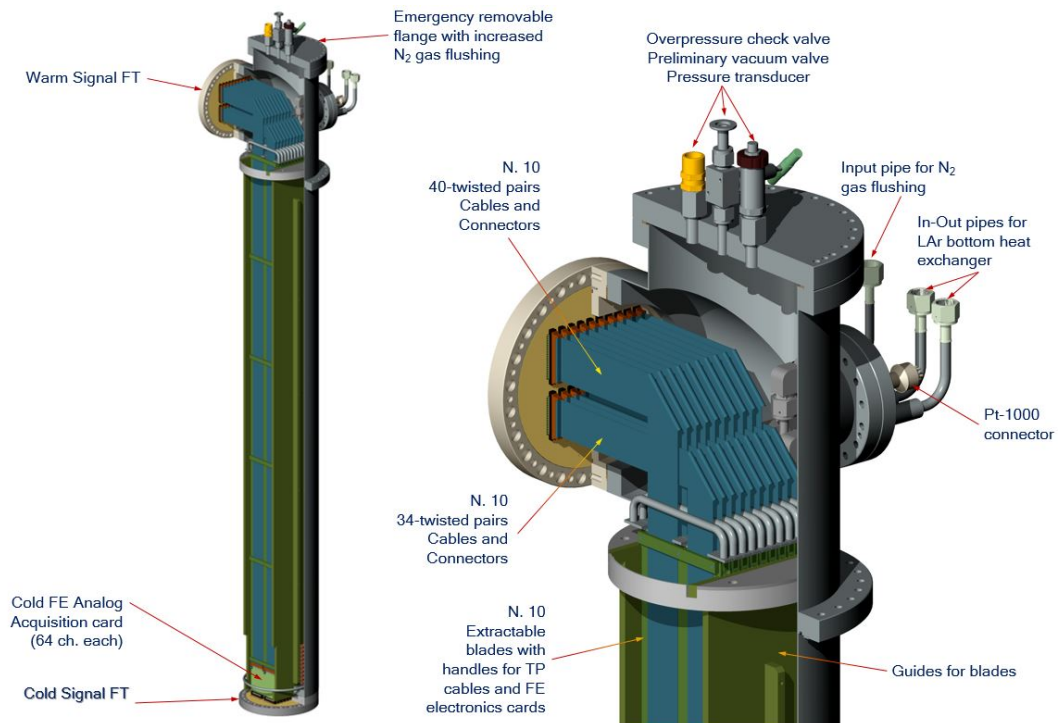


Figure 3.7: Details of the signal feedthrough (SFT) chimney design.

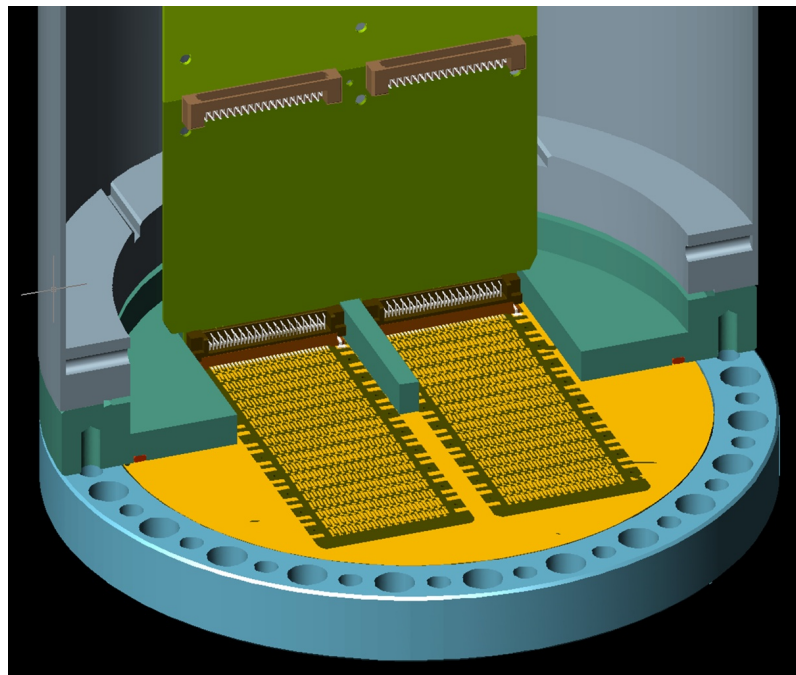


Figure 3.8: SFT chimney cold feedthrough flange with one of the FE cards mounted.



The analog FE cards are inserted directly onto the PCB of the cold feedthrough of SFT chimney (see Figure 3.8). The other side of the PCB (facing inside the cryostat) hosts the connectors for the flat cables coming from the CRP anodes. The FE cards are mounted on 2 m long blades made from FR4 that enable the insertion and extraction of the electronics, and also support the flat cables carrying signals, low voltages, and slow control to and from the warm flange interface. The blades slide along the rails installed inside the chimney at opposite sides; these rails guide the FE cards to their respective connectors on the cold feedthrough.

Prior to the commissioning of a DP module, the chimneys are evacuated via a dedicated ISO standard KF16 port (see Figure 3.7) and then filled with nitrogen gas. This ensures the removal of any moisture that would otherwise condense around the FE cards, once the DP module is filled with the LAr, damaging the electronics. To access the FE cards once the DP module is cold, the stainless steel flange at the top of the SFT chimney (Figure 3.7) must be removed. This procedure requires continuous flushing of nitrogen gas at slight over-pressure (with respect to atmospheric) in order to prevent the humid air entering. Once a chimney is opened, it is possible to extract the blades with the FE cards after unplugging the flat cables (two per card) connected on the inner side of the warm flange (Figure 3.7).

The procedure to access the FE cards under cold operation was successfully tested during the operation of the WA105 DP demonstrator detector. The top of the chimney was very close to room temperature, allowing manipulation of the cable connections on the warm feedthrough flange without cryogenic gloves. The movement of the blades on the rails and the FE card extraction and insertion did not indicate any mechanical problems due to the shrinking of various elements at lower temperatures. The signals from the FE cards that underwent this process were also checked and all channels functioned properly.

### 3.2.3 Digital Advanced Mezzanine Card Electronics for Charge Readout

The CRO AMC cards read and digitize the data from the FE amplifiers and transmit them to the DAQ system. The cards also include a last stage of analog shaping before the ADC input. The analog FEs produce differential unipolar signals defined with respect to a baseline offset. Prior to the digitization, this offset is removed and the signals are subtracted in the analog input stage of the digital electronics. Each card has eight ADC chips (Analog Devices, AD9257<sup>4</sup>, Table 3.4), two dual-port memories (Integrated Device Technology IDT70T3339<sup>5</sup>), and an field programmable gate array (FPGA) (Altera<sup>6</sup> Cyclone V) on board. The FPGA provides a virtual processor (NIOS) that handles the readout and the data transmission. The choices for all of the components have been optimized with respect to the design requirements and technical criteria such as costs, chip footprint (small enough to fit on the AMC), power consumption, and ease of use (available functionality).

Figure 3.9 shows block diagram of the AMC functionality. Each AMC generates a continuous

<sup>4</sup>Analog Devices™, <http://www.analog.com/media/en/technical-documentation/data-sheets/AD9257.pdf>.

<sup>5</sup>Integrated Device Technology™ (IDT), <https://www.idt.com/document/dst/70t33391999-data-sheet>.

<sup>6</sup>Altera™, <https://www.altera.com/products/fpga/cyclone-series/cyclone-v/overview.html>.

Table 3.4: Main characteristics of ADC AD9257.

| Item                       |  |
|----------------------------|--|
| Channels                   | 8  |
| Sampling                   | up to 40 MSPS  |
| Resolution                 | 0.122 mV   |
| Dynamic range              | 14 bit/ 2.0V   |
| Differential non-linearity | typical $\pm 0.6$ LSB<br>with min. $-1.0$ and max. $1.7$ LSB |
| Integral non-linearity     | typical $\pm 1.1$ LSB<br>with min. $-3.1$ and max. $3.1$ LSB |

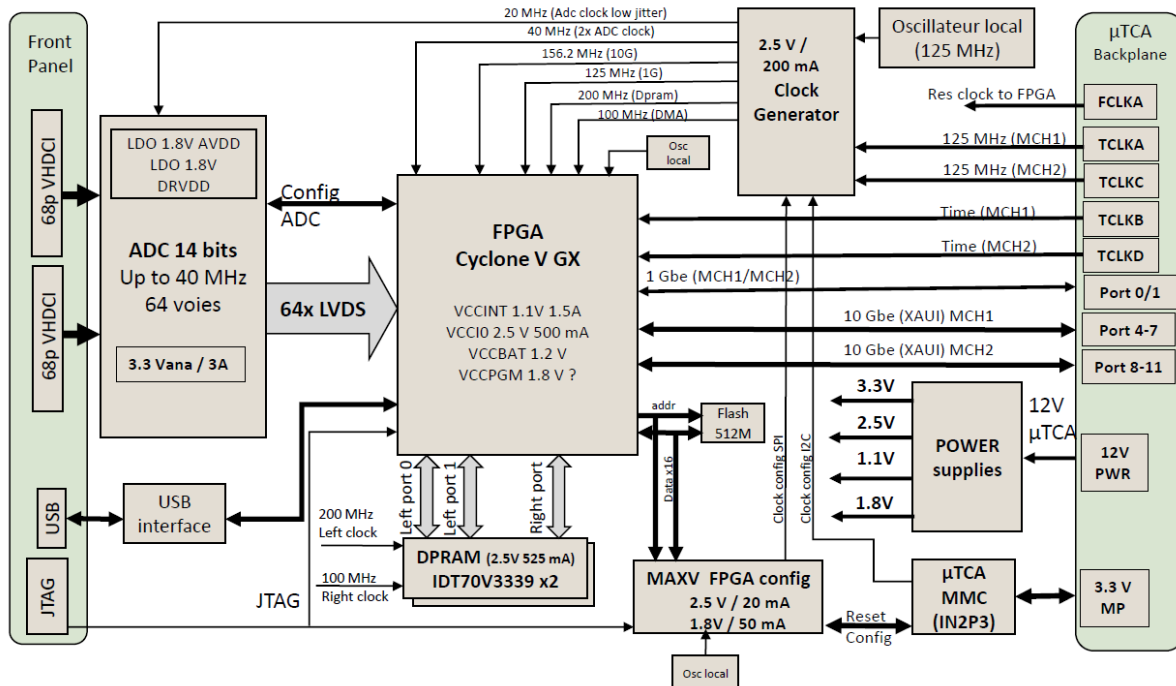


Figure 3.9: Block diagram of AMC.

compressed stream of 2.5 MSPS 12 bit data per readout channel. The on-board ADCs operate at a rate of 25 MHz per channel. The data are down-sampled in the FPGA to 2.5 MHz by performing ten-sample averaging, which leads to further digital filtering of the noise. The data, consisting of only the 12 most significant bits from each digitized 14 bit sample, are then compressed using an optimized version of the Huffman algorithm and organized in frames for transmission. The frames contain the absolute timing information of the first data sample for reliability purposes. In the current design, each AMC has 64 channels and reads one analog FE card.

The AMCs are housed in  $\mu$ TCA crates and send their data via the MCH switch. The timing synchronization of AMCs is achieved via a WR-MCH module (also housed in the crate) that is connected to the WR network. In addition, a WR-MCH could also be used for triggered readout of AMCs by sending it dedicated packets containing trigger timestamp information over the WR network.

In ProtoDUNE-DP, AMCs are operated in the triggered mode, reading a 4 ms drift time window at a trigger rate of 100 Hz, which is not far from continuous readout mode. The analog data are continuously digitized and buffered. It is possible to acquire a sub-sample of these data by providing AMC with a timestamp generated by an external trigger. The timestamp defines the start time for the data sequence to be read, while the length of the sequence is determined by the size of the drift window. In ProtoDUNE-DP this length corresponds to 10,000 400 ns samples per full drift window (4 ms). Triggers (beam counters, cosmic-ray counters, PMTs detecting the UV light, and starts of beam spills) are time stamped in a dedicated WR slave node (WR-TSN), an FMC-DIO mezzanine mounted on WR SPEC carrier card, which runs a custom firmware and is hosted in a computer. The WR-TSN is connected to the WR grandmaster for synchronization and for transmission of the trigger information. The timestamp data produced by the WR-TSN are sent over the WR network as Ethernet packets with a customized protocol.

### 3.2.4 Electronics for Light Readout

The LRO card is a 16 channel AMC containing one 16 channel 14 bit 65 MHz ADC (AD9249) and one CATIROC ASIC. A block diagram of the prototype board used for ProtoDUNE-DP is shown in Figure 3.10 and a photo in Figure 3.11 . In this prototype a mezzanine board containing the ASIC and ADC sits on a commercial mother board (Bittware S4 AMC<sup>7</sup>) with a high specification FPGA (Altera<sup>8</sup> Stratix IV). In the final implementation for the DP module, the mezzanine is integrated with the layout of the AMC board developed for the charge readout. A proposed upgrade is a 32 channel card, which would reduce the number of cards required and increase the channel density to 352 channels per  $\mu$ TCA crate.

The analog signals from each PMT channel are split equally into two separate branches (see Figure 3.10) . One path (waveform branch), through an anti-aliasing low-pass filter and the 14 bit 65 MHz ADC (AD9249), produces continuous digitization of the PMT waveform data, which are down-sampled to 2.5 MHz prior to the transmission to DAQ. The other (CATIROC branch)

<sup>7</sup>Bittware™, Inc., <https://www.bittware.com/fpga/intel/boards/s4am/>.

<sup>8</sup>Altera™, <https://www.altera.com/products/fpga/stratix-series/stratix-iv/overview.html>.

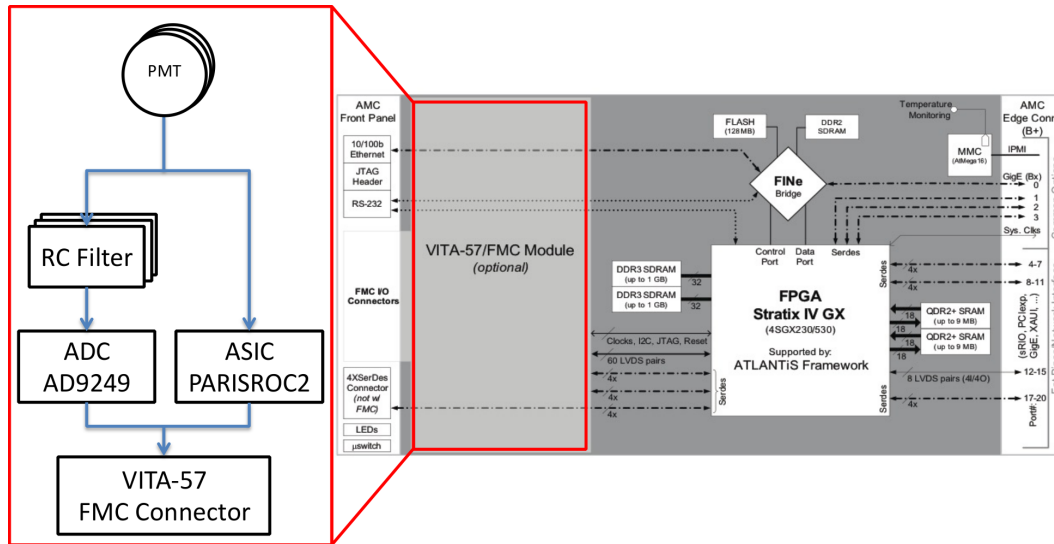


Figure 3.10: Block diagram of LRO prototype.



Figure 3.11: A photo of the LRO prototype.

is routed directly to the CATIROC ASIC for precise measurements of pulse charge and timing. Both paths produce data continuously and independently.

### 3.2.4.1 Waveform branch

The main characteristics of the ADC used for continuous digitization of the PMT signals are shown in Table 3.5.

Table 3.5: Main characteristics of ADC AD9249.

| Item                       |  |
|----------------------------|--|
| Channels                   | 16   |
| Sampling                   | 65 MSPS  |
| Resolution                 | 0.122 mV   |
| Dynamic range              | 14 bit/ 2V   |
| Differential non-linearity | typical $\pm 0.6$ LSB<br>with min. $-0.9$ and max. $1.6$ LSB |
| Integral non-linearity     | typical $\pm 0.9$ LSB<br>with min. $-3$ and max. $3$ LSB     |

For normal operation, in the continuous mode, the digitized signals are down-sampled by the FPGA to a coarse 400 ns sampling to match that of the CRO and limit the quantity of data streamed. The use of a higher specification ADC, with time-sampling of 15.4 ns, allows for greater flexibility. For particular calibration runs, waveforms with finer time sampling could be read-out, allowing studies of, e.g., the LAr scintillation time profiles. During normal operation, as well, online pulse processing is possible within the FPGA using the finer time-sampled waveforms (before the down sampling; this would enable continuous measurements of quantities such as the rise and fall times of the pulses. Even at the coarse sampling rate of 400 ns, studies of the LAr scintillation time profile are possible (given the long fall-time constant of  $\sim 1500$  ns) as is matching of the electroluminescence signal (also known as proportional scintillation light) to that of the charge signal. Low light-level signals, as from single or a few photoelectrons, will show no time structure, but will consist of one sample several LSB above the baseline.

### 3.2.4.2 CATIROC branch

The CATIROC is a 16 channel ASIC dedicated to measurement of charge and precision timing of negative-polarity PMT signals [3]. It auto-triggers on single photoelectrons and can sustain a high dark rate of up to 20 kHz/channel. Charge measurements are possible over the range of 160 fC to 70 pC (corresponding to approximately to a range of 1 to 400 photoelectrons with a PMT gain of  $1 \times 10^6$ ). Timing measurements per channel can reflect an accuracy of 200 ps.

Figure 3.12 shows the schematic of the CATIROC ASIC. Its main properties are summarized in Table 3.6. The slow channel, from which precision charge and timing measurements are made,

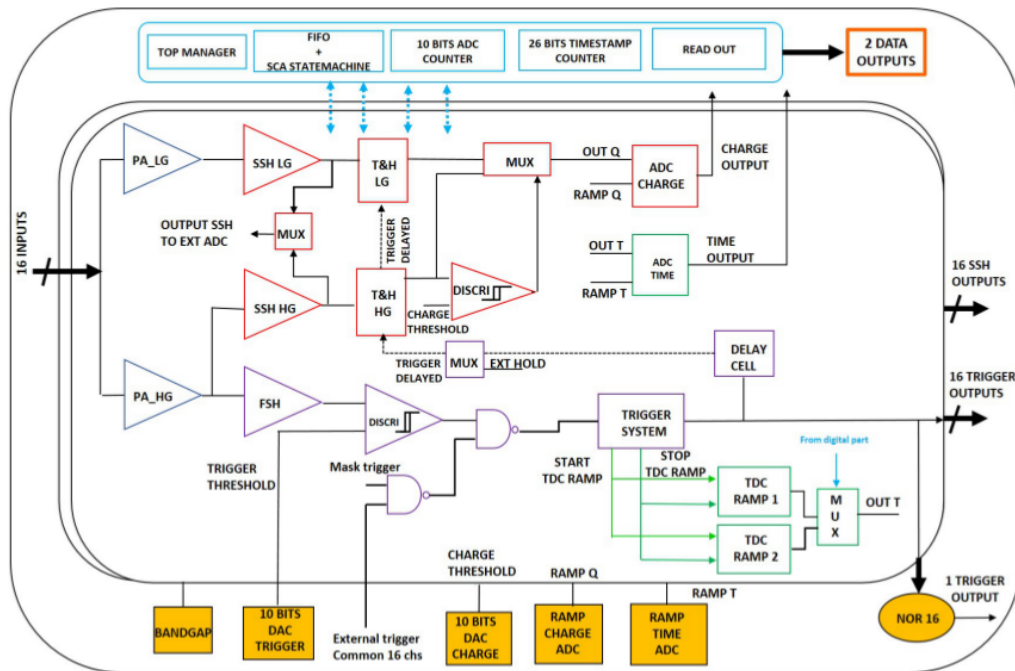


Figure 3.12: Functional diagram of CATIROC ASIC.

is formed by two variable-gain (8 bit) amplifiers followed by two variable slow shapers; one high gain for small signals, and one low gain for larger signals, and two track-and-hold stages. The slow shaper has a tunable shaping time (up to 100 ns) and a variable gain. If the high gain is saturated, corresponding to passing a predetermined threshold common to all 16 channels, the lower gain value is chosen. The chosen charge value is converted by an internal 10-bit Wilkinson ADC operating at 160 MHz. This slow channel operates in a ping-pong mode, with two capacitors to store the slow shaper signals, giving an effective buffer of 2 events. If both capacitors are full, a deadtime of 5  $\mu$ s arises.

The fast channel is used to auto-trigger the ASIC and make the fine-timing measurement. It comprises a high gain preamplifier, fast shaper (shaping time 5 ns) and discriminator with a 10 bit programmable threshold that is common to all 16 channels. The output of the discriminator is used for the two time-to-digital convertors to get the fine timing. A coarse timestamp could also be obtained from a 26 bit counter running at 40 MHz. Only the data from the triggered channels are digitized; their information is transferred to the internal memory, which is read by the external FPGA.

### 3.2.5 Network-based $\mu$ TCA Architecture

The digital electronics is based on  $\mu$ TCA standard which offers an industrial solution with a very compact and easily scalable architecture to handle a large number of channels at low cost. The standard (or related standards such as Advanced Telecommunications Computing Architecture (ATCA) or xTCA) is widely used in the telecommunication industry and is being adopted by the HEP community. The backplane of the  $\mu$ TCA crates host high-speed serial links that support

Table 3.6: Main characteristics of CATIROC.

| Item                                |  |
|-------------------------------------|--|
| Number of channels                  | 16   |
| Signal polarity                     | negative   |
| Timing                              | Timestamp: 26 bit counter at 40 MHz<br>Fine time: resolution <200 ps   |
| Charge Dynamic Range                | 160 fC to 100 pC   |
| Trigger                             | auto-trigger<br>Noise = 5 fC Minimum threshold = 25 fC ( $5\sigma$ )   |
| Digital                             | 10-bit Wilkinson ADC at 160 MHz<br>Read-out frame of 50 bits   |
| Outputs                             | 16 trigger outputs<br>NOR16<br>16 slow shaper outputs<br>Charge measurement over 10 bits<br>Time measurements over 10 bits |
| Main Internal Programmable Features | Variable preamplifier gain<br>Variable shaping and gain<br>Common trigger threshold<br>Common gain threshold               |

a variety of transmission protocols (Ethernet, PCI Express, SRIO, etc.). In addition, dedicated lanes are available for the distribution of the clock signals to all the boards hosted in the crate. The Ethernet-based solution has been adopted for both the data and clock distribution in this design of the DP electronics system for both charge and light readout.

Each AMC for either charge or light readout plugged into the  $\mu$ TCA is connected to the crate MCH board through the backplane serial links. The MCH provides the switch functionality that enables AMCs to communicate with each other or external systems through the MCH uplink interface. In the DP electronics system design, MCH also manages the WR clock distribution.

Table 3.7: Bandwidth requirements per  $\mu$ TCA crate for continuous data streaming. A compression factor of 10 for the charger readout data is assumed

| Parameter                | Value      |
|--------------------------|------------|
| CRO data rate            | 1.8 Gbit/s |
| LRO data rate            | 4.7 Gbit/s |
| Current MCH bandwidth    | 10 Gbit/s  |
| Upgradable MCH bandwidth | 40 Gbit/s  |

In the current design, as used for ProtoDUNE-DP, the MCH operates with a 10 Gbit/s uplink. Given that a  $\mu$ TCA crate hosts 10 AMCs for charge readout, the required bandwidth to stream the data to DAQ is about 1.8 Gbit/s. This assumes that the data exiting the AMCs are losslessly compressed with the compression factor 10. The bandwidth required per crate link for streaming the LRO data is 4.7 Gbit/s. The 10 Gbit/s MCH is therefore sufficient to support these data

rates. However, the technology is moving towards supporting the 40 Gbit/s rates. In addition, the channel density per AMC could also be increased for cost optimization. For these reasons an upgrade to a 40 Gbit/s MCH could be foreseen in the future. This would also imply that the optical links connecting the DAQ system to  $\mu$ TCA MCH should be operable at 40 Gbit/s. A summary of the required and supported bandwidths per  $\mu$ TCA crate for continuous data streaming is provided in Table 3.7.

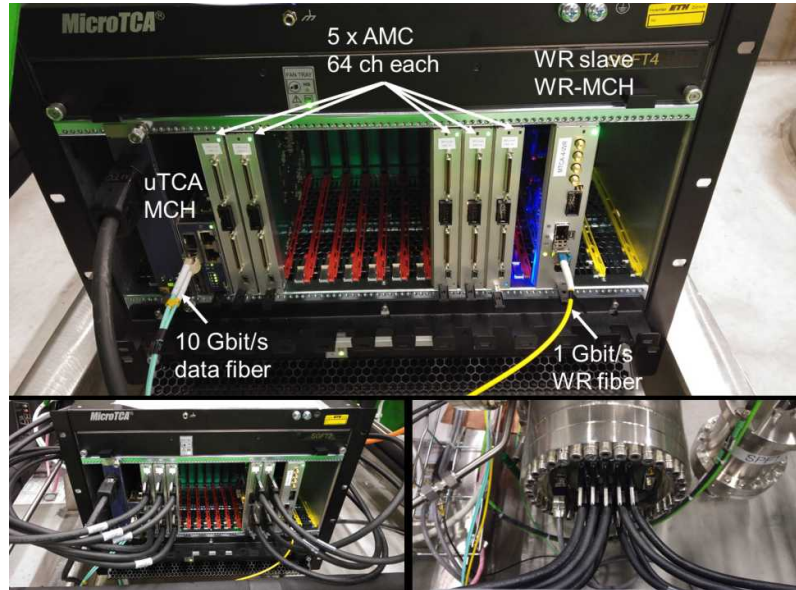


Figure 3.13: Pictures of an instrumented  $\mu$ TCA crate from the WA105 DP demonstrator. The crate contains five AMC cards, correspondingly to the number of readout channels per the SFT chimney. The images below show the crate after the cables are connected to the warm flange of the SFT chimney.

As an illustration, Figure 3.13 shows pictures of one of the instrumented  $\mu$ TCA crates used for the charge readout of the WA105 DP demonstrator at CERN. In this detector each SFT chimney reads 320 channels, thus requiring only five AMCs per the  $\mu$ TCA crate. The two optical fiber links, one (10 Gbit/s) for data and the other (1 Gbit/s) for clock and trigger timing distribution, are visible in the images.

### 3.2.6 Timing Distribution

The time synchronization system selected for the DP module utilizes a WR network, which combines the synchronous 1 Gbit/s Ethernet (SyncE) technology with the exchange of PTPV2 packets, to synchronize clocks of distant nodes to a common time. A high stability GPS disciplined oscillator (GPSDO) with accuracy similar to that of an atomic clock provides a clock reference signal to be distributed over the physical layer interface of the WR Ethernet network. The network topology is built using specially designed switches that have the standard IEEE802.1x Ethernet bridge functionality with an addition of WR-specific extensions to preserve the clock accuracy. Time and frequency information are distributed to the nodes on the WR network via optical fibers. The WR protocol automatically performs dynamic self-calibrations to account for any propagation delays and keeps all connected nodes continuously synchronized to sub-ns precision.



The sub-ns precision on the clock synchronization is not strictly needed for aligning samples in the different AMC digitization units, since the timing granularity on the data is 400 ns. However, the WR timing system offers readily available industrial components and the necessary protocols for synchronization with automatic calibration of delay propagation. R&D on this timing distribution solution started in 2006; the final design for integrating this system, planned for the WA105 DP demonstrator, ProtoDUNE-DP, and the DP module readout, was completed in 2016.

In the implementation specific to ProtoDUNE-DP, a GPS-disciplined clock unit (Meinberg LAN-TIME M600<sup>9</sup>) feeds 10 MHz and 1 PPS reference signals to a commercial WR switch (Seven Solutions WRS v3.4<sup>10</sup>). The switch acts as grandmaster of the WR network. It is connected via 1 Gbit/s optical links to the dedicated WR timestamping node (WR-TSN) and the WR end-node slave cards present within each  $\mu$ TCA crate (WR-MCH) keeping these synchronized to its reference time. The WR grandmaster also communicates through a standard Ethernet port with the LANTIME unit for its date and time synchronization via NTP. The WR-TSN module receives analog TTL-level trigger signals, generates their timestamps, and transmits them over the WR network to the connected WR-MCH units. This timestamp information is then used by AMCs to find the data frame corresponding to the trigger.



Figure 3.14: Picture of the WR slave node card (WR-MCH) present in each  $\mu$ TCA crate for time synchronization. The WR-LEN mezzanine card is visible in the bottom right corner.

The WR-MCH card (Figure 3.14) enables clock/timing/trigger distribution to AMCs. It communicates with them via dedicated lines in the backplane of the  $\mu$ TCA crate using a customized data-frame protocol. The module contains a commercial WR slave node card, the WR Lite Embedded Node (Seven Solutions OEM WR-LEN<sup>11</sup>), as mezzanine card. WR-LEN runs on a customized firmware which also enables it to decode the trigger timestamp data packet received over the WR network.

The architecture of the WR network layout for one DP module is illustrated Figure 3.15. It is built in a hierarchical structure from 16 WR switches with 18 ports each, chained with 1 Gbit/s optical fibers. The switch at the top of the hierarchy interconnects the synchronization WR grandmaster from the DAQ system with the 15 switches in the middle layer. These are in turn connected to the WR-MCH slave nodes in each  $\mu$ TCA crate (245 in total for charge and light readout).

<sup>9</sup>Meinberg™, <https://www.meinbergglobal.com/english/products/advanced-1u-ntp-server.htm>.

<sup>10</sup>Seven Solutions™, <http://sevensols.com/index.php/products/white-rabbit-switch/>.

<sup>11</sup>Seven Solutions™, <http://sevensols.com/index.php/products/oem-wr-len/>.



Figure 3.15: Architecture of WR network for time synchronization of digital readout electronics.

## 3.3 Production and Quality Assurance

### 3.3.1 Cryogenic Analog FE Electronics

The production of the cryogenic ASICs and analog FE cards is envisioned to be split between several sites located in France and Japan at the moment. The delivered cards are then split between five institutions in France (IPNL), Japan (KEK, NITKC, IU), and USA (SMU), where they are tested for various performance parameters such as noise levels, dead channels, hot channels, gain and its uniformity across channels, etc., at both room and operating cold temperature. An appropriate and common database will be developed and populated with test results.

### 3.3.2 Signal Feedthrough Chimneys

A number of items require manufacture in order to produce the SFT chimneys. These include

- the PCB flanges for the warm and cold feedthrough flange interfaces,
- the stainless steel pipe structure,

- the flanges containing the interfaces to the gas and liquid lines and slow control,
- the blades and railing, and
- the heat exchanger system.

The flat cables that connect the FE cards to the warm flange are commercially available products and are part of the SFT chimney procurement process.

The manufactured components are delivered to designated institutions participating in the DP electronics consortium where teams verify the signal continuity for both cold and warm flanges, then assemble them into SFT chimneys and test for leaks. They also check the blade insertion, test the flat cables, then, once verified, pack the assembled SFT chimneys and ship them to SURF.

### 3.3.3 The Timing System and $\mu$ TCA

The timing system components, the 16 WR switches and the 245  $\mu$ TCA crates containing the power modules, carrier hubs (MCH), and fan units, are commercially available. The manufacturer takes the responsibility for the necessary quality control and quality assurance of these components, requiring no further testing on the part of the DP electronics consortium. Once the components are delivered to the designated institutions, they can be sent to SURF for the installation.

The commercial VHDCI signal cables (connecting the AMCs to the SFT chimneys) are procured and tested with the SFT chimney warm flanges.

### 3.3.4 Charge Readout Electronics

The production of the AMC cards for the charge readout as well as the WR-MCH slave cards for synchronization is currently shared between four institutions (IPNL, KEK, NITKC, IU). The cards ordered and delivered to each respective institution are subjected to quality assurance tests agreed upon by all participants.

### 3.3.5 Light Readout Electronics

The production of the LRO AMC cards is occurs in the same manner as the cards for ProtoDUNE-DP since the number of cards to be produced and the channels to test are both small. The cards' electronic components, meeting required specifications, are purchased commercially. The project will be managed by a qualified engineer, working with a specialist in quality assurance (QA).

The produced cards are delivered to designated consortium institutions. Upon delivery, teams conduct basic quality tests, including visual inspection and electrical testing, to ensure conformity

of production. Another series of tests is performed on the cards to ensure their correct functionality and to evaluate their performance. Measurements include: linearity measurements (DNL and INL) of each ADC channel, and linearity of response of the ASIC. The level of cross-talk on the ASIC is also quantified.

A dedicated single-channel setup, with PMT (Hamamatsu R5912-02-mod), and identical cabling and splitter as in the far detector (FD), can be used to characterize the expected noise level of each channel, and response to single photoelectrons up to saturation. Multiple cards are operated in a  $\mu$ TCA crate with the DAQ.

After shipment to SURF and installation on-site, a small series of tests is performed with a pulse generator to verify the good working condition of the cards. Noise-level measurements are included in the integration effort.

## 3.4 Interfaces

The DP electronics system interfaces to several other systems, starting with the CRP and the PD systems. The digitized data must in turn flow to the DAQ via the optical links in each  $\mu$ TCA crate. The SFT chimneys integrate into the cryostat structure and connect to the cryogenics and gas systems. The slow-control system takes on management of the low-voltage power supplies for the FE analog electronics and  $\mu$ TCA crates, and monitors various sensors in the SFT chimneys. Table 3.8 provides the references to the relevant interface documents for each interface, stored in the DUNE document database (DocDB).

Table 3.8: Interface documents relevant to DP electronics system.

| Interface document                            | DUNE DocDB No. |
|---|----------------|
| DP TPC electronics to DP CRP                  | 6751           |
| DP TPC electronics to DP PD                   | 6772           |
| DP TPC electronics to Joint DAQ               | 6778           |
| DP TPC electronics to Joint CISC              | 6784           |
| Facility Interfaces to DP TPC electronics     | 6982           |
| Installation interfaces to DP TPC electronics | 7009           |
| Integration facility to DP TPC electronics    | 7036           |
| Calibration to DP TPC electronics             | 7063           |
| DUNE physics to DP TPC electronics            | 7090           |
| Software and computing to DP TPC electronics  | 7117           |

### 3.4.1 Electronics System to CRP and Photon Detection Systems

The cold feedthrough flange of the SFT chimneys forms the interface between the CRP and the CRO electronics system. On the side facing the cryostat the flange PCB has 20 68 pin connectors

(KEL 8930E-068-178MS-F<sup>12</sup>) for plugging the flat cables from the CRP. These are 68 channel twisted-pair flat cables, each carrying signals from 32 anode strips and are within the scope of the CRP system. Each analog FE card reads 64 anode strips, i.e., signals from two KEL connectors. The order in which the cables are connected to the cold flange determines the mapping of the electronic channels to the physical location of the strips on the CRP and is coordinated carefully with the CRP consortium. Figure 3.16 shows two images of the cold feedthrough from the WA105 DP demonstrator.

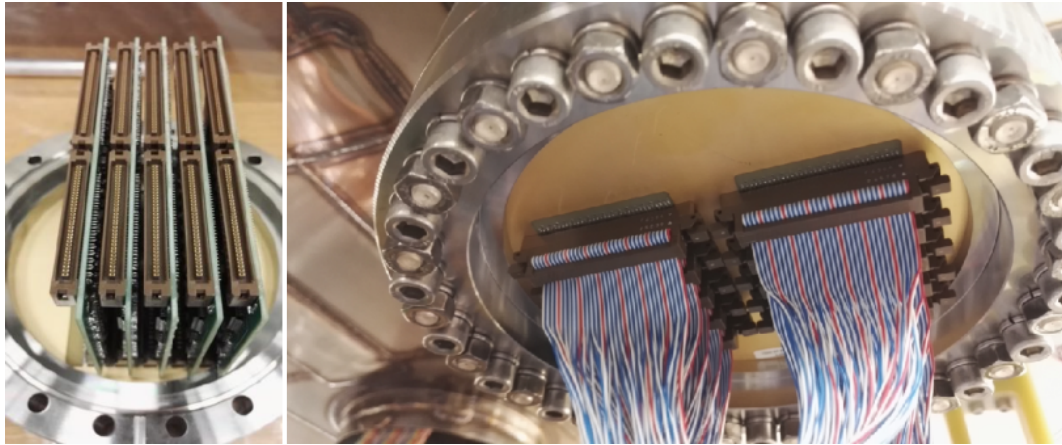


Figure 3.16: Images of the WA105 DP demonstrator SFT cold feedthrough with the FE cards inserted (right) and signal cables from CRP connected (left). The WA105 DP demonstrator SFT chimneys read only 320 channels thus requiring 5 FE cards.

The LRO electronics system is connected to the specific LRO signal feedthrough flanges on top of the cryostat via coaxial cables, which are within the scope of the PDS. The LRO electronics is designed for negative polarity PMT signals, with the amplitude of single photoelectrons on the input of the card between 1 and 10 mV. Assuming a typical PMT gain of  $1 \times 10^6$  (not accounting for attenuation of the signals), the Catiroc ASIC can measure a range of 1 to 400 photoelectrons (160 fC to 70 pC). The ADC samples from 1 mV to 1 V corresponding to 1 to 1000 photoelectrons, including the time response of the scintillator the range can increase to  $\sim 6000$ . Increasing the gain of the PMT to  $1 \times 10^7$ , lowers the upper values by a factor of 10. The internal noise level of the CATIROC is below 0.1 mV. The objective for the noise level of the ADC is for each channel to have the RMS noise level greater than 0.5 LSB, aiming for 1 LSB 0.1 mV.

### 3.4.2 Electronics System to DAQ System

The hardware interface between the DP CRO and LRO electronics sub-systems and DAQ has two components. The first interface is the 10 Gbit/s optical fibers for data transfer between the  $\mu$ TCA crates and the network interface of the DAQ system. The second one is a 1 Gbit/s optical fiber that connects the DAQ WR grandmaster switch to the DP electronics timing system.

In the current design a given DP module would have 245 10 Gbit/s optical links for streaming the digitized data to the DAQ from the CRO (240 links) and LRO (5 links) electronics housed in  $\mu$ TCA

<sup>12</sup>KEL Corporation™, [https://www.kel.jp/english/product/product\\_detail/?id=490&pageID=3%20](https://www.kel.jp/english/product/product_detail/?id=490&pageID=3%20).

crates on top of the cryostat structure. In the current specifications, the fibers are multimode OM3 fibers [4] with LC-LC connectors suitable for the transmission over distances of up to 300 m. They are provided by the DAQ consortium. On the side of the  $\mu$ TCA crate, the fibers are connected to an optical transceiver in the MCH (two SFP+XAUI links) [5]. On the DAQ, they go to the level-1 machines of the trigger farm, or switches, depending on the network topology adopted in the DAQ system design.

The 1 Gbit/s link going from the WR grandmaster to the DP electronics time distribution network serves to provide the synchronization to the reference clock common for the entire FD and derived from a GPSDO clock unit installed on the surface. The clock information is distributed to the WR-MCH slave module in each  $\mu$ TCA crate via a set of WR switches. These switches and the interconnecting 1 Gbit/s fibers form the timing sub-system of the DP electronics system and are included in the design of the latter. The WR synchronization protocol includes the automatic and continuous calibration of the propagation delays between the master and the connected slaves. This allows maintaining the overall synchronization between different nodes at sub-ns level. The WR grandmaster will be located either:

- On the surface near the GPSDO. In this case, a single fiber connects it to the DP timing system underground. The system automatically accounts for the incurred latency due to the extensive fiber length.
- Underground in the central utility cavern (CUC). In this case, calibration of the propagation delays between GPSDO and the WR grandmaster is performed manually, and a timing correction is applied to the data afterward.

The TPC electronics design assumes that the data are streamed continuously via the 10 Gbit/s links to the DAQ, where they are buffered until a trigger decision is made. The triggers are to be issued by processing the buffered data in some suitable sliding time window on the trigger farm machines. The window may be as long as 10 s for supernova neutrino burst (SNB)-triggered events. The triggers determine whether the data contained in the buffers are to be written on disk.

The software interface between the DAQ and the electronics system includes the tools for handling the data transmission and buffering, i.e., data formatting in user datagram protocol (UDP) packets, compression and decompression, and exchange of the control packets.

### 3.4.3 Electronics System to Cryostat and Cryogenics

The interface point between the cryostat and the DP electronics system is at the cryostat penetrations where the SFT chimneys are installed. Each penetration accommodates the chimney (of external diameter 254 mm). Each chimney has a CF-273 flange welded to its outer structure (see Figure 3.17). After the chimney is inserted, this flange is in contact with the corresponding flange on the crossing (or penetration) pipe embedded in the cryostat structure to which it is eventually fastened. In order to avoid any leaks at this interface a CF-273 copper gasket is used to ensure the vacuum tightness.

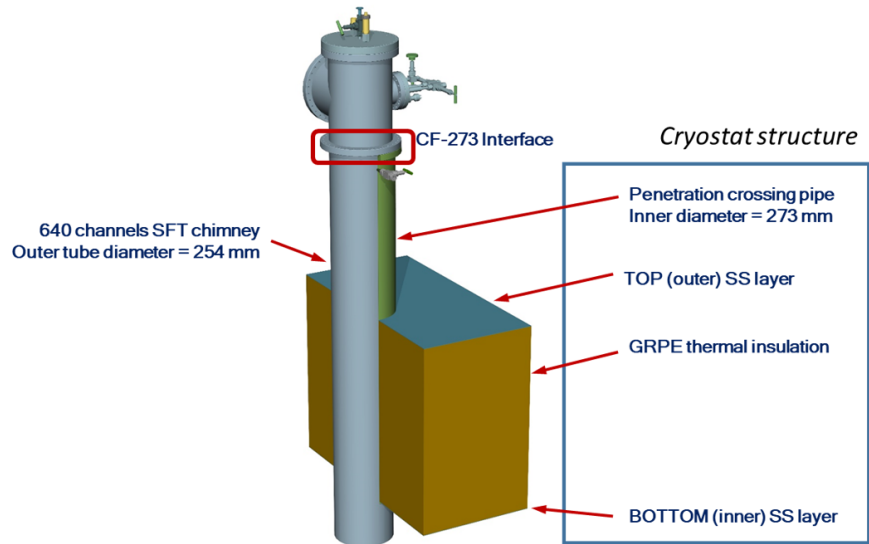


Figure 3.17: Details of SFT chimney interface to the cryostat structure.

Each chimney contains a heat exchanger copper coil cooled with LAr. There are two (inlet and outlet) stainless steel pipe connections with 10 mm and 12 mm inner and outer diameters, respectively, that need to be branched to the respective system for the LAr delivery and recirculation. In addition, a connection for nitrogen gas line with the same pipe dimensions as those for the LAr cooling, is used for filling the chimney after it is closed following the installation of the FE electronics. The nitrogen line is also required for flushing the chimney in the case of an access to the FE cards after the DP module is cooled for the operation.

The  $\mu$ TCA crates for charge readout are installed within a short  $<0.5$  m distance from the SFT chimneys on top of the cryostat roof. The five  $\mu$ TCA crates for the light readout are also placed on the roof of the cryostat at optimal locations defined by the routing of the PMT signal cables. The required volume to accommodate the crates is roughly  $60 \times 50 \times 40$  cm<sup>3</sup>.

### 3.4.4 Electronics System to Slow Control System

The integration with the slow control of the low-voltage power supply system for the FE cards and  $\mu$ TCA crates is required to enable the remote management and monitoring (current consumption by ASICs, set voltage, etc.). In addition, the SFT chimneys contain several sensors that need to be monitored. These include a pressure transducer that measures the pressure inside the chimney and at least two temperature probes (PT1000) that monitor the gas temperature inside near the cold flange at the bottom and close to the warm flange at the top. The readout of the  $\mu$ TCA crate information and the sensors in the SFT chimneys is part of the Slow Control system.

## 3.5 Transport and Handling

The SFT chimneys are 2350 mm long and weigh 180 kg. The cold and warm flanges are mounted on them at the assembly site, and the chimneys undergo leak-testing prior to shipping in wooden crates (approximate dimensions  $2.5 \times 0.5 \times 0.5 \text{ m}^3$ ). Once at SURF the crates are moved underground and placed on the roof of the cryostat by the underground installation team (UIT). The DP electronics consortium is then responsible for unpacking the crates and installing the SFT chimneys.

The boxes containing the electronic cards and  $\mu$ TCA crates are also handled by DP electronics consortium personnel. These are expected to be lightweight and easy to carry. A box containing 100 AMC cards has a maximal dimensions of 60 cm and weighs less than 10 kg.

## 3.6 Installation, Integration and Commissioning

The installation of the TPC electronics systems proceeds in several stages. In order to cable the CRPs to the SFT chimneys, the chimneys are installed first, prior to the start of the CRP installation inside the cryostat. Next the FE cards are mounted on the blades and inserted. The installation of the digital electronics and  $\mu$ TCA crates is postponed until all of the heavy work finishes on top of the cryostat in order to prevent damage to the fragile components (e.g., optical fibers) due to movement of material and traffic. Once the  $\mu$ TCA crates are installed and all the digital cards are inserted, the AMCs are cabled to the warm flanges of the SFTs for the charge readout and are connected to the PMT signal cables for the light readout. Finally, to complete the installation and integrate the system with the DAQ, the 10 Gbit/s and 1 Gbit/s optical links to the DAQ and WR timing network are connected. At this stage the full system is ready for commissioning.

### 3.6.1 SFT Chimneys

The installation of the SFT chimneys requires a compact gantry crane with movable supports along the length of the cryostat. The crane itself moves along the transverse direction. The crates containing the SFT chimneys are placed along the edges of the cryostat roof. An unpacked chimney is hoisted and transported to the appropriate penetration crossing pipe for installation. Once in place, the chimney is fastened to the flange on the crossing pipe. Enough overhead room to accommodate a chimney's 2.4 m length is required to allow to free movement of the chimney with the crane along the direction transverse to the beam axis.

In parallel with the SFT chimney installation, the FE cards are unpacked on top of the cryostat and mounted on the blades prior to their insertion in the chimneys. With SFT chimneys secured in the cryostat structure, the blades with mounted FE cards are inserted prior to sealing the chimney. At this stage, the LAr and gas nitrogen delivery pipes are already installed, and it is possible to make the connections with them. The pressure probes and temperature sensors are also connected



to the slow control system.

### 3.6.2 Digital $\mu$ TCA Crates

The installation of the  $\mu$ TCA crates with the digital electronics takes place in the final stage of the DP module installation to avoid damaging the fragile equipment. The crates are placed in their designated positions on the cryostat and connected to the power distribution network. The AMC cards and WR-MCH modules are inserted in their slots. The VHDCI cables are then attached connecting the CRO AMCs to the warm flange interface of the SFT chimneys. The fibers from the timing system are connected to WR-MCH.

### 3.6.3 Integration within the DAQ

The integration of the DP TPC electronics with the DAQ system requires connecting the 10 Gbit/s fiber links to each of 245  $\mu$ TCA crates. The connection of the timing system to the synchronization WR grandmaster is done via a single 1 Gbit/s fiber link.

The necessary software for the DAQ to read and decode the data packets sent by each  $\mu$ TCA crate would also be provided by the electronics consortium.

### 3.6.4 Integration with the Photon Detection System

The cables carrying the PMT signals from the splitter boxes are connected to the LRO analog electronics in each  $\mu$ TCA crate. The position of the crates is optimized with respect to the layout of PMT cables. In addition, the calibration system of the PDS is connected to specified inputs on the cards.

### 3.6.5 Commissioning

The SFT chimneys are commissioned as a first step. This consists of evacuating and then filling them with nitrogen gas at slight overpressure. It is necessary to check the leak rate when the chimney is under vacuum and to monitor the nitrogen pressure once it is filled in order to verify that no damage occurred to the flange interfaces during installation.

The electronics system is commissioned after completing the installation of the  $\mu$ TCA crates with the AMCs, and the timing system. The functionality of the full DAQ system is not strictly required at this stage. The data from each crate is read with a portable computer connected to the crate MCH 10 Gbit/s or 1 Gbit/s interface. The non-functioning channels are identified by

pulsing the CRP strips and the data quality is examined to ensure the correct functioning of the digital electronics and the temporal alignment of the data segments.

## 3.7 Risks and Vulnerabilities

The design of the DP electronics system takes into account several risk factors:

- **Obsolescence of electronic components over the period of experiment:** allocation of enough spares (preferably complete cards instead of components) should be sufficient to address this issue.
- **Modification to FE electronics due to evolution in design of PDs:** Strict and timely follow-up of the FE requirements from the DP PDS is required.
- **Damage to electronics due to HV discharges or other causes:** The FE cards should include suitable protection components. The TVS diodes used in the current design have been sufficient to protect the electronics in the WA105 DP demonstrator. In addition, the cards are accessible and could be replaced if damaged.
- **Overpressure in the SFT chimneys:** The SFT chimneys are equipped with safety valves that vent the excess gas in case of the sudden pressure rise. The overpressure threshold must be set low enough such that no significant damage could happen to the flanges.
- **Leak of nitrogen inside the DP module via cold flange:** The chimney volume is filled with argon gas instead of nitrogen.
- **Mechanical problems with FE card extraction due to insufficient overhead clearance:** This is addressed by imposing a requirement for LBNF to ensure enough overhead clearance to extract the blades from the SFT chimneys.
- **Data flow increase due to inefficient compression caused by higher noise:** Currently there is a factor of 5 margin in the available bandwidth with 10 Gbit/s MCH.
- **Damage to  $\mu$ TCA crates due to presence of water on the roof of the cryostat:** This is addressed by imposing a requirement for LBNF to ensure that the top cryostat surface remains dry.
- **Problems with the ventilation system of the  $\mu$ TCA crates due to bad air quality:** Normal conditions similar to any industrial environment (e.g., at CERN or Fermilab) is expected to be sufficient for proper crate functioning. It is important to avoid liberation of large quantities of dust in the detector caverns at SURF.

## 3.8 Organization and Management

### 3.8.1 Dual-Phase TPC Electronics Consortium Organization

The DP TPC electronics consortium consists of seven participating institutions from France (3), Japan (3), and the USA (1). The consortium leader is from IPNL, France, and the technical leader is from KEK, Japan. The consortium includes members from APC, IPNL, and LAPP in France; Iwate University, KEK, and NITKC in Japan; and SMU in the USA.

### 3.8.2 Planning Assumptions

The design of the DP TPC electronics system largely on the elements that have already been developed and tested in the WA105 DP demonstrator. Commissioning of the ProtoDUNE-DP towards the end of 2018 should provide some additional information, but is not expected to affect the design of principal components. Some additional improvements related to the increase in the channel density supported by AMCs is possible for the purpose of further cost reduction.

### 3.8.3 WBS and Responsibilities

The description of the work breakdown structure (WBS) including the assignments of the responsible institutions is documented in DUNE-doc-5594.

### 3.8.4 High-level Cost and Schedule

The key milestones are listed in Table 3.9. Table 3.10 shows an extract from the international project schedule pertaining to the technical activities of this consortium. The detailed cost model has been developed based on the scaling of the costs for the electronics system of ProtoDUNE-DP. It is provided in an addendum.

Table 3.9: DP TPC electronics consortium key milestones.

| Date           | Milestone  |
|----------------|--|
| September 2018 | Number of LRO channels finalized                             |
| November 2018  | Final routing for LRO AMCs for production                    |
| March 2019     | Costing model for technical design report (TDR) finalized    |
| March 2019     | Firmware for CRO AMCs finalized                              |
| March 2019     | Commissioning of ProtoDUNE-DP finished                       |
| January 2023   | Start of component production and procurement                |
| July 2023      | $\mu$ TCA infrastructure components produced                 |
| July 2023      | Components of WR system delivered and validated              |
| January 2024   | SFT chimneys produced and tested                             |
| January 2024   | Cryogenic FE analog electronics produced and tested          |
| January 2024   | AMCs for CRO and LRO produced and tested                     |
| August 2024    | Cryostat of the second detector module is ready              |
| November 2024  | SFT chimneys installed                                       |
| December 2024  | Cryogenic FE electronics installed                           |
| December 2024  | $\mu$ TCA crates and WR network installed                    |
| January 2025   | Installation of AMCs completed                               |
| January 2025   | Commissioning of the DP TPC electronics system               |
| August 2025    | Closure of the cryostat temporary construction opening (TCO) |

Table 3.10: DP TPC electronics consortium schedule.

| Technical activity                                     | Days | Start date | End date |
|--|------|------------|----------|
| Preparation of costing for interim design report (IDR) | 20   | 02/26/18   | 03/23/18 |
| Initial development of installation schedule           | 20   | 02/26/18   | 03/23/18 |
| Further development of installation schedule           | 145  | 09/03/18   | 03/22/19 |
| Installation and commissioning of ProtoDUNE-DP         | 320  | 01/01/18   | 03/22/19 |
| Finalization of the number of channels for LRO         | 20   | 09/03/18   | 09/28/18 |
| Implementation of routing for digital cards of LRO     | 40   | 10/01/18   | 11/23/18 |
| Preparation of final costing for TDR                   | 85   | 11/26/18   | 03/22/19 |
| Firmware development for charge readout cards          | 145  | 09/03/18   | 03/22/19 |

# Chapter 4

## High Voltage System

### 4.1 High Voltage System (HV) Overview

#### 4.1.1 Introduction

A liquid argon time-projection chamber (LArTPC) requires an equipotential cathode plane at high voltage (HV) and a precisely regulated interior E field to drive electrons from particle interactions to sensor planes. In the case of the DUNE dual-phase technology, this requires a horizontal cathode plane, held at negative HV; a horizontal charge-readout plane (CRP) in the gas phase as described in Chapter 2.1.1; and formed sets of conductors at graded voltages surrounding the central drift volume, collectively called the field cage as shown in Figure 4.1. The field cage (FC) consists of continuous field shaping rings that provide voltage degradation in the vertical direction and forms one continuous active volume.

The HV consortium supplies the systems that operate at the nominal voltages to establish the uniform 500 V/cm E field in the time projection chamber (TPC) drift volume. As a result, its systems constitute a large fraction of the internal structures of the TPC. Mechanical and structural concerns are taken into account, together with the electrical design to meet the requirements.

The design presented in this chapter is primarily based on the ProtoDUNE-DP design, which includes a set of basic elements (i.e., FC sub-modules, cathode, and ground grid modules) that are deployed to build a TPC with a  $6 \times 6 \times 6 \text{ m}^3$  active volume. The extrapolation to the DP module structure with  $12 \text{ m} \times 12 \text{ m} \times 60 \text{ m}$   $\text{m}^3$  active volume requires some electrical and mechanical adaptations. The size of each element is kept within a roughly  $3 \times 3 \text{ m}^2$  envelope, matching the size of the CRP modules, which was optimized for underground transportation and assembly.

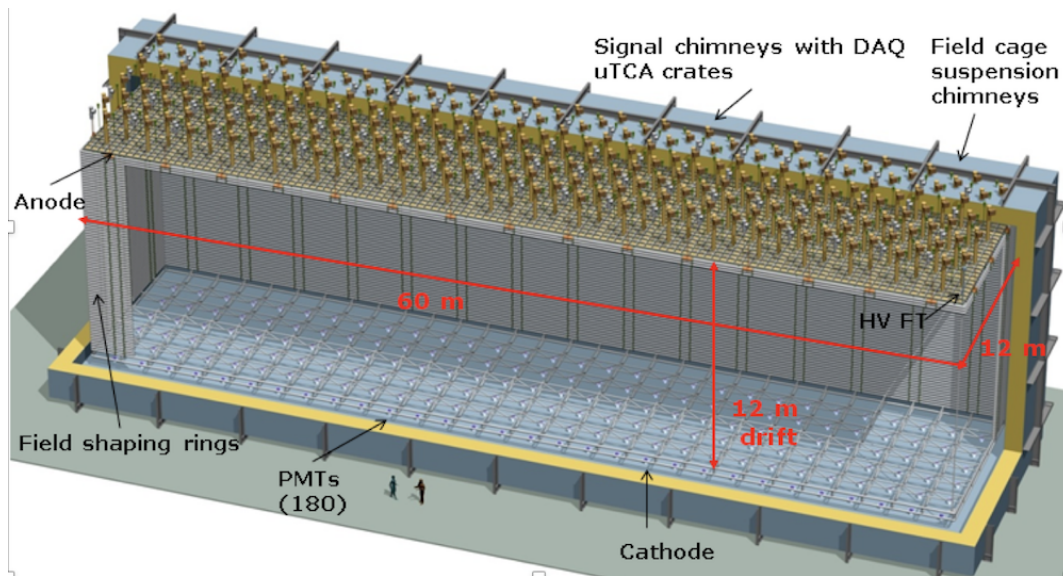


Figure 4.1: A cutaway showing an overview of a DP module, with the cathode plane and the PDS on the floor, the 12 m tall FC modules surrounding the active volume, and the top view of the CRPs showing the anode plane (the only portion visible from this angle).

## 4.1.2 Design Considerations

The HV system is designed to meet the physics requirements of the DUNE experiment. This includes both physical requirements (e.g., an E field that allows robust event reconstruction) and operational (e.g., avoidance of over-complication in order to maximize data collection efficiency). A collection of essential requirements for the HV system is shown in Table 4.1.

## 4.1.3 Scope

The scope of the HV system includes the continued procurement of materials for, and the fabrication, testing, delivery, and installation of systems to generate, distribute, and regulate voltages so as to create a precision E field within the detector module volume.

The HV system consists of components both exterior and interior to the cryostat. The HV power supply is located external to the cryostat. In the DP module, the HV power supply is expected to be located on top of the HV feedthrough. The HV is further distributed by interior components that form part of the TPC structure, as depicted in Figure 4.2.a. These components are:

- power supply (similar to that shown in Figure 4.2b),
- HV feedthrough (similar to that shown in Figure 4.2c),
- HV extender and voltage degrader,

Table 4.1: HV System Requirements

| No. | Requirement  | Physics requirement driver  | Requirement   | Goal  |
|-----|--|---|---|---|
| 1   | Exceed minimum E field TPC drift volume  | Maintain adequate particle ID, which is impacted by slower drift speed and increased recombination, diffusion and space charge effects.     | >250 V/cm   | 500 V/cm  |
| 2   | Do not exceed maximum E field in LAr volume  | Avoid damage to detector to enable data collection over long periods.   | 30 kV/cm  | as low as reasonably achievable (ALARA)         |
| 3   | Minimize power supply ripple   | Keep readout electronics free from external noise   |   |   |
| 4   | Maximize power supply stability  | Maintain the ability to reconstruct data taken over long period. Maintain high operational uptime to maximize experimental statistics.      |   |   |
| 5   | Provide adequate decay time constant for discharge of the cathode plane and FC as well as cathode plane resistive segmentation | Avoid damage to detector to enable data collection over long periods. Maintain high operational uptime to maximize experimental statistics. | G $\Omega$ resistors per each connection of the 3 $\times$ 3 m <sup>2</sup> cathode units |   |
| 6   | Provide redundancy in all HV connections   | Avoid single-point failures in detector that interrupt data taking.   | >2 voltage divider chains to distribute HV to the FC profiles                             | One voltage divider chain every four FC modules |

- cathode plane and ground plane (GP),
- field cage,
- HV return feedthrough and resistor box (similar to that shown in Figure 4.2d).

#### 4.1.4 System Overview

A DP detector module has a single modular cathode plane that forms the bottom of the single 12 m (W)  $\times$  12 m (H)  $\times$  60 m (L) drift volume. It is constructed from eighty 3 m  $\times$  3 m contiguous units each consisting of a stainless steel tube frame holding a stainless steel grid. A similar but highly transparent GP is placed just above the PDS, which is located near the bottom of the cryostat and below the cathode to shield it from the HV. The cathode bias voltage of  $-600$  kV is provided by an external HV power supply through a HV feedthrough and a voltage extender unit that reaches the cathode.

The FC surrounds the drift volume in a set of equidistant, stacked, horizontal, rectangular-shaped aluminum rings. Its function is to ensure a uniform drift field of  $500$  V cm $^{-1}$ . This is accomplished by gradually decreasing the voltage over the 12 m height from the cathode voltage of  $-600$  kV to  $-10$  kV at the top-most field shaping ring, to allow for electron extraction into the gas volume of the CRP. The FC consists of aluminum field-shaping rings, made up of mechanically and electrically connected 3 m long aluminum profiles. This is a cost-effective system for establishing the required equipotential surfaces.

## 4.2 HV System Design

### 4.2.1 High Voltage Power Supply and Feedthroughs

The HV delivery system consists of

- one power supply,
- HV cryogenic feedthroughs,
- HV cryogenic extender.

To ensure the nominal E field of  $500$  V/cm over the 12 m drift distance, an external power supply must deliver  $-600$  kV to the cathode through one HV cryogenic feedthrough, with a maximum current draw of  $0.5$  mA. At present such a power supply does not exist, but Heinzinger, the industrial partner and leader in the production of HV power supplies, is executing a vigorous R&D program towards this goal, relying on the following facts:



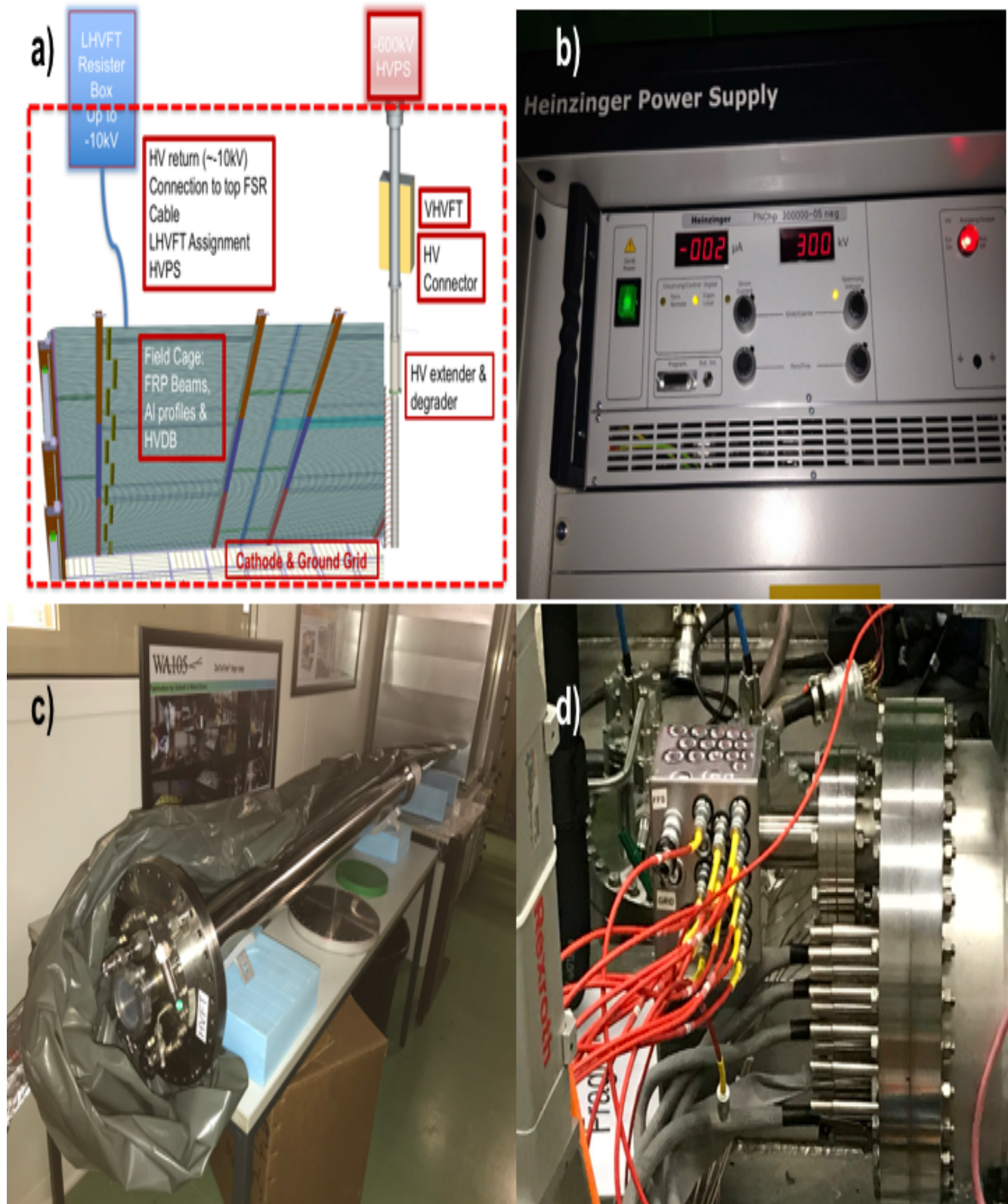


Figure 4.2: (a) Schematic overview of the VHV system for a DP detector module, (b) photo of the 300 kV Heinzinger power supply<sup>2</sup>, (c) the VHV feedthrough, and (d) the VHV return connection. (All photos from the WA105 DP demonstrator.).

- 600 kV power supplies are feasible, scaling from present industrial technology;
- The same is possibly true for the HV cryogenic feedthrough, scaling to large diameter and longer size with respect to the present 300 kV prototypes;
- The critical points of the HV distribution are then the cable and its connectors on the power supply and on the HV-feedthrough.

The joint R&D program between DUNE and Heinzinger aims to eliminate cables and connectors, and build a power supply that can be connected directly on the top of the HV-feedthrough. A sample schematic and some details are shown in Figure 4.3. Heinzinger is motivated to pursue this effort because of possible new industrial applications.

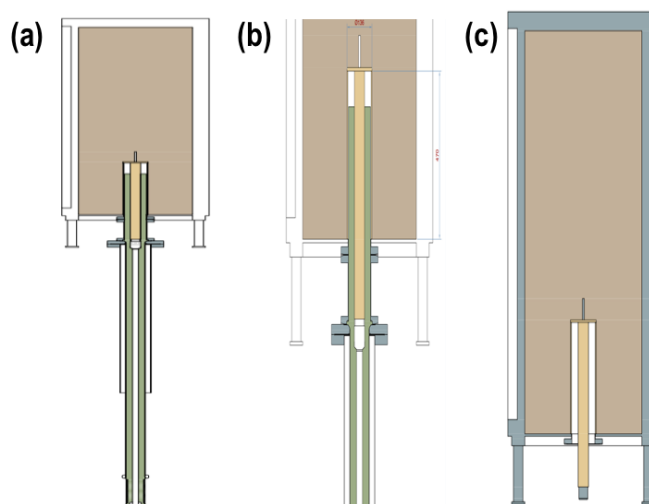


Figure 4.3: (a) Vertical cross section of the proposed VHV power supply inserted over the 750 kV HVFT for a DP detector module, (b) Insertion detail of the proposed VHV power supply inserted over the 750 kV HVFT. The female HDPE of the HVFT is indicated in green. The male plug of the HVPS, shown inserted, is a metallic conductor inserted in a HDPE insulating tube (indicated in yellow). The gap between male and female is filled, via a tube inside the HVPS (not indicated) by a silicone oil such as RHODORSIL 47 V1000. (c) Vertical cross section of the HVPS. The front panel is on the left. The HV multiplication and regulation (not indicated) is in the beige region.

Typical Heinzinger power supplies have ripples in the range of  $\sim 30$  kHz with an amplitude of  $0.001\%V_{\text{nom}} \pm 50$  mV. A low-pass RC filter designed to reduce the voltage ripple could be integrated into the output of the power supply. It should be noted, however, that the required ripple suppression does not need to be as high as for the SP module due to the DP module's more effective shielding of the anodic structure, performed by the extraction grid and by the CRP signal amplification stage.

The HV feedthrough is based on the same successful ICARUS design that was adopted in both ProtoDUNE-SP and ProtoDUNE-DP. In this design, the voltage is transmitted along a stainless steel center conductor on the warm exterior of the cryostat, where this conductor mates with a cable end. Inside the cryostat, the end of the center conductor has a spring-loaded tip that contacts a receptacle cup mounted on the cathode, from which point HV is delivered to the FC. The center

conductor of the feedthrough is surrounded by Ultra-High Molecular Weight Polyethylene (UHMW PE).

To first order, the upper bound of operating voltage on a feedthrough is set by the maximum E field on the feedthrough. Increasing the insulator radius reduces the E field. For the target voltage, the feedthrough uses a UHMW PE cylinder of at least 15.2 cm (6 in) diameter. In the gas space and into at least 15.2 cm of the liquid, a tight-fitting stainless steel ground tube surrounds the insulator. The ground tube has a CF-type flange of at least 25.4 cm (10 in) welded on for attachment to the cryostat. A prototype<sup>3</sup> has been successfully tested up to  $-300$  kV in pure argon in a dedicated setup; two similar prototypes are currently being installed in ProtoDUNE-SP and ProtoDUNE-DP.

## 4.2.2 High Voltage Extender and Voltage Degradar

Since the HV has to be guided from the top of the cryostat to the cathode (12 m below the liquid argon (LAr) surface), an extension of the HV feedthrough is required, as shown in Figure 4.4a, b and c. The extender contains an inner conductor at  $-600$  kV surrounded by an insulator. Since the extension runs the entire height of the drift volume, metallic rings (degrader rings) are installed on the periphery of the extension close to the field-shaping ring. Each degrader ring is electrically connected to the field shaping ring at the same height thus guaranteeing that the E field in the LAr between the extender and the FC remains at zero.

## 4.2.3 Cathode Plane

The DP detector module's cathode plane forms the bottom of the single 12 m (W)  $\times$  12 m (H)  $\times$  60 m drift volume and provides a constant potential surface at  $-600$  kV. It receives its HV from the central conductor of the extender that carries the voltage from the power supply through the HV feedthrough.

The cathode plane consists of eighty 3 m  $\times$  3 m modules. The cathode module design is based on the design used in ProtoDUNE-DP, for which the cathode consists of a stainless steel (316L) mechanical structure made from two types of tubes: an external frame made from 60 mm diameter tubes, and the internal portion is made from oval pipes of 20 mm  $\times$  40 mm with 1.5 mm thickness, as shown in Figure 4.5. This frame is filled with smaller tubes of 12 mm diameter (not shown in the figure), forming a grid, to provide a uniform equipotential surface, while ensuring 60 % optical transparency. All diameters are optimized to guarantee a uniform potential across the cathode, to satisfy the maximum local field requirement of 30 kV/cm, and to minimize the local E fields to ground. The cathode plane components are bolted together and fixed to the supporting fiber-reinforced plastic (FRP) I-beams of the FC. Modules of the same size as for ProtoDUNE-DP are foreseen for the DP detector module cathode. Some mechanical modifications will be performed in order to guarantee the flatness over the longer distance of 12 m compared to the 6 m of ProtoDUNE-

---

<sup>3</sup>The prototype was manufactured by the company CINEL™ Strumenti Scientifici Srl.

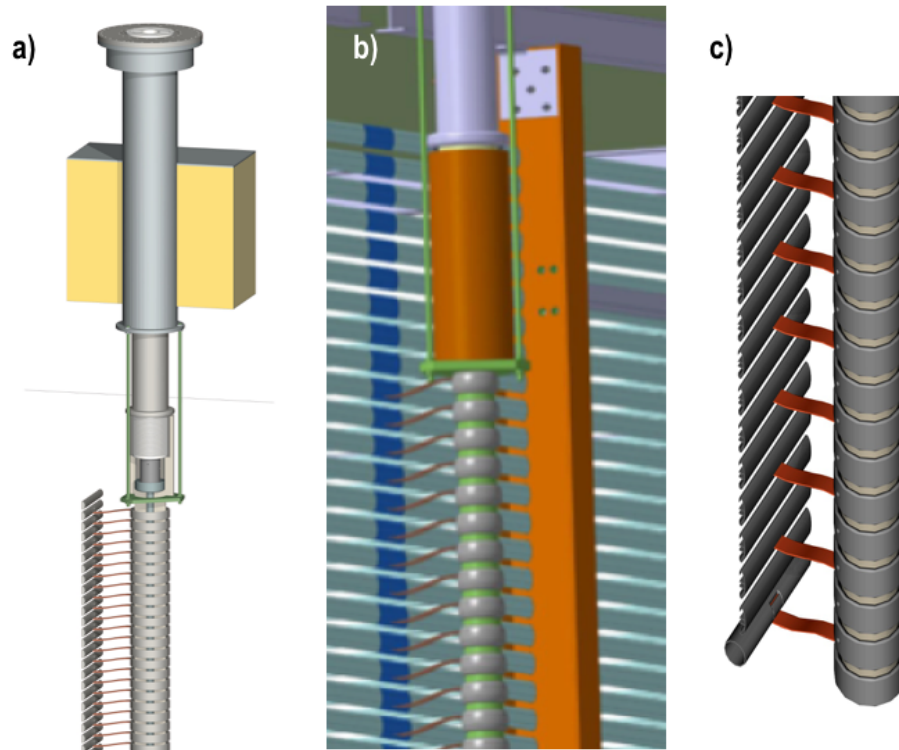


Figure 4.4: Pictures of HV feedthrough and HV extender-degrader; a) Overview of the HV FT, HV extender and the degrader chain, b) details of the top portion of the HV extender and its connections to the field shaping rings, c) detail of the HV extender and degrader connection to the bottom part of the FC, including the connection to the cathode plane.

DP. In addition, the shape of the conductors could undergo some slight modifications in order to lower the local E field values based on the ProtoDUNE-DP experience.

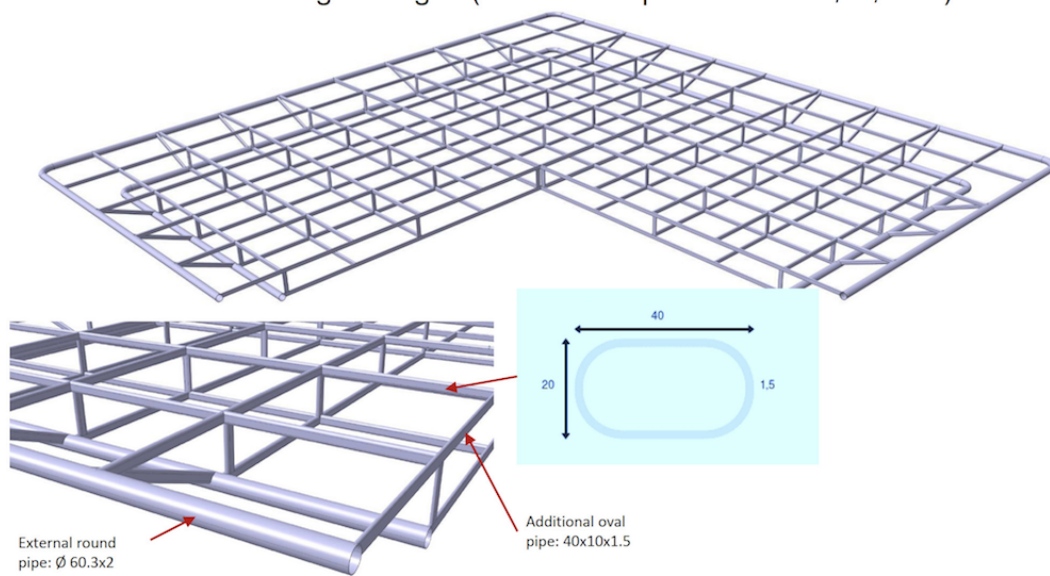


Figure 4.5: A cutaway view of ProtoDUNE-DP cathode (Credit: ETHZ)

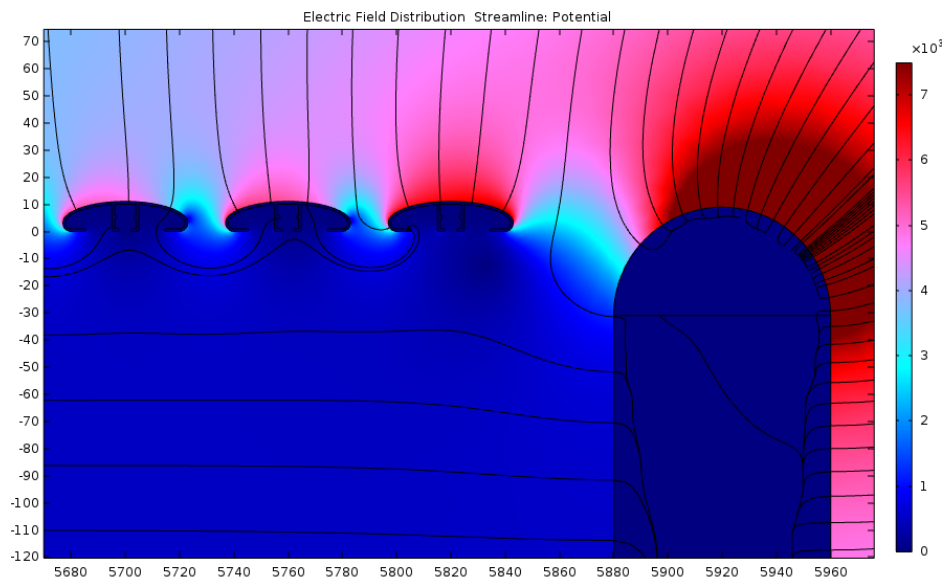


Figure 4.6: Electric field map near the cathode, showing the maximum local field at  $<30$  kV/cm, satisfying the requirement.

The energy stored in the volume between the cathode plane and the ground grid (which sits under the cathode and above the photon detectors (PDs)) is estimated to be about 1.7 kJ over the  $12\text{ m} \times 60\text{ m}$  area, based on the cathode voltage and the distance of 1 m between the cathode and the ground grid described in Section 4.2.4. A sudden discharge from the cathode frame to the cryostat membrane could cause severe damage to the membrane. The modular construction of the cathode helps minimize this effect in case of discharge. During assembly in the cryostat, the cathode units are kept electrically insulated and connected to their adjacent neighbors through  $\text{G}\Omega$  resistors. Given the 100 pF capacitance of each cathode unit, any discharge occurring in one

unit will release at most 21 J of stored energy while the discharge rate to the other units is slowed to the several-hundred-millisecond range.

Detailed calculations are in progress to determine the final shape and the size of the cathode and ground grid frames to limit the maximum E field to  $30 \text{ kV cm}^{-1}$  throughout the LAr volume (Figure 4.6), as per requirement 2 (Table 4.1). Structural calculations are also in progress to verify the planarity of the cathode as it hangs on the FC supports. Value and voltage characteristics of the connecting resistors will also be defined according to results from dedicated simulations of the cathode electrical model.

## 4.2.4 Ground Grid

The ground grid is installed between the PD and the cathode plane to shield the PMTs from a discharge.

The ground grid consists of 316 L stainless tubes, as does the cathode. It is made of eighty  $3 \text{ m} \times 3 \text{ m}$  modules. Unlike the cathode, the ground grid has a single layer supported by a set of feet resting on the membrane floor. Detailed studies on the grid geometry are ongoing to ensure that the requirement on the maximum local field is satisfied.

## 4.2.5 Field Cage

### 4.2.5.1 Mechanical Structure

The field shaping rings of the FC are made up of extruded roll-formed aluminum open profiles. The profiles are stacked horizontally and constructed into continuous rectangular rings that form the vertical sides of the drift volume. The aluminum profiles are attached to structural elements made of pultruded FRP.

FRP is non-conductive and strong enough to withstand the FC loads in the temperature range of  $-150 \text{ C}$  to  $23 \text{ C}$ . This material meets the Class A International Building Code classification for flame spread and smoke development, as characterized by ASTM E84.

Each of these modules is composed of three styles of submodules of dimensions  $3 \text{ m (W)} \times 2 \text{ m (H)}$ . These submodules are supported by two  $15.2 \text{ cm (6 in)}$  FRP I-beams (with profile slots cut out) and two  $7.62 \text{ cm (3 in)}$  cross bar I-beams that form a rectangular frame.

The FC is modular, each module covering a vertical area of  $3 \text{ m (W)} \times 12 \text{ m (H)}$ . There are two types of modules, straight section and corner, both types having the dimensions  $3 \text{ m (W)} \times 12 \text{ m (H)}$ . A total of 40 straight section modules (i.e., with straight profiles) and eight corner section modules, with profiles bent 45 degrees at one corner to allow straight connections via clips at the corner, as shown in Figure 4.7.c. A photo of the ProtoDUNE-DP FC is shown in Figure 4.7.d.

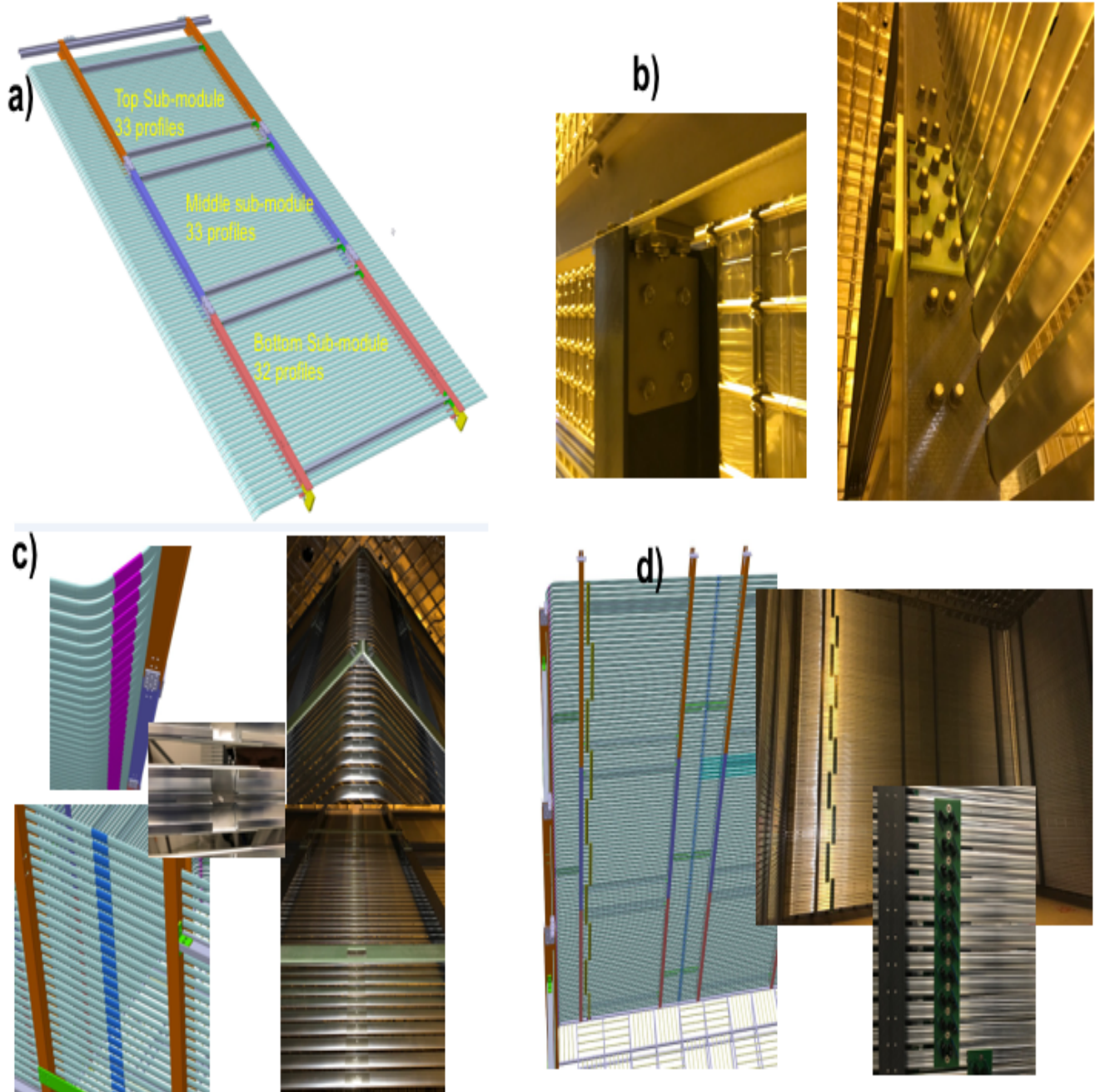


Figure 4.7: FC parts and connections for ProtoDUNE-DP. a. One ProtoDUNE-DP FC panel consisting of three submodules. The DP module has virtually the identical structure, except for the number of middle submodules, which is four, b. A photo of the top module connection to the stainless steel I-beam and an inter-submodule connection, c. Aluminum clip connection at the corner and at the straight sections, d. HV divider boards and their connections on ProtoDUNE-DP FC.

Each FC module is made of six submodules of three distinct types: top, bottom and middle. The dimensions for all submodules are 3 m (W)  $\times$  2 m (H). Each module has one top submodule with 33 profiles, four middle submodules with 33 profiles each, and one bottom submodule with 32 profiles, for a total of 197 profiles per module. The voltage of the top-most field shaping ring is  $-9$  kV. The top submodules make the mechanical connection to the ceiling of the cryostat from which the entire FC hangs, as shown in Figure 4.10, left. The bottom modules make both mechanical and electrical connections to the cathode.

A railed rib runs along the length of the aluminum profiles at the center of the profile. The rib provides mechanical strength and acts as the rail for the slip nuts that hold the profiles onto the supporting FRP frame. The rib also serves as the rail for the nuts that hold the HV divider boards and the slip nuts for inter-module profile connections. All profiles at a given height are electrically connected via an aluminum clip screwed onto the slip nut across two neighboring profiles. A resistive divider chain interconnects the aluminum profiles to provide a linear voltage gradient between the cathode and the top field-shaping ring.

The extruded aluminum profiles are mounted to the 15.2 cm (6 in) I-beam via two stainless screws and aluminum slip nuts in the center enforcement rail of the profile. The mounting is only on one of the 15.2 cm I-beams to allow contraction on either side of the profile. The top submodule has an extended 15.2 cm FRP beam with holes to connect it to the stainless steel I-beam hanging from the ceiling. The bottom submodule has a cutout to hold the cathode plane onto it. The four middle submodules are symmetric, and thus interchangeable. FC modules are horizontally interconnected with six G10 bars screwed to the vertical FRP I-beams at positions evenly distributed along the 12 m height. This interconnection guarantees the required alignment of the adjacent aluminum profiles for clipping. Given this interconnection, the full FC can be considered as single skeleton that is mostly composed of FRP, which will shrink by about 12 cm over 60 m once the cryostat is filled with LAr. To compensate for this, the G10 bars are designed to be slightly longer than their final length in the LAr.

#### 4.2.5.2 Electrical Interconnections

An aluminum clip connects the ends of each set of two end-to-end FC profiles, forming continuous equipotential rectangular rings 144 m long. Rows of HVDBs, consisting of two resistors and a series of four surge-protection varistors in parallel, bridge the gap between the two neighboring stacked profile rings. The total number of rows will be determined based on the redundancy and the current-limit requirements; one row of HVDBs is in principle sufficient to provide the required potential difference of 3 kV between neighboring rings, but more are desirable for redundancy.

The resistive chain for voltage division between the profiles provides a linear voltage gradient between the cathode and the top-most field shaping ring. It is critical as it determines the strength of the E field between one profile and its neighbors, as well as between the profile and other surrounding parts, e.g., the grounded stainless steel membrane. The E field needs to be kept well below  $30 \text{ kV cm}^{-1}$  at all points in the LAr bath to enable safe TPC operation.



The identified profile, Dahlstrom Roll Form #1071<sup>4</sup> is estimated to lead to E fields of up to  $12\text{ kV cm}^{-1}$ , for the planned FC configuration and operating voltage. Figure 4.8 illustrates results from an E field calculation.

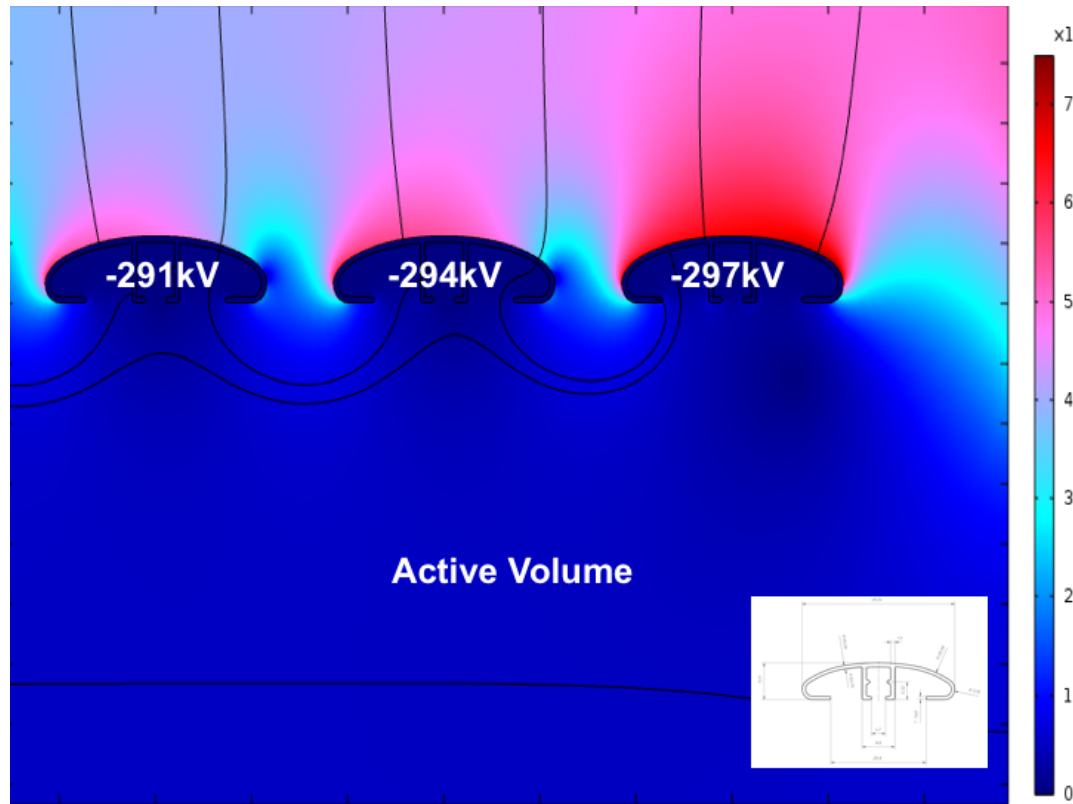


Figure 4.8: E field map (color) and equipotential contours of an array of roll-formed profiles biased up to  $-300\text{ kV}$  and a ground clearance of about  $100\text{ cm}$  in ProtoDUNE-DP (CAD model)

Two distinct types of HV divider boards are used for ProtoDUNE-DP: 10 stage and 8 stage boards. Each stage consists of two  $2\text{ G}\Omega$  resistors in parallel and four varistors of threshold voltage  $1.28\text{ kV}$  to protect the resistors in case of a sudden discharge. The total expected current at  $600\text{ kV}$  is therefore  $3\text{ }\mu\text{A}$  per row. Since multiple rows, which are connected in parallel, are used for redundancy, the expected current in the entire system is simply the number of rows times the current per each row. For optimization purposes, one DP module HVDB will connect 11 stages. This enables one  $12\text{ m}$  tall module to be covered by fifteen 11 stage HVDB and one 10 stage HVDB at the bottom to make the final connection.

Figure 4.9 shows one HVDB board and Figure 4.7.d. shows the connection of one row of HVDB along the entire height of the FC as installed in ProtoDUNE-DP. The  $12\text{ m (W)} \times 60\text{ m (L)}$  ground plane consists of 80 unit planes (each  $3\text{ m} \times 3\text{ m}$ ). The cathode plane is mounted to the bottom of the FC, together forming one contiguous unit of field-providing structure. The bottom-most HVDB makes the connection between the cathode and the bottom-most field-shaping ring. For redundancy, a total of two HVDB rows are used in ProtoDUNE-DP. The DP detector module will use one HVDB chain every four FC modules, providing an ample redundancy. However, the final number of rows of HVDB must take into account the impact of the underlying current through

<sup>4</sup>Dahlstrom Roll Form #1071, Dahlstrom™.

the FC due to the particle interactions.

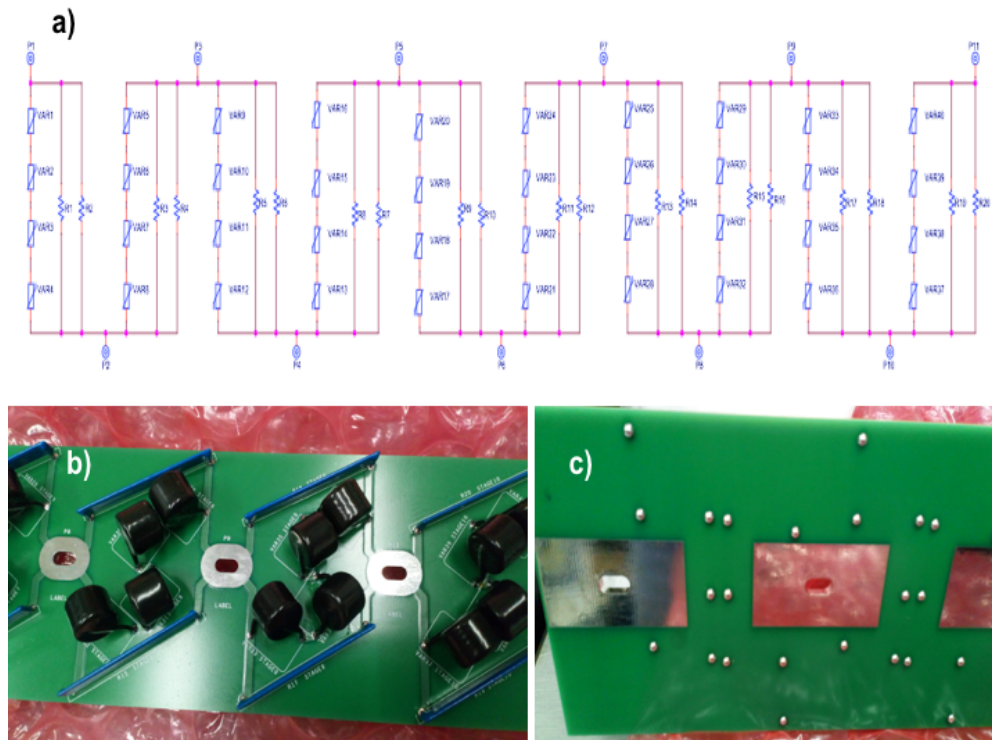


Figure 4.9: ProtoDUNE-DP HV divider board (a) schematic circuit diagram, (b) photo of the top of the board, (c) photo of the bottom of the board

## 4.2.6 HV Return and Monitoring Devices

In order to maintain the potential difference between the top-most field shaping ring and the extraction grid of the charge readout plane, either a dedicated HV supply and an adjustable resistor chain is used in the HV return outside of the cryostat. This requires an independent 10 kV feedthrough similar to those developed for the extraction grid.

Multiple devices are planned for monitoring the HV.

- The Heinzinger units have typical sensitivities down to tens of nanoamperes with current readback capability. The units are able to sample the current and voltage every few 100 ms.
- Inside the cryostat, so-called pick-off points near the anode will monitor the current through the HVDB resistor chain.
- Additional pick-off points could be implemented on the ground grid below the cathode to monitor possible stray currents.

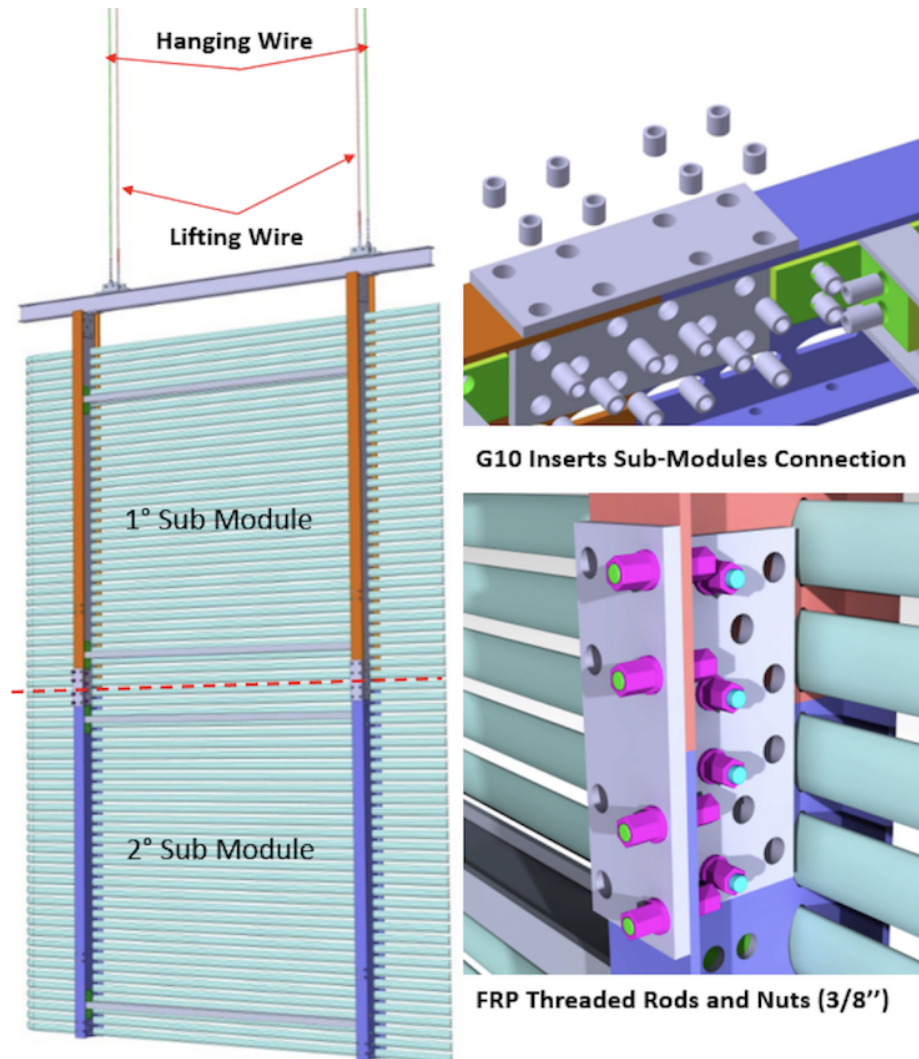


Figure 4.10: Left: Two submodules connected and hanging from the two sets of stainless steel cables on the ceiling. The lifting wires are used to raise the module to its position as submodules are connected; the hanging wires keep the fully integrated module in its final position. Right: Inter-submodule connections. Each connection is made by two 1cm thick G10 plates along the height of the I-beams and one 1cm thick G10 plate on the flange.

## 4.3 Quality Assurance

**Field Cage FRP Parts** Upon delivery of the FRP I-beams and other parts, all parts undergo a visual inspection process to look for defects, in particular those affecting structural integrity, such as cracks, air bubble holes, depression and flatness. The parts are sorted into three preliminary categories: category 0 (pass), category 1 (problematic but could be repairable) and category 2 (severe and unusable) .

The visual inspection is followed by critical dimension measurements to verify individual submodule assembly and module interconnection integrity. These measurements focus on cross sectional dimensions for rods, plates and bars, and on the length, straightness, flatness and camber of the beams and flanges. All measurements must satisfy the mechanical tolerance provided by the design drawings and the standard industry quality criteria.

The FRP I-beams and parts in category 1 undergo a repair process during the preparation stage through defibering, deburring and sanding. Another set of measurements is performed after the repair to redetermine the part's category.

Those in category 2 are returned to the vendor for replacements.

**HV Divider Board** All resistors used for board production are numbered and undergo a three-stage quality assurance (QA) test for final selection. Resistance is measured at voltages up to 4kV in 500 V steps for each stage. The first stage is done at room temperature, the second at LN temperature, and the third again at room temperature after warming up. The measured values are histogrammed for the final selection, in order to look for groupings of values. It is more important that the resistance values be close to each other than that they be at any particular value (unless they are too far from the design values). The resistors for which the resistance values are within 1% of each other are selected.

All varistors for board production are also numbered for QA purposes and undergo a three-stage QA testing program for the final selection. Each stage is a clamping voltage measurement, first at room temperature, then at LN temperature, and again after warming back up up to room temperature. The measured values are histogrammed for the final selection; those for which the clamping voltage is closer to the design values are selected, to ensure proper protection.

Once the electrical parts are mounted on the HVDB by the vendor, they undergo a three-stage QA testing program. Each stage involves a resistance measurement, first at room temperature, then at LN temperature, and again after warming back up up to room temperature. The measured values are histogrammed for the final selection. The boards can fall into three categories: 0. Pass, 1. Repairable and 2. Rejected. If at any testing stage the resistance is more than 0.5 % away from the mean, the part does not fall into category 0, pass. Boards in category 1 are sent back to the vendor with the selected resistors so that the parts in the failed stages can be replaced.

**Aluminum Profiles and Clips** The QA testing of the aluminum profiles and clips is done on prototype production samples prior to full production. The samples are visually inspected for

their shape and their adherence to the design drawing, the surface smoothness, the surface-coating quality, and the smoothness of the bend (for the profiles with the 45° bend). Clip samples are visually inspected for their shape and their adherence to the drawing, their edge smoothness, their mechanical fitness, and how tightly they fit to the profiles.

**Cathode, HVFT and the Extender** The QA for other components is under development as part of the ProtoDUNE-DP construction efforts.

**Power Supply and Feedthrough** The power supply is tested extensively along with the controls and monitoring software. Capabilities to test include:

- Ramp and change the voltage; including rate change and pause capabilities and settings.
- Accept user-defined current limit. This parameter sets the value of current at which the supply reduces the voltage output in order to stay below it. The current limiting itself is done in hardware.
- Accept a setting for the trip threshold current. At this threshold the software would reduce the voltage output. In previous experiments, the trip function in software would set the output to 0 kV.
- Record the current and voltage readback values with a user-defined frequency, and also to record any irregular current or voltage events.

## 4.4 Production and Assembly

### 4.4.1 Field Cage Submodule Frames

All FRP parts that pass the QA process undergo the preparation process, which involves quality control (QC) at each step. Each of the parts is first defibered, deburred, sanded to smooth the edges, and then varnished to suppress any remaining fibers. Once the part completes the preparation process, it is stored in a humidity- and temperature-controlled drying area for 24 to 48 hours to fully cure the varnish. Upon full curing, each module is laser-engraved with a unique part number and recorded in a QC database.

At this point the submodule is pre-assembled on a table prior to packaging to ensure fitness of all parts, including inserts, screws and slip nuts. When the fitness is verified, the submodule is disassembled and packaged into a 2 cm×20 cm×2 m compact package with the edges wrapped with a thick plastic layer to protect the parts from mechanical damage, e.g., from a fall. This package includes all necessary parts to assemble the given submodule along with 10 to 20% spare parts. This ensures that each package is self-sufficient for the final assembly. Each package is given a submodule number for further tracking purposes. This submodule number stays with it throughout assembly at SURF and final installation so that the submodule can be assigned to its

specific module and in its proper location within the module.

These packages are shipped to SURF and transported underground for final assembly prior to the installation. The 3 m long aluminum profiles are produced and shipped to SURF separately for final assembly. The final QC of the profiles is conducted during submodule assembly. Profiles with deep scratches and sharp protrusions that could cause excess charge concentration will be rejected. This process must be done underground at the time of submodule assembly because of the delicate nature of the coated surface and the smoothness requirement.

Assembly of submodules from the parts is carried out inside the cryostat. An assembly table with a precision alignment bar for rapid profile alignment is used for this task. The package is opened on the table and the FRP frame is assembled with four L-brackets and sixteen 5.61 cm (2.21 in) threaded rods through the G10 insert and eight 5.77 cm (2.27 in) threaded rods through G10 inserts held by the plastic nuts. These nuts are first hand-tightened and then set with a torque wrench.

Once the frame is assembled, aluminum profiles are inserted through the corresponding slots on the 15.2 cm (6 in) on either side. One slip-nut is inserted onto the center rib rail prior to the profile insertion. Care must be taken to ensure that the profiles are not scratched during the insertion process.

Once all profiles are inserted into the frame, each of the profiles is mounted onto the I-beam using two 45 mm M4 button head hex drive stainless steel screws into the aluminum slip nut. When all screws are hand-tightened as much as possible, the final torque is applied using a torque wrench. The final alignment of the profiles is then made by hand, tightening only one or two screws, as necessary. A wheel base made of unistrut bars is then mounted to the bottom of the submodule and the entire unit is placed in a designated area to await installation. The wheel is clearly labeled with the submodule number for tracking purposes.

#### **4.4.2 Cathode Plane**

Each cathode module is assembled off-site and shipped to SURF in its transport container. The containers are transported underground to the cryostat and opened in front of the cryostat. The cathode module is then inserted into the cryostat for installation.

#### **4.4.3 Ground Plane**

Each ground grid module is assembled off-site and shipped to SURF in its transport container. The containers are transported underground to the cryostat and opened in front of the cryostat. The ground grid module is then inserted into the cryostat for installation.

#### 4.4.4 Electrical Interconnections

The HVDBs are mounted on the profiles as the submodules are built. For optimization purposes, one DP module HVDB connects 11 FC stages. One 12 m tall module is covered by fifteen 11-stage HVDBs, and one 10-stage HVDB is at the bottom to make the final connection. One row of HVDBs is mounted every four FC modules. All connections and electrical functionality must be checked with a high-sensitivity electrometer.

### 4.5 Interfaces to the HV System

#### 4.5.1 Cryostat

Each FC module is suspended and raised by two ropes hung from the cryostat roof through the FC suspension feedthroughs, by winches as in ProtoDUNE-DP.

Once an FC module of the full height is completed for DP module, it will be hung from the cables attached to the final suspension hooks. The suspension feedthroughs are then fully sealed. A possible improvement on the ProtoDUNE-DP interface is to use remote-controlled electrical winches (as opposed to manual) to ensure synchronized lifting of the modules.

#### 4.5.2 Charge Readout Plane

No direct hardware interface exists between the HV and CRP systems. The cryostat penetrations and feedthroughs for the two systems are completely independent, as are their control electronics. The only interface envisaged includes a system to ensure the appropriate physical separation between the top-most field-shaping profile and the CRP extraction grid.

#### 4.5.3 Photon Detection System

No direct hardware interface exists between the HV and PD systems. The cryostat penetrations and feedthroughs for the two systems are completely independent, as are their control electronics. The only interfaces envisaged include (1) maintenance of a safe minimum distance between the PDs and the  $-600$  kV cathode; and (2) definition of the PD power dissipation limit (production of bubbles would compromise the HV stability). The power dissipation depends on the final PD density chosen, which is awaiting simulation results. Aspects of the cathode design are also awaiting simulation results to determine its impact on the PDS. These interfaces are effectively at the level of design requirements.

## 4.6 Transport, Handling and Integration

The FC FRP beams and G10 parts are shipped in a standard wooden crate. Parts for each submodule are packed into one flatpack of dimensions  $0.2\text{ m} \times 0.2\text{ m} \times 2\text{ m}$  sealed in multiple layers of shrink wrap and a thick soft cushion of plastic for edge protection. Due to the compact size of each submodule package and since a total of 530 or so submodules are expected, including 10% spare, the total number of crates for FRP parts to be transported down the shaft will be small. Given the dimensions of the hoist cage, an optimal crate size could be  $1.2\text{ m} \times 1.5\text{ m} \times 2.3\text{ m}$ , each containing 30 flatpacks of FRP parts.

The extruded aluminum profiles for FC are shipped separately in standard wooden crates. A total of 197 profiles are needed for each 12m module. Therefore, the total number of profiles to be transported down underground would be of the order 18,000, including 10% spares. The same number of aluminum clips are also shipped in standard wooden crates and are transported underground separately.

The cathode modules of dimension  $3\text{ m} \times 3\text{ m}$  are assembled off-site and shipped to SURF in their transport containers. Given the paucity of storage space at the 4850L, the cathode plane is assembled as each unit cathode plane arrives at the cavern – in its assigned order – and is unwrapped. The cathode plane is assembled inside the cryostat by connecting the cathode units mechanically and electrically, taking into account the constraints imposed by the installation of the ground grid modules and the photomultiplier tubes (PMTs).

The integration starts from the cryostat end opposite to the temporary construction opening (TCO). The field cage modules covering the 12 m long side of the cryostat are installed first. This installation is followed by the CRP installation, which requires access to the cryostat floor. Once a  $3 \times 12\text{ m}^2$  strip of CRP modules is installed, the corresponding field cage side modules are installed followed by the installation of the four cathode modules. The four ground grid modules are initially attached to the cathode modules allowing access for the removal of the false floor and the subsequent installation and cabling of the photomultipliers below the cathode modules. After the installation of the photomultipliers, the ground grid modules are lowered to their final positions. This installation sequence is repeated until the entire detector is complete. The field cage modules covering the endwall on the TCO side are installed before the installation of the last  $3 \times 12\text{ m}^2$  cathode strip.

The power supply, feedthroughs and HV extender are sent to SURF in standard shipping crates. Unwrapping requires clean areas and careful handling. Surfaces can be cleaned with alcohol and allowed to dry.

## 4.7 Quality Control

The assembly, testing, transport, and installation procedures required to ensure adequate QC of all HV system components are being defined, tested and documented during the construction of



ProtoDUNE-DP.

The FC submodules are assembled inside the cryostat on an assembly table with a precision alignment bar, as in ProtoDUNE-DP. Each submodule-FRP part package is visually inspected for external damage and is opened carefully to avoid damage to the FRP parts. The bags of hardware are removed and set aside. The two 15.2 cm (6 in) I-beams, two 7.62 cm (3 in) I-beams and connecting L-brackets are visually inspected for damage during transport. Once the FRP parts pass the inspection, they are assembled into the frame on the table.

The aluminum profiles are visually inspected and felt by hand for severe scratches and any excess sharp points. The profiles that pass are inserted into the profile slots on the FRP submodule frame, with one alignment-fixing slip nut inserted into the rail on the reinforcement rib, and follow the assembly and alignment process described in Section 4.4.1. The alignment of the profiles is checked using a straight-edge along one end of the profile. The submodules that pass are put on the wheel base and stored for installation.

The HV divider boards are tested on-site for resistance of each stage at room temperature to ensure the integrity of the board and each electrical connection of the resistors before installation onto the submodule.

At SURF, cathode and GP modules are checked for the required planarity and mechanical integrity. Also during the installation phase the electrical continuity between the modules is checked.

The feedthrough and the HV extender are tested simultaneously at the testing facility site (possibly at CERN or the integration and test facility (ITF)), preferably with the planned power supply. To pass, the feedthrough must hold the goal voltage ( $-600$  kV) in ultra pure LAr (TPC-quality purity corresponding to a free electron lifetime,  $\tau \geq 7$  ms) for at least 24 hours. The ground tube submersion and E field environment of the test setup must be comparable to the real FC setup or more challenging. Additionally, the feedthrough must be UHV-grade leak-tight.

Upon arrival at SURF the power supply used in the DP module HV system is tested before installation, with output voltages and currents checked on a known load.

## 4.8 Safety

In all phases of HV system development of the DP detector module, including fabrication, installation, and operations, safety is the highest priority. As for ProtoDUNE-DP, assembly, testing, transport, and installation procedures will be documented. Explicit attention is paid to the transferability of the ProtoDUNE-DP procedures to the DP detector module; the most critical of these are noted in the preliminary ProtoDUNE-DP risk assessment document<sup>5</sup>.

The structural and electrical designs for the dual-phase (DP) HV system are based on designs that are vetted and validated in the ProtoDUNE-DP construction, which is currently in its final phase

---

<sup>5</sup>CERN EDMS document number 1856841.

of deployment at CERN. In parallel with the ProtoDUNE-DP construction and operation, HV tests at CERN are planned using a full-voltage and full-scale HV feedthrough, power supply, and monitoring system in dedicated HV test facilities. This also provides an opportunity to complete full safety reviews.

Operating the FC at its full operating voltage produces a substantial amount of stored energy. The modular design of the cathode specifically addresses this safety concern: in the event of a power supply trip or other failure that unexpectedly drops the HV, the charge stored in the segmented cathode structure limits the power dissipated. This design will be tested in ProtoDUNE-DP at 300 kV voltage over 9 m<sup>2</sup> surfaces segmented in four cathode modules.

Integral to the DP FC design, both in ProtoDUNE-DP and the DP detector module, is the concept of pre-assembled modular panels of field-shaping conductors with individual voltage divider boards. The structural design and installation procedures used in ProtoDUNE-DP were selected to be compatible with use at the far detector (FD) site and were vetted by project engineers, engineering design review teams, and CERN's safety engineers. Some revisions to these designs are expected based on lessons learned in installation and operations; these revisions will be reviewed both within the DUNE project and by Fermilab EH&S personnel. The overall design is on solid footing.

Assembly of the FC panels and resistor-divider boards does not present unusual hazards. The HV consortium will work closely with each assembly site to ensure that procedures meet both Fermilab's and institutional requirements for safe procedures, personal protective equipment, environmental protection, materials handling, and training. The vast majority of part fabrication will be carried out commercially, and shipping will be contracted through approved commercial shipping companies. Prior to approving a site as a production venue, the site will be visited and reviewed by an external safety panel to ensure best practices are in place and maintained.

## 4.9 Organization and Management

### 4.9.1 HV Consortium Organization

At present, the HV consortium is gathering institutions to participate in the design, construction and assembly of the HV systems for both SP modules and DP modules. The consortium needs to grow in the near future, and it hopes to attract new institutions, in particular from EU to balance USA participation with additional international participants.

The consortium management structure currently includes a consortium leader from CERN, a technical lead from BNL, and technical design report (TDR) editors from CERN and UTA.

In the current HV consortium organization, each institution is naturally assuming the same responsibilities it had for ProtoDUNE-DP. The consortium is organized into six working groups (WG) that are addressing the design and R&D phases, and the hardware production and installation.

Table 4.2: HV Consortium Participants

| Institution                                      |
|--|
| EU: CERN   |
| USA: Argonne National Lab                        |
| USA: Brookhaven National Lab                     |
| USA: University of California (Berkeley)         |
| USA: University of California (Davis)            |
| USA: Fermi National Accelerator Lab              |
| USA: University of Houston                       |
| USA: Kansas State University                     |
| USA: Lawrence Berkeley National Lab              |
| USA: Louisiana State University                  |
| USA: South Dakota School of Mines and Technology |
| USA: Stony Brook University                      |
| USA: University of Texas (Arlington)             |
| USA: Virginia Tech.                              |
| USA: College of William and Mary                 |

- WG1. Design optimization for SP and DP; assembly, system integration, detector simulation, physics requirements for monitoring and calibrations.
- WG2. R&D activities and facilities.
- WG3. SP-CPA: Procurement, in situ QC, resistive panels, frame strips, electrical connections of CPA modules, QC, assembly, shipment to assembly site / QC.
- WG4. DP Cathode.
- WG5. FC modules.
- WG6. HV supply and filtering, HV power supply and cable procurement, R&D tests, filtering and receptacle design and tests.

Merging of SP and DP groups is envisaged for the working groups where synergies are being identified: HV feedthroughs, voltage dividers, aluminum profiles, FRP beams, and assembly infrastructures.

## 4.9.2 Planning Assumptions

The present baseline design for all elements of the HV system for DP module strictly follows the ProtoDUNE-DP design as it has been produced and is being assembled. It is also assumed that no major issues in the HV system operation of ProtoDUNE-DP will be encountered and therefore

that the basic HV system concepts are sound.

However some design modifications and simplifications must be implemented to take into account the doubled drift distance, implying an increase in HV delivery to the cathode from  $-300$  kV to  $-600$  kV.

The DP HV system distribution and the related cathode structure still require intense R&D, given the unprecedented value of the required HV ( $-600$  kV). The related results could lead to revision of design details such as the shape of the cathode elements and of the GP structures, the distance from the cryostat walls, the distance between the cathode and the GP protecting the PDs, and resistive connections of the cathode modules. It is important to ensure that the E field intensity in the LAr is below the critical value of about  $30$  kV/cm everywhere and that the energy stored in the FC is not released catastrophically to the detector membrane.

As for the SP module, ProtoDUNE-SP serves as the test-bed for understanding and optimizing detector element assembly, installation sequence, and integration as well as requirements in human resources, space and tooling, and schedule.

# Chapter 5

## Photon Detection System

### 5.1 Overview

#### 5.1.1 Introduction

The dual-phase (DP) photon detection system (PDS) primarily serves three purposes. It provides the trigger for non-beam events; it enables determination of the event absolute time for beam and non-beam events; and it enables calorimetric measurements. It is essential to ensure that the DP PDS is optimized for the full DUNE physics program. In particular, low-energy signals like supernova neutrino burst (SNB) neutrinos and multi-messenger astronomy, other low-energy signals, and proton decay, impose more stringent requirements on PDS performance than the primarily higher energy, beam-synchronous, neutrino oscillation physics. The final specifications of the system will be determined so as to achieve these physics requirements. A number of scientific and technical issues impact the DP PDS and SP PDS in a similar way, and the consortia for these two systems cooperate closely. See Volume 2: Single-Phase Module, Chapter 5 for details on the SP PDS.

This chapter concentrates on direct projection of the ProtoDUNE-DP design to the DUNE scale. The optimization and final design of the DP PDS is driven by the ProtoDUNE-DP [6] data and simulation studies.

The chapter begins with an overview of the system in Section 5.1. Section 5.2 describes the photosensors, namely photomultiplier tubes (PMTs) and the related high voltage (HV) system, wavelength shifters and light collectors. The mechanics associated with the PMTs is described in Section 5.3, and the readout electronics in 5.4. Section 5.5 details the photon calibration system to monitor the PMT gain and stability. Then, the photon detector (PD) performance is described in Section 5.6, and the operations in Section 5.7. Interfaces with other subsystems are described in Section 5.8. Section 5.9 includes the installation, integration and commissioning plans. The quality control (QC) procedures are outlined in Section 5.10. The main safety issues to consider are

specified in Section 5.11. To finish, the management and organization is described in Section 5.12.

### 5.1.2 Physics and the Role of Photodetection

The main physics goals of the DP module are to register beam events and to operate outside of the beam spill as an efficient observatory for SNBs and proton decays. DUNE will also collect atmospheric neutrino and muon events, and will conduct searches for a number of exotic phenomena postulated by extensions of the standard model. Expected or searched for signals can range in energy from a few MeV to many GeV and have characteristic time duration and topological features that challenge the performance of large noble liquid TPCs. A critical part of the LArTPC is the PDS, sensitive to light produced by interactions in argon [7]. In DP TPCs, the timing of prompt scintillation light (usually referred to as the S1 signal) in LAr is needed for time stamping of events and propagation of tracks in the detector. The extraction and amplification of drift electrons in the gas phase (usually referred to as the S2 signal) yields information on the drift time and amount of ionization charge, thus supplementing information from the charge readout on the anode plane. The interplay between the charge and light from an event enables pattern recognition and the measurement of energy of interactions.

Ionizing radiation in liquid noble gases leads to the formation of excimers in either singlet or triplet states, which decay radiatively to the dissociative ground state with characteristic S1 fast and slow lifetimes (fast is about 6 ns, slow is about 1.3  $\mu$ s in LAr with the so-called second continuum emission spectrum peaked at the wavelength of approximately 127 nm, 126.8 nm with a full width at half maximum of 7.8 nm [8]). This prompt and relatively high-yield (about 40,000 photons per MeV) of 127 nm scintillation light is exploited in a LArTPC to provide the absolute time ( $t_0$ ) of the ionization signal collected at the anode, thereby providing the absolute value of the drift coordinate of fully contained events, as well as a prompt signal used for triggering purposes.

The secondary scintillation light S2 is produced in the gas phase of the DP module when electrons, extracted from the liquid, are accelerated in the E field between the liquid phase and the anode. The secondary scintillation in the argon gas (i.e., the vapor phase) is the luminescence in gas caused by accelerated electrons in the E field and in the large electron multiplier (LEM) anode through Townsend amplification. For a given argon gas density, the number of photons of this S2 signal is proportional to the number of electrons, the E field, and the length of the drift path in gas covered by the electrons. In an extraction field of 2.5 kV/cm in gas, one electron generates about 75 photons. The time scale of S2 reflects the extraction time of original ionization in the liquid phase into the gas phase, thus for about 1 kV/cm E field, this time scale is of the order of hundreds of microseconds. The time between the occurrence of the primary scintillation light and the secondary scintillation light is equivalent to the drift time of the electrons from the ionization coordinate to the LAr surface.

The baseline design of the light collection system calls for 20.3 cm (8 in) diameter cryogenic PMTs distributed uniformly on the floor of the cryostat and electrically shielded from the bottom cathode plane. The proposed density of PMTs and their arrangement follows the design of the ProtoDUNE-DP detector. On the other hand, modeling and simulations of light collection both for ProtoDUNE-DP and the DUNE detector modules are still ongoing. Therefore, even critical system parameters

and their impact on the physics reach are still tentative. Results from the ProtoDUNE-DP will provide the critical validation of simulations and will guide optimizations for the large DP module.

### 5.1.3 Technical Requirements

PMTs provide the sharpest time information of events in the LArTPC and in the gas phase of the extraction stage. Due to necessary wavelength-shifting of photons from the argon luminescence and shadowing by the cathode plane, the efficiency of light detection is challenging and requires careful mechanical, electrical, and optical designs. The DP PD consortium is presently in contact with PMT manufacturers, including Hamamatsu Photonics<sup>1</sup> in Japan, Electron Tubes Limited<sup>2</sup> in the USA and UK, and HZC<sup>3</sup> in China, to define optimal choice and configuration of PMTs satisfying our requirements, tentatively summarized in Table 5.1. These requirements will be reviewed based on the physics needs. For this, simulations and ProtoDUNE-DP results will be key.

PMTs will be installed at a baseline density of one per  $1 \text{ m}^2$ . The choice of the Hamamatsu R5912-MOD20 PMT is assumed as the baseline plan. Extension of the PMT light sensitivity region to the LAr light emission wavelength of 127 nm requires use of a wavelength shifter. Therefore, in the baseline plan, the hemispherical windows of the PMTs are coated with a thin layer of tetra-phenyl butadiene (TPB) [10] for wavelength-shifting into the range suitable for R5912 PMT photocathode sensitivity [9]. The PMTs have to be rigidly anchored to the bottom of the cryostat. Different PMT densities and placements along the walls are also being considered in simulations. The HV signal cables are routed along the cryostat walls to feedthroughs installed in the roof of the cryostat. Each PMT is controlled individually so that its gain can be individually adjusted to match the front-end (FE) dynamic range and S/N ratio. An average light yield of 2.5 photoelectron/MeV is required based on ProtoDUNE-DP simulations (see Section 5.6). The precision of the light yield requirement will be established after the completion of the full DUNE simulations.

The cathode plane, described in Chapter 4, is placed at a height of about 2 m above the bottom of the cryostat, and the PMT plane is distant enough from the cathode plane, taking into account the high electrical rigidity of the LAr phase. In order to protect the PMTs, the ground grid is installed and placed at an identical potential as the PMT photocathode (0 V). The PMTs are powered to values between 1.5 to 2.0 kV such that the PMT gain is  $\sim 10^7$  to  $10^9$ . Future developments on the quantification of possible TPB dissolution in LAr will be encouraged and followed [11].

### 5.1.4 Detector Layout

The PMT plane is placed far enough below the cathode plane to be sufficiently electrically shielded. According to the baseline plan, the PMTs are uniformly distributed across this plane with a density of 1 PMT/ $\text{m}^2$ , with a total of 720 PMTs installed. Other PMT configurations as determined by the simulations are also being considered. The PMTs are individually mounted to the cryostat floor.

<sup>1</sup>Hamamatsu Photonics™, [http://www.hamamatsu.com/resources/pdf/etd/LARGE\\_AREA\\_PMT\\_TPMH1286E.pdf](http://www.hamamatsu.com/resources/pdf/etd/LARGE_AREA_PMT_TPMH1286E.pdf)

<sup>2</sup>Electron Tubes Ltd™, <http://www.electron-tubes.co.uk//>

<sup>3</sup>HZC Photonics™, [http://hzcphotonics.com/en\\_index.html](http://hzcphotonics.com/en_index.html).

Table 5.1: Summary of tentative requirements for the DP module PDS. This table represents the baseline choice for the R5912-MOD20 PMT as manufactured by Hamamatsu Photonics [9] is made.

| Feature   | Goal                  | Comment  |
|---|-----------------------|--|
| <b>Optical</b>                                  |                       |  |
| Spectral response                               | 127 nm                | Wavelength shifters are required.  |
| Light yield                                     | 2.5 photoelectron/MeV | For ProtoDUNE-DP, final value depends on simulation results.                           |
| <b>Electronic</b>                               |                       |  |
| Minimum light signal                            | SPE                   | Required to perform the PMT gain measurement.  |
| Gain  | $\sim 10^6$ - $10^9$  | Given by PMT specifications.   |
| Noise (or signal/noise)                         | <1 mV                 | To distinguish SPE from noise, depends on PMT gain.                                    |
| Timing resolution                               | few ns                | To distinguish S1 from S2 component.   |
| Power   | < 0.2W/PMT            | Used successfully in the WA105 DP demonstrator.  |
| analog-to-digital converter (ADC) dynamic range | TBD                   | Depends on simulation results, see Section 5.4.3                                       |
| <b>Electrical</b>                               |                       |  |
| HV range  | 0–2500V               | Individual cable per PMT.  |
| HV resolution                                   | 1 V                   | Fine tuning of PMT gain.   |
| HV noise  | <100 mV               | Extra filtering is required.   |
| HV grounding                                    | Isolated              | HV outputs are floating, crate ground is independent of the return of the HV channels. |
| PMT placement                                   | Isolated              | PMTs electrically shielded from the TPC cage.  |
| <b>Mechanical</b>                               |                       |  |
| Temperature                                     | Cryogenic             | PMTs operated in LAr and tested in liquid nitrogen.                                    |
| Pressure  | 2 bar                 | The argon column is about 10 m high.   |



The exact location of the PMTs will be determined by the location of the other floor structures like the cryogenic piping. The outline of the DP module is shown in Figure 5.1.

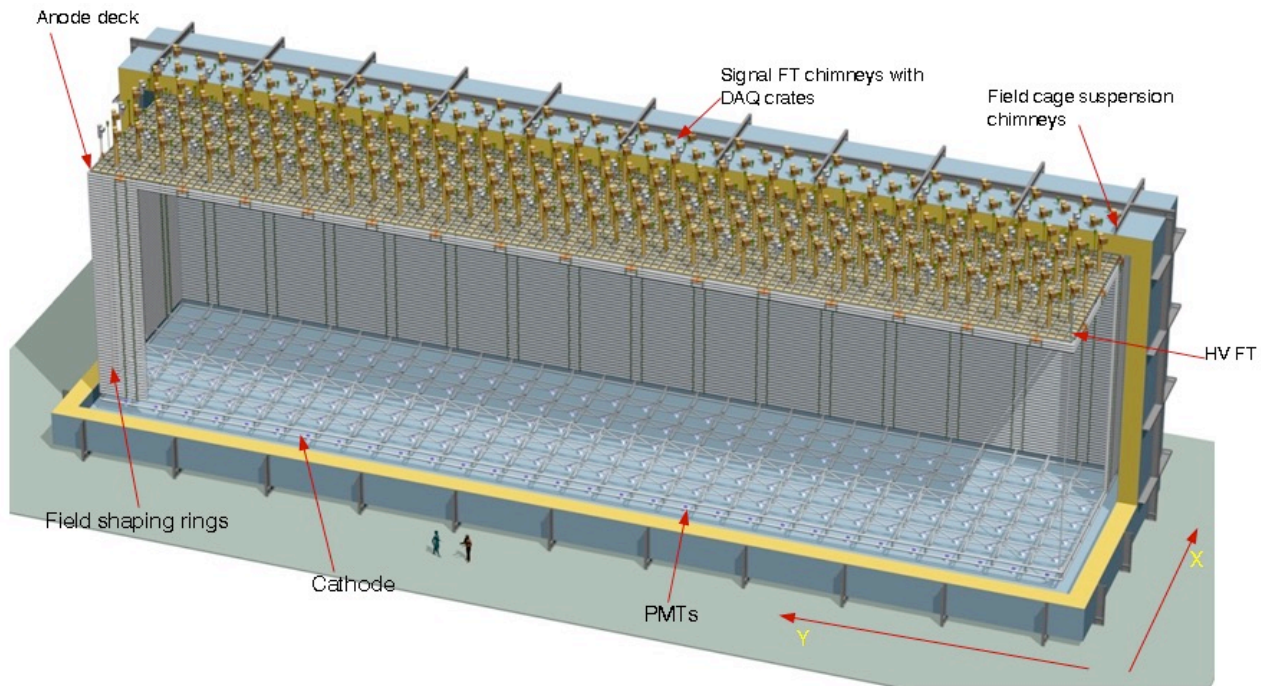


Figure 5.1: The DP module (partially open) with cathode, PMTs, FC and anode plane with chimneys.

Since few light sensors are directly sensitive to 127 nm, a wavelength shifter is required. A TPB coating directly on the PMT is the default plan. Light collectors to increase the photons detected are under study. A single cable per PMT carries power and signal, and splitters are placed outside the cryostat. A photon calibration system will be formed by external light sources and internal optical fibers.

The cable trays from the side walls of the cryostat to the PMTs carry the cables and calibration fibers. The cables and fibers are routed from the feedthrough flanges at the top of the cryostat and combined at the side wall trays. These side trays carry the HV/signal cables in blocks of 24 PMTs and four calibration fibers. Each block of 24 PMTs in a  $6 \times 4 \text{ m}^2$  area forms a sector of underground installation, with a total of 30 sectors.

### 5.1.5 Operation Principles

The physics program defines the operation principles of the DP module: the measurement of the neutrino oscillation parameters requires recording events based on an external trigger coming from the beam, while non-beam physics such as SNBs, proton decay, or other exotic transitions events, require special trigger conditions, including the PDS. PMT calibration, which has to be performed regularly, presents another operation mode wherein a hardware trigger provided by the calibration system starts the data recording.

Thus, the operation modes are:

- External trigger: the typical case is when the beam generates a hardware trigger, but it also includes software-generated triggers for test data;
- Non-beam physics trigger: the electronics based on the PDS signals provides the trigger for SNB, proton decay events, etc.;
- Calibration: during PDS calibrations, the trigger is provided by the light calibration system.

The external and non-beam physics triggers run in parallel to ensure that rare events such as SNBs are recorded effectively.

## 5.2 Photosensor System

### 5.2.1 Photodetector Selection and Procurement

The PD selected as baseline for the light-readout system is the Hamamatsu R5912-MOD20 PMT as used in ProtoDUNE-DP. The Hamamatsu R5912-MOD20, see Figure 5.2, is an 8-inch, 14-stage, high gain PMT (nominal gain of  $10^9$ ). In addition, this PMT was designed to work at cryogenic temperature adding a thin platinum layer between the photocathode and the borosilicate glass envelope to preserve the conductance of the photocathode at low temperature. This particular PMT has proven reliability on other cryogenic detectors. The same or similar PMTs have been successfully operated in other LAr experiments like MicroBooNE [12], MiniCLEAN [13], ArDM, ICARUS T600 [14], as well as in ProtoDUNE-DP [6]. Contacts with other manufacturers such as Electron Tubes Limited (UK) [15] and HZC (China) [16] are on-going to engage them in the program.

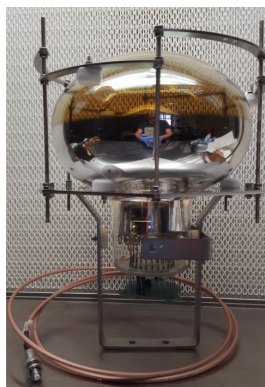


Figure 5.2: Picture of the Hamamatsu R5912-MOD20 PMT [9].

As the baseline number of PMTs,  $720 + 80$  spares, is high and several operations and tests have to be performed with them before the installation, the PMTs have to be ordered with sufficient time in advance to complete the following planned operations: assembly of the voltage divider

circuit, mounting on the support structure, testing at room and cryogenic temperatures, application of TPB coating, packing and shipment. They are re-tested at SURF before installation (see Sections 5.9 and 5.10). Considering the large number of PMTs required by DP PD, the purchase order must be completed at least two years ahead of installation. A staged or staggered order allowing us to receive a steady supply of PMTs would be most convenient.

## 5.2.2 Photodetector Characterization

Prior to installation, the most important parameters of the PMT response have to be measured with two aims: first, to reject under-performing PMTs and second, to store the characterization information in a database for later use during the DP module commissioning and operation.

The basic and most important parameters to characterize are the dark count rate versus voltage and the gain versus voltage. Both parameters must be measured at both room and cryogenic temperatures. Prepulsing and afterpulsing are not expected to be an issue, but will be measured, too.

From the mechanical point of view, the test setup requires a light-tight vessel filled with a cryogenic liquid (argon or nitrogen) plus the infrastructure for filling and operating the vessel with temperature and liquid-level controls. For ProtoDUNE-DP, 10 PMTs were tested at a time over the course of a week, as cryogenic tests of PMTs require several days for the PMT thermalization. Figure 5.3 shows the ProtoDUNE-DP PMTs being installed in the testing vessel. Increasing the capacity of the vessel, and thus the number of PMTs to test simultaneously, will reduce the characterization test duration.



Figure 5.3: Picture of the PMTs being installed in the testing vessel used for the ProtoDUNE-DP PMTs.

Figure 5.4 shows the sketch of the envisaged setup for PMT characterization tests. From the electronics point of view, the test setup requires a HV power supply, a discriminator, a counter for

the dark rate measurements, a pulsed light source, and a charge-to-digital or analog-to-digital converter for the PMT gain versus voltage measurements. All those instruments must allow computer control to automate the data acquisition.

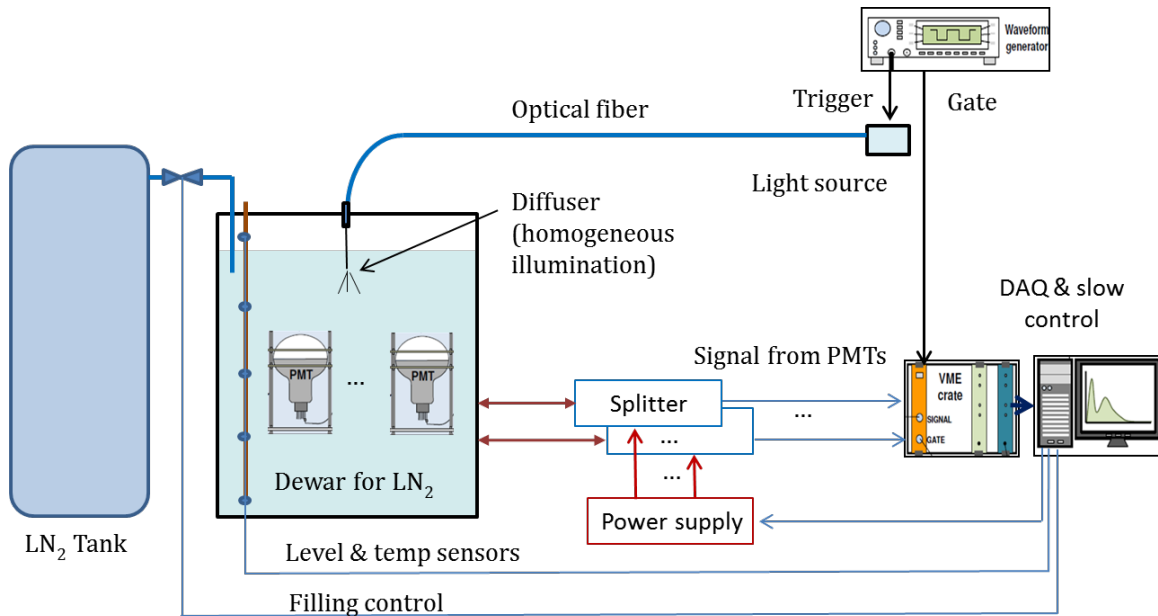


Figure 5.4: Sketch of the setup for PMT characterization tests.

### 5.2.3 High Voltage System

Based on the experience with the WA105 DP demonstrator prototype, the A7030 power supply modules from CAEN<sup>4</sup> form the baseline design of the PMT HV system. These modules provide up to 3 kV with a maximal output current of 1 mA and a common floating ground to minimize the noise. Module versions with 12, 24, 36, or 48 HV channels are available. The HV polarity can be chosen for each module. According to the baseline PMT powering scheme, modules with positive HV polarity will be acquired for the experiment. Modules with 48 HV channels and Radiall 52<sup>5</sup> connectors are under consideration. The corresponding HV cable connects the modules with the HV splitters, described in Section 5.4.2. This choice allows the design of a compact and most cost-effective system occupying only 1 to 2 racks. For 720 PMTs, 15 A7030 modules (+ 2 spares) are needed. These 15 HV modules will be installed in mainframes from CAEN.

Each PMT is powered individually thus allowing the gain of all PMTs to be equalized by adjusting the operating voltage. This will be software-controlled. The software must interface to the PMT calibration system (Section 5.5) in order to extract the calibration factors needed for the gain equalization.

<sup>4</sup>CAEN™, <http://www.caen.it/csite/CaenFlyer.jsp?parent=222>

<sup>5</sup>Radiall™, <https://www.radiall.com/>.

## 5.2.4 Wavelength Shifters

The DP module PDS requires waveshifting the 127nm scintillation photons into visible photons. Coating the PMT windows with a thin film of TPB has already been validated [10] and is adopted as the baseline plan. TPB is a wavelength shifter with high efficiency for conversion of LAr scintillation VUV photons into visible light, where the PMT cathode is sensitive. The TPB is deposited on the PMT by means of a thermal evaporator which consists of a vacuum chamber with two copper crucibles (Knudsen cells) placed at the bottom of the chamber, following the sanding of the PMT window. A PMT is fixed at the top of the evaporator, with its window pointing downwards, on a rotating support in order to ensure a uniform coating. The crucibles, filled with the TPB, are heated to 220 C. At this temperature, the TPB evaporates through a split in the crucible lid into the vacuum chamber, eventually reaching the PMT window.

Several tests were performed to tune some parameters, e.g., the coating thickness (TPB surface density) and the deposition rate. A PMT mock up covered with mylar foils was used for the tests. A TPB density of  $0.2 \text{ mg/cm}^2$  – the value where the PMT efficiency is stable as a function of the density – was chosen for ProtoDUNE-DP. Efficiency measurements were performed using a VUV monochromator by comparing the cathode current of a coated PMT with the current value of a calibrated photodiode. As a result of the efficiency tests, about 0.8 g of TPB must be placed in the crucibles at each evaporation, in order to achieve the desired PMT coating density. This value optimizes the quantity of TPB used per evaporation while keeping the coating density fluctuations below 5%. With these specifications, two to four PMTs can be coated per day at a single coating station. Multiple coating stations will be required in order to remain on schedule.

## 5.2.5 Light Collectors

Although we are still lacking detailed physics simulations of photon collection in the full DP modules, it can be generally argued that further optimization (i.e., cost balanced against physics reach) of light collection is desirable. In addition to maximizing the overall light yield, another crucial figure of merit is the uniformity of the light collection efficiency within the full DP modules active volume. Geometrical acceptance effects, as well as light absorption processes at the detector boundaries and within the LAr itself, can greatly degrade the uniformity in response. Active detector regions close to the FC and further away from the cathode are the most affected. As a result, differences of up to an order of magnitude in response throughout the active volume are not uncommon in a LArTPC.

In the case of a LArTPC, there are at least four main parameters for optimizing the light yield and the uniformity in response: (1) the number of PMTs per unit area, (2) the placement of PMTs, (3) the augmentation of PMTs with additional light collectors, and (4) the choice of where and how the original 127 nm photons can be wavelength-shifted. The most obvious direction for optimizing cost effectiveness are the latter two options. Detector components that are not strictly part of the PDS may also play a role in this optimization process, one relevant example being the transparency of the cathode plane. The options to use shifter-reflectors (Winston cones) to increase the effective area of individual PMT windows, or to move shifting of light closer to the cathode and attaching

wave guides coupled to the PMTs, are under study.

Another promising and cost-effective option to increase both light yield and response uniformity is the use of TPB-coated reflector foils covering the detector inner walls. This option is routinely used in DP LArTPCs searching for dark matter, such as the ArDM [17] experiment. This is also under investigation for the SP module concept, building on the experience already accumulated with the LArIAT experiment, and the one to be gained with SBND. In the DP case, up to four of the six inner faces of the TPC – those corresponding to the FC structure – could be covered with dielectric foils. The same wavelength shifting (WLS) used to coat the PMT windows, TPB, would be vacuum-evaporated on the foils. The shifted blue light emitted by the foils would then have a greater chance of reaching the PMT windows compared to 127 nm light, owing to the better reflective properties given by the combination of foils and blue light. To be adopted, this concept would first need to demonstrate satisfactory stability on the timescale of the experiment duration.

## 5.3 Mechanics

An individual PMT mount has been designed and tested in the WA105 DP demonstrator prototype [18]. The same design is used for ProtoDUNE-DP and is planned for the DP module. A PMT with this mechanical structure is shown in Figure 5.2. The support frame structure is mainly composed of 304L stainless steel with some small Teflon (PTFE) pieces assembled by A4 stainless steel screws that minimize the mass while ensuring the PMT support to the cryostat membrane. The design takes into account the shrinking of the different materials during the cooling process so as to avoid breakage of the PMT glass. Over-pressure tests were carried out for ProtoDUNE-DP, and further tests to ensure the correct performance under pressure will be carried out.

A uniform array of 720 cryogenic Hamamatsu R5912-MOD20 PMTs, below the transparent cathode structure, is fixed on the membrane floor in the areas between the membrane corrugations. The arrangement of the PMTs accommodates the cryogenic piping on the membrane floor, and other elements installed in this area.

The mechanics for the attachment of the PMTs has been carefully studied for ProtoDUNE-DP. It must counteract the PMT buoyancy while avoiding stress to the PMT glass due to differentials in the thermal contraction between the support and the PMT itself. The attachment is done via a stainless steel supporting base that could be point-glued to the membrane. The weight of the support and PMT exceeds the buoyancy force of the system. Given the large standing surface of the stainless steel plate support basis, these supports also ensure stability against possible lateral forces acting on the PMTs due to the liquid flow. Figure 5.5 depicts the PMT together with its support base attached to the bottom of the cryostat.

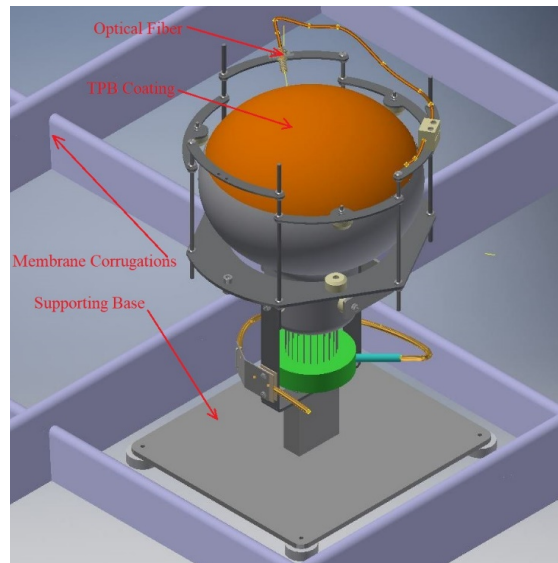


Figure 5.5: Cryogenic Hamamatsu R5912-MOD20 PMT fixed on the membrane floor, with the optical fiber of the calibration system.

## 5.4 Readout Electronics

### 5.4.1 Photomultiplier High Voltage Dividers

The ProtoDUNE-DP PMT power supply has a grounded cathode and positive HV applied to the anode. A single cable for each PMT carries both power and signal. This configuration, which requires half as many cables and feedthroughs on the detector as would the negative voltage configuration, offers a clear advantage given the large number of PMTs in the detector module. In addition, the cathode grounding shows fewer dark counts than the anode grounding scheme. Although a coupling capacitor must be used to separate the HV from the PMT signal, this signal and power splitting can be done externally, mitigating this drawback. Figure 5.6 shows the positive power supply and cathode grounding scheme.

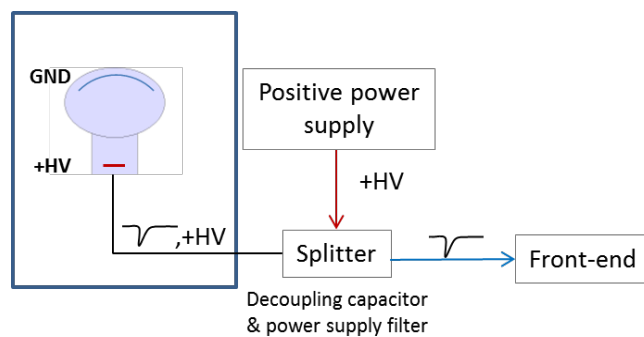


Figure 5.6: Positive power supply and cathode grounding scheme.

The PMT base circuit uses only resistors and capacitors. The components are carefully selected and tested to minimize the variations in their characteristics with temperature. The polarization

current of the voltage divider (total circuit resistance) is chosen to meet the PMT light linearity range and maximum power requirements. The dynodes' voltage ratio will follow the manufacturer recommendations for increased linearity range on the space-charge effect area (tapered divider). In addition, capacitors are added to the last stages to increase the PMT linearity in pulsed mode. The precise values for the components have not been decided yet, as they depend on concrete requirements and also on the results from ProtoDUNE-DP. The ProtoDUNE-DP design is considered as the baseline solution.

For the connection between the PMT base and the feedthrough, the RG-303/U cable was selected for its low attenuation and its proven reliability in cryogenic environments. This cable is directly soldered to the PMT base on one side, and it ends with an SHV connector on the other side for attachment to the flange.

## 5.4.2 High Voltage and Signal Splitters

HV and signal splitters are used to separate the fast PMT response signal from the positive HV with capacitive decoupling. A low-pass filter between the HV supply and the PMT reduces the noise.

It is possible for radiated electromagnetic interference (EMI) picked up by the cables and conducted noise from the HV power supply to be synchronous across many PMT channels (i.e., coherent noise). This noise could add up to produce false detector triggers. Since the PMT signal can be as low as a few mV, control of the EMI over the circuit is very important. The splitter HV input filter is intended to reduce the EMI induced and conducted by the power supply cables. Enclosing each splitter channel in its own metallic grounded box reduces the EMI directly received in the splitter circuit and the cross-talk between different splitter channels.

Figure 5.7 shows a generic splitter circuit where R1 and C1 form the HV input low-pass filter (with a cut-off frequency below 60 Hz). The resistor R7 and the LED are for safety purposes only, warning when HV is applied to the splitter. The C4 capacitor splits the signal coming from the PMT from the HV, and R2 prevents the PMT signal from going to ground through the C1 capacitor. R4 and R5 are zero  $\Omega$  optional resistors that allow some flexibility in the grounding configuration. Finally, R3 ensures the discharging of C4 if the splitter is not connected to the 50  $\Omega$  input at the data acquisition (DAQ) system. The RC constant of the capacitor C4 and the load (50  $\Omega$ ) must be as large as possible to minimize baseline oscillations due to the charge-discharge of the capacitor. Values of C4 between 150 nF and 300 nF have already been tested in the WA105 DP demonstrator.

For the connections between the HV power supply and the splitters, and between the splitters and the cryostat feedthroughs, the HTC 50-3-2 cables have been chosen as baseline. The HTC 50-3-2 has a similar attenuation as the RG-303/U (used inside the cryostat), but with a factor of 8 to 10 lower cost. Both cables are attached on one side directly to the HV splitter and have an SHV connector on the other end. An RG-58 cable terminated on the connector required by the FE card provides the connection between the splitter and the FE.





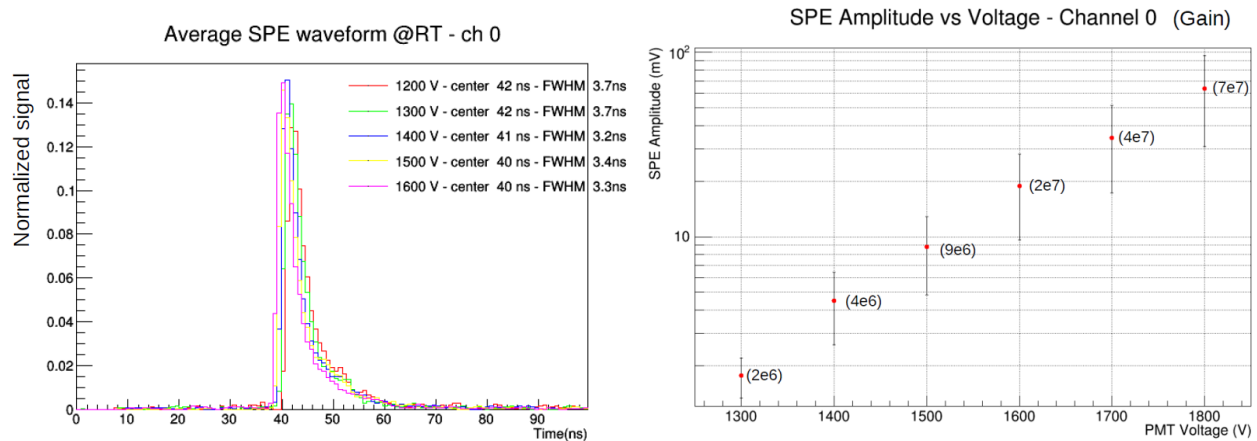


Figure 5.8: SPE waveforms and amplitudes from the WA105 at different voltages.

To calculate the PMT gains, the SPE charge measurement will be performed. Depending on the PMT gain, the SPE amplitude varies from the mV level to hundreds of mV, as shown in Figure 5.8. Due to the very long cables from the PMTs to the FE electronics, the noise into the cables could be high. If one considers a noise level around 1 mV, the PMT gain must be set to  $10^6$  or higher in order to distinguish the SPE from noise. The average SPE pulse width is around 3.5 ns full width at half maximum (FWHM). In order to digitize this signal to reconstruct it with fidelity, a sampling period on the order of ns is required.

The sampling frequency also affects the time tagging precision. The time uncertainty due to the PMT alone is around 3 ns (transit time spread). Other factors, e.g., Rayleigh scattering, increase this uncertainty, as does the sampling period; therefore, the lower sampling frequency, the better. In the WA105 DP demonstrator 4 ns sampling was used to digitize waveforms.

The rate of the events observed in the WA105 DP demonstrator was around 300 kHz with the threshold at the SPE level. The rate at the DP module, is not yet known, but expected to be much larger despite the underground location. The time-tagging system needs to process events at high rates to ensure that no events are lost. Figure 5.9 shows the event rates for different trigger thresholds observed in the WA105 DP demonstrator.

The light signal has to be synchronized with the DAQ. All the DAQ electronics use the White Rabbit (WR) protocol for synching. A dedicated WR Micro Telecommunications Computing Architecture ( $\mu$ TCA) [19] slave node is on the light readout FE electronics as sync receiver, distributing clocks to the different FE cards.

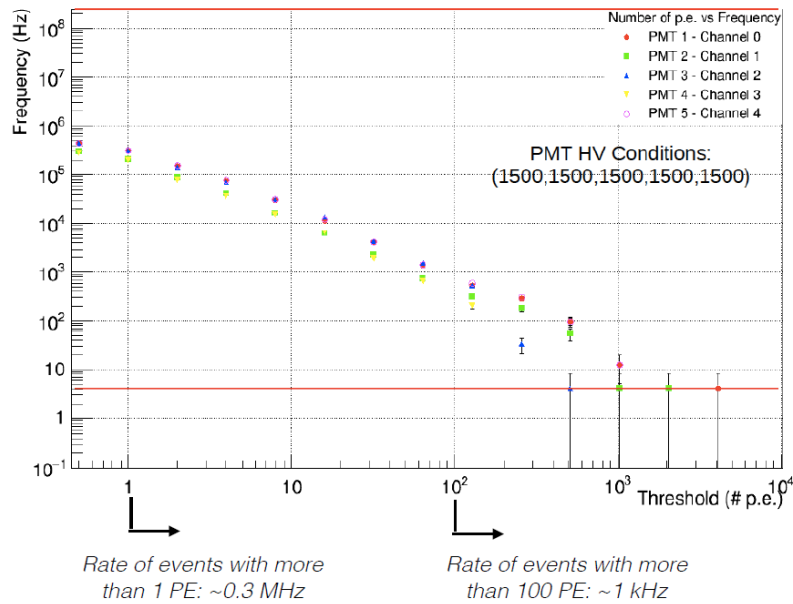


Figure 5.9: Event rates for different trigger thresholds observed in the WA105 DP demonstrator .

## 5.5 Photon Calibration System

### 5.5.1 System Design and Procurement

A photon calibration system is required to be integrated into the DP module to calibrate the PMTs installed in the LAr volume. The goal is to determine the PMT gain and maintain the PMT performance stability. A design similar to the one used in ProtoDUNE-DP will be used although some R&D measurements are planned to make it more effective, reduce the cost and mitigate issues related to the scaling.

In ProtoDUNE-DP, an optical fiber is installed at each PMT in order to provide a configurable amount of light (see Figure 5.5). The calibration light is provided by a blue LED of 460 nm using a Kapuschinski circuit as LED driver; this is much less expensive than using a laser. One LED is connected to one fiber that goes to one female optical feedthrough from Allectra <sup>6</sup> In total, six LEDs are placed in a hexagonal geometry. The direct light goes to the fiber, and the stray light to a silicon photomultiplier (SiPM) used as a single reference sensor in the center. Fibers of length 22.5 m (from Thorlabs  $\phi$  800  $\mu$ m, FT800UMT, <sup>7</sup> and stainless-steel jacket) are used inside the cryostat. Each of these fibers is attached to a 1 to 7-fiber bundle (from Thorlabs  $\phi$  200  $\mu$ m, FT200UMT <sup>8</sup> stainless-steel jacket common end, and black jacket at split ends), so that one fiber is finally installed at each PMT. A diagram of the ProtoDUNE-DP photon calibration system is shown in Figure 5.10.

<sup>6</sup>Allectra™, <http://www.allectra.com/index.php/en/>.

<sup>7</sup>Thorlabs™, <https://www.thorlabs.com/thorproduct.cfm?partnumber=FT800UMT>.

<sup>8</sup>Thorlabs™, <https://www.thorlabs.com/thorproduct.cfm?partnumber=FT200UMT>.

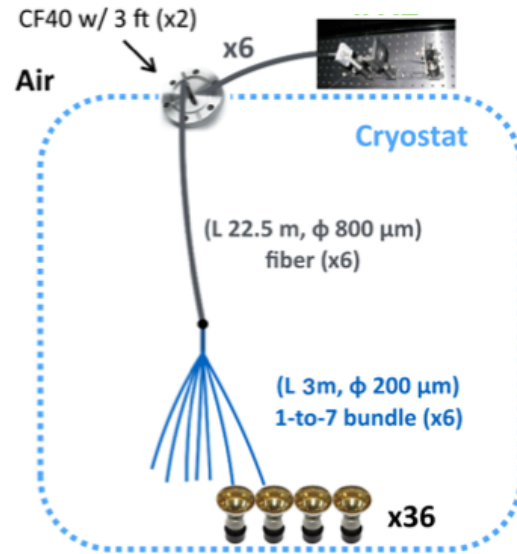


Figure 5.10: Diagram of the photon calibration system to be implemented in ProtoDUNE-DP

Assuming the ProtoDUNE-DP design for the DUNE DP module with 720 PMTs, 120 bundles, 120 fibers, 120 light sources, 120 flange feedthroughs, and 20 reference sensors are needed. The length of the fibers and bundles has to be calculated considering the exact position of the feedthrough flanges. The number of flanges required to host 120 SMA feedthroughs will depend on their size. However, alternatives to this design will be pursued with R&D measurements in order to reduce the amount of fibers, study other options for the reference sensor, and increase the input light if necessary. In order to reduce the number of fibers, light diffusers can be used, so that one fiber can illuminate at least 4 PMTs. For instance, a diffuser could be placed at the ground grid.

## 5.5.2 Validation Tests

In order to validate the design, the most important result will come from the ProtoDUNE-DP performance. In any case, since the fibers to be used in DUNE FD will be longer, dedicated calculations and measurements to confirm that sufficient light reaches the PMTs will be performed. Also, alternative designs, will be validated in different laboratories. The possibility of using a diffuser can be tested in a vessel. The light source will also be validated by studying the different options in the lab. All these measurements will be performed at room temperature and in liquid nitrogen to test the behavior at cryogenic temperatures.

Once the design is fixed, basic characterization measurements will be performed on the fibers upon receiving them from the manufacturer. Those measurements will consist of providing light with a known source and measuring the output with a power meter. Measurements at cryogenic temperatures may not be needed at this point.

Finally, during the photon calibration system installation, each fiber and source will be re-tested to check that the expected light is arriving to each PMT using a photodiode. A dedicated procedure

will be designed with this purpose, similar to the one used in ProtoDUNE-DP.

## 5.6 Photon Detector Performance

To define the PDS performance, a good understanding of the light generation is needed. For this, optical simulations and a good knowledge of the light properties are required. The DUNE experiment expects to record not only accelerator neutrino interactions, but also rare non-beam events such as SNBs or nucleon decays. In those cases, an internal trigger is required: an optimized light collection system is hence mandatory. This section describes the tools developed in the consortium for the light simulation in large detector volumes for these purposes.

The main feature of a LArTPC detector is to collect electrons produced by the energy loss of charged tracks when crossing the volume. This signal provides a high resolution 3D image of the event. The reconstructed topology and the amount of charge collected gives the characterization of the tracks (identification and energy). Together with the charge, scintillation light is also produced in LAr. There are many advantages to collect and exploit the scintillation signal. As only a fraction of the initial energy deposition is converted into electrons, the rest being emitted as photons, light collection can improve the calorimetry of the detector. The light signal can provide the  $t_0$  of the event, which is a necessary observable for a proper reconstruction. The study of the slow component can give insights into the purity of the LAr.

When energy deposition occurs, either the knocked argon atom gets excited or an electron is ejected. In the latter case, the probability of the ejected electron being recaptured by an argon ion depends on the drift field and on the amount of energy deposited. This case also produces an excited argon state. In either case, in order to decay to the ground state, the excited argon atom combines with another argon atom to form an excited excimer. A photon at 127 nm is then emitted, returning the excimer to the ground state. As the excimer can be formed in a singlet or triplet state, two time constants will be observed: the singlet at 6 ns and the triplet at 1.3  $\mu$ s. These principles are sketched in Figure 5.11.

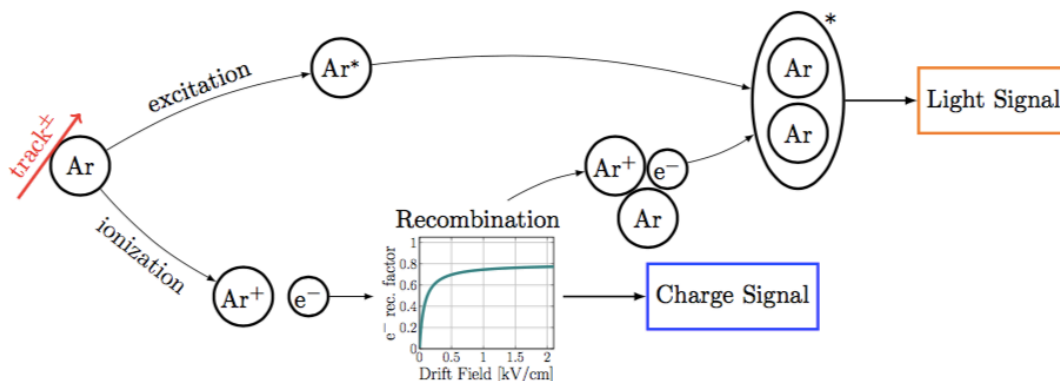


Figure 5.11: A sketch depicting the mechanism of light production in argon.

In the DP technology two light signals produced, one (S1) when a charged particle crosses the LAr volume and the second (S2) once the particle is above the liquid surface in the argon gas. As

electrons drifting in the gas enter high field regions (such as the extraction field or the amplification field in the LEMs), their velocities increase and Townsend avalanches occur. This current of electrons produces electroluminescence light with the same wavelength and similar time structure as for the S1 signal. The S2 light is expected to be an irreducible background for the light studies in ProtoDUNE-DP, since the detector is on the surface. Indeed, the S2 signal can last as long as the total drift time of the electrons: 0.625 ms per meter of drift at a drift field of 500 V/cm.

Table 5.2 summarizes the default optical parameters chosen for the light simulation methods described in Section 5.6.1. The LAr optical properties are the subject of significant discussions in the community, in particular regarding the LAr absorption length and the Rayleigh scattering length. The former affects the collected light yield whereas the latter mostly affects its uniformity and timing resolution. The absorption and reflection of the VUV photons on stainless steel (i.e., the drift cage, cathode, extraction grid and ground grid) and on copper (the LEM surfaces) are poorly known, largely because those reflection coefficients depend strongly on the polishing procedure.

The measurement of the quantum efficiency of the PMTs at VUV wavelengths requires a specific setup operating in vacuum since VUV photons are absorbed in air. The PMT quantum efficiencies in the WA105 DP demonstrator PMTs were measured before and after the TPB coating using a LED that could emit light in the 200 to 800 nm range.

Finally, the electroluminescence gain  $G$ , defined as the number of S2 photons produced per extracted drifting electron, is also subject to discussion. Experimental measurements of  $G$  have been performed in a setup quite similar to the amplification design of the DP technology, although the measurements were made above the LEM [20]. In our case, the S2 photons are the ones leaving the LEM from below, where the number can be significantly lower.

Table 5.2: Default optical parameters chosen for the light simulation methods. Below the thick line are presented some quantities used in our studies although they are not linked to the optical properties of the LAr.

|                            | VUVs photons<br>$\lambda = 127 \text{ nm}$ | Shifted photons<br>$\lambda = 435 \text{ nm}$ |
|----------------------------|--|---|
| Absorption length          | $\infty$                                   |   |
| Rayleigh scattering length | 55 cm                                      | 350 cm  |
| Absorption coefficients    | 100%                                       | 50%   |
| LAr refractive index       | 1.38                                       | 1.25  |
| PMT quantum efficiency     | 0.2  |   |
| Electroluminescence gain   | 300  |   |

To understand the performance of the PDS, it is important to take into account the following indicators:

- Overall detected light yield, in photoelectrons per MeV of deposited energy in LAr;
- Uniformity of the light yield across the entire LArTPC active volume;
- Event time resolution extracted from the detected photon signal.

In turn, these indicators directly affect the strategy and performance of the DP module trigger system (Section 5.7), and determine whether the PD technical design is sufficient to meet the DUNE physics goals. These higher-level studies will be available on the technical design report (TDR) timescale.

Our current understanding of these performance indicators is largely based on ProtoDUNE-DP simulations and the current status of the simulation work is discussed in detail in Section 5.6.1. Work is focused on ProtoDUNE-DP in a first phase, and will expand to the DP module. For a realistic ProtoDUNE-DP geometry, an average light yield of 2.5 photoelectron/MeV is expected across the entire active volume. This promising yield assumes 36 8in PMTs located below the ProtoDUNE-DP cathode plane, averaging to one PMT per  $\text{m}^2$ . On the other hand, spatial non-uniformities in the PD response are found to be important and need to be modeled in detail. Variations as large as one order of magnitude both parallel to the drift direction (due to geometrical effects and absorption of light by LAr) as well as perpendicular to it (due to light absorption on detector boundaries) are obtained. The event time resolution due solely to light production and light propagation times, i.e., neglecting electronics and DAQ effects for now, is expected to be of order  $\mathcal{O}(100 \text{ ns})$  and hence largely sufficient for our purposes. These initial low-level performance estimates will be refined with more realistic simulations and with ProtoDUNE-DP data (Section 5.6.2) in the future. They will also be extended to the full DP module geometry on the TDR timescale.

## 5.6.1 Simulations

At zero drift field, when the electron recombination is maximum, roughly  $40,000 \gamma/\text{MeV}$  are produced. At the nominal drift field of  $500 \text{ V/cm}$ , then  $24,000 \gamma/\text{MeV}$  are generated. For reference, the energy deposited by a minimum ionizing particle (MIP) track is  $2.12 \text{ MeV/cm}$ . Given the size of the ProtoDUNE-DP ( $6 \times 6 \times 6 \text{ m}^3$ ) and the fact that it is located on surface, roughly 100 muons are expected to cross the fiducial volume during the 4 ms time window of the DAQ. With a full GEometry ANd Tracking, version 4 (Geant4) [21] simulation, it takes more than three hours to propagate all the photons emitted by a single MIP track crossing the ProtoDUNE-DP detector. A full optical simulation is hence computationally prohibitive. Three simulation approaches are being explored to provide the light simulation needed for the design optimization of the DP module.

### 5.6.1.1 Generation of light maps

In this method, the photons are propagated in a full dedicated Geant4 simulation only once. The main light characteristics needed for light studies (photon detection probability, called *visibility* hereafter, and time profile) are stored in a map in a ROOT [22] file format which can then be read by any other simulation program. This work was done first using LightSim, a dedicated software developed at LAPP, France. These maps have been adapted to be readable by LArSoft, where light maps are known as *photon libraries*. Work to generate them directly in LArSoft is in progress, in particular for S2 light, which has not yet been simulated for DP technology.

In the dedicated Geant4 code, special care has been taken to precisely describe all subdetector

components that might affect the light propagation: LEM plates, extraction grid, FC rings, the cathode and its supporting structure, and the ground grid above the PMTs. The LAr fiducial volume is then divided into voxels of  $25\text{ cm}^3$  and  $10^8$  photons are isotropically generated at the center of each voxel. The number of photons reaching each PMT, and their arrival times are stored. The light map can then be built from these results. For each voxel and for each PMT, the visibility is computed as:  $w = N\gamma^{\text{collected}}/N\gamma^{\text{generated}}$ . In order to be able to reproduce the time profile, each distribution is fit to a Landau function. From the fits, three parameters are extracted: the minimum time for photons to arrive to the PMT,  $t_0$ ; the peak of the distribution,  $t_{\text{peak}}$  from the Landau most probable value (MPV); and the distribution spread, the  $\sigma$  of the Landau function. These three parameters are stored in the light maps for each PD. The same procedure is done for the gaseous phase, although the voxel size is smaller in height (only 5 mm). In Figure 5.12, two fitted time distributions are presented. As is visible, the shapes of the time distributions depend strongly on the source-to-PMT distance. For close sources, the distributions are very sharp and the Landau description may not be the optimal function to use. On the other hand, for longer distances, the distribution is broader and the Landau fit reproduces the simulations quite well. For practical purposes, the Landau parametrization was used for all cases.

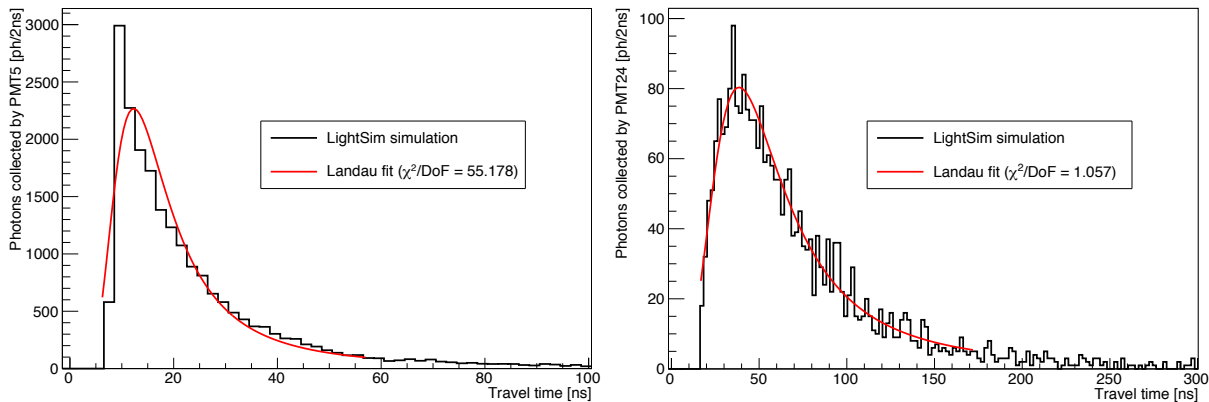


Figure 5.12: Landau fits (red line) of the travel time distributions (black histogram) for a source close to (left) and far from (right) the PMT.

As the map has been computed with discrete entries, an interpolation of the four light parameters ( $w$ ,  $t_0$ ,  $t_{\text{peak}}$ ,  $\sigma$ ) between the actual source position and the closest voxel centers is performed. An example of the distribution of the visibility and its 3D interpolation is presented in Figure 5.13. The loss of photons due to the cathode and ground grid are visible. For the ProtoDUNE-DP cathode and supporting structure design, and using the default optical parameters presented in Table 5.2, it has been shown that up to  $\sim 70\%$  of the photons generated in the active volume are absorbed by those structures before reaching the PMT array.

Table 5.2 presents the light propagation parameters used during the generation of the light maps. After generation, it is possible to study the loss of photons due to absorption using an approximation of the probability that the medium absorbs the photon as:  $p_{\text{abs}} = \exp(-\frac{D_{\text{travel}}}{\lambda_{\text{abs}}})$ . For the study of other light propagation parameters (Rayleigh scattering and absorption on the stainless-steel and copper) new maps have to be generated.

It takes roughly three days of computing to generate the light maps for ProtoDUNE-DP, even though only an eighth of the voxels need to be simulated, since the detector and the PMT po-



sitioning are symmetric. Generating maps for larger volumes such as the DP module, where the maximum source-to-PMT distance is around 60 m, could be too time-consuming. Moreover, the light simulation for the DP module is foreseen to drive the optimization of the positioning of the PMTs and will guide the studies of possible implementation of light reflectors. As most of the light propagation parameters in LAr are still subject to large uncertainties, these studies will have to consider various absorption and diffusion values. Therefore, it is crucial to find a faster way to simulate the light reliably, even at the cost of losing some precision.

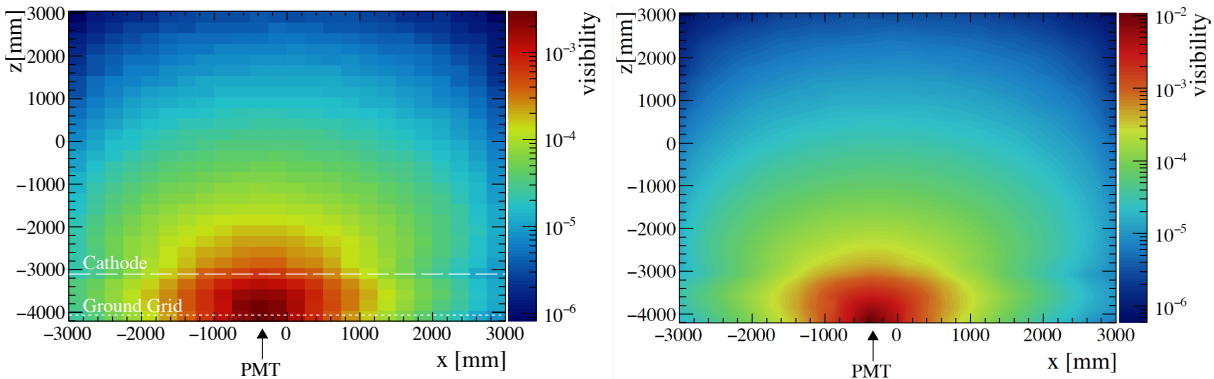


Figure 5.13: Evolution of the visibility seen by a central PMT (see arrow) in ProtoDUNE-DP as a function of different source positions in  $x$  and  $z$  ( $y$  is set at 0 mm). The position of the cathode and the ground grid are highlighted. Results are limited by the number of photons generated ( $10^7$  photons per voxel), and voxels with less than 50 photons arriving to the PMT are not taken into account. Left: discrete values from the maps, right: after 3D interpolation.

### 5.6.1.2 Parametrization from the Light Maps

Without considering the border effects where the photons are mostly absorbed, the visibility and the time profile depend only on the source-to-PMT distance.

This approach has been followed for the SBND [23] light simulation and is under consideration for the DP module as well. In Figure 5.14 the evolution of the visibility and the peak time as a function of the source-to-PMT distance are shown. On the left, the borders are taken into account, and the visibility structure is quite complicated due to the complexity of the light simulation in a closed space. However, on the right, the same evolutions are presented only for voxels at least 1 m from the active volume boundaries, and a clear correlation between distance and visibility is observed. As for the time distribution (here for the peak time, but the same goes for  $t_0$  and  $\sigma$  parameters), one can notice two different regimes when looking at all voxels, with a transition at a propagation distance of around 2 m. When considering only the central voxels, the evolution of the peak time is fully correlated with the propagation distance. The parametrization of the light propagation parameters as a function of the propagation distance is a promising option for very large volumes such as the DP module, at least for light sources far from the fiducial volume boundaries.

This preliminary study is quite encouraging for the light simulation in the DP module, at least for light sources far from the fiducial volume boundaries. Since it is complicated to disentangle the

effects due to the propagation and absorption parameters from the light maps, a careful dedicated study should be performed to get parametrization of the visibility and time distribution parameters as a function of the photon traveling distance.

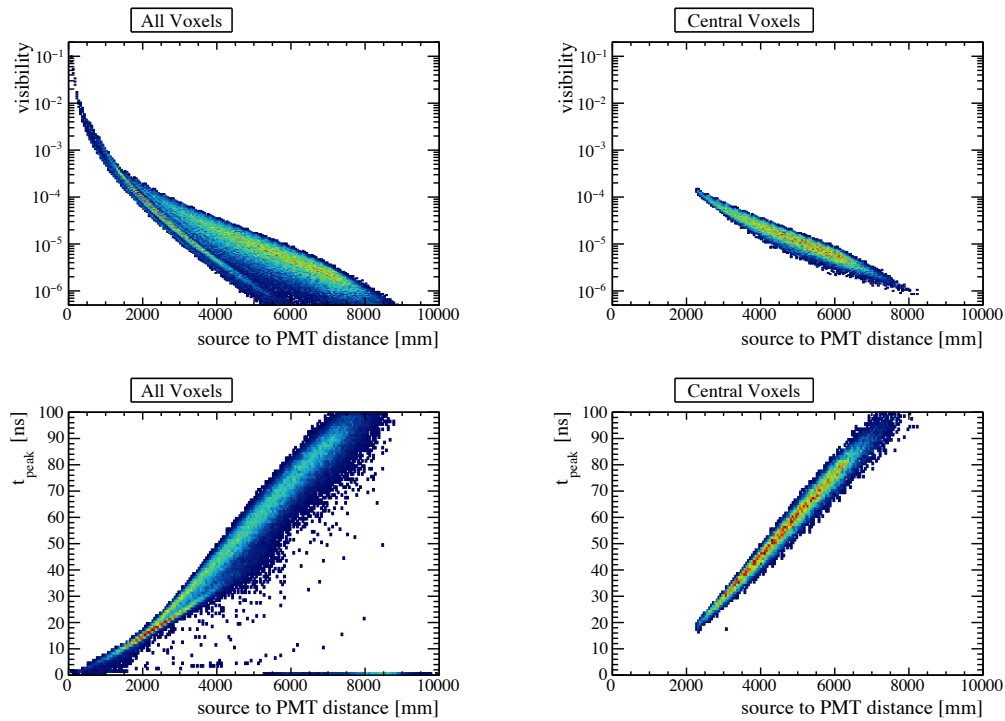


Figure 5.14: Evolution of the visibility (top) and peak time (bottom) as a function of the source-PMT distance as simulated in the ProtoDUNE-DP geometry (preliminary study). On the left, all voxels are included, on the right only the voxels at least 1 m away from the fiducial border are included.

### 5.6.1.3 Analytical approach

The propagation of light in a uniform material such as LAr can be described by the Fokker-Planck diffusion equation:

$$\frac{\partial}{\partial t} p(x, y, z, t) = D \left[ \frac{\partial^2}{\partial x^2} p(x, y, z, t) + \frac{\partial^2}{\partial y^2} p(x, y, z, t) + \frac{\partial^2}{\partial z^2} p(x, y, z, t) \right]$$

where  $D$  is the diffusion coefficient. In an unbound medium, the Fokker-Planck equation is solved by the Green function:

$$G(\mathbf{r}, t; \mathbf{r}_0, t_0) = \frac{1}{[4\pi Dc(t - t_0)^{3/2}]} \exp\left(-\frac{|\mathbf{r} - \mathbf{r}_0|^2}{4Dc(t - t_0)}\right)$$

$$D = \frac{1}{3(\mu_A + (1 - g)\mu_S)}$$

where  $\mu_A$  and  $\mu_S$  are the absorption and scattering coefficients, respectively (both in units of  $\text{m}^{-1}$ ),  $g$  is the average scattering cosine ( $g = 0.025$ ). In LAr with the default optical properties in Table 5.2,  $D = 18.8$  cm. In a bound medium, with full absorption of the photons by the FC and LEMs, a few additional techniques have to be used to obtain a solution. With this method, it takes only a few ms to generate the photon density at a given PD from a specific point source. From preliminary studies, relatively good agreement between analytical approach and full simulation has been found. In particular, the arrival time distributions of photons on the PMTs are well reproduced. The only drawback is that one cannot easily implement or study a complicated geometry including regions that are semi-transparent to light. Hence, the visibilities generated by the two methods are not in agreement in the overall light yield, but have a very similar trend in terms of spatial dependences. Studies to improve the analytical method results are in progress since this approach could be extremely powerful for physics studies in the SP module.

#### 5.6.1.4 Simulation of light yield

The light collected per PMT can be simulated together with the charge for crossing tracks in a standard simulation code where a detailed description of the detector is not needed. At each step of the track propagation, the energy deposited is computed by Geant4. This energy is converted into number of electrons and photons produced. As for the light simulation, the number of photons reaching each PMT and their time of arrival is now obtained from the light maps. As an example, the light yield from a uniform generation of 10 MeV electrons in the active volume is shown in Figure 5.15. The number of photoelectrons/MeV shown is summed over all PMTs and averaged along the  $y$  axis ( $z$  being the drift direction). One can notice the large spread in terms of light yield.

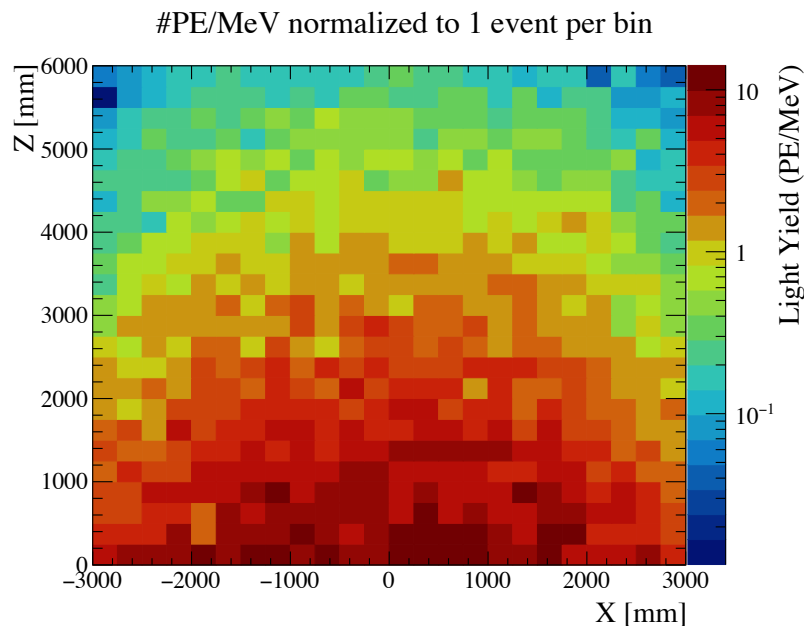


Figure 5.15: Light yield in terms of photoelectron/MeV summed over all PMTs and averaged along the  $y$ -axis. The mean of all voxels gives a light yield of 2.5 photoelectron/MeV, although the distribution is not uniform, in particular along the  $z$  (drift) axis.

For larger volumes such as the DP module, the light maps might be too big and the time spent

accessing the four parameters might strongly reduce the speed of the simulation. Either the parametrization method or the analytical approach are foreseen to replace the current light map usage, the exact strategy is yet to be defined.

## 5.6.2 Light Data in DP Prototypes

The WA105 DP demonstrator was operated from June to November 2017 with cosmic data. About 5 million light events were taken with various configurations. The study of the S1 light as a function of the drift field was performed. An example of an averaged waveform fitted to a fast and a slow scintillation components is shown in Figure 5.16. The amount of S2 light can be monitored as a function of the extraction and LEM amplification fields.

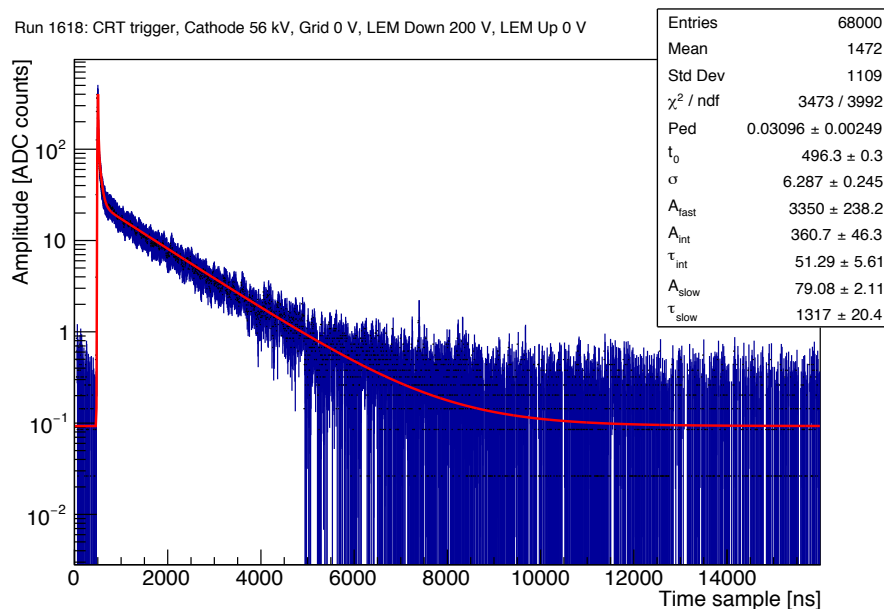


Figure 5.16: Averaged waveform of the S1 light signal taken with one PMT from the WA105 DP demonstrator, fitted with a function (red line) that is the sum of a Gaussian, parametrized by  $t_0$  and  $\sigma$ , and two exponential functions, with decay time constants  $\tau_{fast}$  and  $\tau_{slow}$ , and normalization factors  $A_{fast}$  and  $A_{slow}$

Light maps have also been generated with the demonstrator geometry, and data-Monte Carlo (MC) comparisons are ongoing. The preliminary results look promising, although the statistics in each setting and the relatively small size of the detector still constitute a challenge to extract the entire optical properties of the LAr.

## 5.6.3 Simulation of Physics Events

A preliminary study to understand whether the DP PD technical design meets the experiment's physics requirements has been performed. In this study, event topologies of interest for DUNE

physics have been simulated using LArSoft fast optical simulation tools.

The simulation framework used represents the current state of the art. It includes realistic models for the primary scintillation production yields in LAr, for Rayleigh scattering in LAr, for detector optical properties (such as FC reflectivity and cathode transparency), for the density of PMTs underneath the cathode, and for the quantum efficiency of the TPB-coated PMTs (taken to be 20%). On the other hand, these simulations do not yet include the full DP module geometry, but rather are performed in a ProtoDUNE-DP geometry with the same average PMT density as the one proposed here for the DP module (one PMT per  $\text{m}^2$ ). Relevant aspects such as secondary scintillation light emission in gaseous argon (a nuisance for event  $t_0$  determination), light absorption in LAr, electronics effects, reconstruction effects, and background contributions coming from  $^{39}\text{Ar}$  decays are not accounted for either in this study. While more realistic simulation results including the above effects will be produced on the DUNE TDR timescale, this preliminary study already provides a sense of the capabilities of the planned PD design.

Figure 5.17 shows the expected light yield for SNB neutrino CC interactions. As a representative  $\nu_e$  flux from a SNB, we assume a Fermi-Dirac distribution with  $T=3.5$  MeV temperature and no neutrino oscillation effects, yielding an average neutrino energy of about 11 MeV. Low-energy  $\nu_e$  CC interactions throughout the entire LArTPC active volume are generated with the LArSoft-based Marley package. For the assumed SNB neutrino flux and for a single interacting neutrino (hence, after convoluting flux and cross-section effects), Marley expects about 19 MeV of energy deposited in the LAr active volume, primarily from the final state electron and from nuclear de-excitation gamma rays. The left panel of Figure 5.17 shows a broad light yield distribution, averaging at about 50 detected photoelectrons per interaction and after summing all PMTs. This is as expected from the light yield distributions per deposited energy shown in Figure 5.15. The right panel shows the fraction of SNB  $\nu_e$  CC interactions within the LArTPC active volume above a given photoelectron detection threshold, as a function of the photoelectron threshold. From the figure, we conclude that about a 70% fraction of SNB  $\nu_e$  CC interactions would be seen by the PD, if the detector threshold was set at 10 photoelectrons on the sum of the PMT charges.

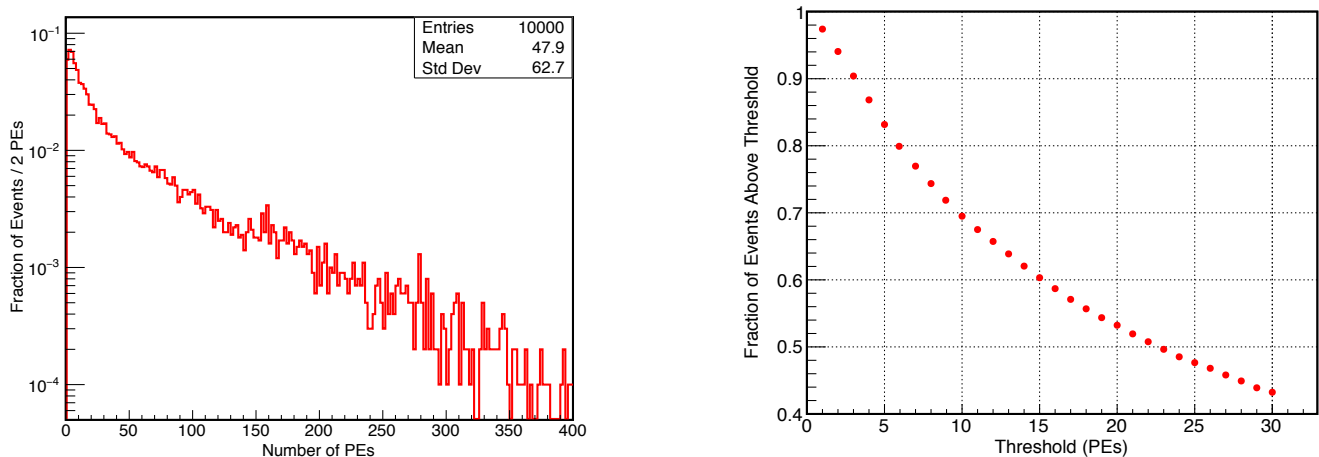


Figure 5.17: Photon detector response for simulated SNB neutrino interactions in the ProtoDUNE-DP geometry. Left panel: distribution of detected photoelectrons per neutrino interaction, for SNB  $\nu_e$  CC interactions throughout the active volume. Right panel: fraction of SNB  $\nu_e$  CC interactions above photoelectron threshold, as a function of the photoelectron threshold.

Figure 5.18 shows the corresponding plots for a representative nucleon decay final state in DUNE, namely  $p \rightarrow \bar{\nu}K^+$ . Nucleon decay events are generated using Generates Events for Neutrino Interaction Experiments (GENIE), accounting for both initial and final state nuclear effects in argon nuclei. Particles exiting the nucleus are then propagated in LAr using all relevant, Geant4-based, physics processes. The deposited energy per nucleon decay, of order 300 MeV, is much higher than the one per SNB neutrino interaction. As a result, the expected light yield for  $p \rightarrow \bar{\nu}K^+$  events throughout the active volume, shown in the left panel of Figure 5.18, averages to about 800 photoelectrons in this case. The right panel of Figure 5.18 shows that about a 98% fraction of  $p \rightarrow K^+\bar{\nu}$  decays in the TPC active volume are expected to be seen by the PD, for a PD threshold of 10 photoelectrons on the PMT charge sum.

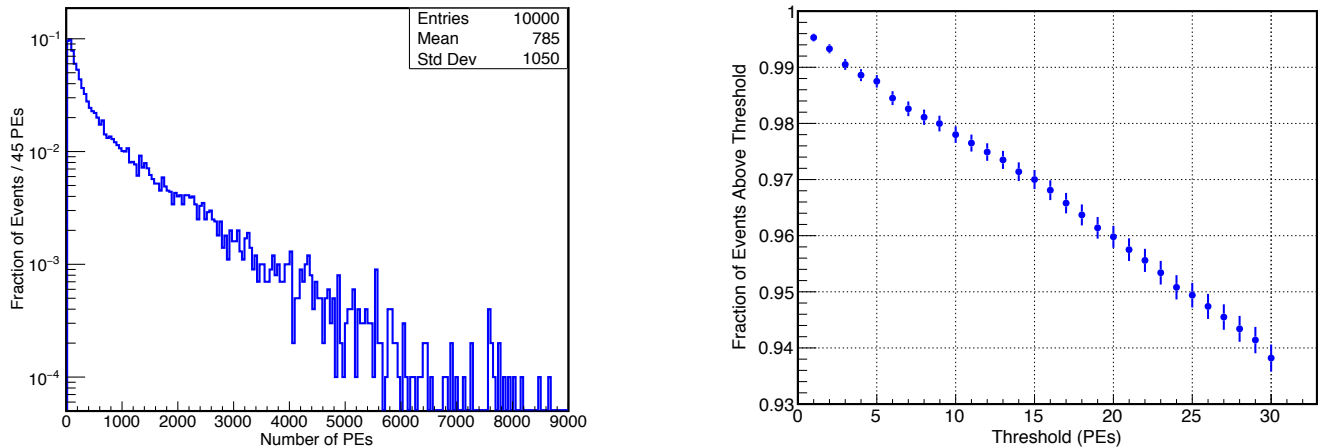


Figure 5.18: Photon detector response for simulated nucleon decays in the ProtoDUNE-DP geometry. Left panel: distribution of detected photoelectrons per nucleon decay, for  $p \rightarrow \bar{\nu}K^+$  decays throughout the active volume. Right panel: fraction of  $p \rightarrow K^+\bar{\nu}$  decays above photoelectron threshold, as a function of the photoelectron threshold.

## 5.7 Photon Detector Operations

### 5.7.1 Trigger Strategy

As explained in Section 5.1.5, the PDS operates in different acquisition modes. These modes include the external trigger (used for the beam events), the trigger for non-beam events, and the calibration mode.

In the LArTPC there are different uses of the light signal: cosmic ray and track timing for the reconstruction; non-beam events trigger such as SNB, atmospheric neutrinos, and proton decay; and calorimetry, as the light and charge signal are anti-correlated. These physics studies imply different requirements in terms of dynamics of the electronics and data sampling, from a few photoelectron to a much higher level.

For the non-beam event trigger strategies, the requirements can be very different. In the event

of a nearby (10 kpc) SNB, it is expected that a few thousands of neutrinos will homogeneously interact in the detector module for a period as long as  $\sim 100$  s. Hence, the SNB trigger strategy is mostly driven by the energy threshold set for  $\nu$  detection and its efficiency: 30 MeV is sufficient for a galactic SN, 5 MeV is needed for a burst in Andromeda. A high-efficiency trigger for proton decay events has to be designed considering the worst case scenario, e.g., the event happening at the top of the detector module, 12 m away from the closest PMT. In order to minimize the amount of spurious triggers, one can think of signal thresholds for a cluster of close-by PMTs.

All these important studies will be further investigated once a reliable light simulation of the DP module is available. For the DP technology, the main light trigger concerns are the amount of light collectable for a photon traveling distance of 12 m and the S1-S2 separation. The data that is collected in the ProtoDUNE-DP will provide crucial inputs for the optimization of the DP module light-collection system and for the design of an efficient trigger strategy for rare non-beam events.

The PDS trigger design is flexible so as to fulfill the different physics requirements. The light readout FE board controls the PDS trigger generation. The trigger is decided based on the coincidence of several PMT signals over a threshold during a time window. The number of PMTs that contribute to the trigger, the signal threshold and the length of the coincidence time window will be programmable online in order to be adaptable to different physics cases.

## 5.7.2 Data Quality Monitoring

The PMTs installed at the bottom of the tank will be operated for 10 to 20 years with no possibility to access them. Monitoring tools to ensure data quality of the PDS will have to be developed to catch any malfunctioning detector before data analysis. For instance, the amount of dark noise and the stability of the PMT response will have to be monitored over time. For the gain evolution, either studies of standard candles, e.g., from Michel electrons or average collected light produced by cosmic tracks, or with the dedicated calibration system are under consideration.

Monitoring tasks were performed during the six-month WA105 DP demonstrator operation with no dedicated light calibration system. This and the forthcoming operation of the ProtoDUNE-DP will again provide crucial input towards the PDS monitoring system in the DP module.

## 5.8 Interfaces

The PDS has several interfaces with other subsystems and the global DUNE systems. The interface documents related to DP module PDS are given in Table 5.3. Only some of the basic interfaces are summarized below.

- DP module electronics: The PDS shares the same FE electronics standard as the charge readout, which is  $\mu$ TCA-based [19]. Specifications of both PDS and FE electronics will be determined by the simulations and ProtoDUNE-DP data.

Table 5.3: DP PD interface documents

| DP PD Interface Document                           | DUNE docdb number |
|--|-------------------|
| DP module electronics                              | 6772 [24]         |
| DP module HV                                       | 6799 [25]         |
| DAQ  | 6802 [26]         |
| Cryogenic instrumentation and slow controls (CISC) | 6781 [27]         |
| DUNE Physics                                       | 7087 [28]         |
| Software and Computing                             | 7114 [29]         |
| Calibration  | 7060 [30]         |
| Integration and test facility (ITF)                | 7033 [31]         |
| Detector and Facilities (LBNF) Infrastructure      | 6979 [32]         |
| Installation                                       | 7006 [33]         |

- HV: This interface includes the consideration of the distance between the cathode and the PMT planes, power dissipation from the PMTs and the combined impact on the simulations.
- DAQ: The hardware interface is mainly through optical fibers. DP module PDS provides trigger and data in continuous streaming; the interface also includes the DAQ software.
- cryogenic instrumentation and slow controls (CISC): The main interface points are the layout of the cryogenic instrumentation (e.g., purity monitors and light emitting system for the cameras) and the PMT support structures and cabling; and the slow control and the PDS power supplies and calibration system.
- DUNE physics: DP PD has interfaces with the overall physics requirements on energy and time together with classification of events, decay modes and neutrino flavors.
- Software and Computing: This interface is on the development of simulation, reconstruction and analysis tools.
- Calibration: The PDS is participating in the DUNE global calibration task force and will provide handles to allow global monitoring of the PMT performance.
- integration and test facility (ITF): The operations at the ITF are described in Section 5.9.2. The interface items can be summarized as shipping and receiving of the PDS components and basic testing and repairing at the facility. The interface includes recycling and returning the packaging materials.
- Detector and Facilities (LBNF) Infrastructure: The PDS PMT mounting structures stand on the cryostat membrane; cold cables are routed in cable trays to the ceiling feedthrough flanges and racks and to cable trays on top of the cryostat. Other interfaces with the facility include access to conventional facilities and participation in the detector safety systems.
- Installation: This interface includes the transportation of the PDS components to and between underground areas, clean room activities and storage, and installation coordination



with the other teams.

## 5.9 Installation, Integration and Commissioning

### 5.9.1 Transport and Handling

The 720 PMTs of the PDS are shipped from various locations following base and cable assembly for the TPB coating at the ITF. They are shipped in boxes of 24, for a total of 30 deliveries. The PMTs are individually wrapped with special wrapping materials.

The PMTs are placed in modular shock-absorbing assemblies inside the boxes. The boxes have integrated pallets for easy handling and short-distance transportation, and a limited amount of inclination for the assemblies is safely allowed. The PMTs reach the ITF by air and ground transportation. Each box has a dedicated bar code visible on each side. This bar code is also associated with the shipping documents.

### 5.9.2 Integration and Testing Facility Operations

The ITF receives the PMT boxes and manages a shipping and delivery database. The received status of the boxes is available to the DP PD consortium as the boxes arrive at the ITF. The PDS characteristics database managed by the DP PD consortium is updated accordingly to reflect the received status of the contents of the boxes. Each PMT assembly gets an identifying bar code that is directly connected to the PDS characteristics database. This database stores the PMT serial number, the base board serial number, special information about TPB coating and assembly if any, and performance and calibration characteristics. This database forms the basis of the operations database, providing the initial calibration values. It also stores information about the ITF tests and underground installation and commissioning tests.

The TPB coating is performed at the ITF in the coating stations, after which the PMTs are placed back in their boxes and dedicated testing electronics are connected to the PMT cables soldered to the PMT bases. The test electronics enables connecting several PMTs at a time. The tests include basic functionality checks of both the PMTs and the base boards to assess the performance after transportation. No detailed performance characteristics are measured at the ITF. The tests are performed in a dedicated room with light and climate control. Once the performance of the PMTs in a box is validated, the box is closed with the original cover. Before closing, additional quality checks on the shock-absorbing assemblies are made.

The preparation of the PMT boxes for underground transportation includes installing holding and lifting fixtures to the top and sides that allow crane operation. The boxes are delivered to the surface station by ground transportation with appropriate updates to the shipping database.

### 5.9.3 Underground Installation and Integration

Once the PMT boxes are underground, the same top and side covers are opened as at the ITF. The PMTs are carried to the underground storage area in sub-units of the modular shock-absorbing assemblies. The underground storage area for the PDS is expected to be sufficiently large to store at least 30 PMTs, enabling continuous installation operations.

The removal of the individual PMT wrappings is done in the clean room. PMTs together with their base boards undergo visual inspection by the PDS installation supervisor. Once signed-off, the installation can proceed with multiple PMTs at a time by multiple teams. Cabling is carried out in parallel and relevant database updates are made in situ. The installation time management is done in coordination with the cathode and FC installation groups.

The bundles of cables are routed through the cable trays along the cryostat walls from the PDS flanges. Following the mechanical mounting of the PMTs to the cryostat floor, the PMT cables are connected to the cables coming from the flanges. In parallel, the calibration fibers are installed and routed through cable trays.

### 5.9.4 Commissioning

The commissioning of the PDS is performed in partitions. The size of a single partition will mainly be determined by the DAQ and the HV systems. The DAQ and HV partitions are commissioned, including the relevant control systems, prior to the connection of the PMTs to these systems. Once the physical sector corresponding to a partition is installed, the PMTs are powered up, and basic functionality and performance checks are performed. These include pedestal data taking, i.e., recording event data with external periodic triggering, and tests with the calibration system where the data taking is triggered in synchronization with a light source, as described in Section 5.5.

As a result of the commissioning tests, the basic performance characteristics of the PMTs, e.g., the dark count rate and gain, are measured in their final places. Installation-related issues are identified and eliminated at this stage. A commissioned sector becomes a part of the overall detector and can join the global calibration data taking and commissioning.

## 5.10 Quality Control

### 5.10.1 Production and Assembly

The QC performed at the different institutions labs includes reception of PMTs from the manufacturer and execution of the QC tests to accept or return the PMTs according to the acceptance and rejection criteria.

- The PMT support structure design is validated by immersing its mounted PMT in cryogenic temperatures and at an over-pressure equivalent to a depth of 12 m in LAr.
- Design validation tests are carried out to confirm that the PMT base design fulfills the specifications at room and cryogenic temperatures. A cable with SHV connector is soldered to each PMT base to facilitate the different base and PMT tests and the final PMT connection during the installation. The PMT bases are labeled (on the cable) in order to keep track of them. After production of the PMT base boards they are individually tested before mounting to the PMT to verify that components are correctly mounted. Later they are cleaned and tested at maximum voltage in an argon gas environment to confirm that there are no sparks on these (worst case conditions). After mounting the bases on the PMTs they are tested again in argon gas at maximum voltage to confirm that there are no sparks due to bad soldering.
- All the light readout units (PMT + base + support) are tested and characterized in liquid nitrogen in order to check their performance at cryogenic temperature and to obtain a database with the most important parameters from each PMT (gain versus voltage, dark counts, etc.). The PMT base number attached to each PMT is also included in the database.
- The wrapping materials and techniques are studied with one fully assembled light readout unit. The handling, transportation and installation scenarios are carefully studied and the transportation box design is validated. The transport box and PMT wrapping must ensure complete darkness.
- The light output of the LEDs and the fibers' light transmission from the photon calibration system are measured with a power meter.

### 5.10.2 Post-Factory Installation

Upon receipt at ITF, the PMTs go through verification measurements in order to identify any items damaged during transport. Gain versus voltage and dark current values are compared with those obtained before transportation.

The TPB coating is also performed at the ITF. The first few samples undergo microscopic examination and surface uniformity tests, and the coating procedure is validated. The production PMTs are randomly sampled for basic coating QC.

After transport from the ITF to SURF the PMTs are tested again before installation to confirm that no damage occurred during the last stage of transportation. During the installation, the PMTs database is updated with the position in the detector module of each PMT (identified by its serial number and base number). After installation, the full connection from the FE to the PMTs is checked. The FE channel and splitter number connected to each PMT are also included in the PMT database. Once it is possible to fully darken the detector module, voltage can be applied to the PMTs to test the signal with a scope or, if available, with the FE electronics.

## 5.11 Safety

Safety is the highest priority at all stages of DP PD operations. Since DUNE is an international project, the international safety regulations will be followed closely and safety documents will be prepared accordingly.

The main risks at the production and testing sites are electrocution, exposure to excessive heat, chemicals and cryogenics, and heavy lifting. Detailed procedures will be developed by the relevant institutes and approved by the DP PD consortium. Contents of the electrical safety rules will range from utilizing regular power equipment to handling PMTs for testing. The chemical and heat exposure hazards only concern the sites where the TPB coating is performed. The heavy-lifting risks concern mainly the PMT delivery boxes.

The ITF DP PD safety procedures will be developed in a similar way. The main hazards at this site are electrocution and heavy lifting. Also, due to the quantity and frequency of shipments from all other subsystems, tripping and operating in a limited space will be considered.

The underground operation and installation safety rules will follow the general facility rules on e.g., working in confined spaces, oxygen deficiency hazard and emergency procedures. The DP PD-specific safety rules are particularly related to lifting the boxes and their contents for installation and working at heights for cabling.

## 5.12 Management and Organization

The DP PD consortium was formed in 2017 and it is composed of eleven institutes from France, Peru, Spain, UK and USA. The charge of the DP PD consortium is to plan and execute the construction, installation and commissioning of the DP module PDS.

### 5.12.1 Consortium Organization

The current DP PD consortium Leader (CL) is from CIEMAT (Spain) and the Technical Lead (TL) is from LAPP (France). They are members of the DUNE Technical Board and they represent the consortium to the overall DUNE collaboration. The CL is responsible for the subsystem deliverables and for the effective management of the consortium. The TL acts as the overall project manager and is the interface to the International Project Office (IPO); he is responsible for monitoring and reporting on progress with respect to the agreed schedule and for issues related to interface documentation.

The institutions participating in the consortium are responsible for the design or construction of a particular subsystem. It is hoped that the national groups within the consortia will be able to approach relevant funding agencies with a specific construction-phase proposal, such that a likely

funding line can be established in or before 2019. The DP PD consortium is open to any new institution willing to join the current effort.

The current institutions participating in the DP PD consortium are LAPP (France); PUCP (Peru); IFAE, CIEMAT, and IFIC (Spain); UCL (UK); and ANL, Duke U., U. of Iowa, SDSMT, and UTA (USA).

The DP PD consortium is divided into four working groups: photosensors and electronics, calibration system, mechanics and integration, and simulation and physics. The corresponding current WG convener institutions are:

- WG1: Photosensors and Electronics - CIEMAT
- WG2: Calibration System - CIEMAT
- WG3: Mechanics and Integration - U. of Iowa
- WG4: Sim. & Phys. - Duke U., IFIC, LAPP

### 5.12.2 Planning Assumptions

The optimization and final design of the DP PD system will be driven by:

1. ProtoDUNE-DP data (expected by beginning of 2019)
2. Simulation studies (in progress)

ProtoDUNE-DP operation and data analysis are fundamental steps to understanding whether the current PDS design considered as baseline, based on cryogenic PMTs with TPB coating, is able to provide  $t_0$  for non-beam events, background rejection and triggering on non-beam events. These data will be used to tune the MC simulations and extrapolate the performance of the system to the DP module.

Simulations are needed to determine and optimize the DP PD system to meet the physics requirements in terms of:

- light collection efficiency,
- number of channels,
- photosensor requirements,
- dynamic range of readout electronics and timing resolution, and
- trigger strategy on non-beam events.

The performance requirements on the PDS will be provided by the DUNE physics working group. Alternate designs for aspects of the DP module's baseline PDS [34] will be developed based on the compatibility of ProtoDUNE-DP data and MC light simulation results with the DUNE physics requirements.

### 5.12.3 WBS and Responsibilities

The DP PD consortium has developed a detailed breakdown of deliverables and responsibilities included in the overall DUNE collaboration work breakdown structure (WBS) [35] coordinated by the IPO. The main deliverables are based on the ProtoDUNE-DP PDS and are divided into seven topics. These are listed along with the participating institutions:

1. Management DP PDS (includes milestones and review dates) - *LAPP, CIEMAT*
2. Physics and Simulations - *Duke, LAPP, IFIC, SDSMT, CIEMAT, PUCP, UCL, Texas-Austin*
3. Design, Engineering, R&D and validation tests - *Iowa, CIEMAT, IFIC, UCL, Texas-Austin, IFAE, SDSMT*
4. Production Setup (includes tooling) - *UCL*
5. Production (includes component production, assembly, testing, and QC) - *Iowa, CIEMAT, IFAE, IFIC, UCL, Texas-Austin, Duke, SDSMT, LAPP*
6. Integration (contributions to activities at global integration facility) - *SDSMT*
7. Installation (contributions to activities at SURF) - *CIEMAT, IFIC, SDSMT, Iowa*

### 5.12.4 High-Level Cost and Schedule

The cost of the baseline DP PDS will be defined in a separate document.

The DP PDS consortium's main activities during the next 16 months are focused on developing the TDR. The main high-level milestones are detailed in Table 5.4 for this period. The plan for the activities in the post-TDR period is summarized in Table 5.5.

Table 5.4: Pre-TDR key milestones

| Milestone   | End date |
|---|----------|
| Simulations and physics: Implementation of DP optical simulation in LArSoft for ProtoDUNE-DP  | 08/2018  |
| Simulations and physics: Optimization of the DP module performance to fulfill the physics requirements and definition of a trigger strategy | 05/2019  |
| Photosensors: Components selection and final design   | 03/2019  |
| PMT calibration system design and selection of components   | 03/2019  |
| Cabling definition and design of flange   | 03/2019  |
| Design review in light of ProtoDUNE-DP calibration data   | 03/2019  |
| QC plan   | 06/2018  |
| Identification of Interfaces  | 06/2018  |
| Integration, installation and commissioning plans   | 12/2018  |
| DP module TDR   | 06/2019  |

Table 5.5: Post-TDR key milestones

| Milestone   | Start date | End date |
|---|------------|----------|
| <b>PMT preparation and installation</b> (can be done in batches)                                      |            |          |
| PMT procurement procedure and production  | 01/2021    | 12/2022  |
| PMT base design and manufacturing   | 01/2022    | 12/2022  |
| PMT support structure production and assembly   | 08/2022    | 01/2023  |
| PMT characterization - 10 PMTs/week (two facilities)  | 02/2023    | 12/2023  |
| TPB coating (two facilities similar to that for CERN ICARUS)  | 01/2024    | 12/2024  |
| Splitter production and tests   | 05/2024    | 12/2024  |
| <b>Installation at SURF</b>   |            |          |
| PMT cable and fiber routing in cryostat from flange to bottom (depends on FC and flange installation) | 09/2024    | 09/2024  |
| PMT testing, installation in cryostat and cabling (72 PMTs/month)                                     | 10/2024    | 07/2025  |
| PMT support installation on the membrane (in parallel by sector with PMT installation)                | 10/2024    | 07/2025  |
| Splitter installation (in parallel with PMT installation to test cabling and connections)             | 10/2024    | 07/2025  |
| <b>Light calibration system</b>   |            |          |
| Fibers, light source tests and procurement  | 06/2023    | 05/2024  |
| Fiber calibration system installation (in parallel with PMT installation with validation test)        | 09/2024    | 07/2025  |

# Chapter 6

## Data Acquisition System

### 6.1 Data Acquisition (DAQ) System Overview

#### 6.1.1 Introduction

The DUNE far detector (FD) data acquisition (DAQ) system must enable the readout, triggering, processing and distribution to permanent storage of data from all detector modules, which includes both their electrical time projection chamber (TPC) and optical photon detection system (PDS) signals. The final output data must retain, with very high efficiency and low bias, a record of all activity in the detector that pertains to the recognized physics goals of the DUNE experiment. The practical constraints of managing this output requires that the DAQ achieve these goals while reducing the input data volume by almost four orders of magnitude.

The current generation of liquid argon time-projection chamber (LArTPC) DAQs, such as used in ProtoDUNE and MicroBooNE, produce data spanning a fixed window of time that is chosen based on the acceptance of an external trigger. The DUNE DAQ faces several major challenges beyond those of the current generation. Foremost, it must accept data from about two orders of magnitude more channels and from that data it must form its own triggers. This self-triggering functionality requires immediate processing of the full-stream data from a large portion of all TPC channels with a throughput of approximately one terabyte per second per detector module. From this data stream, triggers must be raised based on two very different patterns of activity. The first is activity localized in a small region of one detector module, such as due to beam neutrino interactions or the passage of relatively rare cosmic-ray muons. This activity tends to correspond to a relatively large deposition of energy, around 100 MeV or more. The second pattern that must lead to a trigger is lower energy activity dispersed in both time and spatial extent of the detector module, such as due to a supernova neutrino burst (SNB).

The DAQ must also contend with a higher order of complexity compared to the current generation. The FD is not monolithic but ultimately will consist of four detector modules each of 10 kt fiducial



mass. Each module will implement somewhat different technologies and the inevitable asymmetries in the details of how data are read out from each must be absorbed by the unified DAQ at its front end. Further, each detector module is not monolithic but has at least one layer of divisions, here generically named detector units. For example, the single-phase (SP) detector module has anode plane assemblies (APAs) each providing data from a number of warm interface boards (WIBs) and the dual-phase (DP) detector module has charge readout (CRO) and light readout (LRO) units associated with specific electronics crates. In each detector module, there are on the order of 100 detector units (150 for SP and 245 for DP) and each unit has a channel count that is of the same order as that of an entire LArTPC detector of the current generation. The DUNE DAQ, composed of a cohesive collection of DAQ instances called DAQ partitions, must run on a subset of all possible detector units for each given detector module. Each instance effectively runs independently of all the others, however some instances indirectly communicate through the exchange of high-level trigger information. This allows, for example, each detector module to take data in isolation. It also allows for all detector modules to contribute to forming and accepting global SNB triggers, and to simultaneously run small portions – consisting of a few detector units – separately in order to debug problems, run calibrations or perform other activities while not interfering with nominal data taking in order to maintain high uptime.

Substantial computing hardware is required to provide the processing capability needed to identify such activity while keeping up with the rate of data. The nature of various technical, financial and physical constraints leads to the need for much of the computing hardware required for this processing to reside underground, near the detector modules. In such an environment, power, cooling, space, and access is far more costly than in typical data centers.

Past LArTPC and long-baseline (LBL) neutrino detectors have successfully demonstrated external triggering using information related to their beam. The DUNE FD DAQ will accept external information on recent times of Main Injector beam spills from Fermilab. This will assure triggering with high efficiency to capture activity pertaining to interactions from the produced neutrinos.

However, even if the DUNE experiment were interested only in neutrinos from beam spills, an external beam trigger alone would not be sufficient. Absent any other information, such a trigger must inevitably call for the readout of all possible data from the FD over at least one LArTPC drift time. This would lead to an annual data volume approaching an exabyte ( $10^{18}$  bytes), the vast majority of which would consist of just noise. This entire data volume would have to be saved to permanent storage and then processed offline in order to get to the signals.

DUNE's physics goals of course extend beyond beam-related interactions, including cosmic-ray muons, which provide an important source of detector calibration, and atmospheric neutrino interactions, which give a secondary source from which to measure neutrino properties. Taken together, recording their activity will dominate the data rate. The DAQ must also record data with sensitivity to rare interactions (both known and hypothetical) such as nucleon decay, other baryon number violating processes (such as neutron-antineutron oscillation), and interactions from the products of SNBs as well as possibly being able to observe isolated low-energy interactions from solar neutrinos and diffuse supernova neutrinos.

Some of these events, while rare in themselves, produce patterns of activity that can be mimicked by other higher-rate backgrounds, particularly in the case of SNBs. While the exact processes involved

in SNBs are not fully understood, it is expected that a prolonged period of activity of many tens of seconds will occur over which their neutrino interactions may be observed. Individually, these interactions will be of low energy (relative to that of beam neutrino interactions, for example), and will be spread over time and over the bulk of the detector modules. Because of their signature and their importance, special attention is required to first ascertain that a SNB may be occurring and to save as much data as possible over its duration.

Thus the DAQ must greatly reduce the full-stream of its input data while using the data itself to do so. It must do this efficiently both in terms of recording essentially all activity important to the physics goals of DUNE and in terms of a rate of data output that is manageable. To perform these primary duties the DAQ provides run control, configuration management, monitoring of both its processes and the general health of the data, and a user interface for these activities.

## 6.1.2 Design Considerations

The different detector modules vary in terms of their readout technology and schemes, timing systems, channel counts and data throughput and format. These aspects determine the nature of the digital data input to the DAQ. The design of the DAQ strives to contain the unique layers that adapt to the variation in the detector modules toward its front end in order to allow as many of its back end components to remain as identical across the detector modules as possible. In particular, the DAQ must present a unified interface to the ultimate consumer of its data, DUNE offline computing. It must also accept and process the data from a variety of other sources including the accelerator, various calibration systems (including laser, cold electronics (CE), photon detectors (PDs), and potentially others) as well as trigger sources external to DUNE. The modular nature of the DUNE FD implies that the DAQ instances running on each module must also exchange trigger information. In particular, exchanging module-local SNB trigger information will allow higher efficiency for this important physics. The DAQ must be optimized for the above while also retaining the flexibility to scale to handle risks such as excess noise, changes in high voltage (HV), cut network connectivity and other issues that could arise.

Currently, two major variations for the DUNE DAQ are under consideration. The eventual goal is to reduce this to a single high-level design which will service both SP and DP detector modules and be reasonably expected to support the third and fourth modules to come. The first design, designated in this proposal as *nominal*, is illustrated in a high-level way in terms of its data and trigger flow in Figure 6.1. The second design, designated as the alternate, is similarly illustrated in Figure 6.2. The two variants differ largely at their FEs in terms of the order in which they buffer the data received from the detector module electronics and use it to form trigger primitives. They also differ in how they treat triggering and data flow due to a potential SNB. As their FEs are also sensitive to differences between the detector module electronics, this further variation for each general design is described below in Sections 6.2.2 and 6.2.3 for the detector module specific to this volume.

At this general high level, the two designs are outlined. For both, the diagrams are centered on one DAQ front-end fragment FE, which is a portion of the entire DAQ partition servicing a detector module that has one front-end computer (FEC) accepting about 10 to 20 Gbit/s of data

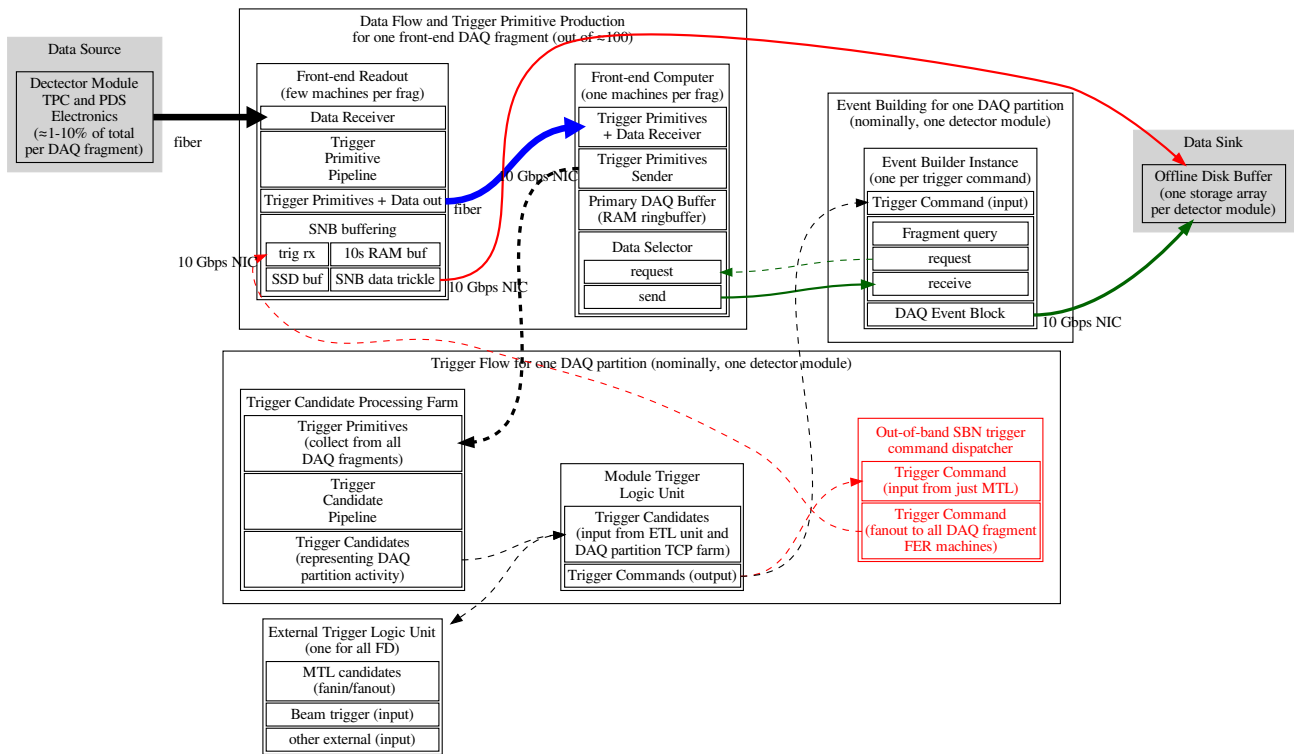


Figure 6.1: The high-level, *nominal* design for the DUNE FD DAQ in terms of data (solid) and trigger (dashed) flows between one DAQ front-end fragment FE and the trigger processing and event building back end for one DAQ partition. Line thickness indicates relative bandwidth requirements. Blue indicates where the full data flow for the DAQ front-end fragment is concentrated to one endpoint. Green indicates final output of normally triggered (non-SNB) data. Red indicates special handling of potential SNB. Each detector module has specialized implementation of some of these high level components, particularly toward the upstream FE as described in the text. The grayed boxes are not in the DAQ scope.

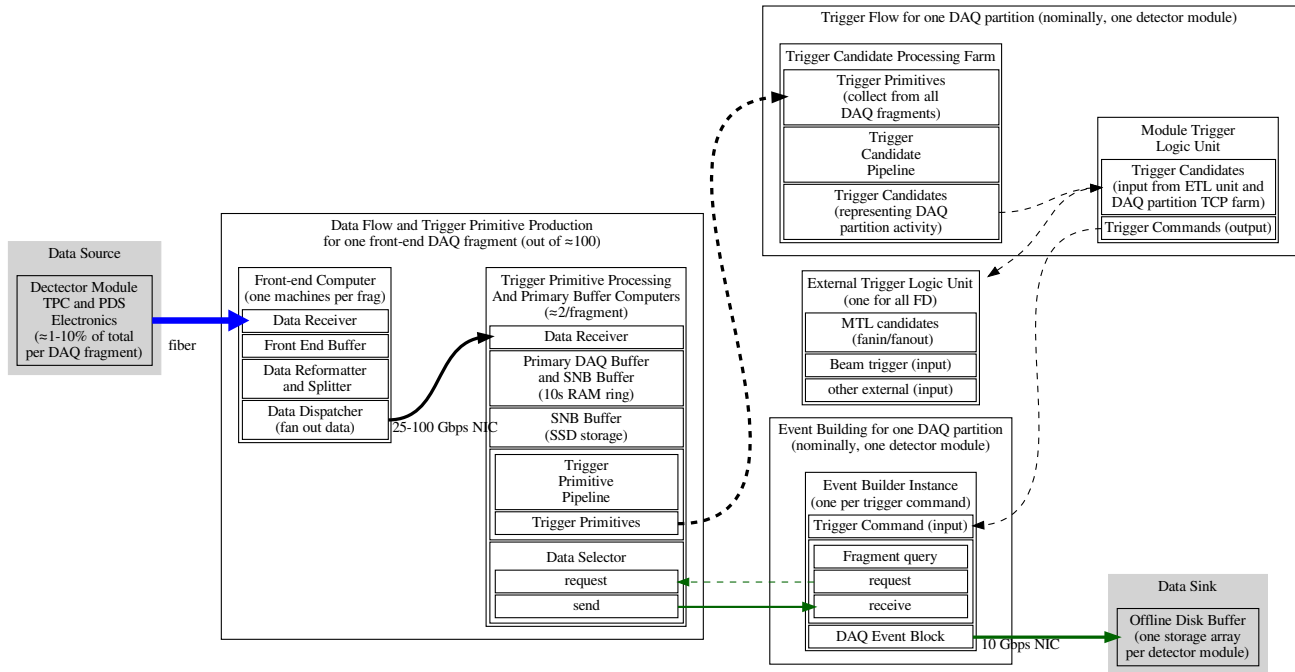


Figure 6.2: The high-level, alternate design for the DUNE FDFD DAQ in terms of data (solid) and trigger (dashed) flows between one DAQ front-end fragment FE and the trigger processing and event building back end for one DAQ partition. Line thickness indicates relative bandwidth requirements. Blue indicates where the full data flow for the DAQ front-end fragment is concentrated to one endpoint. Green indicates final output. Note, except for a longer readout, SNB is handled symmetric to normal data. Each detector module has specialized implementation of some of these high level components, particularly toward the upstream front-end as described in the text. The grayed boxes are not in the DAQ scope.

(uncompressed rate) from some integral number of detector units. Each of the participating DAQ front-end fragments do the following:

- Accept TPC and PDS data from the detector units associated with the DAQ front-end fragment.
- Produce and emit a stream of per-channel trigger primitives.
- Buffer the full data stream long enough for the trigger decision to complete (at least 10 s as driven by SNB requirements).
- Accept data selection requests and return corresponding data fragments.

All participating DAQ front-end fragments in the particular DAQ partition (i.e., the DAQ instance) servicing a portion of one detector module communicate with one trigger processing and event building system. The trigger processing system must:

- Receive the stream of per-channel trigger primitives from all DAQ front-end fragments.
- Correlate the primitives in time and spatially (across channels), and otherwise use them to form higher-level trigger candidates.
- Exchange trigger candidates with the external trigger logic (ETL).
- From them form trigger commands, each of which describes a portion of the data in time and a channel to be read out, such that no two trigger commands overlap.
- Dispatch these commands as required (in general to the event builder (EB)).

The event building system is responsible for performing the following actions:

- Accept a trigger command and allocate one EB instance to dispatch it.
- Interpret and execute the command by making data selection requests to referenced DAQ front-end fragments.
- Accept the returned data fragment from each DAQ front-end fragment and combine them into a DAQ event block.
- Write the result to the secondary DAQ buffer, which is the boundary shared with DUNE offline computing.

The nominal and the alternate DAQ designs differ largely in where the trigger primitive and SNB buffering exist. The *nominal* design places these functions in machines comprising a DAQ front-end readout (FER), which is upstream of the FEC. This then requires the SNB data and trigger handling to be different than that for normal (non-SNB) data. When a SNB trigger command is raised it is forwarded to the out-of-band trigger command dispatcher (OOB dispatcher) which sends

it down to the FERs. After the SNB data is dumped to solid-state disks (SSDs) it is “trickled” out via a path separate from the normal data to the secondary DAQ buffer. The *alternate* design, on the other hand, places these functions downstream of the FEC in trigger processing and data buffering nodes. The RAM of these nodes is used to provide the primary DAQ buffer for normal triggering as well as the deeper buffers needed for SNB. This design handles the SNB data somewhat symmetrically with normal data. When an EB makes a request for SNB data, it differs only in its duration, spanning tens of seconds of instead just a few milliseconds. The FE buffering nodes, instead of directly attempting to return the full SBN data immediately, streams it to local SSD storage. From that storage, the data is sent to the EB as low priority (i.e., also trickled out). Since the module trigger logic (MTL) ensures no overlapping commands, the buffer nodes may service subsequent requests from post-dump data that is in the RAM buffer. Since each trigger command is handled by an individual EB instance, the trickle proceeds asynchronously with respect to any subsequent trigger command handled by another EB instances.

Further description of these designs is given in Section 6.2.

The most critical requirements for the DUNE FD DAQ are summarized in Table 6.1.

Table 6.1: Important requirements on the DAQ system design

| Requirement     | Description  |
|-----------------|--|
| Scalability     | The DUNE FD DAQ shall be capable of receiving and buffering the full raw data from all four detector modules   |
| Zero deadtime   | The DUNE FD DAQ shall operate without deadtime under <i>normal</i> operating conditions  |
| Triggering      | The DUNE FD DAQ shall provide full-detector triggering functionality as well as self-triggering functionality; the data selection shall maintain high efficiency to physics events while operating within a total bandwidth of 30 PB/year for all operating detector modules |
| Synchronization | The DUNE FD DAQ shall provide synchronization of different detector modules to within $1\ \mu\text{s}$ , and of different subsystems within a module to within 10 ns   |

The input bandwidth and processing needs of the DAQ are expected to be dominated by the rate of data produced by the TPC system of each detector module. These rates vary between the modules and their estimations are summarized in Table 6.2.

The ultimate limit on the output data rate of the DUNE FD DAQ is expected to be provided by the available bandwidth to the tape, disk and processing capacity of Fermilab. An ample guideline has been established that places this limit at about 30 PB/year or 8 Gbit/s. Extrapolating to four detector modules, this requires a DAQ data reduction factor of almost four orders of magnitude. This is achieved through a simple self-triggered readout strategy.

An overestimate of the annual triggered but uncompressed data volume for one 10 kt detector module is summarized in Table 6.3. It assumes a very generous and simple trigger scheme whereby the data from the entire detector module is saved for a period longer than two drift times around

Table 6.2: The parameters governing the pre-trigger data rate from units of each detector module TPC CEs and the aggregate throughput into the FECs of the DAQ DAQ front-end fragments. Compression is an estimate and will be reduced if excess noise is introduced.

| Parameter                  | single-phase          | dual-phase           |
|----------------------------|-----------------------|----------------------|
| TPC unit                   | APA                   | CRO crate            |
| Unit multiplicity          | 150                   | 240                  |
| Channels per unit          | 2560 (800 collection) | 640 (all collection) |
| ADC sampling               | 2 MHz                 | 2.5 MHz              |
| ADC resolution             | 12 bit                | 12 bit               |
| Aggregate from CE          | 1440 GB/s             | 576 GB/s             |
| Aggregate with compression | 288 GB/s (5×)         | 58 GB/s (10×)        |

the trigger time. This essentially removes any selection bias at the cost of recording a substantial amount of data that will simply contain noise. Detailed trigger efficiency studies still remain to be performed. Initial understanding indicates that trigger efficiency should be near 100 % for localized energy depositions of at least 10 MeV. Sub-MeV signals can be ascertained from noise in existing LArTPCs so the effective trigger threshold may be even lower with high efficiency. Of course, data rates rise quickly when the threshold drops into the range of an MeV. Additional simulation and use of early data will be used to better optimize this threshold.

The data volume estimates also assume that any excess noise beyond what is expected due to intrinsic electronics noise will not lead to an increase in trigger rates. If, for example, excess noise occurs such that it frequently mimics more than about 10 MeV of localized ionization, this would lead to an increase in various types of triggers and subsequently more data. However, at the same time, these estimates do not take into account that some amount of lossless compression of the TPC data will be achieved. In the absence of excess noise it is expected that a compression factor of at least 5× can be achieved with the SP data and up to 10× may be achieved with the DP data, although the actual factor achieved will ultimately depend on the level of excess noise experienced in each detector module. Studies using data from the DUNE 35 ton prototype and early MicroBooNE running have shown that a compression factor of at least 4× can be expected even in the case of rather high levels of excess noise.

One category that will be particularly sensitive to excess noise is the trigger primitives. As discussed further in Section 6.2.3, their primary intended use is as transient objects produced and consumed locally and directly by the DAQ in the trigger decision process. However, as their production is expected to be dominated by  $^{39}\text{Ar}$  decays (absent excess noise) they may carry information that proves very useful for calibration purposes. Future studies with simulation and with early data will determine the most feasible methods to exploit this data. These may include committing all or a portion to permanent storage or potentially developing processes that can summarize their data while still retaining information salient to calibration.

Finally, it is important to note that early data will be used to evaluate other selection criteria. It is expected that efficient and bias-free selections can be developed and validated that save a subset of the entire detector module for any given trigger type. For example, a cosmic-muon trigger command for a SP module will indicate which anode plane assemblies contributed to its

Table 6.3: Anticipated annual, uncompressed data rates for a single SP module. The rates for normal (non-SNB triggers) assume a readout window of 5.4 ms. For planning purposes these rates are assumed to apply to a DP module as well, which has a longer readout time but fewer channels. In reality, application of lossless compression is expected to provide as much as a  $5\times$  reduction in data volume for the SP module and as much as  $10\times$  for the DP module.

| Event Type                     | Data Volume<br>PB/year | Assumptions  |
|--------------------------------|------------------------|--|
| Beam interactions              | 0.03                   | 800 beam and 800 dirt muons; 10 MeV threshold in coincidence with beam time; include cosmics           |
| Cosmics and atmospherics       | 10                     | 10 MeV threshold, anti-coincident with beam time   |
| Front-end calibration          | 0.2                    | Four calibration runs per year, 100 measurements per point   |
| Radioactive source calibration | 0.1                    | Source rate $\leq 10$ Hz; single fragment readout; lossless readout                                    |
| Laser calibration              | 0.2                    | $1 \times 10^6$ total laser pulses, lossy readout  |
| Supernova candidates           | 0.5                    | 30 seconds full readout, average once per month  |
| Random triggers                | 0.06                   | 45 per day   |
| Trigger primitives             | $\leq 6$               | All three wire planes; 12 bits per primitive word; 4 primitive quantities; $^{39}\text{Ar}$ -dominated |



formation (i.e., which ones had local ionization activity). This command can then direct reading out these anode plane assemblies, possibly also including their neighbors, while discarding the data from all other anode plane assemblies. This may reduce the estimated 10 PB/year for cosmics and atmospheric by an order of magnitude. A similar advanced scheme can be applied to the DP module by retaining data for the given readout window from only the subset of CRO crates (and again, potentially their nearest neighbors) that contributed to the formation of the given trigger.

### 6.1.3 Scope

The nominal scope of the DAQ system is illustrated in Figure 6.1 by the white boxes. It includes the continued procurement of materials for, and the fabrication, testing, delivery and installation of the following systems:

- FE readout (nominal design) or trigger farm (alternate design) hardware and firmware or software development for trigger primitive generation.
- FE computing for hosting of DAQ data receiver (DDR), DAQ primary buffer (primary buffer) and data selector.
- Back-end computing for hosting MTL, EB and the OOB dispatcher processes.
- External trigger logic and its host computing.
- Algorithms to generate trigger commands that perform data selection.
- Timing distribution system.
- DAQ data handling software including that for receiving and building events.
- The online monitoring (OM) of DAQ performance and data content.
- Run control software, configuration database, and user interface
- Rack infrastructure in the central utility cavern (CUC) for readout electronics, FE computing, timing distribution, and data selection.
- Rack infrastructure on surface at SURF for back-end computing.

## 6.2 DAQ Design

### 6.2.1 Overview

The design for the DAQ has been driven by finding a cost-effective solution that satisfies the requirements. Several design choices have been made and two major variations remain to be studied. From a hardware perspective, the DAQ design follows a standard HEP experiment design, with customized hardware at the upstream, feeding and funnelling (merging) and moving the data into computers. Once the data and triggering information are in computers, a considerable degree of flexibility is available; the processing proceeds with a pipelined sequence of software operations, involving both parallel processing on multi-core computers and switched networks. The flexibility allows the procurement of computers and networking to be done late in the delivery cycle of the DUNE detector modules, to benefit from increased capability of commercial devices and falling prices.

Since DUNE will operate over a number of decades, the DAQ has been designed with upgradability in mind. With the fall in cost of serial links, a guiding principle is to include enough output bandwidth to allow all the data to be passed downstream of the custom hardware. This allows the possibility for a future very-fast farm of computing elements to accommodate new ideas in how to collect the DUNE data. The high output bandwidth also gives a risk mitigation path in case the noise levels in a part of the detector are higher than specified and higher than tolerable by the baseline trigger decision mechanism; it will allow additional data processing infrastructure to be added (at additional cost).

Digital data will be collected from the TPC and PD readout electronics of the SP and DP detector modules. These categories of data sources are viewed as essentially four types of subdetectors within the DAQ and follow the same overall data collection scheme as shown for the nominal design in Figure 6.1 and for the alternate design in Figure 6.2. The readout is arranged to allow making a trigger decision in a hierarchical manner. Initial inputs are formed at the channel level, then combined at the detector unit level and again combined at the detector module level. In addition, the trigger decision process combines information at this level that may come from the other detector modules as well as information from sources external to the DAQ. This hierarchical structure in forming and consuming triggers allows safeguards to be developed so that any problems in one cavern or in one detector unit of one detector module need not overwhelm the entire DAQ. It also allows a SNB to be recorded in all operational parts of the detector while others may be down for calibration or maintenance.

Generally speaking, the DAQ consists of data flow and trigger flow. The trigger flow involved in self-triggering originates from processing a portion of the data flow. The trigger flow is then consumed back by the DAQ in order to govern what portion of the data flow is finally written out to permanent storage. The nominal and alternate designs differ in where in the data flow the trigger flow originates.

In both designs, a single DAQ front-end fragment associates an integral number of detector units with one front-end computer (FEC). This fragment forms one conceptual unit of the FE DAQ. The

processing on a FEC is kept minimal such that each has a throughput limited by I/O bandwidth. The recently released PCIe v4 doubles the bandwidth from the prior version and thus we assume that  $\approx 20$  GB/s throughput (out of a theoretical 32 GB/s max) can be achieved based on tests using PCIe v3. In principle then, this allows one FEC to accept the data from: two (if uncompressed) or ten (if  $5\times$  compressed) of the 150 SP anode plane assemblies, ten of the 240 DP CRO crates given their nominal  $10\times$  compression or the uncompressed data from all five DP LRO crates.

In the nominal design, the data enters the DAQ via the fragment's DAQ front-end readout (FER) component. In the SP the FER consists of eight reconfigurable computing elements (RCEs) and in the DP it consists of a number of Bump On Wire (BOW) computers, (see Section 6.2.2 in each respective detector module volume). The FER is responsible for accepting that data and from it producing channel level trigger primitives. It is also responsible for forwarding compressed data and the primitives to the DAQ data receiver (DDR) in the corresponding FEC. The FER is also responsible for supplying transient memory (RAM) and non-volatile buffer in the form of SSD sufficient for SNB triggering and readout. The DDR accepts the full data stream and transfers it to the DAQ primary buffer of its DAQ front-end fragment. There it is held awaiting a query from the event builder (EB). When the EB receives a trigger command it uses the included information to query all appropriate data selectors and from their returned data fragments an DAQ event block is built and written to file on the secondary DAQ buffer. From there the data becomes responsibility of the offline group to transfer to Fermilab for permanent storage and further processing.

In the alternate design, the data is accepted directly by the DAQ data receiver (DDR) in a FEC from the detector electronics for the particular detector module. The data then flows into the primary buffer and the portion required for forming trigger primitives is dispatched to the trigger computers of the fragment for the production of trigger primitives. Current SSD technology may allow SSD to be directly mounted to the FEC to provide for the SNB dump buffer. Another solution, which puts less pressure on write throughput, is to distribute the SSD for the SNB dumps to the trigger computers. In order to supply enough CPU for trigger primitive pipelines it is expected that at least two hosts per FEC will be needed. While their CPUs are busy finding trigger primitives, their I/O bandwidth will be relatively unused and thus they provide synergistic, cost-effective hosting for the SSDs.

Regardless of where the trigger primitives are produced in either the nominal or alternate design, they are further processed at the DAQ front-end fragment level to produce trigger candidates. At this level, they represent possible activity localized in time and by channel to a portion of the overall detector module. The trigger candidates emitted by all DAQ front-end fragments are sent to the module trigger logic (MTL) associated with the DAQ partition. There, they are time ordered and otherwise processed to form trigger commands. At this level they represent activity localized across the detector module and over some period of time.

The DAQ partition (or DAQ instance) just introduced is the cohesive collection of DAQ parts. One DAQ partition operates essentially independently from any other, and there is typically one per detector module. In some cases multiple DAQ partitions may operate simultaneously in a detector module, such as when some fraction of detector units are undergoing isolated testing or calibration.

Each trigger command is consumed by a single EB instance in order to query back to the DAQ

front-end fragments of its DAQ partition as described above. In addition, the MTL of one module is exchanging messages in the form of trigger candidates with the others. For example, one module may raise a local SNB trigger candidate and forward it to all other modules. Each module is also emitting candidates to sinks and accepting them from sources of external trigger information.

The exact implementation of some of these high-level functions, particularly those near the FE, depends on the particular detector module. The required specialization and in general, more implementation-level details are described in the following sections. Subsequent description proceeds toward the DAQ back end including processes handling dataflow, triggering, event building and data selection.

## 6.2.2 Front-end Readout and Buffering

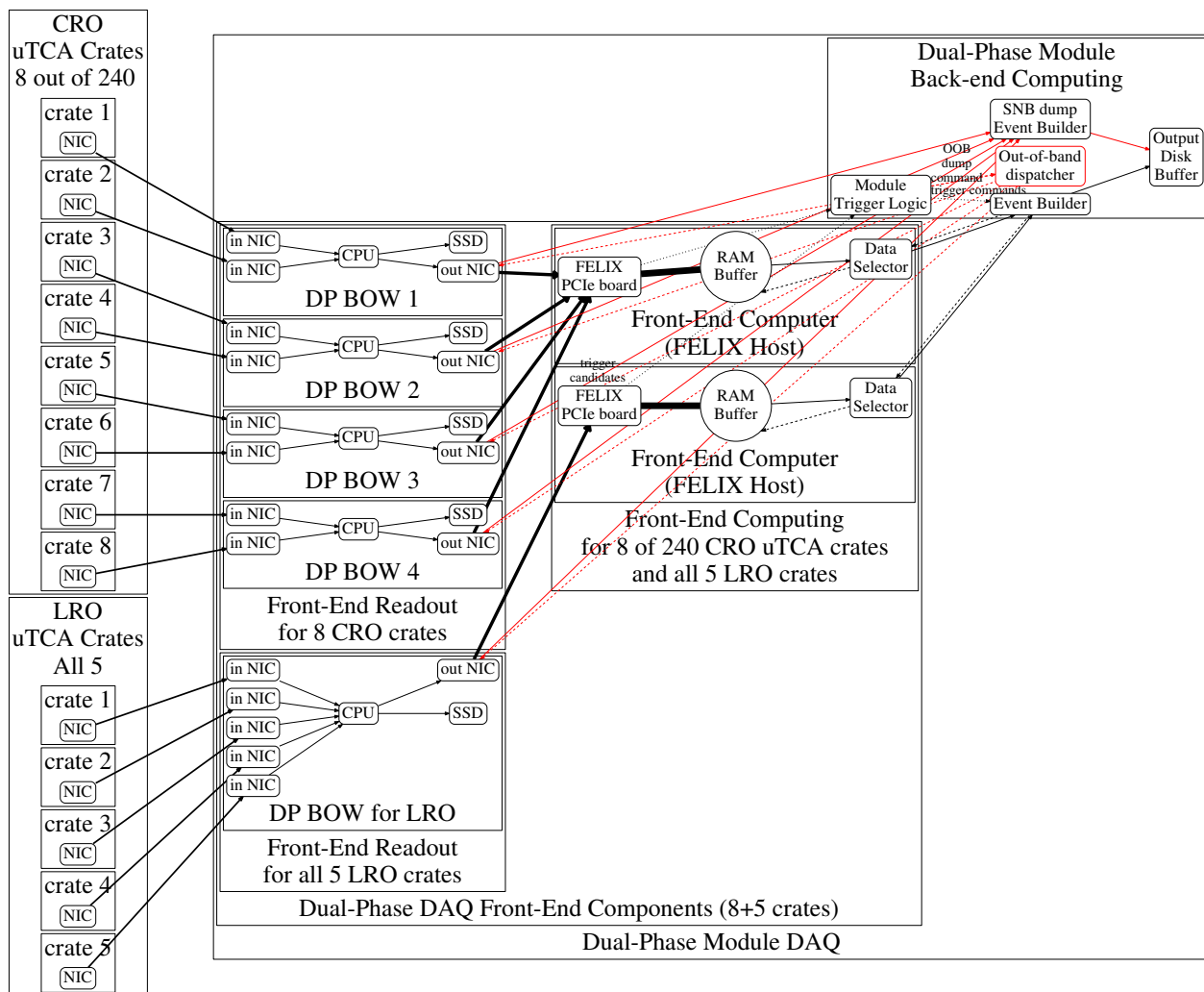


Figure 6.3: Illustration of data (solid arrows) and trigger (dashed) flow for two DP FE DAQ fragments. One servicing eight of 240 CRO crates and the other servicing all five LRO crates. Black arrows indicate nominal flow and red indicate special flow for handling of potential SNB.

Figure 6.3 illustrates DP-specific implementation of the nominal, generic DAQ front-end DAQ front-end fragment design shown in Figure 6.1. The CRO crates deliver data on user datagram protocol (UDP) to BOW computers which implement the FER duties. The CRO data is delivered to the DAQ BOW computers with lossless compression applied and so before the trigger primitives can be produced the data must be decompressed.

In order to save on cost, power, space, cooling, etc., a number of CRO crate data streams can be aggregated into one FEC. The CRO data stream is sent using UDP which is not expected to provide reliable transport of high-throughput data if a network switch intervenes. Thus each CRO requires a corresponding 10 Gbit/s network interface controller (NIC) in the receiving BOW computer. With the expected  $10\times$  lossless compression factor the nominal output from each CRO crate will be 2 Gbps. If noise levels are higher than expected the throughput will increase, however even very noisy data should be compressible enough to fit into the 10 Gbps bandwidth. Noise will be better understood from ProtoDUNE-DP data, and studies are needed to optimize the number of CRO crates per BOW computer.

After processing, the input data is sent out, along with the corresponding primitives to a Front-End Link eXchange (FELIX) board in a FEC. Similar to the argument above about noise, bandwidth and BOW computer multiplicity, the number of BOW data streams that can be aggregated into each FELIX board requires additional study. The current generation of FELIX boards have been tested with a throughput to system RAM of 10 GB/s. The next generation is expected to at least double that. With the caveat that these tests did not receive data on UDP, a nominal 20 GB/s throughput is assumed possible for the next-generation PCIe v4 boards. Given this assumption and that the expected noise levels are achieved, then based solely on bandwidth, as many as 80 CRO data streams might be aggregated into a single next-generation FELIX board. Figure 6.3 indicates the aggregation of eight CRO streams, which represents the multiplicity required to deal with very high noise. Future studies are needed to determine which of these two extremes to favor for optimization of the design, but the basic design itself is fairly elastic between them.

The LRO crates are nominally not involved in self-triggering although the data from all five LRO crates are assumed to flow through a LRO BOW. The data are then sent to a single FELIX board. Given the expected data rates, that FELIX board must ingest about 25 GB/s.

The second duty of the FER in the nominal design is to provide non-volatile storage for receiving full-stream data dumps when an SNB dump trigger command is issued. With today's technology, individual SSDs can write at about 2.5 GB/s. Up to four SSDs have been placed on a 1-lane PCIe v3 board and have achieved about three times this speed. This would allow an individual BOW computer to aggregate 10 to 30 CRO data streams before the SSDs become a bottleneck. The five LRO data streams, each producing 5 Gbps, could together be streamed to a two modern SSDs. The BOW computers must also have sufficient RAM to hold pre-SNB-trigger data of about 10 seconds.

The alternate design (not diagrammed), which corresponds to Figure 6.2, deletes the layer containing BOW computers and directly connects the UDP streams from the CRO and LRO crates to the FELIX boards in the FECs. The CRO (compressed) data is buffered on the FELIX host computer RAM and distributed to the trigger farm for decompression and trigger primitive and trigger candidate processing. The remaining part of the trigger decision is as in the nominal design

except that the SNB dump data stream is handled symmetrically with the normal triggered data.

### 6.2.3 Front-end Trigger Primitive Generation

In the nominal design, the BOW computers decompress the CRO data stream and execute algorithms to search for per-channel localized activity above some threshold based on a recent measure of the noise. These trigger primitives are then sent out along with the original, compressed CRO data to the FEC associated with the BOW.

Initial studies have shown some promise that this type of trigger primitives pipeline can be implemented on commodity CPUs and keep up with the data. The studies made use of SP signal and noise simulation but given the relatively higher signal-to-noise ratio expected in the DP module data, coupled with fewer total channels, these studies should be applicable and even better performance may be expected. With that said, more realistic studies using DP-specific simulations and with ProtoDUNE-DP data are needed.

Most of the same technical triggering issues apply in the nominal and the alternate designs (generically diagrammed in Figure 6.2), as both call for deploying trigger primitive pipelines on commodity CPUs. The main difference is that the BOW hosts become trigger farm hosts. They move from being upstream and inline of the data flow before the FEC to being downstream and receiving the data after it has been buffered. Their trigger candidates no longer have to be inserted into the stream and stripped out by the FEC and instead are sent directly to the MTL. Additional study is required to understand the multiplicity of trigger processing computers and how that might scale as one considers different multiplicities of CRO Micro Telecommunications Computing Architecture ( $\mu$ TCA) crates with respect to each FEC.

In both designs, the LRO data is currently not considered for triggering as the CRO triggering is expected to be more efficient. However, using light information for triggering has not yet been ruled out. Future studies may indicate additional benefit to including LRO information in triggering and both the nominal and alternate design can elastically accommodate this increased scope although possibly at the cost of either more BOW or trigger processor computers. As described elsewhere, the LRO data flow is handled by separate DAQ front-end fragments from those that service the CROs. Thus, if any trigger primitives and trigger candidates are to be formed from LRO data they would come from these separate fragments and be combined in the MTL as peers of the CRO and external candidates.

### 6.2.4 Dataflow, Trigger and Event Builder

In the general data and trigger flow diagrams for the nominal (Figure 6.1) and alternate (Figure 6.2) designs, the dataflow, trigger and event builder functions take as input data from the detector module electronics and culminate in files deposited to the secondary DAQ buffer for transfer to permanent storage by offline computing processes. The continuous, uncompressed data rate of the input from one detector module is on the order of 1 TB/s. The final output data rate, for all

detector modules operating at any given time is approximately limited to 1 GB/s.

To accept this high data-inflow rate and to apply the substantial processing needed to achieve the required reduction factor, which is on the order of 1000, the DAQ follows a distributed design. The units of distribution for the front end of the DAQ must match up with natural units of the detector module providing the data. This unit is called the DAQ front-end fragment and each accepts input at a rate of about 10 to 20 GB/s. The exact choice maps to some integral number of physical detector module units (e.g., SP anode plane assemblies or DP CROs and LROs).

As described in the previous sections, the nominal and alternate designs differ essentially in the order and manner in which the SNB buffering occurs and the trigger primitives are formed. The overall data flow, higher level triggering and building of *event* data blocks for final writing are conceptually very similar. This processing begins with the data being received by the FELIX PCIe board hosted in the FEC. The FELIX board performs a DMA transfer of the data into the primary buffer for the DAQ front-end fragment, which resides in the FEC host system RAM. This buffer is sized to hold ten seconds of data assuming the maximum uncompressed input rate associated with the fragment. While data is being written to the buffer, a delayed portion is also being read in order to dispatch it for various purposes. Any and all requests to further dispatch a subset of this data from the primary buffer must arrive within this buffer time. In the nominal design, the only dispatching will be from a request made by an EB (described more below) upon receipt of a trigger command. In the alternate design, a suitable fraction of the data is also dispatched via high bandwidth (at least 25 to 50 Gbit/s simplex, less if data is compressed at this stage) network connections to a trigger farm so that trigger primitives may be formed. Whether the primitives are formed in this manner or extracted from the stream sent by the FER (as in the nominal design) these trigger primitives from one DAQ front-end fragment are collectively sent for further processing in order to be combined across channels and to then produce trigger candidates. These are finally combined for one detector module in the MTL. It is in the MTL where trigger candidates from additional sources are also considered, as described in section 6.2.5.

In both the nominal and alternate designs the dispatch of data initiated by normal (non-SNB) trigger commands is identical. This dispatch, commonly termed *event building* involves collection of data spanning an identical and continuous period of time from multiple primary buffers across the DAQ. As introduced above, each trigger command is consumed by an EB process. It uses fragment address information in the trigger command to query the data selector process representing each referenced DAQ front-end fragment and accepts the returned a data fragment. In the exceptional case that the delay of this request is so large that the primary buffer no longer contains the data, then an error return is supplied and recorded by the EB in place of the lost data. Such failures lead to indicators displayed by the detector operation monitoring system. The EB finally assembles all responses into a DAQ event block and writes it to file on the secondary DAQ buffer where it becomes the responsibility of DUNE offline computing.

The data selector and EB services are implemented using the general-purpose Fermilab data acquisition framework *artDAQ* for distributed data combination and processing. It is designed to exploit the parallelism that is possible with modern multi-core and networked computers, and has been used in ProtoDUNE and other experiments. The *artDAQ* framework is the principal architecture that will be used for the DUNE DAQ back-end computing. The authors of *artDAQ* have accommodated DUNE-specific requests for feature additions. Also, a number of libraries have been

developed based on existing parts of *artDAQ* used to handle incoming data from data sources. It is likely that future DUNE extensions will be made by one of these two routes.

Unlike the dispatch of data initiated by a normal trigger commands, a command formed to indicate the possibility of a SNB is handled differently between the nominal and alternate designs. Such a command is interpreted to save all data from all channels for a rather extended time of 30s starting from 10s before the time associated with the trigger command. As no data selection is being performed, given the required bandwidth, special buffering to nonvolatile storage, in the form of SSD, is required. Today's technology supplies individual SSD in the M.2 expansion card form factor, which supports individual write speeds up to 2.5 GB/s. The two designs differ as to the location of and data source for these buffers.

In the nominal design, these SSDs reside in the FER as described in Section 6.2.2. In that location, due to larger granularity of computing units, the data rate into any one SSD is within the quoted write bandwidth. However, and as shown in Figure 6.1, the data and trigger flow for SNB in the nominal case takes a special path. Instead of an EB consuming the trigger command as described above, it is sent to the out-of-band trigger command dispatcher (OOB dispatcher), which dispatches it to each FER unit hosting an SSD. This component is used to immediately free up the MTL to continue to process normal triggers. When the command is received, each host must begin to stream data from its local RAM, supplying at least 10s of buffer to the SSD, and continue until the full 30s has elapsed. While it is performing this dump it must continue to form trigger primitives and pass them and the full data stream to the connected FEC.

In the alternate design the same primary buffer provides the 10s of pre-trigger SNB buffering. As in the nominal case, it must rely on fast, local SSD storage to sink the dump. Current SSD technology allows four M.2 SSD devices to be hosted on a PCIe board. Initial benchmarks of this technology show that such a combination can achieve 7.5 GB/s write bandwidth, which is short of linear scaling. To support the maximum of 20 GB/s, three such boards would be required. The alternate design presents a synergy between the need to dump high-rate data and the need to provide CPU to form the trigger primitives. With current commodity computing hardware it is expected that each FEC will need to be augmented with about two computers in the trigger farm. These trigger processors will need to accept the entire DP and three-eighths of the SP data stream from their DAQ front-end fragment. If they instead accept the entire stream, they can also provide RAM buffering and split up the data rate, which must be sunk to SSD buffers.

In both designs, the data dumped to SSD may contain precious information about a potential SNB. It must be extracted from the buffer, processed and either discarded or saved to permanent storage. The requirements on these processes are not easy to determine. The average period between actual SNBs to which DUNE is sensitive is measured in decades. However, to maintain high efficiency for capturing such important physics, the thresholds will be placed as low as feasible, limited only by the ability to acquire, validate and (if validated) write out the data to permanent storage. Notwithstanding, the (largely false positive) SNB trigger rate is expected to be minuscule relative to normal triggers. Understanding the exact rate requires more study, including using early data, but for planning purposes it is simply assumed that one whole-detector data dump will occur per month on average. Using the SP module as an example, and choosing the nominal time span for the dump to be 30s, about 45 PB of uncompressed data would result. In the nominal SP DAQ design, this dump would be spread over 600 SSD units leading to 75 GB per SSD per dump. Thus,



typical SSDs offer storage to allow any given dump to be held for at least one half year before it must be purged to assure storage is available for subsequent dumps. If every dump were to be sent to permanent storage, it would represent a sustained 0.14 Gbit/s (per detector module), which is a small perturbation on the bandwidth supplied throughout the DAQ network. Saved to permanent storage this rate integrates to 0.5 PB/year, which while substantial, is a minor fraction of the total data budget. The size of each dump is still larger than is convenient to place into a single file, so the SNB event-building will likely differ from that for normal triggers in that the entire dump is not held in a single DAQ event block. Finally, it is important to qualify that these rates assume uncompressed data. At the cost of additional processing elements, lossless compression can be expected to reduce this data rate by 5 to 10 $\times$  or alternatively allow lower thresholds that lead to the same factor of more dumps. Additional study is required to optimize the costs against the expected increase in sensitivity.

### 6.2.5 Data Selection Algorithms

Data selection follows a hierarchical design. It begins with forming detector unit-level trigger candidates inside the DAQ front-end fragment FE computing using channel-level trigger primitives. These are then used to form detector module trigger commands in the MTL. When executed, they lead to readout of a small subset of the total data. In addition, trigger candidates are provided to the MTL from external sources such as the ETL in order to indicate external events such as beam spills, or SNB candidates detected by the other detector modules. In addition to supplying triggers to SuperNova Early Warning System (SNEWS), triggers from SNEWS or other cosmological detector sources such as LIGO and VIRGO can be accepted in order to possibly record low-energy or dispersed activity that would not pass the self-triggering. The latency of arrival for these sources must be less than the nominal 10 s buffers used to capture low-level early SNB activity. A high-level trigger (HLT) may also be active within the MTL. The hierarchical approach is natural from a design standpoint and it allows for vertical slice testing and running multiple DAQ partitions simultaneously during commissioning of the system or when debugging of individual detector units is required.

As discussed in Sections 6.2.2 and 6.2.3, trigger primitives are generated in either in FERs (in the nominal design) or in trigger processing computers (in the alternate design). In both designs, and for both SP and DP detector modules, only data from TPC collection channels (three-eighths of SP and all of DP channels) feed the self-triggering, as their waveforms directly supply a measure of ionization activity without computationally costly signal processing. The trigger primitives contains summary information for each channel, such as the time of any threshold-crossing pulse, its integral charge, and time over threshold. A channel with an associated trigger primitive is said to be *hit* for the time spanned by the primitive. Trigger primitives from one detector unit are then further processed to produce a trigger candidate. The candidate represents a cluster of hits across time and channel, localized to the detector unit. The candidates from all DAQ front-end fragments are passed to the MTL.

The MTL arbitrates between various trigger types, determines trigger priority and ultimately the time range and detector coverage for a trigger command, which it emits back to the FECs. The MTL assures that no trigger commands are issued that overlap in time or in detector channel

space. It also may employ a HLT to reduce or aggregate triggers into fewer trigger commands so as to optimize the subsequent readout. For example, aggregating many small readouts into fewer but larger ones may allow for more efficient processing. This can be particularly important during periods of high-rate activity due to e.g., various backgrounds or instrumental effects.

When activity leads to the formation of a trigger command this command is sent down to the FECs instructing which slice of time of its buffered data should be saved. The trigger command information is saved along with this data. At the start of DUNE data taking, it is anticipated that for any given single-interaction trigger (a cosmic-ray track, for example), waveforms from all channels in the detector module will be recorded over a one readout window (nominally, 5.4 ms for SP and 16.4 ms for DP, chosen to be two drift times plus an extra 20%).

Such an approach is clearly very generous in terms of the amount of data saved, but it ensures that associated low-energy physics (such as captures of neutrons produced by neutrino interactions or cosmic rays) are recorded without any need to fine-tune detector unit-level triggering, and does not depend on the noise environment across detector units. In addition, the wide readout window ensures that the data of all associated activity is recorded. As generous as it is, it is estimated that this readout window will not produce an unmanageable volume of data. As shown in Table 6.3, the uncompressed selected data from the SP module will fill about half of the nominal annual data budget. The longer DP drift and its fewer channels will give approximately the same data rate. However, once a modest amount of lossless compression is applied, the nominal data budget can be met. Early running will allow experience to be gained and more advanced data selection algorithms to be validated allowing the DAQ to discard the many data fragments in each trigger consistent with just electronics noise. This has the potential for a reduction of at least another factor of ten.

Other trigger streams – calibrations, random triggers, and prescales of various trigger thresholds – are also generated at the detector module level, and filtering and compression can be applied based upon the trigger stream. For example, a large fraction of random triggers may have zero-suppression (ZS) applied to their waveforms, reducing the data volume substantially, as the dominant data source for these will be  $^{39}\text{Ar}$  events. Additional signal-processing can also be done on particular trigger streams if needed and if the processing is available, such as fast analyses of calibration data.

At the detector module level, a decision can also be made on whether a series of interactions is consistent with an SNB. If the number of detector unit-level, low-energy trigger candidates exceeds a threshold for the number of such events in a given time, a trigger command is sent from the MTL back to the FERs, which store up to 10 s of full waveform data. That data is then streamed to non-volatile storage to allow for subsequent analysis by the SNB working group, perhaps as an automated process. If not rejected, it is sent out of the DAQ to permanent offline storage.

In addition, the MTL passes trigger candidates up to a detector-wide ETL, which among other functions, can decide whether, integrated across all modules, enough detector units have detected interactions to qualify as an SNB, even if within a particular module the threshold is not exceeded. Trigger candidates from the ETL are passed to the MTL for dispatch to the FECs (or FERs in the case of SNB dump commands in the nominal design). That is, to the MTL, an external trigger candidate looks like just one more *external* trigger input.

Detector unit level trigger candidates are generated within the context of one DAQ front-end fragment, specifically in each FEC. The trigger decision is based on the number of nearby channels hit in a given fragment within a time window (roughly 100  $\mu$ s), the total charge collected in these adjacent channels, and possibly the union of time-over-threshold for the trigger primitives in the collection plane. Studies show that even for low-energy events (roughly 10 MeV to 20 MeV) the reduction in radiological backgrounds is extremely high with such criteria. The highest-rate background,  $^{39}\text{Ar}$ , which has an overall rate of 10 MBq within a 10 kt volume of argon, has an endpoint of 500 keV and requires significant pileup in both space and time to get near a 10 MeV threshold. One important background source is  $^{42}\text{Ar}$ , which has a 3.5 MeV endpoint and an overall rate of 1 kBq.  $^{222}\text{Rn}$  decays via a 5.5 MeV kinetic energy  $\alpha$  and is also an important source of background. The radon decays to  $^{218}\text{Po}$ , which within a few minutes leads to a 6 MeV kinetic energy  $\alpha$ , and ultimately to a  $^{214}\text{Bi}$  daughter (many minutes later), which has a  $\beta$  decay with its endpoint near 3.5 MeV kinetic energy. The  $\alpha$  ranges are short, resulting in charge being collected on one or two anode wires at most, but the charge deposit can be large, and therefore the charge threshold must be well above the  $\alpha$  deposits plus any pileup from  $^{39}\text{Ar}$  and noise.

At the level of one detector unit, two kinds of local trigger candidates can be generated. One is a high-energy trigger that indicates local ionization activity corresponding to more than 10 MeV. The per-channel thresholds on total charge and time-over-threshold will be optimized to achieve at least 50% efficiency at this energy threshold, with efficiency increasing to 100% via a turn-on curve that ensures at least 90% efficiency at 20 MeV. The second type of trigger candidate generated is for low-energy events between 5 MeV and 10 MeV. In isolation, these candidates do not lead to formation of a trigger command. Rather, at the detector module level they are combined, time ordered and their aggregate rate compared against a threshold based on fluctuations due to noise and backgrounds in order to form an SNB trigger command.

The MTL takes as input trigger candidates (both low-energy and high-energy) from the participating DAQ front-end fragments, as well as external trigger candidate sources, such as the ETL, which includes global, detector-wide triggers, external trigger sources such as SNEWS, and information about the time of a Fermilab beam spill. The MTL also generates trigger commands for internal consumption, such as random triggers and calibration triggers (for example, telling a laser system to fire at a prescribed time). The MTL can also generate trigger commands from a prescaled fraction of trigger types that otherwise do not generate such commands on their own. For example, a prescaled fraction of single, low-energy trigger commands could be allowed to generate a trigger command, even though those candidates normally only result in a trigger command when aggregated (i.e., as they would be for an SNB).

The MTL is also responsible for checking candidate triggers against the current run control (RC) trigger mask: in some runs, for example, we may decide that only random triggers are accepted, or that certain trigger candidates streams should not be considered because their DAQ front-end fragments have been producing unreasonably large rates in the recent past (such as may be due to noise spikes, flaky hardware or buggy software). In addition, the MTL counts low-energy trigger candidates, and based upon their number and distribution over a long time interval (e.g., 10s), decides to generate an SNB trigger command. The trigger logic will be optimized to record the data due to at least 90% of all Milky Way supernovae, and studies of simple low-energy trigger criteria show that a much higher efficiency can likely be achieved.

The HLT can also be applied at this level, particularly if there are unexpectedly higher rates from instrumental or low-energy backgrounds that require some level of reconstruction or pattern recognition. An HLT might also allow for efficiently triggering on lower-energy single interactions, or allow for better sensitivity for supernovae originating outside the Milky Way galaxy, by employing a weighting scheme to individual trigger candidates – higher-energy trigger candidates receiving higher weights. Thus, for example, two trigger candidates consistent with 10 MeV interactions in 10 s might be enough to create a SNB candidate trigger, while a hundred 5 MeV trigger candidates in 10 s might not. Lastly, the HLT can allow for dynamic thresholding; for example, if a trigger appears to be due to a cosmic-ray muon, the threshold for single interactions can be lowered (and possibly prescaled) for a short time after that to identify spallation products. In addition, the HLT could allow for a dynamic threshold after a SNB, to extend sensitivity beyond the 10 s SNB readout window, while not increasing the data volume associated with SNB candidates linearly.

All low-energy trigger candidates are also passed upwards to the ETL so that they may be integrated across all 10 kt detector modules in order to determine that a SNB may be occurring. This approach increases the sensitivity to trigger on SNBs by a factor of four (for 40 kt), thus extending the burst sensitivity to a distance twice as far as for a single 10 kt detector module.

The MTL is also responsible for including in the trigger command a global timestamp built from its input trigger candidates, and information on what type of trigger was created. Information on trigger candidates is also kept, whether or not they contribute to the formation of a trigger command. As described above, the readout window for nominal trigger commands (those other than for SNB candidates) is somewhat more than two times the maximum drift time. Further, a nominal readout spans all channels in a detector module. The MTL is also responsible for sending the trigger commands that tell the FERs to stream all data from the past 10 s and for a total of 30 s in hopes to catch SNBs. This command may be produced based on trigger candidates from inside the MTL itself or it may be produced based on an external SNB trigger candidate passed to the MTL by the ETL.

## 6.2.6 Timing and Synchronization

The timing distribution is integrated into the TPC electronics design and is described in section 3.4.2 and 3.2.6 using a White Rabbit (WR) network over synchronous 1 Gbit/s Ethernet (SyncE), using Precision Time Protocol-version 2 (PTPV2) packets.

The synchronization between the FD and the beam pulses from the LBNF beamline is done by a single overall system for SP and DP and is described in the following section.

### 6.2.6.1 Beam timing

The neutrino beam is produced at the Fermilab accelerator complex in spills of 10  $\mu$ s duration. A spill location system (SLS) at the Far Detector site will locate the time periods in the data when beam could be present, based on network packets received from Fermilab containing predictions

of the GPS-time of spills soon to occur or absolute time stamps of recent spills. Experience from MINOS and NO $\nu$ A shows that this can provide beam triggering with high reliability with some small fraction of late or dropped packets. To improve reliability further, the system outlined here contains an extra layer of redundancy in the prediction process. Several stages of prediction based on recent spill behavior will be applied, aiming for an accuracy of better than 10% of a readout time (sub-ms) in time for the data to be selected from the DAQ buffers. Ultimately, an offline database will match the actual time of the spill with the data, thus removing any reliance on real-time network transfer for this crucial stage of the oscillation measurements. The network transfer of spill-timing information is simply to ensure that a correctly located and sufficiently wide window of data is considered as beam data. This system is not required, and is not designed to provide signals accurate enough to measure neutrino time-of-flight.

The precision to which the spill time can be predicted at Fermilab improves as the acceleration process of the protons producing the spill in question advances. The spills currently occur at intervals of 1.3 s; the system will be designed to work with any interval, and to be adaptable in case the sequence described here changes. For redundancy, three packets will be sent to the far detector for each spill. The first is approximately 1.6 s before the spill-time, which is at the point where a 15 Hz booster cycle is selected; from this point on, there will be a fixed number of booster cycles until the neutrinos and the time is subject to a few ms of jitter. The second is about 0.7 s before the spill, at the point where the main injector acceleration is no longer coupled to the booster timing; this is governed by a crystal oscillator and so has a few  $\mu$ s of jitter. The third will be at the so called ‘\$74’ signal generated before the beamline kicker magnet fires to direct the protons at the LBNF target; this doesn’t improve the timing at the Far Detector much, but serves as a cross check for missing packets. This system is enhanced compared to that of MINOS-NO $\nu$ A, which only use a third of the above timing signals. The reason for the larger uncertainty in the time interval from 1.6 s to 0.7 s is that the booster cycle time is synchronized to the electricity supply company’s 60 Hz, which has a variation of about 1%.

Arrival-time monitoring information from a year of MINOS data-taking was analyzed, and it was found that 97% of packets arrived within 100 ms of being sent and 99.88% within 300 ms.

The SLS will therefore have estimators of the GPS-times of future spills, and recent spills with associated data contained in the primary buffers. These estimators will improve in precision as more packets arrive. The DAQ will use data in a wider window than usual, if, at the time the trigger decision has to be made, the precision is lower due to missing or late packets. From the MINOS monitoring analysis, this expected to be very rare.

## 6.2.7 Computing and Network Infrastructure

The computing and network infrastructure that will be used in each of the four detector modules is similar, if not identical. It supports the buffering, data selection, event building, and data flow functionality described above, and it includes computing elements that consist of servers that:

- buffer the data until a trigger decision is received;

- host the software processes that build the data fragments from the relevant parts of the detector into complete events;
- host the processes that make the trigger decision;
- host the data logging processes and the disk buffer where the data is written;
- host the real-time data quality monitoring processing;
- host the control and monitoring processes.

The network infrastructure that connects these computers has the following components:

- subnets for transferring triggered data from the buffer nodes to the event builder nodes; these need to connect underground and above-ground computers;
- a control and monitoring subnet that connects all computers in the DAQ system and all FE electronics that support Ethernet communication; this sub-network must connect to underground and above-ground computers;
- a subnet for transferring complete events from the event builder servers to the storage servers; this subnet is completely above-ground.

## 6.2.8 Run Control and Monitoring

The online software constitutes the backbone of the DUNE DAQ system and provides control, configuration and monitoring of the data taking in a uniform way. It can be subdivided logically into four subsystems: the run control, the management of the DAQ and detector module electronics configuration, the monitoring, and the non-physics data archival. Each of these subsystems has a distinct function, but their implementation will share underlying technologies and tools.

In contrast to experiments in which data taking sessions, i.e., runs, are naturally subdivided into time slots by external conditions (e.g., a collider fill, a beam extraction period), the DUNE experiment aims to take data continuously. Therefore, a classic run control with a coherent state machine and a predefined and concurrently configured number of active detector and DAQ elements does not seem adequate.

The DUNE online software is thus structured according to the architecture principle of loose coupling: each component has as little knowledge as possible of other components. While the granularity of the back-end DAQ components may match the individual software processes, for the front-end DAQ a minimum granularity must be defined, balancing fault tolerance and recovery capability against the requirement of data consistency. The smallest independent component is called a DAQ front-end fragment, which is made up of the detector units associated with a single front-end computer. In the nominal design, this corresponds to two SP anode plane assemblies and about ten DP CRO crates.

The concept of a *run* represents a period of time in which the same FE elements are active or the same data selection criteria are in effect (possibly with maximum lengths for offline processing reasons). More than just orchestrating data taking, the run control provides the mechanisms allowing DAQ applications to publish their availability, subscribe to information, and exchange messages. In addition, the online software provides a configuration service for DAQ elements to store their settings and a conditions archive, keeping track of varying detector electronics settings and status.

Another important aspect of the online software is the monitoring service. Monitoring can be subdivided into two main domains: the monitoring of the data taking operations (rates, number of data fragments in flight, error flags, application logs, network bandwidth, computing and network infrastructure) and the monitoring of the physics data. Both are essential to the success of the experiment and must be designed and integrated into the DAQ system from the start. In particular, for such a large and distributed system, the information sharing and archival system is very important, as are scalable and easily accessible data visualization tools, which will evolve during the lifetime of the experiment. The online software provides the glue that holds the DAQ applications together and enables data taking. Its architecture guides the approach to DAQ application design and also shapes the view that the operators will have of the experiment.

## 6.3 Interfaces

### 6.3.1 TPC Electronics

Details about the interfaces between the DAQ and the DP charge readout TPC electronics are documented in [36].

In the case of the DP detector module, signals from the charge readout electrodes are amplified and then digitized by advanced mezzanine card (AMC) boards residing in 240  $\mu$ TCA crates. Each crate produces 2.5 MHz samples from 640 channels on a 10 Gbit/s optical fiber. Data is losslessly compressed and sent via UDP producing a stream with an expected average throughput of 2 Gbit/s. The DAQ consortium will be responsible for acquiring the fibers while the DP electronics consortium will be responsible for their installation on the cryostat roof down to their connection to the  $\mu$ TCA crates.

### 6.3.2 PD Electronics

Details about the interfaces between the DAQ the DP light readout [26] are documented.

For the DP LRO, the signals are digitized in 14 bits at 65 MHz and then downsampled to 2.5 MHz. The data is then handled largely symmetrically with the CRO data except that only five  $\mu$ TCA crates are required and their average uncompressed output is expected to fill 5 Gbit/s on 10 Gbit/s

fiber optical connections. The installation of these fibers is similar to that described above for the CROs fibers.

### 6.3.3 Offline Computing

The interface between the DAQ and offline computing is described in [37]. The DAQ team is responsible for reducing the data volume to the level that is agreed upon by all interested parties, and the raw data files are transferred from SURF to Fermilab using a dedicated network connection. A disk buffer is provided by the DAQ on or near the SURF site to hold several days worth of data so that the operation of the experiment is not affected if there happens to be a network disruption between SURF and Fermilab.

During stable running, the data volume produced by the DAQ systems of all four detector modules will be no larger than 30 PB/year. The maximum data rate is expected to be independent of the number of detector modules that are operational. During the construction of the second, third, and fourth detector modules, the extra rate per detector module will be used to gather data to aid in the refinement of the data selection algorithms. During commissioning, the data rate is expected to be higher than nominal running and it is anticipated that a data volume corresponding to (order) one year will be necessary to commission a detector module.

The disk buffer at SURF is planned to be 300 TB in size. The data link from SURF to Fermilab will support 100 Gbit/s (30 PB/year corresponds to about 8 Gbit/s). The offline computing team is responsible for developing the software to manage the transfer of files from SURF to Fermilab. The DAQ team is responsible for producing a reference implementation of the software that is used to access and decode the raw electronics data. The offline group is also responsible for providing the framework for real-time data quality monitoring (DQM). This monitoring is distinct from the online monitoring (OM). Developing the payload jobs that run various algorithms to summarize the data is the joint responsibility of the DAQ, offline, reconstruction and other groups. The DQM system includes a visualization system that can be accessed from the Internet and shows specifically where operation shifts are performed.

### 6.3.4 Slow Control

The cryogenic instrumentation and slow controls (CISC) systems monitor detector hardware and conditions not directly involved in taking the data described above. That data is stored both locally (in CISC database servers in the CUC) and offline (the databases will be replicated back to Fermilab) in a relational database indexed by timestamp. This allows bi-directional communications between the DAQ and CISC by reading or inserting data into the database as needed for non time-critical information.

For prompt, time sensitive status information such as *run is in progress* or *camera is on*, a low-latency software status register is available on the local network to both systems.



There is no hardware interface. However, several racks of CISC servers are in the counting room of the CUC, and rack monitors in DAQ racks are read out into the CISC data stream.

Note that life and hardware safety-critical items will be hardware interlocked according to Fermilab standards, and fall outside the scope of this interface.

### 6.3.5 External Systems

The DAQ is required to save data based on external triggers, e.g., when a pulse of beam neutrinos arrives at the FD; or upon notice of an interesting astrophysical event by SNEWS [38] or LIGO. This could involve going back to save data that has already been buffered (see Section 6.2.2), or changing the trigger or zero suppression criteria for data taken during the interesting time period.

#### 6.3.5.1 Beam Trigger

The method for predicting and receiving the time of the beam spill is described in Section 6.2.6.1. Once that time is known to the DAQ, a high-level trigger can be issued to ensure that the necessary full data can be saved from the buffer and saved as an event.

#### 6.3.5.2 Astrophysical Triggers

SuperNova Early Warning System (SNEWS) is a coincidence network of neutrino experiments that are individually sensitive to an SNB observed from a core-collapse supernova somewhere in our galaxy. While DUNE must be sensitive to such a burst on its own, and is expected to be able to contribute to the coincidence network (Section 6.2.5) via a TCP/IP socket, the capability to save data based on other observations provides an additional opportunity to ensure capture of this rare and valuable data. A SNEWS alert is formed when two or more neutrino experiments report a potential SNB signal within 10 s. A script running on the SNEWS server at BNL, provided by a given experiment that wishes to receive an alert, sends out a message with the earliest time in the coincidence. The latency from the neutrino burst is set by the response time of the second fastest detector to report to SNEWS. This could be as short as seconds, but could be tens of seconds. At latencies larger than 10 s, full data might not be available, but selected data is expected to be manageable.

Other astrophysical triggers are available to which DUNE alone is unlikely to have sensitivity, except in rare cases, or if the triggers are taken as an ensemble. Among these are gravitational wave triggers (the details are being worked out during the current LIGO shutdown), and high-energy photon transients, most notably gamma ray bursts. In fact, the use of network sockets on the timescale of seconds enabled cooperation between LIGO, VIRGO, the Gamma Ray Coordinates Network (GCN) <sup>1</sup>, and a number of automated telescopes to make the discovery that *short/hard*

---

<sup>1</sup>Described in detail at [https://gcn.gsfc.nasa.gov/gcn\\_describe.html](https://gcn.gsfc.nasa.gov/gcn_describe.html)

gamma ray bursts are caused by colliding neutron stars [39].

## 6.4 Production and Assembly

### 6.4.1 DAQ Components

The FD DAQ system comprises the classes of components listed below. In each case, we outline the production, procurement, quality assurance (QA), and quality control (QC) strategies.

#### 6.4.1.1 Custom Electronic Modules

Custom electronic modules, specified and designed by the DAQ consortium, are used for two functional components in the DAQ FE. The first is to interface the detector module electronics to the DAQ FEC systems, which are likely to be based on the FELIX PCIe board. The other is for real-time data processing (particularly for the SP module), which will likely be based on the Cluster On Board (COB) ATCA blade. PROTODUNE-SP currently implements both designs, and new designs optimized according to DUNE requirements will be developed. It is possible that we will make use of commercially-designed hardware in one or other of these roles. DAQ consortium institutes have significant experience in the design and production of high-performance digital electronics for previous experiments. Our strategy is therefore to carry out design in-house, manufacturing and QA steps in industry, and testing and QC procedures at a number of specialized centers within the DUNE collaboration. Where technically and economically feasible, modules will be split into subassemblies (e.g., carrier board plus processing daughter cards), allowing production tasks to be spread over more consortium institutes.

DUNE electronic hardware will be of relatively high performance by commercial standards, and will contain high-value subassemblies such as large field programmable gate arrays (FPGAs). Achieving a high yield will require significant effort in design verification, prototyping and pre-production tests, as well as in tendering and vendor selection. The production schedule is largely driven by these stages and the need for thorough testing and integration with firmware and software before installation, rather than by the time for series hardware manufacture. This is somewhat different from the majority of other DUNE FD components.

#### 6.4.1.2 Commercial Computing

The majority of procured items will be standard commercial computing equipment, in the form of compute and storage servers. Here, the emphasis is on correct definition of the detailed specification, and the tracking of technology development, in order to obtain the best value during the tendering process. Computing hardware will be procured in several batches, as the need for DAQ throughput increases during the construction period.

### 6.4.1.3 Networking and data links

The data movement system is a combination of custom optical links (for data transmission from the cryostats to the CUC) and commercial networking equipment. The latter items will be procured in the same way as other computing components. The favored approach to procurement of custom optics is purchase of pre-manufactured assemblies ready for installation, rather than on-site fiber preparation and termination. Since transmission distances and latencies in the underground area are not critical, the fiber run lengths do not need to be of more than a few variants. It is assumed that fibers will not be easily accessible for servicing or replacement during the lifetime of the experiment, meaning that procurement and installation of spare *dark* fibers (including, if necessary, riser fibers up the SURF hoist shafts) is necessary.

### 6.4.1.4 Infrastructure

All DAQ components will be designed for installation in 48.3 cm (standard 19 in) rack infrastructure, either in the CUC or above ground. Standard commercial server racks with local air-water heat exchangers are likely to be used. These items will be specified and procured within the consortium, but will be pre-installed (along with the necessary electrical, cooling and safety infrastructure) under the control of technical coordination (TC) before DAQ beneficial occupancy.

### 6.4.1.5 Software and firmware

The majority of the DAQ construction effort will be invested in the production of custom software and firmware. Based on previous experiments, these projects are likely to use tens to hundreds of staff-years of effort, and will be significant projects even by commercial standards, mainly due to the specialized skills required for real-time software and firmware. A major project management effort is required to guide the specification, design, implementation and testing of the necessary components, especially as developers will be distributed around the world. Use of common components and frameworks across all areas of the DAQ is mandatory. Effective DAQ software and firmware development has been a demonstrated weakness of several previous experiments, and substantial work is required in the next two years to put in place the necessary project management regime.

## 6.4.2 Quality Assurance and Quality Control

High availability is a basic requirement for the DAQ, and this rests upon three key principles:

- A rigorous QA and QC regime for components (including software and firmware);
- Redundancy in system design, to avoid single points of failure;

- Ease of component replacement or upgrade with minimal downtime.

The lifetime of most electronic assemblies or commercial computing components will not match the 20 year lifespan of the DUNE experiment. It is to be expected that essentially all components will therefore be replaced during this time. Careful system design will allow this to take place without changes to interfaces. However, it is intended that the system run for at least the first three to four years without substantial replacements, and QA and QC, as well as spares production, will be steered by this goal. Of particular importance is adequate burn-in of all components before installation underground, and careful record-keeping of both module and subcomponent provenance, in order to identify systematic lifetime issues during running.

### 6.4.3 Integration testing

Since the DAQ will use subcomponents produced by many different teams, integration testing is a key tool in ensuring compatibility and conformance to specification. This is particularly important in the prototyping phase before the design of final hardware. Once pre-production hardware is in hand, an extended integration phase will be necessary in order to perform final debugging and performance tuning of firmware and software. In order to facilitate ongoing optimization in parallel with operations, and compatibility testing of new hardware or software, we envisage the construction of one or more permanent integration test stands at DAQ institutions. These will be in locations convenient to the majority of consortium members, i.e., at major labs in Europe and the USA. A temporary DAQ integration and testing facility near SURF will also be required as part of the installation procedure.

## 6.5 Installation, Integration and Commissioning

### 6.5.1 Installation

The majority of DAQ components will be installed in a dedicated and partitioned area of the CUC as shown in Figure 6.4, starting as soon as the consortium has beneficial occupancy of this space. The conventional facilities (CF) is responsible for running fiber from the SP module's WIBs to the DAQ, and from the DAQ to the surface. This is currently projected to take place eighteen months before anode plane assemblies are installed in the SP module, allowing time for final component acceptance testing in the underground environment, and to prepare the DAQ for detector testing and commissioning. Some DAQ components (event builder, storage cluster and WAN routers, plus any post-event-builder processing) will be installed above ground.

A total of 500 kVA of power and cooling will be available to run the computers in the counting room. Twelve 48.3 cm (standard 19 in) server racks (of up to 58U height) per module have initially been allocated for each detector module, with two more each for facilities and CISC. An optimized layout, including the necessary space for hardware installation and maintenance, plus on-site spares, will be

developed once the DAQ design is finalized. The racks will be water cooled with local air-to-water heat exchangers. To allow expanded headroom for initial testing, development, and commissioning throughput, the full complement of rack infrastructure and network equipment for four detector modules will be installed from the start.

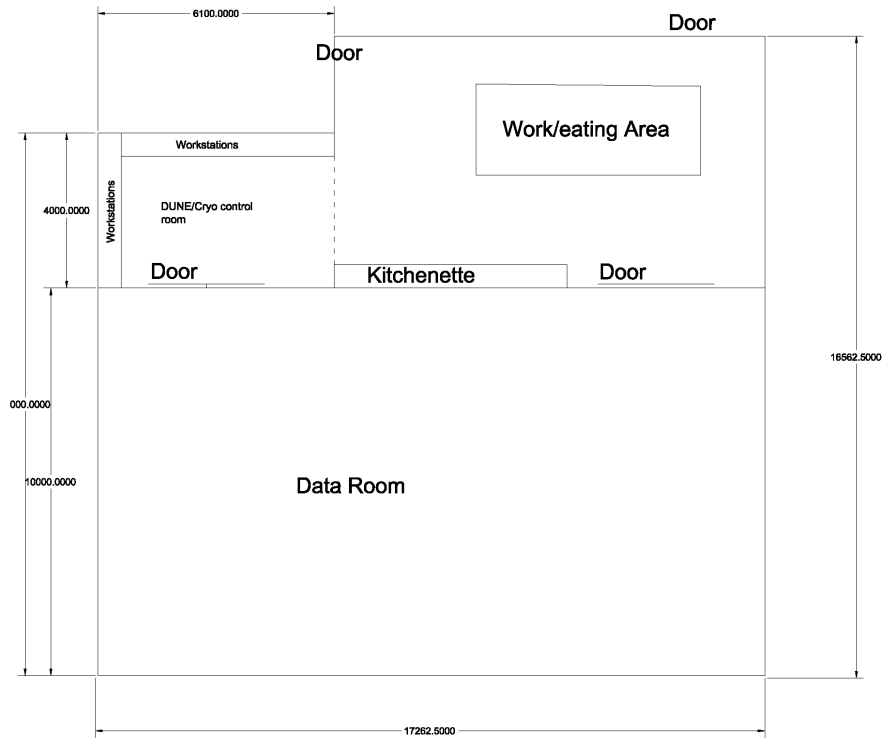


Figure 6.4: Floor plan for the DAQ and control room space in the CUC. The DAQ Room has space for at least 52 racks of servers and routers. Fiber from the WIBs in the detector caverns enter in the upper right of this room, terminate in a breakout panel, and are distributed to the RCEs in these racks, then to FELIX servers (also in this room) as outlined in Figure 6.3. Fibers to the surface enter this room from the lower left.

The counting room is similar to a server room at a university or national lab in terms of the need for cleanliness, ventilation, fire protection, drop flooring, and access control. Networking infrastructure and fiber breakout will take up some of the rack space, but very little of the power budget. Power to individual machines and crates must to be controlled remotely via power distribution units, since it is desirable to minimize DAQ workers' presence underground if there is work that can be done from the surface or remotely. Some uninterruptible power supply (UPS) capacity is needed to allow for an orderly shutdown of computers, but only networking equipment requires longer-duration backup power, this is to enable remote recovery from short-term power failures.

## 6.5.2 Integration with Detector Electronics

Basic technical integration with detector electronics will take place before installation, during a number of integration exercises in the preceding years. We anticipate that the consortium will supply and support small-scale instances of the DAQ system for testing of readout hardware at the production sites, based on prototype or pre-production hardware. Full-scale DAQ testing will have been completed with artificial data sources during internal integration. The work to be done during installation is therefore essentially channel-by-channel verification of the final system as it is installed, on a schedule allowing for any rectifying work to be carried out on the detector immediately (i.e., the DAQ must gather and present data in effectively real time). This implies the presence of a minimal but sufficient functional DAQ system before detector installation commences, along with the timing and fast control system, and the capability to permanently record data for offline analysis. However, it does not require triggering, substantial event building or data transfer capacity. The DAQ installation schedule is essentially driven by this requirement.

In addition, the data pipeline from event builder, via the storage buffer and WAN, to the offline computing facilities, must be developed and tested. We anticipate this work largely happening at Fermilab in parallel with detector installation, and the full-scale instances of these components being installed at SURF in preparation for start of data-taking.

## 6.5.3 Commissioning

System commissioning for the DAQ comprises the following steps:

- Integration with detector subsystems of successive detector modules;
- Final integration and functional testing of all DAQ components;
- Establishment of the necessary tools and procedures to achieve high-efficiency operation;
- Selection, optimization and testing of trigger criteria;
- Ongoing and continuous self-test of the system to identify actual or imminent failures, and to assess performance.

Each of these steps will have been carried out at the integration test stands before being used on the final system. The final steps are to some extent continuous activities over the experiment lifetime, but which require knowledge of realistic detector working conditions before final validation of the system can take place. We anticipate that these steps will be carried out during the cryostat filling period, and form the major focus of the DAQ consortium effort during this time.

## 6.6 Safety

Two overall safety plans will be followed by the FD DAQ. General work underground will comply with all safety procedures in place for working in the detector caverns and CUC underground at SURF. DAQ-specific procedures for working with racks full of electronics or computers, as defined at Fermilab, will be followed, especially with respect to electrical safety and the fire suppression system chosen for the counting room. For example, a glass wall between the server room space and the other areas in Figure 6.4 will be necessary to prevent workers in the server room from being unseen if they are in distress, and an adequate hearing protection regime must be put in place.

There are no other special safety items for the DAQ system not already covered by the more general safety plans referenced above. The long-term emphasis is on remote operations capability from around the world, limiting the need for physical presence at SURF, and with underground access required only for urgent interventions or hardware replacement.

## 6.7 Organization and Management

At the time of writing, the DAQ consortium comprises 30 institutions, including universities and national labs, from five countries. Since its conception, the DAQ consortium has met on roughly a weekly basis, and has so far held two international workshops dedicated to advancing the FD DAQ design. The current DAQ consortium leader is from U. Bristol, UK.

Several key technical and architectural decisions have been made in the last months, that have formed an agreed basis for the DAQ design and implementation presented in this document.

### 6.7.1 DAQ Consortium Organization

The DUNE DAQ consortium is currently organized in the form of five active Working Groups (WG) and WG leaders:

- Architecture, current WG leaders are from: U. Oxford and CERN;
- Hardware, current WG leaders are from: U. Bristol and SLAC;
- Data selection, current WG leader is from: U. Penn.;
- Back-end, current WG leader is from: Fermilab;
- Integration and Infrastructure, current WG leader is from: U. Minnesota Duluth.

During the ongoing early stages of the design, the architecture and hardware WGs have been

holding additional meetings focused on aspects of the design related to architecture solutions and costing. In parallel, the DAQ Simulation Task Force effort, which was in place at the time of the consortium inception, has been adopted under the data selection WG, and simulation studies have continued to inform design considerations. This working structure is expected to remain in place through at least the completion of the interim design report (IDR). During the construction phase of the project we anticipate a new organization, built around major subsystem construction and commissioning responsibilities, and drawing also upon expertise build up during the ProtoDUNE projects.

## 6.7.2 Planning Assumptions

The DAQ planning is based the assumption of a SP module first, followed by a DP module. The schedule is sensitive to this assumption, as the DAQ requirements for the two module types are quite different. Five partially overlapping phases of activity are planned (see Figure 6.5):

- A further period of R&D activity, beginning at the time of writing, and culminating in a documented system design in the technical design report (TDR) around July 2019;
- Production and testing of a full prototype DAQ slice of realistic design, culminating in an engineering design review;
- Preparation and fit out of the CUC counting room with a minimal DAQ slice, in support of the first module installation;
- Production and delivery of final hardware, computing, software and firmware for the first module;
- Production and delivery of final hardware, computing, software and firmware for the second module.

This schedule assumes beneficial occupancy of the CUC counting room by end of the first quarter of 2022, and the availability of facilities to support an extended large-scale integration test in 2020 (e.g., CERN or Fermilab). We assume the availability of resources for installation and commissioning of final DAQ hardware (e.g., surface control room and server room facilities) from around the first quarter of 2023, and the integration and test facility (ITF) from the second quarter of 2022. The majority of capital resources for DAQ construction will be required from the second quarter of 2022, with a first portion of funds for the minimal DAQ slice from the first quarter of 2021.

## 6.7.3 High-level Cost and Schedule

The high-level DAQ schedule, which is based upon the current DUNE FD top-level schedule, is shown in Figure 6.5.





# Chapter 7

## Slow Controls and Cryogenics Instrumentation

### 7.1 Slow Controls and Cryogenics Instrumentation Overview

#### 7.1.1 Introduction

The cryogenic instrumentation and slow controls (CISC) system provides comprehensive monitoring for all detector module components as well as for the LAr quality and behavior, both being crucial to guarantee high-quality of the data. Beyond passive monitoring, CISC also provides a control system for some of the detector components. The structure of the CISC consortium is quite complex. The subsystem chart for the CISC system in Figure 7.1 shows the distinct cryogenic instrumentation and slow controls branches.

The cryogenic instrumentation includes a set of devices to monitor the quality and behavior of the LAr volume in the cryostat interior, ensuring the correct functioning of the full cryogenics system and the suitability of the liquid argon (LAr) for good quality physics data. These devices are purity monitors, temperature monitors, gas analyzers, LAr level monitors, and cameras with their associated light emitting system.

Cryogenic instrumentation also requires significant physics and simulation work such as E field simulations and cryogenics modeling studies using computational fluid dynamics (CFD). E field simulations are required to identify desirable locations for instrumentation devices in the cryostat so that they are not in regions of high E field and that their presence does not induce large field distortions. CFD simulations are needed to understand the expected temperature, impurity and velocity flow distributions and guide the placement and distribution of instrumentation devices inside the cryostat.

From the organizational point of view, the cryogenic instrumentation has been divided into three

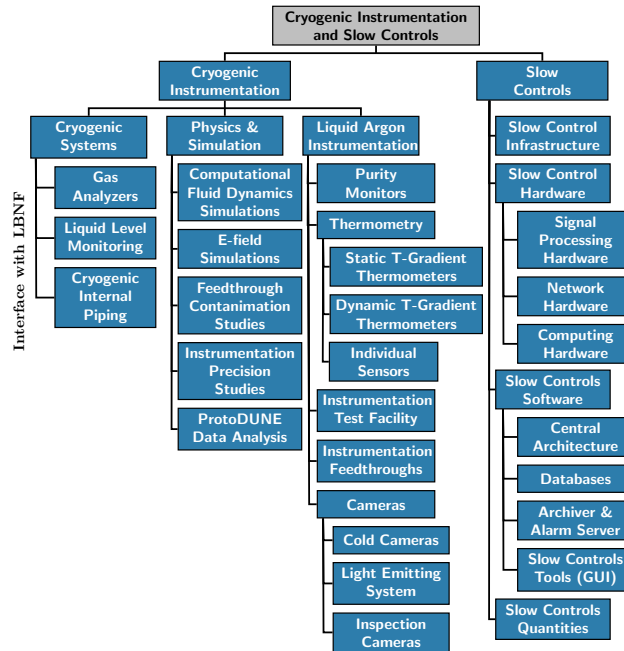


Figure 7.1: CISC subsystem chart

main parts: (1) cryogenics systems, which includes all components directly related to the external cryogenics system, such as liquid level monitoring, gas analyzers and internal cryogenic piping – all having substantial interfaces with LBNF; (2) physics and simulation; and (3) LAr instrumentation, which includes all other instrumentation devices.

The second branch of CISC is the slow controls system, in charge of monitoring and controlling most detector elements, including power supplies, electronics, racks, instrumentation devices, and calibration devices, etc. It includes four main components: hardware, infrastructure, software, and firmware. The slow controls hardware and infrastructure consists of networking hardware, signal processing hardware, computing hardware, and relevant rack infrastructure. The slow controls software and firmware are needed for signal processing, alarms, archiving, and control room displays.

Two other systems have been included by the DUNE management as part of the CISC consortium, a test facility for the instrumentation devices and the cryogenic piping inside the cryostat. Those are included inside the cryogenic instrumentation branch.

## 7.1.2 Design Considerations

For all LAr instrumentation devices, ProtoDUNE-DP designs are considered as the baseline, and requirements for most design parameters are extrapolated from ProtoDUNE. Hence a critical step for the CISC consortium is to analyze data from ProtoDUNE once data sets become available to validate the instrumentation designs and understand their performance. For example, noise

induced by instrumentation devices on the readout electronics can confuse the event reconstruction; the tolerable noise level from this source is a crucial design parameter that should be evaluated in ProtoDUNE.

Some of the common design considerations for instrumentation devices include stability, reliability and longevity, such that the devices can survive for a period of at least 20 years. Since it is uncommon for any device to have such a long lifetime, provisions are made in the overall design to allow replacement of devices where possible.

As for any other element inside the cryostat, the E field on the instrumentation devices is required to be less than 30 kV/cm, so that the risk of dielectric breakdown in LAr is minimized. This requirement imposes stringent constraints on the location and mechanical design of some devices. Electrostatic simulations will be performed to compute the expected field on the boundaries of instrumentation devices and to design the appropriate E field shielding in the case the field approaches the limit.

Another common consideration for all instrumentation devices is their support structure design, which is expected to be substantially different from the one used in ProtoDUNE.

For slow controls, the system needs to be robust enough to support a large number of monitored variables and a broad range of monitoring and archiving rates. It must be capable interfacing with a large number of systems to establish two-way communication for control and monitoring. Table 7.1 shows some of the important CISC system design requirements and parameters.

There are several aspects specific to the DP design impacting the CISC system design requirements:

- At the level of the cryogenic instrumentation, additional care is needed in order to monitor the gas phase above the liquid level. The temperature and the pressure of the gas phase affect the gas density, and consequently, the large electron multiplier (LEM) gain calibration. The gas pressure must be accurately monitored. In proximity to the liquid surface the temperature gradient of the gas is measured with an array of temperature probes with a vertical pitch of about 1 cm. Each charge-readout plane (CRP) is also equipped with 36 thermometers to sample the temperature across its structure.
- The CRP-specific instrumentation also includes:
  - the pulsing system for charge injection in the anode strips,
  - the precision level meters implemented only on the CRPs located at the cryostat borders, and
  - the measurement of the LEM-grid capacitance allowing to know the position of the CRP with respect to the liquid level for all CRPs,
  - the control of the stepping motors, which allows positioning each CRP parallel to the liquid level (keeping the extraction grid immersed in the liquid and the LEMs in the gas phase).

- The slow control system generates and controls the high voltage (HV) for biasing the LEMs (41 channels/CRP) and the extraction grid (1 channel/CRP), at maximum voltages of  $-5$  kV/channel and  $-10$  kV/channel, respectively;
- The requirements related to the photon detection system (PDS) include the generation and control of HV biasing for the photomultiplier tubes (PMTs) (up to  $-3$  kV) and the control of the calibration of the PMTs, performed with a light distribution system with a common light source and a network of optical fibers;
- The front-end (FE) electronics requires the control of the Micro Telecommunications Computing Architecture ( $\mu$ TCA) crates, the control of the analog FE cards, the control of the LV and of the charge injection system connected to the pre-amplifiers mounted on the FE cards;
- The DP design also enables surveying from the cryostat roof the position of reference points connected to the CRP suspension system, to ensure proper CRP alignment. This aspect needs as well to be integrated in the alignment scheme.

### 7.1.3 Scope

As described above, and shown schematically in Figure 7.1, the scope of the CISC system spans a broad range of activities. In the case of cryogenics systems (gas analyzers, liquid level monitors and cryogenic internal piping), LBNF provides the needed expertise and is responsible for the design, installation, and commissioning activities while the CISC consortium provides the resources as needed. In the case of LAr Instrumentation devices (purity monitors, thermometers, cameras and light-emitting system; and their associated feedthroughs) and instrumentation test facility, CISC is responsible from design to commissioning in the far detector modules.

From the slow controls side, CISC provides control and monitoring of all detector elements that provide information on the health of the detector module or conditions important to the experiment. The scope of systems that slow controls includes is listed below:

- **Slow Controls Base Software and Databases:** provides the central tools needed to develop control and monitoring for various detector systems and interfaces.
  - Base input/output software;
  - Alarms, archiving, display panels, and operator interface tools;
  - Slow controls system documentation and operations guidelines.
- **Slow Controls for External Systems:** export data from systems external to the detector and provide status to operators and archiving.
  - Beam status, cryogenics status, data acquisition (DAQ) status, and facilities systems

Table 7.1: Important design requirements on the DP CISC system design

| Design Parameter   | Requirement  | Motivation   | Comment  |
|--|--|--|--|
| Electron lifetime measurement precision                  | $< 1.4\%$ at 3 ms  | Per DUNE-FD Task Force [40], needed to keep the bias on the charge readout in the TPC to be low $0.5\%$ at 3 ms                          | Purity monitors do not directly sample TPC: see Section 7.2.2            |
| Thermometer precision                                    | $< 5$ mK   | Driven by CFD simulation validation; based on ProtoDUNE-SP design  | Expected ProtoDUNE performance 2 mK                                      |
| Pressure meters precision (DP)                           | $< 1$ mbar   | To measure the pressure (density) of the gas phase; based on ProtoDUNE-DP design   | WA105 DP demonstrator / ProtoDUNE-DP design $< 1$ mbar                   |
| Thermometer density                                      | $> 2/m$ (vert.),<br>$\sim 0.2$ m (horiz.)                      | Driven by CFD simulation.  | Achieved by design.  |
| Thermometer density gas phase (DP)                       | $> 1/cm$ (vert.),<br>$\sim 1$ m (horiz.)                       | Vertical array of thermometers with finer pitch close to the liquid level to measure the temperature gradient in the gas phase.          | Achieved by design.  |
| Thermometer density CRP structure (DP)                   | 36 thermometers on each CRP                                    | Monitoring the temperature across the CRP structure.   | Achieved by design.  |
| Liquid level meters precision (DP)                       | $< 1$ mm   | Maintain constant CRP alignment with respect to the liquid surface   | WA105 DP demonstrator / ProtoDUNE-DP design 0.1 mm                       |
| Cameras  | — multiple requirements imposed by interfaces: see Table 7.3 — |  |  |
| Cryogenic Instrumentation Test Facility cryostat volumes | 0.5 to 3 m <sup>3</sup>  | Based on filling costs and turnaround times  | Under design   |
| Max. E field on instrumentation devices                  | $< 30$ kV/cm   | The mechanical design of the system should be such that E field is below this value, to minimize the risk of dielectric breakdown in LAr | ProtoDUNE designs based on electrostatic simulations                     |
| Noise introduced into readout electronics                | Below significant levels                                       | Keep readout electronics free from external noise, which confuses event reconstruction   | To be evaluated at ProtoDUNE   |
| Total no. of variables                                   | 50 to 100k   | Expected number based on scaling past experiments; requires robust base software model that can handle large no. of variables.           | Achievable in existing control systems; DUNE choice in progress.         |
| Max. archiving rate per channel                          | 1 Hz (burst),<br>1 min <sup>-1</sup> (avg.)                    | Based on expected rapidity of interesting changes; impacts the base software choice; depends on data storage capabilities                | Achievable in existing control system software; DUNE choice in progress. |

status;

- For the systems above, import other interesting monitoring data as needed (e.g., pumps data from cryogenics system, heaters data from facility systems, etc.);
  - Building controls, detector hall monitoring, and ground impedance monitoring;
  - Interlock status bit monitoring (but not the actual interlock mechanism).
- **Slow Controls for Detector Hardware Systems:** develop software interfaces for detector hardware devices.
    - Monitoring and control of all power supplies;
    - Full rack monitoring (rack fans, thermometers and rack protection system);
    - Instrumentation and calibration device monitoring (and control to the extent needed);
    - Power distribution units monitoring, computer hardware monitoring;
    - HV system monitoring through cold cameras;
    - Detector components inspection through warm cameras.

In terms of slow controls hardware, CISC develops, installs and commissions any hardware related to rack monitoring and control. While most power supplies might only need a cable from the device to an Ethernet switch, some power supplies might need special cables (e.g., GPIB or RS232) for communication. The CISC consortium is responsible for providing such control cables.

The DP module has historically defined the scope of its slow controls system in a different way from that of the SP module. This chapter respects that historic definition and includes two systems within CISC for now that could be taken on by other consortia at a later date. These are: HV biasing for the LEM and extraction grid, and HV biasing for the DP PDS; and (2) a calibration system for the CRPs.

In addition to the listed activities, CISC also has activities that span outside the scope of the consortium and require interfacing with other groups. This is discussed in Section 7.4.

## 7.2 Cryogenics Instrumentation

Instrumentation inside the cryostat must ensure that the condition of the LAr is adequate for operation of the TPC. This instrumentation includes devices to monitor the impurity level of the argon, e.g., the purity monitors, which provide high-precision electron lifetime measurements, and gas analyzers to ensure that the levels of atmospheric contamination drop below certain limits

during the cryostat purging, cooling and filling. The cryogenics system operation is monitored by temperature sensors deployed in vertical arrays and at the top and bottom of the detector, providing a detailed 3D temperature map that can help to predict the LAr purity across the entire cryostat. The cryogenics instrumentation also includes LAr level monitors and a system of internal cameras to help in locating sparks in the cryostat and for overall monitoring of the cryostat interior. As mentioned in the introduction, cryogenics instrumentation requires simulation work to identify the proper location for these devices inside the cryostat and for the coherent analysis of the instrumentation data.

Figure 7.2 shows the current map of cryostat ports for the SP module, highlighting the ones assigned to instrumentation devices, as well as the preliminary location for some of these devices. Vertical temperature profilers are located behind the anode plane assemblies (APAs) ( $T_S$ ) and behind the east end wall ( $T_D$ ). They are complemented by a coarser 2D grid of sensors at the top and bottom of the cryostat (not shown in the figure). Purity monitors and level meters are planned in each detector side, behind the two front end walls. Inspection cameras will use some of the multipurpose instrumentation ports, but their exact locations are yet to be decided.

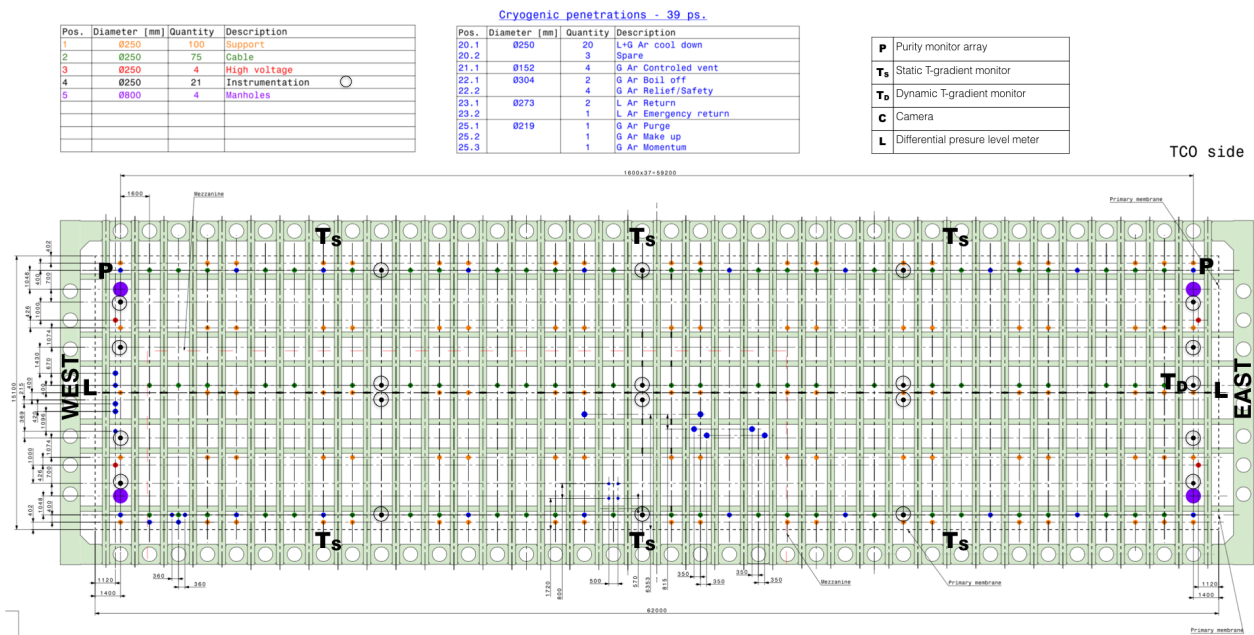


Figure 7.2: Cryostat ports and preliminary location of some instrumentation devices.

For DP, additional care must be taken to monitor the gas phase above the liquid level as the temperature and pressure of argon gas affect gas pressure, and consequently the LEM calibration. The gas pressure must be monitored to 1 mbar precision and accuracy. In proximity to the liquid surface the temperature gradient of the gas has to be measured with an array of temperature probes with a vertical pitch of about 1 cm, and with a coarser 5 cm pitch up to the cryostat roof. Each CRP is also equipped with 36 thermometers to sample the temperature across its structure.



## 7.2.1 Fluid Dynamics Simulations

Proper placement of purity monitors, thermometers, and liquid level monitors within the detector module requires knowledge of how LAr behaves within the cryostat in terms of its fluid dynamics, heat and mass transfer, and distribution of impurity concentrations. Fluid motion within the cryostat is driven primarily by small changes in density from thermal gradients, although pump flow rates and inlet and outlet locations also contribute. Heat sources include exterior heat from the surroundings, interior heat from the electronics, and heat flow through the pump inlet.

The fluid flow behavior can be determined through simulation of LAr flow within the detector using ANSYS CFX<sup>1</sup>, a commercially available computational fluid dynamics (CFD) code. Such a model must include proper definition of the fluid characteristics, solid bodies and fluid-solid interfaces, and a means for measuring contamination, while still maintaining reasonable computation times. Although simulation of the detector module presents challenges, there exist acceptable simplifications for accurately representing the fluid, the interfacing solid bodies, and variations of contaminant concentrations. Because of the magnitude of thermal variation within the cryostat, modeling of the LAr is simplified through use of constant thermophysical properties, calculation of buoyant force through use of the Boussinesq Model (using constant a density for the fluid with application of a temperature dependent buoyant force), and a standard shear stress transport turbulence model. Solid bodies that contact the LAr include the cryostat wall, the cathode planes, the anode planes, the ground plane, and the field cage (FC). As in previous CFD models of the DUNE 35 ton prototype and ProtoDUNE by South Dakota State University (SDSU)[41], the FC planes, anode planes, and ground plane (GP) can be represented by porous bodies. Since impurity concentration and electron lifetime do not impact the fluid flow, these variables can be simulated as passive scalars, as is commonly done for smoke releases [42] in air or dyes released in liquids.

Significant discrepancies between real data and simulations can have potential impacts on detector performance, as simulation results contribute to decisions about where to locate sensors and monitors, as well as definitions of various calibration quantities. However, methods of mitigating such risks include well established convergence criteria, sensitivity studies, and comparison to results of previous CFD simulation work by SDSU and Fermilab. Additionally, the simulation will be improved with input from temperature measurements and validation tests.

Figure 7.3 shows an example of the temperature distribution on a plane intersecting a LAr inlet and at a plane halfway between an inlet and an outlet; the geometry used for this simulation is shown in Figure 7.4. Note the plume of higher temperature LAr between the walls and the outer APA on the inlet plane. The current locations of instrumentation in the cryostat as shown in Figure 7.2 were determined using the temperature and impurity distributions from these previous simulations.

The initial strategy for the future computational fluid dynamics (CFD) simulation effort is to understand the performance of ProtoDUNE cryogenics system and model the far detectors (FDs) to derive requirements for instrumentation devices. The following is a prioritized set of studies planned to help drive the requirements for other systems:

---

<sup>1</sup>ANSYS™, <https://www.ansys.com/products/fluids/ansys-cfx>.

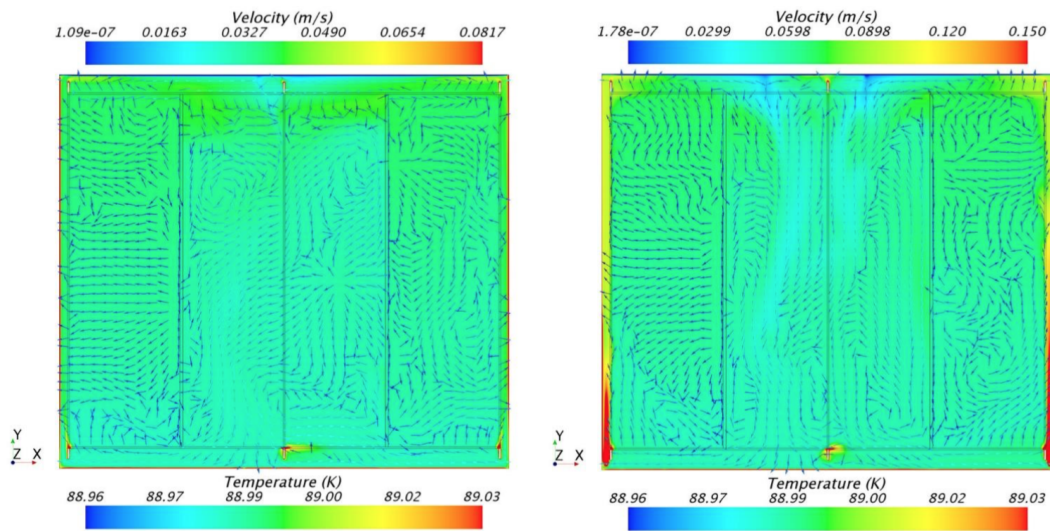


Figure 7.3: Distribution of temperature on a plane intersecting an inlet (right) and halfway between an inlet and an outlet (left), as predicted by SDSU CFD simulations [41]. (See Figure 7.4 for geometry.)

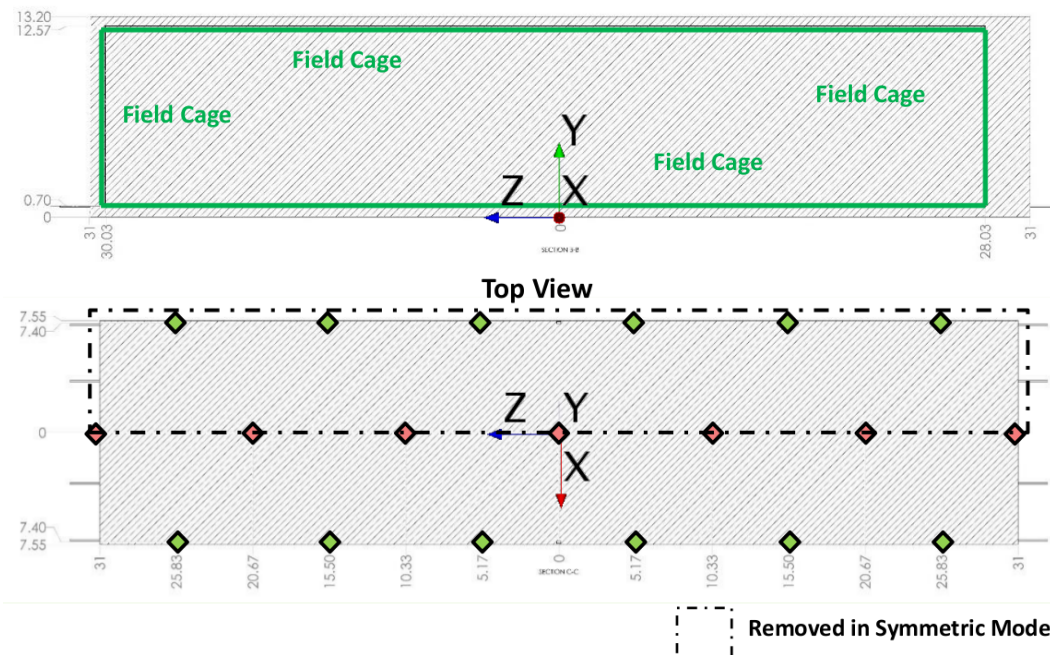


Figure 7.4: Layout of the TPC within the cryostat (top) and positions of LAr inlets and outlets (bottom) as modeled in the SDSU CFD simulations [41]. The Y axis is vertical and the X axis is parallel to the TPC drift direction. Inlets are shown in green and outlets are shown in red.

1. Review the DUNE FD cryogenics system design and verify the current implementation in simulation; this is important to ensure that the model represents what will be built.
2. Model the ProtoDUNE-DP liquid and gas regions with the same precision as the FD. Presently only the liquid model exists. The liquid model is needed to interpret the thermometer data, and the gas model is needed to understand how to place thermometers in the ullage and verify the design of the gaseous argon purge system.
3. Perform a CFD study to determine the feasibility of a wiper for DP; this helps to determine if it can be used to clean the LAr surface before the extraction grid is submerged in the DP module.
4. Verify the SP module SP CFD model in simulation performed by LBNF; this defines the requirements for instrumentation devices (e.g., thermometry).
5. Model the ProtoDUNE-DP liquid and gas regions with the same precision as the FD.

## 7.2.2 Purity Monitors

A fundamental requirement of a LAr TPC is that ionization electrons drift over long distances in LAr. Part of the charge is inevitably lost due to the presence of electronegative impurities in the liquid. To keep such loss to a minimum, purifying the LAr during operation is essential, as is the monitoring of impurities.

Residual gas analyzers are an obvious choice when analyzing argon gas and can be exploited for the monitoring of the gas in the ullage of the tank. Unfortunately, commercially available and suitable mass spectrometers have a detection limit of  $\sim 10$  parts per billion (ppb), whereas DUNE requires a sensitivity down to the parts per trillion (ppt) level. Instead, specially constructed purity monitors measure LAr purity in all the phases of operations, and enable the position-dependent purity measurements necessary to achieve DUNE's physics goal.

Purity monitors also serve to mitigate LAr contamination risk. The large scale of the detector modules increases the risk of failing to notice a sudden unexpected infusion of contaminated LAr being injected back into the cryostat. If this condition were to persist, it could cause irreversible contamination to the LAr and terminate useful data taking. Strategically placed purity monitors mitigate this risk.

Purity monitors are placed inside the cryostat, but outside of the detector TPC, as well as outside the cryostat within the recirculation system before and after filtration. Continuous monitoring of the LAr supply lines to the detector module provides a strong line of defense against contaminated LAr. Gas analyzers (described in Section 7.2.5) provide a first line of defense against contaminated gas. Purity monitors inside the detector module provide a strong defense against all sources of contamination in the LAr volume and contamination from recirculated LAr. Furthermore, multiple purity monitors measuring lifetime with high precision at carefully chosen points can provide key inputs to CFD models of the detector, such as vertical gradients in impurity concentrations.

Purity monitors have been deployed in the ICARUS and MicroBooNE detectors and in the 35 ton prototype detector at Fermilab. In particular during the first run of the 35 ton prototype, two out of four purity monitors stopped working during the cooldown, and a third was intermittent. It was later found out that this was due to poor electrical contacts of the resistor chain on the purity monitor. A new design was then implemented and successfully tested in the second run. The ProtoDUNE-SP and ProtoDUNE-DP employ purity monitors based on the same design principles. ProtoDUNE-SP utilizes a string of purity monitors similar to that of the 35 ton prototype, enabling measurement of the electron drift lifetime as a function of height. A similar system design is exploited in the DUNE FD, with modifications made to accommodate the instrumentation port placement relative to the purity monitor system and the requirements and constraints coming from the different geometric relations between the TPC and cryostat.

### 7.2.2.1 Physics and Simulation

A purity monitor is a small ionization chamber that can be used to independently infer the effective free electron lifetime in the LArTPC. The operational principle of the purity monitor consists of generating a known electron current via illumination of a cathode with UV light, followed by collecting at an anode the current that survives after drifting a known distance. The attenuation of the current can be related to the electron lifetime. The electron loss can be parameterized as  $N(t) = N(0)e^{-t/\tau}$ , where  $N(0)$  is the number of electrons generated by ionization,  $N(t)$  is the number of electrons after drift time  $t$ , and  $\tau$  is the electron lifetime.

For the SP module, the drift distance is 3.53 m and the E field is  $500 \text{ V cm}^{-1}$ . Given the drift velocity at this field of approximately  $1.5 \text{ mm } \mu\text{s}^{-1}$ , the time to go from cathode to anode is around  $\sim 2.4 \text{ ms}$  [43]. The LAr TPC signal attenuation,  $[N(0) - N(t)]/N(0)$ , is to be kept less than 20% over the entire drift distance [40]. The corresponding electron lifetime is  $2.4/[-\ln(0.8)] \simeq 11 \text{ ms}$ .

For the DP module, the maximum drift distance is 12 m, therefore the requirement on the electron lifetime is much higher.

The 35 ton prototype at Fermilab was instrumented with four purity monitors. The data taken with them during the first part of the second phase is shown in Figure 7.5 and clearly shows the ability to measure the electron lifetime between 100  $\mu\text{s}$  and 3.5 ms.

### 7.2.2.2 Purity Monitor Design

The basic design of a purity monitor is based on those used by the ICARUS experiment (Figure 7.6)[44]. It is a double-gridded ion chamber immersed in the LAr volume. The purity monitor consists of four parallel, circular electrodes: a disk holding a photocathode, two grid rings (anode and cathode), and an anode disk. The cathode grid is held at ground potential. The cathode, anode grid, and anode are electrically accessible via modified vacuum grade high-voltage feedthroughs and separate bias voltages held at each one. The anode grid and the field shaping rings are connected to the cathode grid by an internal chain of  $50 \text{ M}\Omega$  resistors to ensure the uniformity of the

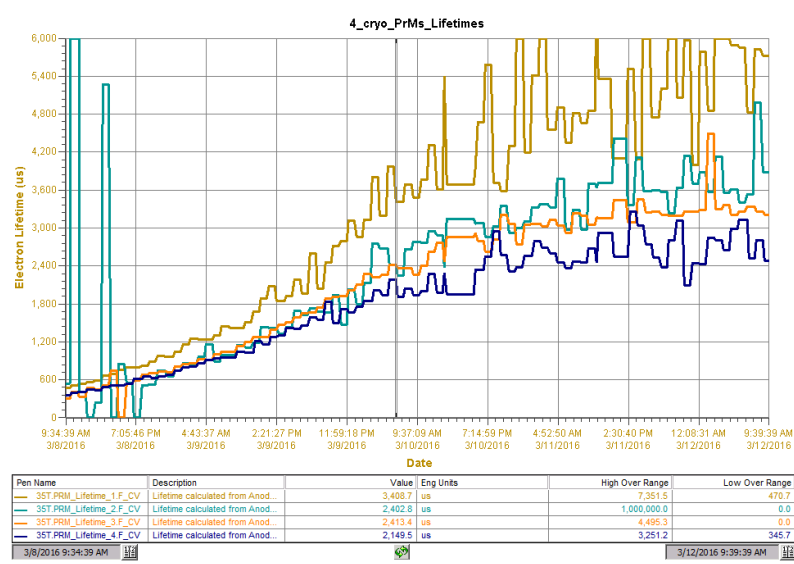


Figure 7.5: The measured electron lifetimes in the four purity monitors as a function of time at Fermilab 35 ton prototype.

E fields in the drift regions. A stainless mesh cylinder is used as a Faraday cage to isolate the purity monitor from external electrostatic backgrounds.

The purity monitor measures the electron drift lifetime between its anode and cathode. The electrons are generated by the purity monitor's UV-illuminated gold photocathode via the photoelectric effect. As the electron lifetime in LAr is inversely proportional to the electronegative impurity concentration, the fraction of electrons generated at the cathode that arrive at the anode ( $Q_A/Q_C$ ) after the electron drift time  $t$  gives a measure of the electron lifetime  $\tau$ :  $Q_A/Q_C \sim e^{-t/\tau}$ .

It is clear from this formula that the purity monitor reaches its sensitivity limit once the electron lifetime becomes much larger than the drift time  $t$ . For  $\tau \gg t$  the anode to cathode charge ratio becomes  $\sim 1$ . But, as the drift time is inversely proportional to the E field, by lowering the drift field one can in principle measure any lifetime no matter the length of the purity monitor (the lower the field, the lower the drift velocity, i.e., the longer the drift time). In practice, at very low fields it is hard to drift the electrons all the way up to the anode. Currently, specific sensitivity limits for purity monitors with a drift distance of the order of  $\sim 20$  cm are still to be determined in a series of tests. If the required sensitivity is not achieved by these “short” purity monitors, longer ones may be developed.

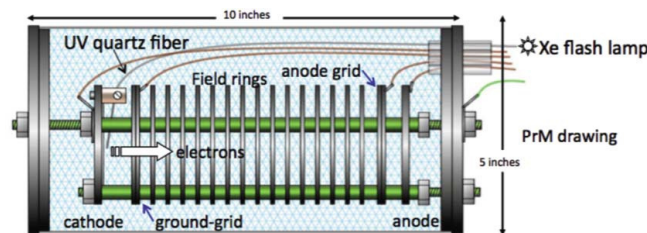


Figure 7.6: Schematic diagram of the basic purity monitor design [44].

The photocathode that produces the photoelectrons is an aluminum plate coated with 50 Å of titanium and 1000 Å of gold and attached to the cathode disk. A xenon flash lamp is used as the light source in the baseline design, although this could potentially be replaced by a more reliable and possibly submersible light source in the future, perhaps LED driven. The UV output of the lamp is quite good around  $\lambda = 225$  nm, which is close to the work function of gold (4.9 eV to 5.1 eV). Several UV quartz fibers are used to carry the xenon UV light into the cryostat to illuminate the gold photocathode. Another quartz fiber is used to deliver the light into a properly biased photodiode outside of the cryostat to provide the trigger signal for when the lamp flashes.

### 7.2.2.3 Electronics, DAQ and Slow Controls Interfacing

The purity monitor electronics and DAQ system consist of FE electronics, waveform digitizers, and a DAQ PC. The block diagram of the system is shown in Figure 7.7.

The baseline design of the FE electronics is the one used for the purity monitors at the 35 ton prototype, LAPD, and MicroBooNE. The cathode and anode signals are fed into two charge amplifiers contained within the purity monitor electronics module. The amplified outputs of the anode and cathode are recorded with a waveform digitizer that interfaces with a DAQ PC.

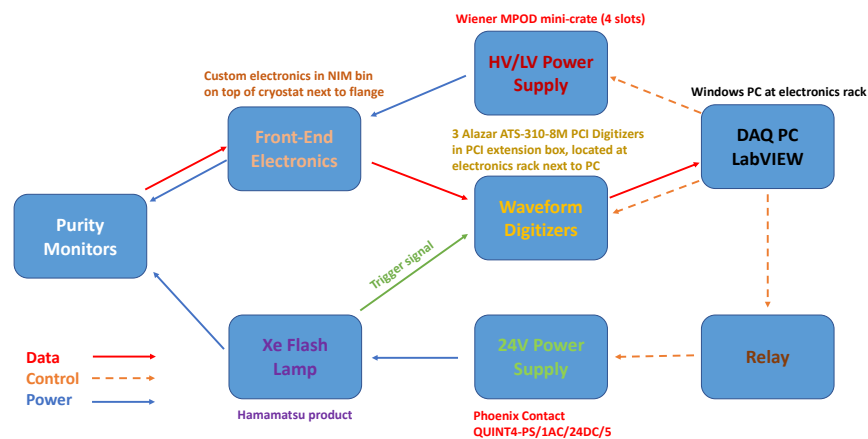


Figure 7.7: Block diagram of the purity monitor system.

A custom LabVIEW application running on the DAQ PC is developed and executes two functions: it controls the waveform digitizers and the power supplies, and it monitors the signals and key parameters. The application configures the digitizers to set the sampling rate, the number of waveforms to be stored in the memory, pre-trigger data, and a trigger mode. A signal from a photodiode triggered by the xenon flash lamp is directly fed into the digitizer as an external trigger to initiate data acquisition. The LabVIEW application automatically turns on the xenon flash lamp by powering a relay at the start of data taking and then turns it off when finished. The application continuously displays the waveforms and important parameters, such as measured electron lifetime, peak voltages, and drift time of electrons in the purity monitors, and shows these parameters over time.

The xenon flash lamp and the FE electronics are installed close to the purity monitor flange, to reduce light loss through the optical fiber and prevent signal loss. Other pieces of equipment are mounted in a rack separate from the cryostat. They distribute power to the xenon flash lamp and the FE electronics, as well as collect data from the electronics. The slow control system communicates with the purity monitor DAQ software and has control of the HV and LV power supplies of the purity monitor system. As the optical fiber has to be very close to the photocathode (less than 0.5 mm) for efficient photoelectron extraction, no interference with the PDS is expected. Nevertheless light interference will be evaluated more precisely at ProtoDUNE.

Conversely the electronics of purity monitors may induce noise in the TPC electronics, largely coming from the current surge in the discharging process of the main capacitor of the purity monitor xenon light source when producing a flash. This source of noise can be controlled by placing the xenon flash lamp inside its own Faraday cage, allowing for proper grounding and shielding; the extent of mitigation will be evaluated at ProtoDUNE. If an unavoidable interference problem is found to exist, then software can be implemented to allow the DAQ to know if and when the purity monitors are running and to veto purity monitor measurements in the event of a supernova neutrino burst (SNB) alert or trigger.

#### 7.2.2.4 Production and Assembly

Production of the individual purity monitors and their assembly into the string that gets placed into the detector module cryostat follows the same methodology that is being developed for ProtoDUNE. Each of the individual monitors is fabricated, assembled and then tested in a smaller test stand. After confirming that each of the individual purity monitors operates at the required performance, they are assembled together via the support tubes used to mount the system to the inside of the cryostat such that three purity monitors are grouped together to form one string, as shown in Figure 7.8. Each monitor is assembled as the string is built from the top down, and in the end three individual purity monitors hang from a single string. The assembly of the string concludes once the purity monitors are each in place, but with the Faraday cages removed and the HV cables and optical fibers yet to be run. This full string assembly is then shipped to the FD site for installation into the cryostat.



Figure 7.8: Design of the purity monitor string that will contain three purity monitors.

#### 7.2.3 Thermometers

A detailed 3D temperature map is important to monitor the correct functioning of the cryogenics system and the LAr uniformity. Given the complexity and size of purity monitors, those can only be installed on the cryostat sides to provide a local measurement of the LAr purity. While a direct measurement of the LAr purity across the entire cryostat is not viable, a sufficiently detailed 3D temperature map can be used to predict the LAr purity using CFD simulations. Measuring

the vertical temperature profile is especially important since this is closely related to the LAr recirculation and uniformity.

High-precision temperature sensors are distributed near the TPC walls in two ways: (1) in high-density ( $> 2$  sensors/m) vertical arrays (the T-gradient monitors), and (2) in coarser ( $\sim 1$  sensor/5 m) 2D arrays at the top and bottom of the detector, which are the most sensitive regions (the individual sensors).

Since temperature variations inside the cryostat are expected to be very small (0.02 K, see Figure 7.3), to properly measure the 3D temperature map sensors must be cross-calibrated to better than 0.005 K. Most sensors are calibrated in the laboratory, prior to installation, as described in Section 7.2.3.1. This is in fact the only viable method for sensors in areas where the available space is restricted: on the long sides of the detector (behind the anode plane assemblies for SP, and behind the lateral endwall field cage (endwall FC) for DP) and top/bottom of the detector. Given the precision required and the unknown longevity of the sensors (which could require a new calibration after some time), a complementary method is used for T-gradient monitors behind the front endwalls, at least for the SP module. In those areas there is sufficient space for a movable system that can be used to cross-calibrate in situ the temperature sensors.

In the baseline design for all three systems mentioned above, three elements are common: sensors, cables and readout system. Platinum sensors with  $100\ \Omega$  resistance, PT100 series, produced by Lakeshore<sup>2</sup>, are adequate for the temperature range of interest, 83 K to 92 K, since in this range those sensors have  $\sim 5$  mK reproducibility and absolute temperature accuracy of 100 mK. In addition, using four-wire readout greatly reduces the issues related to the lead resistance, any parasitic resistances, connections through the flange, and general electromagnetic noise pick-up. The Lakeshore PT102 sensors have been previously used in the 35 ton prototype and ProtoDUNE-SP detector, giving excellent results. For the inner readout cables a custom cable made by Axon<sup>3</sup> is the baseline. It consists of four AWG28 teflon-jacketed copper wires forming two twisted pairs, with a metallic external shield and an outer teflon jacket. The readout system is described below in Section 7.2.3.5.

Another set of lower-precision sensors is used to monitor the filling of the cryostat in its initial stage. Those sensors are epoxied into the cryostat bottom membrane with a density to be determined, not to exceed one sensor every 5 m. Finally, the inner walls and roof of the cryostat are instrumented with the same type of sensors in order to monitor their temperature during cooldown and filling. The baseline distribution has three vertical arrays of sensors epoxied to the membrane: one behind each of the two front endwall FCs and the third one in the middle of the cryostat (behind the anode plane assemblies for SP and behind the lateral endwall FCs for DP).

### 7.2.3.1 Static T-gradient Monitors

Several vertical arrays of high-precision temperature sensors cross-calibrated in the laboratory are installed near the lateral walls (behind the anode plane assemblies for SP and behind the lateral

<sup>2</sup>Lakeshore™, <https://www.lakeshore.com/Pages/Home.aspx>.

<sup>3</sup>Axon™, [http://www.axon-cable.com/en/00\\_home/00\\_start/00/index.aspx](http://www.axon-cable.com/en/00_home/00_start/00/index.aspx)



endwall FCs for DP). For the SP module, since the electric potential is zero behind the anode plane assemblies, no E field shielding is required, simplifying enormously the mechanical design. This does not apply for the DP module, for which the proper shielding must be provided.

Sensors are cross-calibrated in the lab using a well controlled environment and a high-precision readout system, described below in Section 7.2.3.5. Although the calibration procedure will certainly improve, the one currently used for ProtoDUNE-SP is described here. Four sensors are placed as close as possible (such that identical temperature can be assumed for all of them) inside a small cylindrical aluminum capsule, which protects the sensors from thermal shocks and helps in minimizing convection. One of the sensors acts as reference while the other three are calibrated. Five independent calibrations are performed for each set of three sensors, such that the reproducibility of each sensor can be computed. For each calibration the capsule is introduced in a 3D printed polylactic acid (PLA) box of size  $9.5 \times 9.5 \times 19 \text{ cm}^3$ , with two concentric independent volumes of LAr and surrounded by a polystyrene box with 15 cm thick walls. A small quantity of LAr is used to slowly cool down the capsule to  $\sim 90 \text{ K}$ , avoiding thermal shocks that could damage the sensors. Then the capsule is immersed in LAr such that it penetrates inside, fully covering the sensors. Once the temperature stabilizes to the 1-2 mK level (after 5-15 minutes) measurements are taken. Then the capsule is taken out from LAr and exposed to room temperature until it reaches 200 K. As mentioned above, this procedure is repeated five times, before going to the next set of three sensors. As shown in Figure 7.10 a reproducibility (RMS of the mean offset in the flat region) of  $\sim 2 \text{ mK}$  has been achieved in the ProtoDUNE-SP design.

The baseline design for the mechanics of the SP system consists of two stainless strings anchored at top and bottom corners of the cryostat using the available M10 bolts (see Figure 7.9). One of the strings is used to route the cables while the other, separated by 340 mm, serves as support for temperature sensors. Given the height of the cryostat, the need of intermediate anchoring points is under discussion. For the DP module no baseline design exists yet, since additional complications due to the required E field shielding must be taken into account. Figure 7.9 shows the baseline design of the PCB support for temperature sensors, with an IDC-4 male connector. It has a size of  $52 \times 15 \text{ mm}^2$ . Each four-wire cable from the sensor to the flange has an IDC-4 female connector on the sensor side; on the other side, it is directly soldered into the inner pins of male SUBD-25 connectors on the flanges. The CF63 side ports on the detector support system (DSS)/cryogenic ports are used to extract the cables.

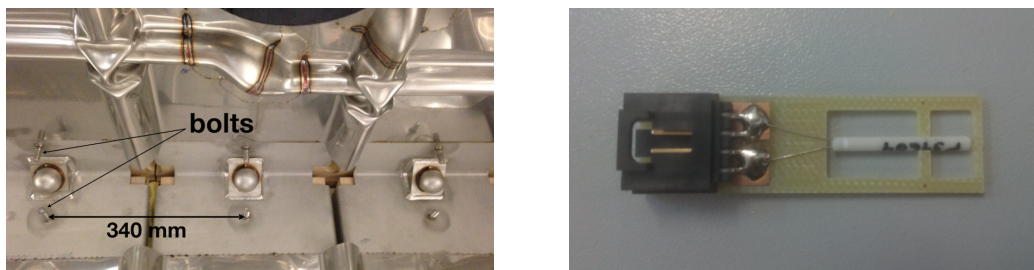


Figure 7.9: Left: bolts at the bottom corner of the cryostat. Right: Lakeshore PT102 sensor mounted on a PCB with an IDC-4 connector.

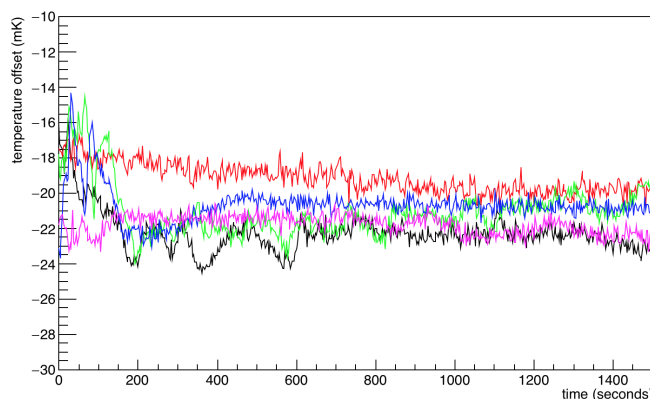


Figure 7.10: Temperature offset between two sensors as a function of time for five independent immersions in LAr. The reproducibility of those sensors, defined as the RMS of the mean offset in the flat region, is  $\sim 2$  mK, The resolution for individual measurements, defined as the RMS of one of the offsets in the flat region, is better than 1 mK.

### 7.2.3.2 Dynamic T-gradient Monitors

The dynamic temperature monitor is a vertical array of high precision temperature sensors with the goal of measuring vertical temperature gradient with precision of few mK. The design of the system is driven by two factors:

- A few-mK uncertainty in the measured vertical temperature profile over the entire detector height is required in order to monitor LAr purity and provide useful feedback of efficiency of cryogenic recirculation and purification.
- Simulations of the cryogenic recirculation predict very slow change in temperature at meter scale except at the bottom and top of the cryostat. Thus, sensors are placed every 50 cm along the detector module height with increased frequency in the first 50 cm, closest to the bottom of the cryostat and the last 50 cm, closest to the top of the cryostat, where spacing between sensors is reduced to 10 cm.

In order to address concerns related to possible differences in the sensor readings prior to and after installation in a detector module, a dynamic temperature monitor allows cross-calibration of sensors in situ. Namely, this T-gradient monitor can move vertically while installed in the detector module, which allows for precise cross-calibration between the sensors in situ at predefined locations, as well as in between them. The procedure for cross-calibrations is the following: the temperature reading is taken at the lowest position with all sensors. The stepper motor then moves the carrier rod up 50 cm, putting all sensors in the previous location of their neighbor that was 50 cm above them. Then the second reading is taken. In this manner, except for the lowest position we have temperature measurement at each location with two adjacent sensors, and by linking the temperature offsets between the two readings at each location, temperature readings from all sensors are cross-calibrated in situ, cancelling all offsets due to electromagnetic noise or any parasitic resistances that may have prevailed despite the four point connection to the sensors that should cancel most of the offsets. These measurements are taken with very stable current

source, which ensures high precision of repeated temperature measurements over time. The motion of the dynamic T-monitor is stepper motor operated, delivering measurements with high spatial resolution.

### 7.2.3.3 Dynamic T-gradient Monitor Design

A dynamic T-gradient monitor consists of three distinct parts: a carrier rod on which sensors are mounted, an enclosure above the cryostat housing the space that allows vertical motion of the carrier rod 1.5 m above its lowest location, and the motion mechanism. The motion mechanism consists of a stepper motor connected to a gear and pinion through a ferrofluidic dynamic seal. The sensors have two pins that are soldered to a printed circuit board (PCB). Two wires are soldered to the common soldering pad for each pin, individually. There is a cutout in the PCB around the sensor that allows free flow of argon for more accurate temperature reading. Stepper motors typically have very fine steps allowing high-precision positioning of the sensors. Figure 7.11 shows the overall design of the dynamic T-gradient monitor with the sensor carrier rod, enclosure above the cryostat and the stepper motor mounted on the side of the enclosure. The enclosure consists of two parts connected by a six-way cross flange. One side of this cross flange is used to for the signal wires, another side is used as a viewing window, while the two other ports are spares. Figure 7.12 (left) shows the mounting of the PCB board on the carrier rod and mounting on the sensor on the PCB along with the four point connection to the signal readout wires. Finally, Figure 7.12 (right) shows the stepper motor mounted on the side of the rod enclosure. The motor is kept outside, at room temperature, and its power and control cables are also kept outside.



Figure 7.11: An overview of the dynamic T-gradient monitor.

### 7.2.3.4 Individual Temperature Sensors

T-Gradient monitors provide a vertical temperature profiling outside the TPCs. They are complemented by a coarser 2D array at the top and bottom of the detector. Sensors, cables and readout system are the same as for the T-gradient monitors.

In principle, a similar distribution of sensors is used at top and bottom. Following the ProtoDUNE-SP design, bottom sensors use the cryogenic pipes as a support structure, while top sensors are anchored to the GPs. Teflon pieces (see Figure 7.13) are used to route cables from the sensors to the CF63 side ports on DSS-cryogenics ports, which are used to extract the cables. The PCB sensor's support, cables and connection to the flanges are the same as for the static T-gradient monitors.

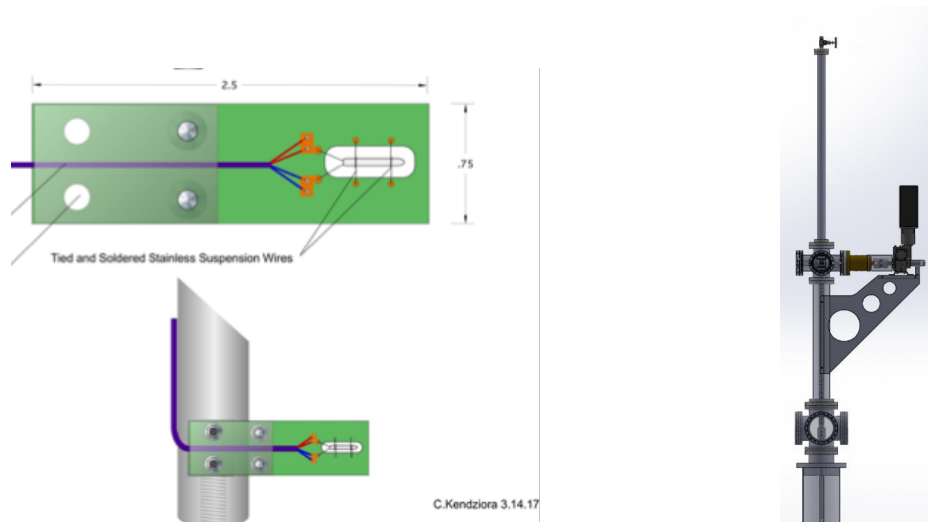


Figure 7.12: Left: Sensor mounted on a PCB board and PCB board mounted on the rod. Right: The driving mechanism of the dynamic T-gradient monitor. It consists of a stepper motor driving the pinion and gear linear motion mechanism.

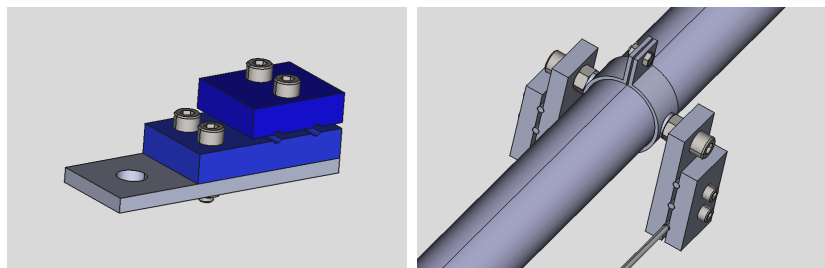


Figure 7.13: Left: support for two cables on ground planes. Right: Supports for three cables mounted on cryogenics pipes using split clamps

### 7.2.3.5 Readout System for Thermometers

A high precision and very stable system is required to achieved the design precision of  $< 5$  mK. The proposed readout system is the one used in ProtoDUNE-SP, which is based on a variant of an existing mass PT100 temperature readout system developed at CERN for one of the LHC experiments. The system consists of three parts:

- An accurate current source for the excitation of the temperature sensors, implemented by a compact electronic circuit using a high-precision voltage reference from Texas Instruments <sup>4</sup>;
- A multiplexing circuit based on an Analog Devices ADG707<sup>5</sup> multiplexer electronic device;
- A high-resolution and accuracy voltage signal readout module based on National Instruments <sup>6</sup> NI9238, which has 24 bit resolution over a 1 V range. This module is inserted in a National Instruments compact RIO device that distributes the temperature values to the main slow control software through the standard OPC UA protocol. The Ethernet DAQ also includes the multiplexing logic.

The current mode of operation averages over 2000 samples taken every second for each sensor. As inferred from Figure 7.10 the system has a resolution better than 1 mK, the RMS of one of the offsets in the stable region.

## 7.2.4 Liquid Level Monitoring

The goals for the level monitoring system are basic level sensing when filling, and precise level sensing during static operations.

For filling the detector module the differential pressure between the top of the detector and known points below it can be converted to depth with the known density of LAr. The temperatures of RTDs at known heights may also be used to determine when the cold liquid has reached each RTD.

During operation, the purpose of liquid level monitoring is twofold: the cryogenics system uses it to tune the LAr flow and the detector module uses it to guarantee that the top GPs are always submerged (otherwise the risk of dielectric breakdown is high). Two differential pressure level meters are installed as part of the cryogenics system, one on each side of the detector module. They have a precision of 0.1 %, which corresponds to 14 mm at the nominal LAr surface. This precision is sufficient for the single phase detector, since the plan is to keep the LAr surface at least 20 cm above the GPs (this is the value used for the HV interlock in ProtoDUNE-SP); thus, no additional level meters are required for the single phase. However, in the DP LAr system the surface level should be controlled at the millimeter level, which can be accomplished with capacitive

---

<sup>4</sup>Texas Instruments™, <http://www.ti.com/>.

<sup>5</sup>Analog Devices™, [http://www.analog.com/media/en/technical-documentation/data-sheets/ADG706\\_707.pdf](http://www.analog.com/media/en/technical-documentation/data-sheets/ADG706_707.pdf).

<sup>6</sup>National Instruments™, <http://www.ni.com/en-us.html/>.

monitors. Using the same capacitive monitor system in each detector reduces design differences and provides a redundant system for the SP. Either system could be used for the HV interlock.

Table 7.2 summarizes the requirements for the liquid level monitor system.

Table 7.2: Liquid level monitor requirements

| Requirement                                      | Physics Requirement Driver                                     |
|--|--|
| Measurement accuracy (filling) $\sim 14$ mm      | Understand status of detector during filling                   |
| Measurement accuracy (operation, DP) $\sim 1$ mm | Maintain correct depth of gas phase. (Exceeds SP requirements) |
| Provide interlock with HV                        | Prevent damage to detector module from HV discharge in gas     |

Differential pressure level meters will be purchased from commercial sources. Installation methods and positions will be determined as part of the cryogenics internal piping plan. Sufficient redundancy will be designed in to ensure that no single point of failure compromises the level measurement.

Multiple capacitive level sensors are deployed along the top of the fluid to be used during stable operation and checked against each other.

During operations of the WA105 DP demonstrator, the cryogenic programmable logic controller (PLC) continuously checked the measurements from one level meter on the charge readout plane (CRP) in order to regulate the flow from the liquid recirculation to maintain a constant liquid level inside the cryostat. Continuous measurements from the level meters around the drift cage and the CRP illustrated the stability of the liquid level within the  $100\ \mu\text{m}$  intrinsic precision of the instruments. The observation of the level was complemented by live feeds from the custom built cryogenic cameras, hereby providing qualitative feedback on the position and flatness of the surface.

In the DP module each CRP is suspended with three ropes actuated by step motors and can be individually adjusted with respect to the liquid level in terms of parallelism and distance. The CRP has a gap of 1 cm in between the bottom of the surface of the LEMs and the extraction grid. The CRP positioning requirements include its parallelism to the liquid surface and the liquid level situated across this gap, namely the extraction grid is required to be immersed and the LEMs are required to not be wet. The distance of the CRP with respect to the liquid level is required to be measured with the accuracy of 1 mm. The slow control system takes care of the control of the step motors, which control the CRP suspensions. The positions of the motors (and of the corresponding suspension points) can be surveyed from the cryostat roof with a typical 0.2 mm accuracy. By reading the controls of the motors and by knowing the results of this survey, the position of the CRPs with respect to the liquid can be predicted in absolute terms, provided that the liquid level is measured also with respect to the same reference system by the cryostat level meters.

The horizontal alignment of the CRPs can be measured as well thanks to the survey of the reference points on the suspension feedthroughs. The relative position of a CRP with respect to the liquid

level can be measured with high-accuracy level meters mounted on the CRP itself. These level meters are multi-parallel plate capacitors with the capacitance changing as a function of the liquid level between the plates. These level meters can be attached to the CRP borders and they guarantee a measurement accuracy at the level of 0.1 mm. It is possible to install these level meters only on the borders of the CRPs, which are at the periphery of the detection surface and not on the borders where the CRPs are side by side. In addition to the installed level meters, the liquid height in the extraction region of all CRPs can be inferred by measuring the capacitance between the grid and the bottom electrode of each LEM. Averaging over all 12 LEMs, the measured values of this capacitance typically ranged from 150 pF with the liquid below the grid to around 350 pF when the LEMs are submerged. This method offers the potential advantage of monitoring the liquid level in the CRP extraction region with a  $50 \times 50 \text{ cm}^2$  granularity and can be used for the CRP level adjustment in the future large-scale detectors where, due to the space constraints, placement of the level meters along the CRP perimeter is not possible.

## 7.2.5 Gas Analyzers

Gas analyzers are commercially produced modules that measure trace quantities of specific gases contained within a stream of carrier gas. The carrier gas for DUNE is argon, and the trace gases of interest are oxygen ( $\text{O}_2$ ), water ( $\text{H}_2\text{O}$ ), and nitrogen ( $\text{N}_2$ ). Oxygen and water impact the electron lifetime in LAr, while  $\text{N}_2$  impacts the efficiency of scintillation light production. In the LAr environment, these trace gases represent contaminants that need to be kept at levels below 0.1 ppb. The argon is sampled from either the argon vapor in the ullage or from the LAr by the use of small diameter tubing run from the sampling point to the gas analyzer. Typically the tubing runs from the sampling points are connected to a switchyard valve that is used to route the sample points to the desired gas analyzers. Figure 7.14 is a photo of such a switchyard.

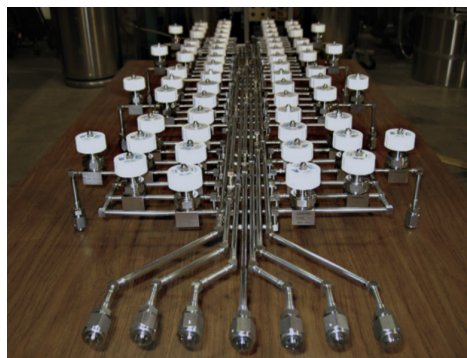


Figure 7.14: A Gas Analyzer switchyard that routes sample points to the different gas analyzers.

Gas analyzers can be used to:

1. Eliminate the air atmosphere from the cryostat after detector installation to levels low enough to begin cooldown is an argon piston purge followed by a recirculation of the remaining argon gas through the filtration system. This process is described more fully in Section 7.5. Figure 7.15 shows the evolution of the  $\text{N}_2$ ,  $\text{O}_2$ , and  $\text{H}_2\text{O}$  levels from gas analyzer data taken during the purge and recirculation stages of the DUNE 35 ton prototype phase 1 run.

- Track trace  $O_2$  and  $H_2O$  contaminants from the tens of ppb to the hundreds of ppt. This is useful when other means of monitoring the impurity level (e.g., purity monitors, or TPC tracks) are not yet sensitive. Figure 7.16 shows an example plot of the  $O_2$  level at the beginning of LAr purification from one of the later 35t HV runs.
- Monitor the tanker LAr deliveries purity during the cryostat-filling period. This allows tracking the impurity load on the filtration system and rejecting any deliveries that are out of specifications. Likely specifications for the delivered LAr are in the 10 ppm range per contaminant.

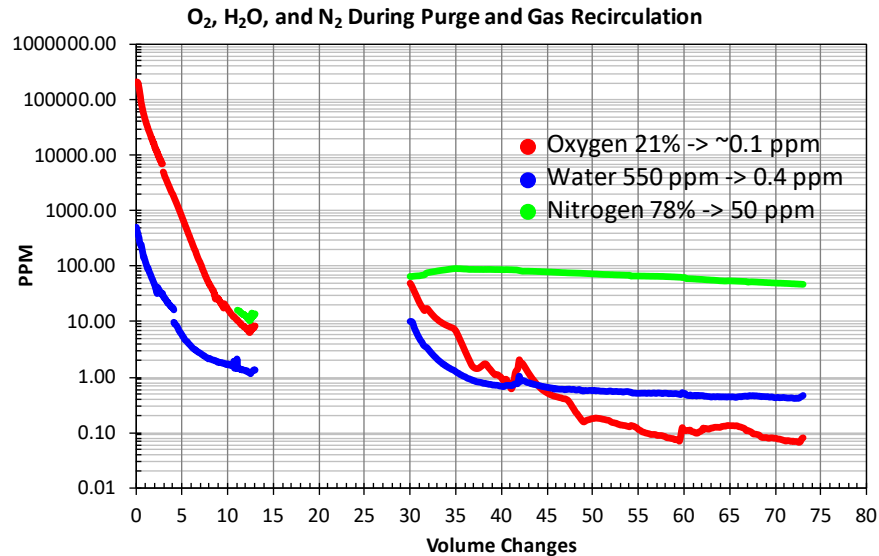


Figure 7.15: Plot of the  $O_2$ ,  $H_2O$ , and  $N_2$  levels during the piston purge and gas recirculation stages of the 35t phase 1 run.

As any one gas analyzer covers only one contaminant species and 3 to 4 orders of magnitude of range, multiple units are needed both for the three contaminant gases and to cover the ranges that are seen between the cryostat closure to the beginning of TPC operations: 20% to  $\lesssim 100$  ppt for  $O_2$ , 80% to  $\lesssim 1$  ppm for  $N_2$ , and  $\sim 1\%$  to  $\lesssim 1$  ppb for  $H_2O$ . Since the total cost of these analyzers exceeds \$100k, it is useful to be able to sample more than a single location or cryostat with the same gas analyzers. At the same time, the tubing run lengths from the sample point should be as short as possible in order to keep the response of the gas analyzer timely. This puts some constraints on the sharing of devices since, for example, the argon deliveries are at the surface, perhaps necessitating a separate surface gas analyzer.

## 7.2.6 Cameras

Cameras provide direct visual information about the state of the detector module during critical operations and when damage or unusual conditions are suspected. Cameras in the WA105 DP demonstrator allowed spray from cool-down nozzles to be seen and the level and state of the LAr to be observed as it covered the CRP [45]. A camera was used in the Liquid Argon Purity Demonstrator cryostat[44] to study HV discharges in LAr, and in EXO-100 during operation of a



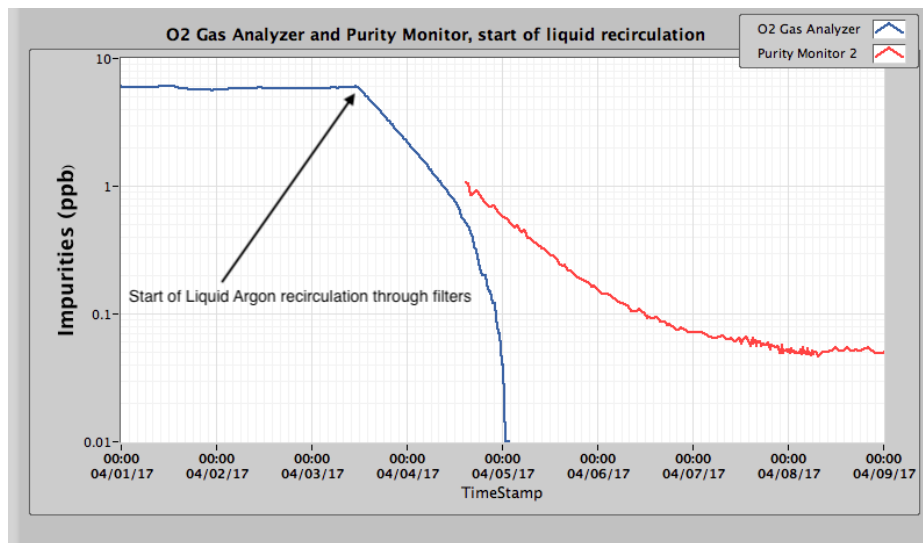


Figure 7.16:  $O_2$  as measured by a precision  $O_2$  analyzer just after the 35 ton prototype was filled with LAr, continuing with the LAr pump start and beginning of LAr recirculation through the filtration system. As the gas analyzer loses sensitivity, the purity monitor is able to pick up the impurity measurement. Note that the purity monitor is sensitive to both  $O_2$  and  $H_2O$  impurities giving rise to its higher level of impurity.

TPC [46]. Warm cameras viewing LAr from a distance have been used to observe HV discharges in LAr in fine detail [47]. Cameras are commonly used during calibration source deployment in many experiments (e.g., the KamLAND ultra-clean system [48]).

In DUNE, cameras are used to verify the stability, straightness, and alignment of the hanging TPC structures during cool-down and filling; to ensure that there is no bubbling near the GPs (SP) or CRPs (DP); to inspect the state of movable parts in the detector module (calibration devices, dynamic thermometers) as needed; and to closely inspect parts of the TPC as necessary following any seismic activity or other unanticipated occurrence. These functions are performed using a set of fixed *cold* cameras permanently mounted at fixed points in the cryostat for use during filling and commissioning, and a movable, replaceable *warm* inspection camera that can be deployed through any free instrumentation flange at any time throughout the life of the experiment. Table 7.3 summarizes the requirements for the camera system.

The following sections describe the design considerations for the cold and warm cameras and the associated lighting system. The same basic design may be used for both the single and dual phase detectors.

### 7.2.6.1 Cryogenic Cameras (Cold)

The fixed cameras monitor the following items during filling:

- Positions of corners of APA or CRP, cathode plane assembly (CPA) or cathode, FCs, GPs (1 mm resolution);

Table 7.3: Camera system requirements

| Requirement  | Physics Requirement Driver   |
|--|--|
| <b>General</b>   |  |
| No component may contaminate the LAr.  | High LAr purity is required for TPC operation.   |
| No component may produce bubbles in the liquid argon if the HV is on.  | Bubbles increase risk of HV discharge.   |
| No point in the camera system shall have a field greater than 15 kV/cm when the drift field is at nominal voltage.                                     | Fields must be well below 30 kV/cm to avoid risk of HV discharge.                                |
| The camera system shall not produce measurable noise in any detector system.   | Low noise is required for TPC operation.   |
| Cameras provide the viewing functionality as agreed upon with the other subsystems for viewing, as documented in the ICDs with the individual systems. |  |
| <b>Cold cameras</b>  |  |
| Minimize heat dissipation when camera not in operation.  | Do not generate bubbles when HV is on.   |
| Longevity must exceed 18 months.   | Cameras must function throughout cryostat filling and detector commissioning.                    |
| Frame rate $\geq 10$ /s.   | Observe bubbling, waves, detritus, etc.  |
| <b>Inspection cameras</b>  |  |
| Keep heat transfer to LAr low when in operation.   | Do not generate bubbles, some use cases may require operation when HV is on.                     |
| Deploy without exposing LAr to air.  | Keep LAr free of N <sub>2</sub> and other electronegative contaminants.                          |
| Camera enclosure must be replaceable.  | Replace broken camera, or upgrade, throughout life of experiment.                                |
| <b>Light emitting system</b>   |  |
| No emission of wavelengths shorter than 400 nm   | Avoid damaging tetra-phenyl butadiene (TPB) waveshifter.   |
| Longevity must exceed 18 months.   | Lighting for fixed cameras must function throughout cryostat filling and detector commissioning. |

- Relative straightness and alignment of APA/CRP, CPA/cathode, and FC ( $< \sim 1$  mm);
- Relative position of profiles and endcaps (0.5 mm resolution);
- State of LAr surface: e.g., the presence of bubbling or debris.

There are published articles and unpublished presentations describing completely or partially successful operation of low-cost, off-the-shelf CMOS cameras in custom enclosures immersed in cryogenics. (e.g., EXO-100: [46]; DUNE 35 ton prototype test [49]; WA105 DP demonstrator: [45].) Generally it is reported that such cameras show poor performance and ultimately fail to function below some temperature of order 150 K to 200 K, but some report that their cameras recover fully after being stored (not operated) at temperatures as low as 77 K and then brought up to minimum operating temperature.

However, as with photon sensors, experience has also shown that it is non-trivial to ensure reliable and reproducible mechanical and electrical integrity of such cameras in the cryogenic environment (e.g., [49] and [50]). Off-the-shelf cameras and camera components are generally only specified by the vendors and original manufacturers for operation down to  $-40^\circ\text{C}$  or  $-50^\circ\text{C}$ . In addition, many low-cost cameras use digital interfaces not intended for long distance deployment, such as USB (2 ~ 5 m) or CSI (circuit board scale), leading to signal degradation and noise problems.

The design for the DUNE fixed cameras uses an enclosure based on the successful EXO-100 design[46], which was also used successfully in LAPD (see Figure 7.17). The enclosure is connected to a stainless steel gas line to allow it to be flushed with argon gas at low enough pressure to prevent liquification, using the same design as the gas line for the beam plug tested in the 35 ton prototype HV test and in ProtoDUNE. A thermocouple in the enclosure allows temperature monitoring, and a heating element provides temperature control. The camera transmits its video signal using either a composite video signal over shielded coax or Ethernet over optical fiber. Most importantly, the DUNE CISC consortium must work with vendors to design camera circuit boards that are robust and reliable in the cryogenic environment.

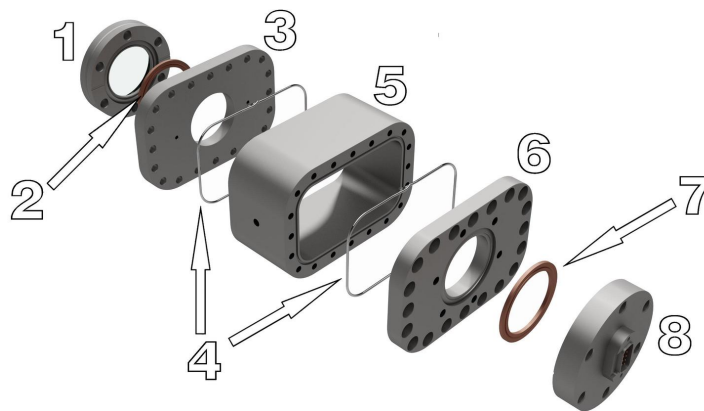


Figure 7.17: CAD exploded view of vacuum-tight camera enclosure suited for cryogenic applications from [46]. (1) quartz window, (2 and 7) copper gasket, (3 and 6) flanges, (4) indium wires, (5) body piece, (8) signal feedthrough.

### 7.2.6.2 Inspection Cameras (Warm)

The inspection cameras are intended to be as versatile as possible. However, the following locations have been identified as likely to be of interest:

- Status of HV feedthrough and cup;
- Status of FC profiles, endcaps (0.5 mm resolution);
- $y$ -axis deployment of calibration sources;
- Status of thermometers, especially dynamic thermometers;
- HV discharge, corona, or streamers on HV feedthrough, cup, or FC;
- Relative straightness and alignment of APA/CRP, CPA/cathode, and FC (1 mm resolution);
- Gaps between CPA frames (1 mm resolution);
- Relative position of profiles and endcaps (0.5 mm resolution);
- Sense wires at top of outer wire planes in SP APA (0.5 mm resolution).

Unlike the fixed cameras, the inspection cameras need operate only as long as inspection lasts, as the camera can be replaced in case of failure. It is also more practical to keep the cameras continuously *warm* (above  $-150^{\circ}\text{C}$ ) during deployment; this offers more options for commercial cameras, e.g., the same model camera used successfully to observe discharges in LAr from 120 cm away [47].

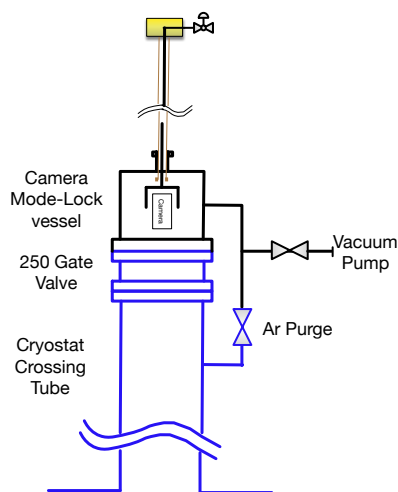


Figure 7.18: An overview of the inspection camera design.

The design for the inspection camera system employs the same basic enclosure design as for cold cameras, but mounted on an insertable fork using a design similar to the dynamic temperature

probes. See Figure 7.18 and Figure 7.12. The entire system is sealed to avoid contamination with air. In order to avoid contamination, the camera can only be deployed through a feedthrough equipped with a gate valve and a purging system, similar to that used for the vertical axis calibration system at KamLAND [48]. The entire system is purged with pure argon gas before the gate valve is opened.

Motors above the flange allow rotation and vertical movement of the fork. A chain drive system, with motor mounted on the end of the fork, allows tilting of the camera assembly, creating a point-tilt mount with vertical motion capability. Taking into account the room above the cryostat flanges and the thickness of the cryostat insulation, a vertical range of motion of 1 m inside the cryostat is achievable. The motors for rotation and vertical motion are located outside the sealed volume, coupled mechanically using ferrofluidic seals, thus reducing contamination risks and allowing for manual rotation of the vertical drive in the event of a motor failure. A significant prototyping and testing effort is needed to finalize and validate this design.

### 7.2.6.3 Light-emitting system

The light-emitting system is based on LEDs with the capability of illuminating the interior with selected wavelengths (IR and visible) that are suitable for detection by the cameras. Performance criteria for the light-emission system are based on the efficiency of detection with the cameras, in conjunction with adding minimal heat to the cryostat. The use of very high-efficiency LEDs helps reduce heat generation; as an example, one 750 nm LED has a specification of 32 % conversion of electrical input power to light.

While data on the performance of LEDs at cryogenic temperatures is sparse, some studies related to NASA projects [51] indicate that LED efficiency increases with reduced temperature, and that the emitted wavelengths may change, particularly for blue LEDs. The wavelength changes cited would have no impact on illumination, however, since in order to avoid degradation of wavelength-shifting materials in the PDS, such short wavelength LEDs would not be used.

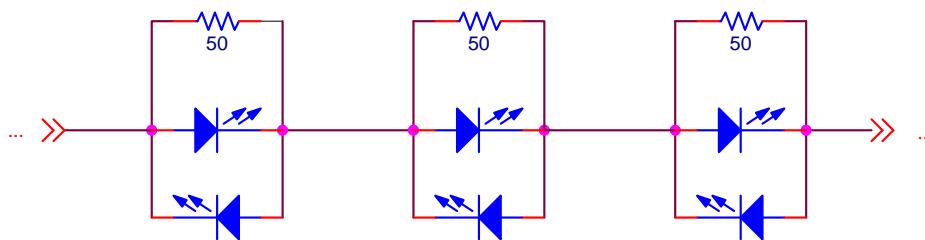


Figure 7.19: Suggested LED chain for lighting inside the cryostat, with dual-wavelength and failure-tolerant operation.

A *chain* of LEDs should be connected in series and driven with a constant-current circuit. It would be advantageous to pair each LED in parallel with an opposite polarity LED and a resistor (see Figure 7.19). This allows two different wavelengths of illumination with a single installed chain (by changing the direction of the drive current) and continued use of an LED chain even if individual LEDs fail.

The LEDs should be placed as a *ring light* around the outside of each camera lens, pointing in the same direction as the lens, to illuminate the part of the detector module within the field of view of the camera. Commercially available LEDs can be obtained with a range of angular spreads, and can be matched to the needs of the cameras without additional optics.

## 7.2.7 Cryogenics Test Facility

The cryogenics test facility is intended to provide the access to a small ( $< 1$  ton) to intermediate ( $\sim 4$  tons) volumes of purified TPC-grade LAr. Hardware that needs liquid of purity this high include any device intending to drift electrons for millisecond time periods. Not all devices require purity this high, but some may need a relatively large volume to provide the needed prototyping environment. Of importance is a relatively fast turn-around time of approximately a week for short prototyping runs.

Figure 7.20 shows the Blanche test stand cryostat at Fermilab.



Figure 7.20: Blanche Cryostat at Fermilab. This cryostat holds  $\sim 0.75$  tons of LAr.

## 7.2.8 Cryogenic Internal Piping

The cryogenic internal piping comprises several manifolds to distribute the liquid and gaseous argon inside the cryostat during all phases (e.g., gaseous purge, liquid distribution, cool down)

and various pipe stands to return argon to the outside (e.g., boil-off gaseous argon). Vacuum-insulated pipe stands are needed to transition from inside to outside in a way that does not affect the purity and does not introduce a significant heat load.

LBNF has the expertise for engineering design and installation of the detector internal piping, while the CISC consortium has the expertise on the physics requirements, the relevant risk registries, and the interfaces with other detector systems. Ultimate responsibility for costing the internal cryogenic piping system also lies with the CISC consortium. It is important for these two groups to interact closely to ensure that the system enables achievement of the physics, avoids interference with other detector systems, and mitigates risks.

DUNE has formed a cryogenics systems working group with conveners from both the CISC consortium and LBNF. This group has both LBNF and CISC members and provides an official forum where we interface and establish the final design.

The initial design for the cryogenic internal piping calls for some 750 m of pipe per cryostat for purging and filling, laid out as shown in Figure 7.21-Left, and 20 flange-pipes assemblies, as the one shown on the right panel of Figure 7.21, with a CF DN250 flange penetrated by two  $\sim 2.2$  m long pipes.

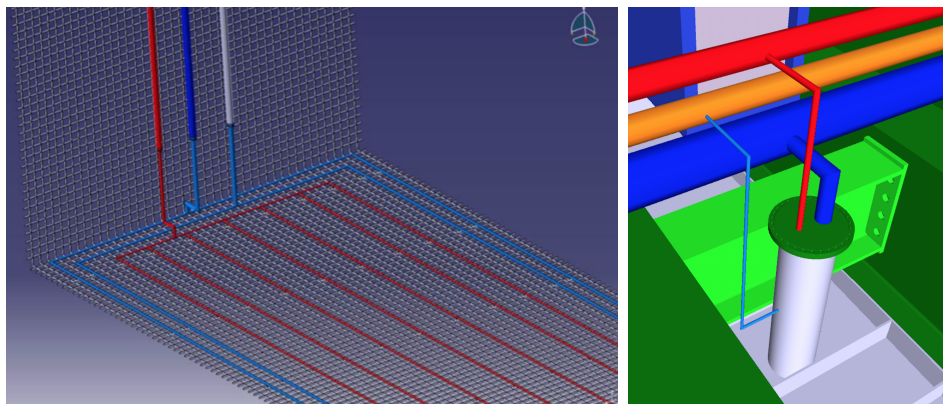


Figure 7.21: Left: Cryogenic internal piping for purging (red) and filling (blue). Right: Cool-down pipes, LAr in blue (vacuum jacketed) and gaseous argon in red.

### 7.3 Slow Controls

The slow controls system collects, archives, and displays data from a broad variety of sources, and provides real time alarms and warnings for detector operators. Data is acquired via network interfaces. Figure 7.22 shows the connections between major parts of the slow controls system and other systems.

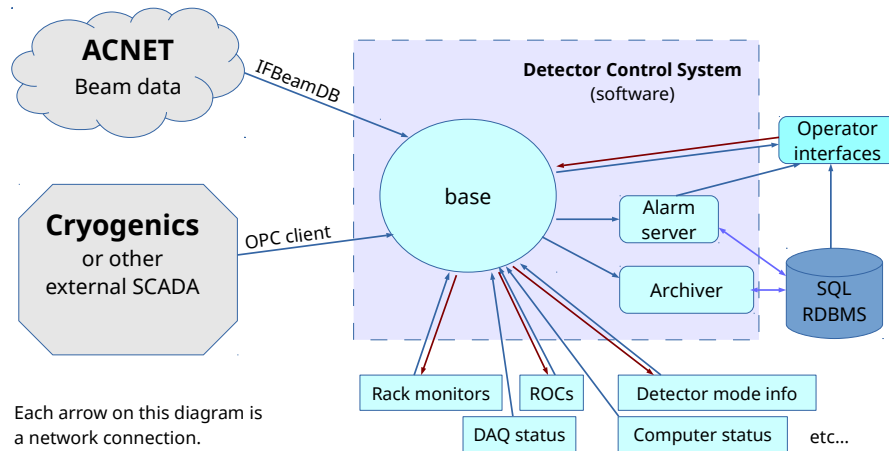


Figure 7.22: Typical Slow Controls system connections and data flow

## 7.3.1 Slow Controls Hardware

The slow controls will always require a small amount of dedicated network and computing hardware as described below. It also relies on common infrastructure, as described in Section 7.3.2.

In the current concept of the DP detector, HV biasing for the LEM, extraction grid, and PDS also falls within the scope of slow controls. This hardware could be assigned to different consortia in the future. For now its description is provided here.

### 7.3.1.1 Slow Controls Network Hardware

The slow controls data originates from the cryogenic instrumentation discussed in Section 7.2 and from other systems, and is collected by software running on servers (Section 7.3.1.2) housed in the underground data room in the central utility cavern, where data is archived in a central CISC database. The instrumentation data is transported over conventional network hardware from any sensors located in the cryogenic plant. However, the readouts that are located in the racks on top the cryostats have to be careful about grounding and noise. Therefore, each rack on the cryostat has a small network switch that sends any network traffic from that rack to the CUC via a fiber transponder. This is the only network hardware specific to slow controls; network infrastructure requirements are described in Section 7.3.2.

### 7.3.1.2 Slow Controls Computing Hardware

Two servers (a primary server and a replicated backup) suitable for the needed relational database discussed in Section 7.3.3 are located in the CUC data room, with an additional two servers to perform FE monitoring interface services: for example, assembling dynamic CISC monitoring web pages from the adjacent databases. Any special purpose software, such as iFix or EPICS, would



also run here. It is expected that one or two more servers will accommodate these programs. Replicating this setup on a per-module basis would allow for easier commissioning and independent operation, accommodate different module design (and the resulting differences in database tables), and ensure sufficient capacity. Including four sets of networking hardware, this would fit tightly into one rack or very comfortably into two.

### 7.3.1.3 High Voltage Biasing

The HV biasing for a LEM requires  $-5\text{ kV/channel}$ , with 41 channels per CRP. The extraction grid requires  $-10\text{ kV/channel}$ , with one channel per CRP. The LEM biasing system requires a current measurement sensitivity of  $50\text{ pA}$ . The biasing of the photomultipliers for the PDS needs of order 1000 channels operating up to a voltage of  $-3\text{ kV}$ .

### 7.3.1.4 CRP and PDS Calibration

Calibration of the charge readout system will be performed by charge injection onto the anode strips of the CRPs and into the preamplifiers. The slow controls system must include a high-accuracy pulser connected to the DAQ system for time-tagging of the pulse triggers. The pulser will be configurable as a function of the different calibration runs (pulsing of the strips or pulsing of the amplifiers) acting as common pulse source. This will be connected to a distribution system that allows dispatching the pulses to the CRP anode strips or to the signal chimneys hosting the analog FE cards. The distribution system will also include the possibility of selecting specific channels to which the pulses will be distributed. The PDS will also require a calibration system constituted by a common light source constantly monitored with reference photodetectors and a network of optical fibers distributing the light to each photomultiplier.

## 7.3.2 Slow Controls Infrastructure

The total number of slow controls quantities and the update rate are low enough that the data rate will be in the tens of kilobytes per second range (Section 7.3.4), placing minimal requirements on the local network infrastructure. Network traffic out of SURF to Fermilab will be primarily database calls to the central CISC database: either from monitoring applications, or from database replication to the offline version of the CISC database. This traffic is of a low enough bandwidth that the proposed general purpose links both out of the mine and back to Fermilab can accommodate it.

Up to two racks of space and appropriate power and cooling are available in the CUC's DAQ server room for CISC usage. Somewhat less space than that is currently envisioned, as described in 7.3.1.2.

### 7.3.3 Slow Controls Software

The slow controls software includes the following components in order to provide complete monitoring and control of detector subsystems:

- Control systems base that performs input and output operations and defines processing logic, scan conditions, alarm conditions, archiving rate, etc.;
- Alarm server that monitors all channels and sends alarm messages to operators;
- Data archiver that performs automatic sampling and storage of values for history tracking;
- Integrated operator interface that provides display panels for controls and monitoring.

An additional requirement for the software is the ability to indirectly interface with external systems (e.g., cryogenics control system) and databases (e.g., beam database) to export data into slow controls process variables (or channels) for archiving and status displays. This allows integrating displays and warnings into one system for the experiment operators, and provides integrated archiving for sampled data in the archived database. In this case, one can imagine an input output controller (IOC) running on a central DAQ server provides soft channels for these data. Figure 7.22 shows a typical workflow of a slow controls system.

In terms of key features of the software, a highly evolved software is needed that is designed for managing real-time data exchange, scalable to large number of channels and high bandwidth if needed. The software should be well documented, supported, and known to be reliable. The base software should also allow easy access of any channel by name. The archiver software should allow data storage in an SQL database with adjustable rates and thresholds such that one can easily retrieve data for any channel by using channel name and time range. Among the key features, the alarm server software should remember state, support arbitrary number of clients and provide logic for delayed alarms and acknowledging alarms. As part of the software, a standard naming convention for channels is followed to aid dealing with large number of channels and subsystems.

### 7.3.4 Slow Controls Quantities

The final set of quantities to monitor will ultimately be determined by the needs of the subsystems being monitored, as documented in appropriate interface control documents (ICDs), and continually revised based on operational experience. The total number of quantities to monitor has been very roughly estimated by taking the total number of quantities monitored in MicroBooNE and scaling by the detector length and the number of planes, giving a number in the range of 50 to 100k. Quantities are expected to update on average no faster than once per minute. The subsystems to be monitored include the cryogenic instrumentation described in this chapter, the other detector systems, and relevant infrastructure and external devices. Table 7.4 lists the kind of quantities expected from each system.

Table 7.4: Slow controls quantities

| <b>System</b>                              | <b>Quantities</b>  |
|--|--|
| <b>Detector Cryogenic Instrumentation</b>  |  |
| Purity monitors                            | Anode and cathode charge, bias voltage and current, flash lamp status, calculated electron lifetime  |
| Thermometers                               | Temperature, position of dynamic thermometers  |
| Liquid level                               | Liquid level   |
| Gas analyzers                              | Purity level readings  |
| Cameras                                    | Camera voltage and current draw, temperature, heater current and voltage, lighting current and voltage   |
| Cryogenic internal piping                  | feedthrough gas purge flow and temperature   |
| <b>Other Detector Systems</b>              |  |
| HV systems                                 | Drift HV voltage, current; end-of-field cage current, bias; ground plane currents  |
| TPC electronics                            | Voltage and current to electronics   |
| photon detector (PD)                       | Bias, current, electronics   |
| DAQ  | Warm electronics currents and voltages; run status; DAQ buffer sizes, trigger rates, data rates, GPS status, etc.; computer and disk health status; other health metrics as defined by DAQ group |
| CRP / APA                                  | Bias voltages and currents   |
| <b>Infrastructure and external systems</b> |  |
| Cryogenics (external)                      | Status of pumps, flow rates, inlet and return temperature and pressure (via OPC or similar SCADA interface)  |
| Beam status                                | Protons on target, rate, target steering, beam pulse timing (via IFBeamDB)   |
| Near detector                              | Near detector run status (through common slow controls database)   |
| Racks power and status                     | PDU current and voltage, air temperature, fan status if applicable, interlock status (fire, moisture, etc.)  |

### 7.3.5 Local Integration

The local integration for the slow controls consists entirely of software and network interfaces with systems outside of the scope of the detector module. This includes the following:

- Readings from the LBNF-managed external cryogenics systems, for status of pumps, flow rates, inlet and return temperature and pressure, which are implemented via OPC or a similar SCADA interfaces;
- Beam status, such as protons on target, rate, target steering, beam pulse timing, which are retrieved via IFBeamDB;
- Near Detector status, which can be retrieved from a common slow controls database.

This integration occurs after both the slow controls and non-detector systems are in place. The LBNF-CISC interface is managed by the Cryogenics Systems working group described in Section 7.2.8. IFBeamDB is already well established. An internal near-detector-FD working group may be established to coordinate detector status exchange between near and far sites interfacing.

## 7.4 Interfaces

The CISC consortium interfaces with all other consortia, task forces (calibration), working groups (physics, software/computing) and technical coordination. This section provides a brief summary; further details can be found in references [52]-[53].

There are obvious interfaces with detector consortia since CISC provides full rack monitoring (rack fans, thermometers and rack protection system), interlock status bit monitoring (not the actual interlock mechanism) and monitoring and control for all power supplies. The CISC consortium must maintain close contacts with all other consortia to ensure that specific hardware choices have acceptable slow controls (SC) solutions. Also, installation of instrumentation devices interferes with other devices and must be coordinated with the respective consortia. On the software side CISC must define, in coordination with other consortia, the quantities to be monitored and controlled by slow controls and the corresponding alarms, archiving and GUIs.

A major interface is the one with the cryogenics system. As mentioned in Section 7.2.2 purity monitors and gas analyzers are essential to mitigate the liquid argon contamination risk. The appropriate interlock mechanism to prevent the cryogenics system from irreversible contamination must be designed and implemented.

Another important interface is the one with the HV system [54] since several aspects related with safety must be taken into account. For all instrumentation devices inside the cryostat, electric field simulations are needed to guaranty proper shielding is in place. Although this is a CISC responsibility, input from HV is crucial. During the deployment of inspection cameras, generation

of bubbles must be avoided when HV is on, as it can lead to discharges.

There are also interfaces with the PDS [55]. Purity monitors and the light-emitting system for cameras both emit light that might damage PDs. Although this should be understood and quantified, CISC and the SP PDS may have to define the necessary hardware interlocks that avoid turning on any other light source accidentally when PDs are on.

The DAQ-CISC interface [56] is described in Section 6.3.4. CISC data is stored both locally (in CISC database servers in the central utility cavern (CUC)) and offline (the databases are replicated back to Fermilab) in a relational database indexed by timestamp. This allows bidirectional communications between DAQ and CISC by reading or inserting data into the database as needed for non-time-critical information.

CISC also interfaces with the beam and cryogenics group since at least the status of these systems must be monitored.

Assuming that the scope of software & computing SWC group includes scientific computing support to project activities, there are substantial interfaces with that group [57]. The hardware interfaces responsibility of the SWC include networking installation and maintenance, maintenance of SC servers and any additional computing hardware needed by instrumentation devices. CISC provides the needed monitoring for power distribution units (PDUs). Regarding software interfaces the SWC group provides: (1) SC database maintenance, (2) API for accessing the SC database offline, (3) UPS packages, local installation and maintenance of software needed by CISC, and (4) SWC creating and maintaining computer accounts on production clusters. Additionally CISC provides the required monitoring and control of SWC quantities including alarms, archiving, and GUIs, where applicable.

The CISC consortium may have additional hardware interfaces with the not-as-yet formed calibration consortium [58]. Indeed, since the shared ports are multi-purpose to enable deploying various devices, both CISC and calibration must interact in terms of flange design and sharing space around the ports. Also, CISC might use calibration ports to extract cables from CISC devices. At the software level, CISC is responsible for calibration device monitoring (and control to the extent needed) and monitors the interlock bit status for laser and radioactive sources.

CISC indirectly interfaces to physics through the shared devices. One specific need for physics is to extract instrumentation or slow controls data to correlate high-level quantities to low-level or calibration data. This requires tools to extract data from the slow controls database (see CISC-SWC interface document [57]). A brief list of what CISC data is needed by physics is given in the CISC-Physics interface document [59].

Interfaces between CISC and technical coordination are detailed in the corresponding interface documents for the facility [60], installation [53] and integration facility [61].

## 7.5 Installation, Integration and Commissioning

### 7.5.1 Cryogenics Internal Piping

The installation of internal cryogenic pipes occurs soon after the cryostat is completed or towards the end of the cryostat completion, depending on how the cryostat work proceeds. A concrete installation plan will be developed by the company designing the internal cryogenics. It depends on how they address the thermal contraction of the long horizontal and vertical runs. We are investigating several options, which each have different installation sequences. All involve delivery and welding together of prefabricated spool pieces inside the cryostat, and vacuum insulation of the vertical lines. The horizontal lines are bare pipes.

The cool-down assemblies are installed in dedicated cool-down feedthroughs at the top, arranged in two rows of ten each in the long direction of the cryostat. Each one features a LAr line connected to a gaseous argon line via a mixing nozzle and a gaseous argon line with spraying nozzles. The mixing nozzles generate droplets of liquid that are circulated uniformly inside the cryostat by the spraying nozzles. They are prefabricated at the vendor's site and delivered as full pieces, then mounted over the feedthroughs.

The current 3D model of the internal cryogenics is developed and archived at CERN as part of the full cryostat model. CERN is currently responsible for the integration of the detector cavern: cryostat, detector, and proximity cryogenics in the detector cavern, including cryogenics on the mezzanine and main LAr circulation pumps.

The prefabricated spool pieces and the cool down nozzles undergo testing at the vendor before delivery. The installed pieces are helium leak-checked before commissioning, but no other integrated testing or commissioning is possible after the installation, because the pipes are open to the cryostat volume. The internal cryogenics are commissioned once the cryostat is closed.

### 7.5.2 Purity Monitors

The purity monitor system is built in a modular way, such that it can be assembled outside of detector module cryostat. The assembly of the purity monitors themselves occurs outside of the cryostat and includes everything described in the previous section. The installation of the purity monitor system can then be carried out with the least number of steps inside the cryostat. The assembly itself is transported into the cryostat with the three individual purity monitors mounted to the support tubes but before installation of HV cables and optical fibers. The support tube at the top and bottom of the assembly is then mounted to the brackets inside the cryostat that could be attached to the cables trays or the detector support structure. In parallel to this work, the FE electronics and light source can be installed on the top of the cryostat, along with the installation of the electronics and power supplies into the electronics rack.

Integration begins by running the HV cables and optical fibers to the purity monitors, coming

from the top of the cryostat. The HV cables are attached to the HV feedthroughs with enough length to reach each of the respective purity monitors. The cables are run through the port reserved for the purity monitor system, along cable trays inside the cryostat until they reach the purity monitor system, and are terminated through the support tube down to each of the purity monitors. Each purity monitor has three HV cables that connect it to the feedthrough, and then along to the FE electronics. The optical fibers are run through the special optical fiber feedthrough, into the cryostat, and guided to the purity monitor system either using the cables trays or guide tubes. Whichever solution is adopted for running the optical fibers from the feedthrough to the purity monitor system, it must protect the fibers from accidental breakage during the remainder of the detector and instrumentation installation process. The optical fibers are then run inside of the purity monitor support tube and to the respective purity monitors, terminating at the photocathode of each.

Integration continues with the connection of the HV cables between the feedthrough and the system FE electronics, and then the optical fibers to the light source. The cables connecting the FE electronics and the light source to the electronics rack are also run and connected at this point. This allows for the system to turn on and the software to begin testing the various components and connections. Once it is confirmed that all connections are successfully made, the integration to the slow controls system is made, first by establishing communications between the two systems and then transferring data between them to ensure successful exchange of important system parameters and measurements.

The purity monitor system is formally commissioned once the cryostat is purged and a gaseous argon atmosphere is present. At this point the HV for the purity monitors is ramped up without the risk of discharge through the air, and the light source is turned on. Although the drift electron lifetime in the gaseous argon is very large and therefore not measurable with the purity monitors themselves, comparing the signal strength at the cathode and anode gives a good indication of how well the light source is generating drift electrons from the photocathode and whether they drift successfully to the anode.

### 7.5.3 Thermometers

Individual temperature sensors on pipes and cryostat membrane are installed prior to any detector component, right after the installation of the pipes. First, all cable supports are anchored to pipes. Then each cable is routed individually starting from the sensor end (with IDC-4 female connector but no sensor) towards the corresponding cryostat port. Once a port's cables are routed, they are cut to the same length such that they can be properly soldered to the pins of the SUBD-25 connectors on the flange. To avoid damage, the sensors are installed at a later stage, just before unfolding the bottom GPs.

Static T-gradient monitors are installed before the outer anode plane assemblies, after the installation of the pipes and before the installation of individual sensors. This proceeds in several steps: (1) installation of the two stainless steel strings to the bottom and top corners of the cryostat, (2) tension and verticality checks, (3) installation of cable supports in one of the strings, (4) installation of sensor supports in the other string, (5) cable routing starting from the sensor end

towards the corresponding cryostat port, (6) cutting all cables at the same point in that port, and (7) soldering cable wires to the pins of the SUBD-25 connectors on the flange. Then, at a later stage, just before moving corresponding APA into its final position, (8) the sensors are plugged into IDC-4 connectors.

For the SP, individual sensors on the top GP must be integrated with the GPs. For each CPA (with its corresponding four GP modules) going inside the cryostat, cable and sensor supports are anchored to the GP threaded rods as soon as possible. Once the CPA is moved into its final position and its top FC is ready to be unfolded, sensors on those GPs are installed. Once unfolded, cables exceeding the GP limits can be routed to the corresponding cryostat port either using neighboring GPs or DSS I-beams.

Dynamic T-gradient monitors are installed after the completion of the detector. The monitor comes in several segments with sensors and cabling already in place. Additional slack is provided at segment joints to ease the installation process. Segments are fed into the flange one at a time. The segments being fed into the detector module are held at the top with a pin that prevents the segment from sliding in all the way. Then the next segment is connected. The pin is removed, and the segment is pushed down until the next segment top is held with the pin at the flange. Then this next segment is installed. The process continues until the entire monitor is in its place inside the cryostat. Use of a crane is foreseen to facilitate the process. Extra cable slack at the top is provided again in order to ease the connection to the D-Sub standard connector flange and to allow vertical movement of the entire system. Then, a four-way cross flange with electric feedthroughs on one side and a window on the other side. The wires are connected to the D-sub connector on the electric flange feedthrough on the side. On the top of the cross, a moving mechanism is then installed with a crane. The pinion is connected to the top segment. The moving mechanism will come reassembled with motor on the side in place and pinion and gear motion mechanism in place as well. The moving mechanism enclosure is then connected to top part of the cross and this completes the installation process of the dynamic T-gradient monitor.

Commissioning of all thermometers proceeds in several steps. Since in the first stage only cables are installed, the readout performance and the noise level inside the cryostat are tested with precision resistors. Once sensors are installed the entire chain is checked again at room temperature. The final commissioning phase occurs during and after cryostat filling.

## 7.5.4 Gas Analyzers

Prior to the piston purge and gas recirculation phases of the cryostat commissioning, the gas analyzers are installed near the tubing switchyard. This minimizes tubing runs and is convenient for switching the sampling points and gas analyzers. Since each is a standalone module, a single rack with shelves, should be adequate to house the modules.

Concerning the integration, the gas analyzers typically have an analog output (4 to 20 mA or 0 to 10V) that maps to the input range of the analyzers. They also usually have a number of relays that indicate the scale they are currently running. These outputs can be connected to the slow controls for readout. However, using a digital readout is preferred since this directly gives the



analyzer reading at any scale. Currently there are a number of digital output connections, ranging from RS-232, RS-485, USB, and Ethernet. At the time of purchase, one can choose the preferred option, since the protocol is likely to evolve. The readout usually responds to a simple set of text commands. Due to the natural time scales of the gas analyzers, and lags in the gas delivery times (depending on the length of the tubing runs), sampling on timescales of a minute most likely is adequate.

Before the beginning of the gas phase of the cryostat commissioning, the analyzers must be brought online and calibrated. Calibration varies for the different modules, but often requires using argon gas with both zero contaminants (usually removed with a local inline filter) for the zero of the analyzer, and argon with a known level of the contaminant to check the scale. Since the start of the gas phase begins with normal air, the more sensitive analyzers are valved off at the switchyard to prevent overloading their inputs and potentially saturating their detectors. As the argon purge and gas recirculation progress, the various analyzers are valved back in when the contaminant levels reach the upper limits of the analyzer ranges.

### 7.5.5 Liquid Level Monitoring

Multiple differential pressure level monitors are installed in the cryostat, connected both to the side penetration of the cryostat at the bottom and to dedicated instrumentation ports at the top.

The capacitance level sensors are installed at the top of the cryostat in coordination with the TPC installation. Their placement relative to the upper ground plane (single phase) or CRP (dual phase) is important as these sensors will be used for a hardware interlock on the HV, and, in the case of the DP module, to measure the LAr level at the millimeter level as required for DP operation. Post installation in situ testing of the capacitive level sensors can be accomplished with a small dewar of liquid.

### 7.5.6 Cameras and Light-Emitting System

Fixed camera installation is in principle simple, but involves a considerable number of interfaces. Each camera enclosure has threaded holes to allow bolting it to a bracket. A mechanical interface is required with the cryostat wall, cryogenic internal piping, or DSS. Each enclosure is attached to a gas line for maintaining appropriate underpressure in the fill gas; this is an interface with cryogenic internal piping. Each camera has a cable for the video signal (coax or optical), and a multiconductor cable for power and control, to be run through cable trays to flanges on assigned instrumentation feedthroughs.

The inspection camera is designed to be inserted and removed on any instrumentation feedthrough equipped with a gate valve at any time during operation. Installation of the gate valves and purge system for instrumentation feedthroughs falls under cryogenic internal piping.

Installation of fixed lighting sources separate from the cameras would require similar interfaces as

fixed cameras. However, the current design has lights integrated with the cameras, which do not require separate installation.

### 7.5.7 Slow Controls Hardware

Slow controls hardware installation includes multiple servers, network cables, any specialized cables needed for device communication, and possibly some custom-built rack monitoring hardware. The installation sequence is interfaced and planned with the facilities group and other consortia. The network cables and rack monitoring hardware are common across many racks and are installed first as part of the basic rack installation, led by the facilities group. The installation of specialized cables needed for slow controls and servers is done after the common rack hardware is installed, and will be coordinated with other consortia and the DAQ group respectively.

### 7.5.8 Transport, Handling and Storage

Most instrumentation devices are shipped to SURF in pieces and mounted in situ. Instrumentation devices are in general small except the support structures for purity monitors and T-gradient monitors, which will cover the entire height of the cryostat. Since the load on those structures is relatively small ( $< 100$  kg) they can be fabricated in parts of less than 3 m, which can be easily transported to SURF. These parts are also easy to transport down the shaft and through the tunnels. All instrumentation devices except the dynamic T-gradient monitors, which are introduced into the cryostat through a dedicated cryostat port, can be moved into the cryostat without the crane.

Cryogenic internal piping needs special treatment given the number of pipes and their lengths. Purging and filling pipes will be most likely pre-assembled by the manufacturer as much as possible, using the largest size that can be shipped and transported down the shaft. Assuming 6 m long sections, pipes could be grouped in bunches of 10 to 15 pipes and stored in five pallets or boxes of about  $6.2 \text{ m} \times 0.8 \text{ m} \times 0.5 \text{ m}$ . These would be delivered to the site, stored, transported down to the detector cavern, and stored again before they are used. Depending on when they are installed, they could be stored inside the cryostat itself or in one of the drifts. Cool-down pipes are easier to handle. They could be transported in 20 boxes of  $2.2 \text{ m} \times 0.6 \text{ m} \times 0.6 \text{ m}$ , although there is room for saving some space using a different packaging scheme. Once in the cavern they could be stored on top of the cryostat.

## 7.6 Quality Control

A series of tests should be done by the manufacturer and the institute in charge of the device assembly. The purpose of quality control (QC) is to ensure that the equipment is capable of performing its intended function. The QC includes post-fabrication tests and also tests to run

after shipping and installation. In case of a complex system, the whole system performance will be tested before shipping. Additional QC procedures can be performed at the integration and test facility (ITF) and underground after installation if possible. The planned tests for each subsystem are described below.

## 7.6.1 Purity Monitors

The purity monitor system undergoes a series of tests to ensure the performance of the system. This starts with testing the individual purity monitors in vacuum after each one is fabricated and assembled. This test looks at the amplitude of the signal generated by the drift electrons at the cathode and the anode. This ensures that the photocathode is able to provide a sufficient number of photoelectrons for the measurement with the required precision, and that the field gradient resistors are all working properly to maintain the drift field and hence transport the drift electrons to the anode. A follow-up test in LAr is then performed for each individual purity monitor, ensuring that the performance expected in LAr is met.

The next step is to assemble the entire system and make checks of the connections along the way. Ensuring that the connections are all proper during this time reduces the risk of having issues once the system is finally assembled and ready for the final test. The assembled system is placed into the shipping tube, which serves as a vacuum chamber, and tested. If an adequately sized LAr test facility is available, a full system test can be performed at LAr temperature prior to installation.

## 7.6.2 Thermometers

### 7.6.2.1 Static T-Gradient Thermometers

Three type of tests are carried out at the production site prior to installation. First, the mechanical rigidity of the system is tested such that swinging is minimized ( $< 5$  cm) to reduce the risk of touching the anode plane assemblies. This is done with a 15 m stainless steel string, strung horizontal anchored to two points; its tension is controlled and measured. Second, all sensors are calibrated in the lab, as explained in Section 7.2.3. The main concern is the reproducibility of the results since sensors could potentially change their resistance (and hence their temperature scale) when undergoing successive immersions in LAr. In this case the QC is given by the calibration procedure itself since five independent measurements are planned for each set of sensors. Sensors with reproducibility (based on the RMS of those five measurements) beyond the requirements (2 mK for ProtoDUNE-SP) are discarded. The calibration serves as QC for the readout system (similar to the final one) and of the PCB-sensor-connector assembly. Finally, the cable-connector assemblies are tested: sensors must measure the expected values with no additional noise introduced by the cable or connector.

If the available LAr test facility has sufficient height or length to test a good portion of the system, an integrated system test is conducted there ensuring that the system operates in LAr

and achieves the required performance. Ideally, the laboratory sensor calibration will be compared with the in situ calibration of the dynamic T-gradient monitors by operating both dynamic and static T-gradient monitors simultaneously.

The last phase of QC takes place after installation. The verticality of each array is checked and the tensions in the horizontal strings are adjusted as necessary. Before soldering the wires to the flange, the entire readout chain is tested with temporary SUBD-25 connectors. This allows testing the sensor-connector assembly, the cable-connector assembly and the noise level inside the cryostat. If any of the sensors gives a problem, it is replaced. If the problem persists, the cable is checked and replaced if needed.

### 7.6.2.2 Dynamic T-Gradient Thermometers

The dynamic T-gradient monitor consists of an array of high-precision temperature sensors mounted on a vertical rod. The rod can move vertically in order to perform cross-calibration of the temperature sensors in situ. Several tests are foreseen to ensure that the dynamic T-gradient monitor delivers vertical temperature gradient measurements with precision at the level of a few mK.

- Before installation, temperature sensors are tested in LN to verify correct operation and to set the baseline calibration for each sensor with respect to the absolutely calibrated reference sensor.
- Warm and cold temperature readings are taken with each sensor after mounting on the PCB board and soldering the readout cables.
- The sensor readout is taken for all sensors after the cold cables are connected to electric feedthroughs on the flange and the warm cables outside of the cryostat are connected to the temperature readout system.
- The stepper motor is tested before and after connecting to the gear and pinion system.
- The fully assembled rod is connected to the pinion and gear, and moved with the stepper motor on a high platform many times to verify repeatability, possible offsets and uncertainty in the positioning. Finally, by repeating the test a large number of times, the sturdiness of the system will be verified.
- The full system is tested after installation in the cryostat: both motion and sensor operation are tested by checking sensor readout and vertical motion of the system.

### 7.6.2.3 Individual Sensors

The method to address the quality of individual precision sensors is the same as for the static T-gradient monitors. The QC of the sensors is part of the laboratory calibration. After mounting six

sensors with their corresponding cables, a temporary SUBD-25 connector will be added and the six sensors tested at room temperature. All sensors should work and give values within specifications. If any of the sensors gives problems, it is replaced. If the problem persists the cable is checked and replaced if needed.

### 7.6.3 Gas Analyzers

The gas analyzers will be guaranteed by the manufacturer. However, once received, the gas analyzer modules are checked for both *zero* and the *span* values using a gas-mixing instrument. This is done using two gas cylinders with both a zero level of the gas analyzer contaminant species and a cylinder with a known percentage of the contaminant gas. This should verify the proper operation of the gas analyzers. When eventually installed at SURF, this process is repeated before the commissioning of the cryostat. It is also important to repeat the calibrations at the manufacturer-recommended periods over the gas analyzer lifetime.

### 7.6.4 Liquid Level Monitoring

The differential pressure level meters will require QC by the manufacturer. While the capacitive sensors can be tested with a modest sample of LAr in the lab, the differential pressure level meters require testing over a greater range. While they do not require testing over the whole range, lab tests in LAr done over a meter or two can ensure operation at cryogenic temperatures. Depth tests can be accomplished using a pressurization chamber with water.

### 7.6.5 Cameras

Before transport to SURF, each cryogenic camera unit (comprising the enclosure, camera, and internal thermal control and monitoring) is checked for correct operation of all operating features, for recovery from 87 K non-operating mode, for no leakage, and for physical defects. Lighting systems are similarly checked for operation. Operations tests will include verification of correct current draw, image quality, and temperature readback and control. The movable inspection camera apparatus is inspected for physical defects, and checked for proper mechanical operation before shipping. A checklist is completed for each unit, filed electronically in the DUNE logbook, and a hard copy sent with each unit.

Before installation, each fixed cryogenic camera unit is inspected for physical damage or defects and checked in the cryogenics test facility for correct operation of all operating features, for recovery from 87 K non-operating mode, and for no contamination of the LAr. Lighting systems are similarly checked for operation. Operations tests include correct current draw, image quality, and temperature readback and control. After installation and connection of wiring, fixed cameras and lighting are again checked for operation. The movable inspection camera apparatus is inspected for physical defects and, after integration with a camera unit, tested in facility for proper mechanical

and electronic operation and cleanliness, before installation or storage. A checklist is completed for each QC check and filed electronically in the DUNE logbook.

### 7.6.6 Light-emitting System

The complete system is checked before installation to ensure the functionality of the light emission. Initial testing of the light-emitting system (see Figure 7.19) is done by first measuring the current when a low voltage (1 V) is applied, to check that the resistive LED failover path is correct. Next, measurement of the forward voltage is done with the nominal forward current applied, to check that it is within 10% of the nominal forward voltage drop of the LEDs, that all of the LEDs are illuminated, and that each of the LEDs is visible over the nominal angular range. If the LEDs are infrared, a video camera with IR filter removed is used for the visual check. This procedure is then duplicated with the current reversed for the LEDs oriented in the opposite direction.

These tests are duplicated during installation to make sure that the system has not been damaged in transportation or installation. However, once the LEDs are in the cryostat a visual check could be difficult or impossible.

### 7.6.7 Slow Controls Hardware

Networking and computing systems will be purchased commercially, requiring quality assurance (QA). However, the new servers are tested after delivery to confirm no damage during shipping. The new system is allowed to *burn in* overnight or for a few days, running a diagnostics suite on a loop. This should turn up anything that escaped the manufacturer's QA process.

The system can be shipped directly to the underground, where an on-site expert performs the initial booting of systems and basic configuration. Then the specific configuration information is pulled over the network, after which others may log in remotely to do the final setup, minimizing the number of people underground.

## 7.7 Safety

Several aspects related to safety must be taken into account for the different phases of the CISC project, including R&D, laboratory calibration and testing, mounting tests and installation. The initial safety planning for all phases is reviewed and approved by safety experts as part of the initial design review, and always prior to implementation. All component cleaning, assembly, testing and installation procedure documentation includes a section on safety concerns relevant to that procedure, and is reviewed during the appropriate pre-production reviews.

Areas of particular importance to CISC include:

- Hazardous chemicals (e.g., epoxy compounds used to attach sensors to cryostat inner membrane) and cleaning compounds: All chemicals used are documented at the consortium management level, with an MSDS (Material safety data sheet) and approved handling and disposal plans in place.
- Liquid and gaseous cryogenics used in calibration and testing: LN and LAr are used for calibration and testing of most of the instrumentation devices. Full hazard analysis plans will be in place at the consortium management level for all module or module component testing involving cryogenic hazards, and these safety plans will be reviewed in the appropriate pre-production and production reviews
- HV safety: Purity monitors operate at  $\sim 2000$  V. Fabrication and testing plans will demonstrate compliance with local HV safety requirements at the particular institution or lab where the testing or operation is performed, and this compliance will be reviewed as part of the standard review process.
- Working at heights: Some aspects of the fabrication, testing and installation of CISC devices require working at heights. This is the case of T-gradient monitors and purity monitors, which are quite long. Temperature sensors installed near the top cryostat membrane and cable routing for all instrumentation devices require working at heights as well. The appropriate safety procedures including lift and harness training will be designed and reviewed.
- Falling objects: all work at height comes with associated risks of falling objects. The corresponding safety procedures, including the proper helmet usage and the observation of well delimited safety areas, will be included in the safety plan.

## 7.8 Organization and Management

### 7.8.1 Slow Controls and Cryogenics Instrumentation Consortium Organization

The organization of the CISC consortium is shown in Figure 7.23. The CISC consortium board is currently formed from institutional representatives from 17 institutes. The consortium leader acts as the spokesperson for the consortium and is responsible for the overall scientific program and management of the group. The technical leader of the consortium is responsible for the project management for the group. Currently five working groups are envisioned in the consortium (leaders to be appointed):

**Cryogenics Systems** gas analyzers, liquid level monitors and cryogenic internal piping; CFD simulations.

**LAr Instrumentation** purity monitors, thermometers, cameras and lightemitting system, and instrumentation test facility; feedthroughs; E field simulations; instrumentation precision stud-

ies; ProtoDUNE data analysis coordination efforts.

**Slow Controls Base Software and Databases** Base software, alarms and archiving databases, and monitoring tools; variable naming convention and slow controls quantities.

**Slow Controls Detector System Interfaces** Signal processing software and hardware interfaces (e.g., power supplies); firmware; rack hardware and infrastructure.

**Slow Controls External Interfaces** Interfaces with external detector systems (e.g., cryogenics system, beam, facilities, DAQ).

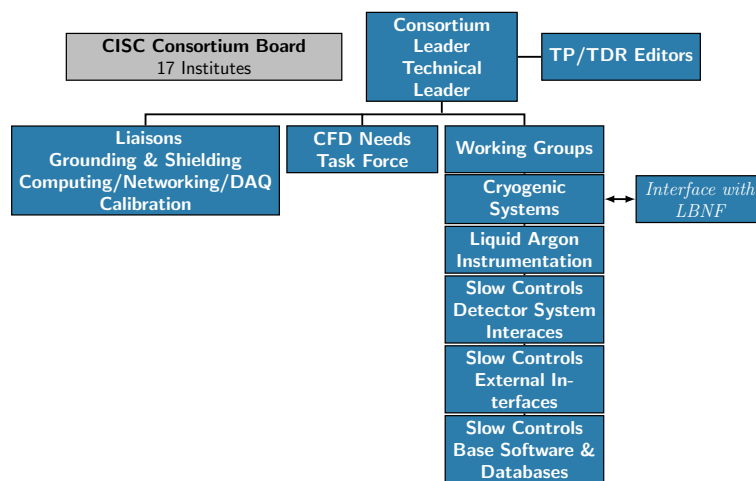


Figure 7.23: CISC consortium organizational chart

Additionally, since the CISC consortium broadly interfaces with other groups, liaisons have been identified for various roles as listed in Figure 7.23. A short-term focus group was recently formed to understand the needs for cryogenics modeling for the consortium. Currently members from new institutes are added to the consortium based on consensus from the consortium board members.

## 7.8.2 Planning Assumptions

The slow controls and cryogenic instrumentation is a joint effort for SP and DP. A single slow controls system will be implemented to serve both SP and DP.

Design and installation of cryogenics systems (gas analyzers, liquid level monitoring, internal piping) is coordinated with LBNF, with the consortium providing resources, and effort and expertise provided by LBNF. ProtoDUNE designs for LAr instrumentation (purity monitors, thermometers, cameras, test facility) provide the basis for DUNE designs. Design validation, testing, calibration, and performance will be evaluated through ProtoDUNE data.



### 7.8.3 High-level Schedule

Table 7.5 shows key milestones on the path to commissioning of the first two DUNE detector modules.

Table 7.5: Key CISC milestones leading towards commissioning of the first two DUNE detector modules.

| Date      | Milestone  |
|-----------|--|
| Aug. 2018 | Validate instrumentation designs using data from ProtoDUNE                       |
| Jan. 2019 | Complete architectural design for slow controls ready                            |
| Feb. 2019 | Full final designs of all cryogenic instrumentation devices ready                |
| Feb. 2023 | Installation of Cryogenic Internal Piping for Cryostat 1                         |
| Apr. 2023 | Installation of support structure for all instrumentation devices for Cryostat 1 |
| Oct. 2023 | All Instrumentation devices installed in Cryostat 1                              |
| Feb. 2024 | All Slow Controls hardware and infrastructure installed for Cryostat 1           |
| May 2024  | Installation of Cryogenic Internal Piping for Cryostat 2                         |
| July 2024 | Installation of support structure for all instrumentation devices for Cryostat 2 |
| Jan. 2025 | All Instrumentation devices installed in Cryostat 2                              |
| Apr. 2025 | All Slow Controls hardware and infrastructure installed for Cryostat 2           |
| July 2025 | Full Slow controls systems commissioned and integrated into remote operations    |

# Chapter 8

## Technical Coordination

The technical coordination (TC) team is responsible for detector integration and installation support. The DUNE collaboration consists of a large number of institutions distributed throughout the world. They are supported by a large number of funding sources and collaborate with a large number of commercial partners. Groups of institutes within DUNE form consortia that take complete responsibility for construction of their system. DUNE has empowered several consortia (currently nine) with the responsibility to secure funding and design, fabricate, assemble, install, commission and operate their components of the DUNE far detector (FD). There are three consortia focusing exclusively on the SP module: anode plane assembly (APA), SP cold electronics (CE) and SP photon detection system (PDS). There are three focusing exclusively on the DP module: charge-readout plane (CRP), DP CE and DP PDS. There are three joint consortia: high voltage (HV), data acquisition (DAQ) and cryogenic instrumentation and slow controls (CISC). Other consortia may be formed over time as concepts more fully emerge, such as a FD calibration system and various aspects of the near detector (ND). DUNE TC, under the direction of the Technical Coordinator, has responsibility to monitor the technical aspects of the detector construction, to integrate and install the detector modules and to deliver the common projects. The DUNE TC organization is shown in Figure 8.1.

The TC organization staffing will grow over time as the project advances. TC will provide staffing for teams underground at SURF, at integration facilities, and at the near site at Fermilab, in addition to the core team distributed among collaborating institutions.

The DUNE Project consists of a FD and a ND. The ND is at a pre-conceptual state; as the conceptual design and organization emerges, it will become part of the DUNE Project. Currently the DUNE Project consists of the DUNE FD consortia and TC. The DUNE Project is moving towards a technical design report (TDR) for the FD, both SP and DP options, in 2019. It is expected that a Conceptual Design Report for the ND will be prepared at the same time.

The FD components will be shipped from the consortia construction sites to the integration and test facility (ITF). TC will evaluate and accept consortia components either at integration facilities or the installation site and oversee the integration of components as appropriate. The scope of the FD integration and installation effort is shown graphically in Figure 8.2.

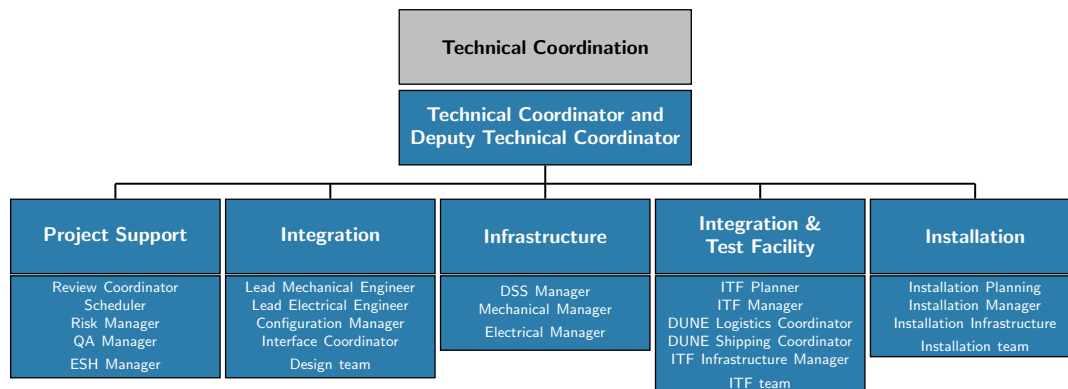


Figure 8.1: Organization of TC. This organization oversees the construction of the FD, both SP and DP, and the ND.

TC interacts with the consortia via three main areas: project coordination, integration, and installation. Construction of the DUNE FD requires careful technical coordination due to its complexity. Given the horizontal nature of the consortia structure and the extensive interdependencies between the systems, a significant engineering organization is required to deliver DUNE on schedule and within specifications and funding constraints.

The responsibilities of TC include:

- management and delivery of all common projects;
- development and monitoring of the consortia interfaces;
- configuration control of all interface documents, drawings and envelopes;
- installation of detectors at the near and far sites;
- logistics for detector integration and installation at the near and far sites;
- survey of the detector;
- primary interface to Long-Baseline Neutrino Facility (LBNF) for conventional facilities, cryostat and cryogenics;
- primary interface to the host laboratory for infrastructure and operations support;

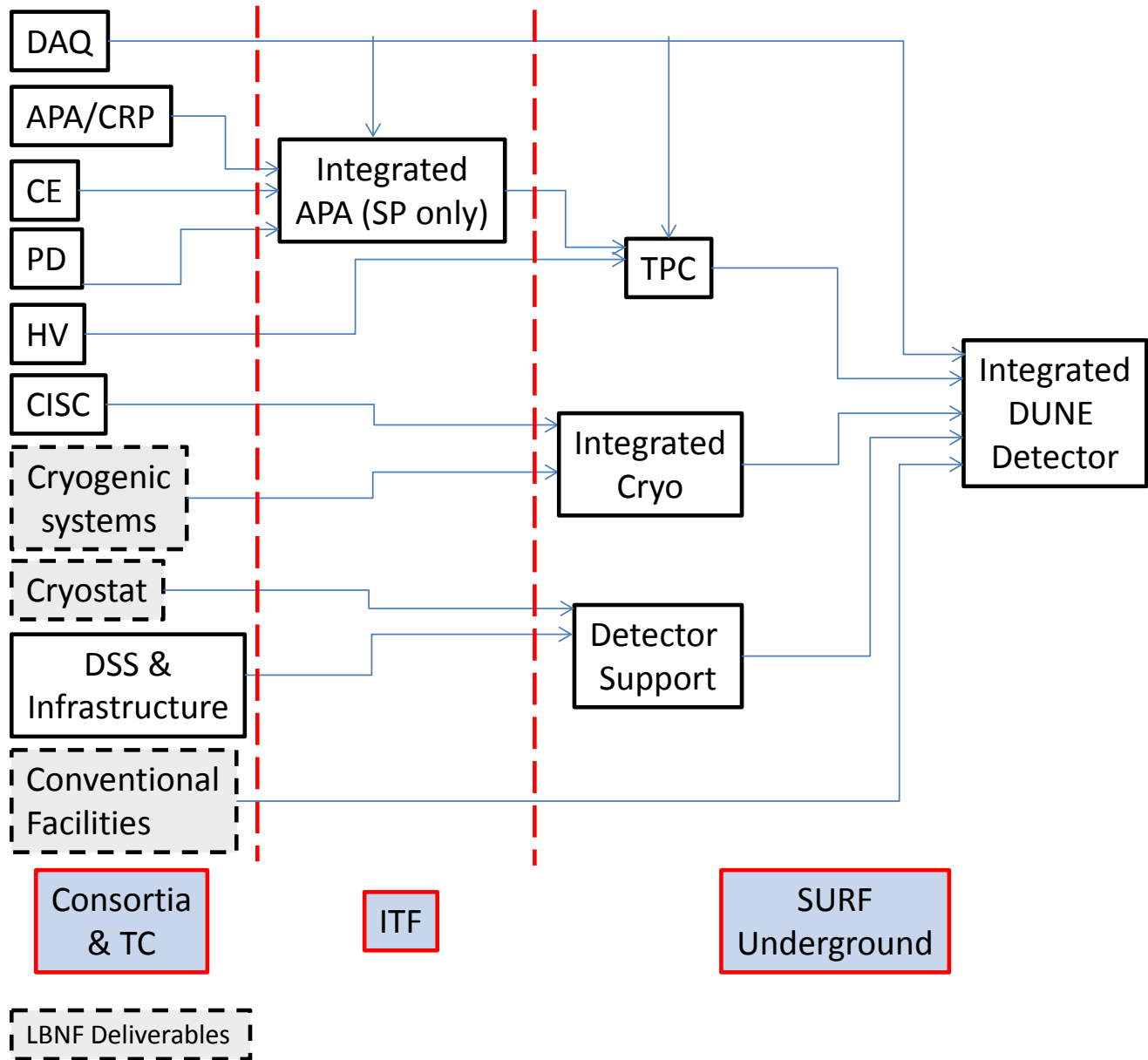


Figure 8.2: Flow of components from the consortia to the FD.

- development and tracking of project schedule and milestones;
- review of all aspects of the project;
- recording and approving all project engineering information, including: documents, drawings and models;
- project work breakdown schedules;
- project risk register;
- DUNE engineering and safety standards, including grounding and shielding;
- monitoring of all consortia design and construction progress;
- quality assurance (QA) and all QA related studies and documents;
- ES&H organization and all safety related studies and documents.

DUNE TC interacts with LBNF primarily through the LBNF/DUNE systems engineering organization. TC provides the points of contact between the consortia and LBNF. TC will work with the LBNF/DUNE Systems Engineer to implement the LBNF/DUNE Configuration Management Plan to assure that all aspects of the overall LBNF/DUNE project are well integrated. TC will work with LBNF and the host laboratory to ensure that adequate infrastructure and operations support are provided during construction, integration, installation, commissioning and operation of the detectors. The LBNF/DUNE systems engineering organization is shown in Figure 8.3.

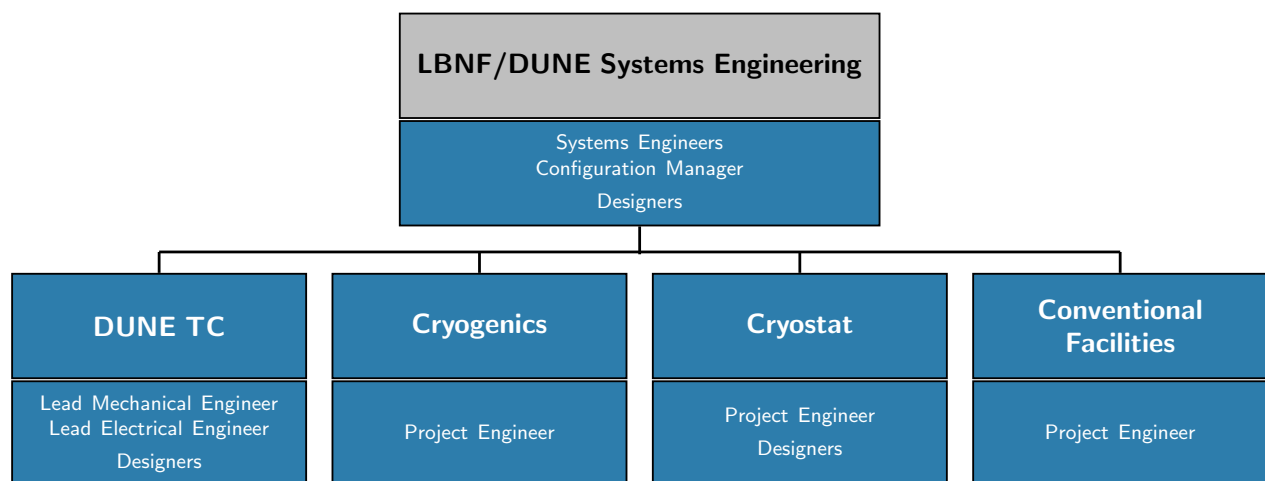


Figure 8.3: LBNF/DUNE systems engineering organizational structure.

Proper integration of the FDs within the supporting facilities and infrastructure at SURF is a major engineering task. The LBNF/DUNE Systems Engineer is responsible for the interfaces between the major LBNF and DUNE systems (conventional facilities, cryostats, cryogenics systems and

detector modules). The LBNF/DUNE systems engineering team includes several engineers and designers with responsibility for maintaining computer aided design (CAD) models. DUNE TC supports an engineering team that works directly with the LBNF/DUNE systems engineering team to ensure that the detector is properly integrated into the overall system.

TC has been working with the LBNF/DUNE systems engineering team to define requirements from DUNE for the conventional facilities final design for the detector chambers, central utility cavern (CUC), drifts and utilities. TC is representing the interests of the DUNE detector in the conventional facilities (CF) design. This includes refining the detector installation plan to understand how much space is needed in front of the temporary construction openings (TCOs) of the cryostats and therefore of the size of the chambers. TC continues to refine the detector needs for utilities in the detector caverns and the CUC where the DAQ will be housed.

Physics requirements on TC include cleanliness in the cryostats, survey and alignment tolerances, and grounding and shielding requirements. The cleanliness requirement is for ISO 8 (class 100,000), which will keep rates from dust radioactivity below those of the inherent  $^{39}\text{Ar}$  background. The alignment tolerances are driven by physics requirements on reconstructing tracks. Grounding and shielding are critical to enable this very sensitive, low-noise detector to achieve the required S/N. The physics requirements for LBNF and DUNE are maintained in DocDB-112.

## 8.1 Project Support

As defined in the DUNE Management Plan (DMP), the DUNE Technical Board (TB) generates and recommends technical decisions to the collaboration executive board (EB) (see Figure 8.4).

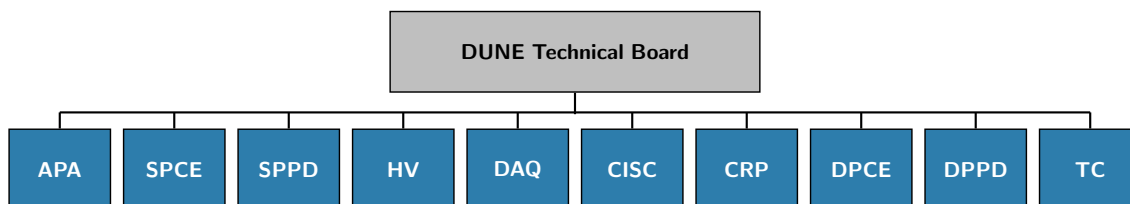


Figure 8.4: DUNE Technical Board.

It consists of all consortia scientific and technical leads. It meets on a regular basis (approximately monthly) to review and resolve any technical issues associated with the detector construction. It reports through the EB to collaboration management. The DUNE TB is chaired by the technical coordinator. DUNE collaboration management, including the EB, is shown in Figure 8.5. The TC engineering team also meets on a regular basis (approximately monthly) to discuss more detailed

technical issues. TC does not have responsibility for financial issues; that will instead be referred to the EB and Resource Coordinator (RC).

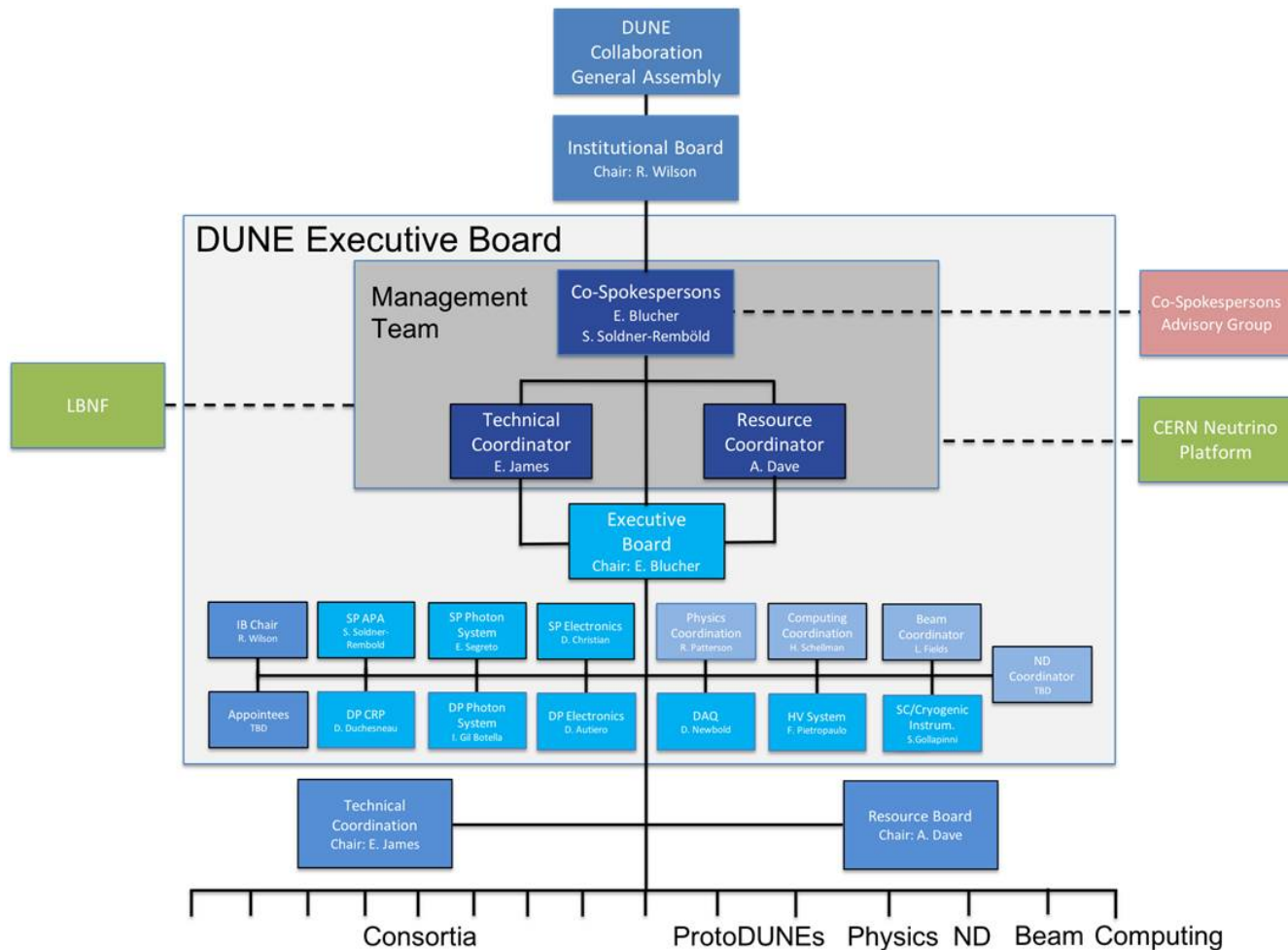


Figure 8.5: DUNE management organizational structure.

TC has several major project support tasks that need to be accomplished:

- Assure that each consortium has a well defined and complete scope, that the interfaces between the consortia are sufficiently well defined and that any remaining scope can be covered by TC through common fund or flagged as missing scope to the EB and RC. In other words, assure that the full detector scope is identified. Monitor the interfaces and consortia progress in delivering their scope.
- Develop an overall project integrated master schedule that includes reasonable production schedules, testing plans and a well developed installation schedule from each consortium. Monitor the integrated master schedule (IMS) as well as the individual consortium schedules.
- Ensure that appropriate engineering and safety standards are developed and agreed to by all key stakeholders and that these standards are conveyed to and understood by each consortium. Monitor the design and engineering work.

- Ensure that all DUNE requirements on LBNF for conventional facilities, cryostat and cryogenics have been clearly defined and understood by each consortium. Negotiate scope boundaries with LBNF. Monitor LBNF progress on final conventional facility design, cryostat design and cryogenics design.
- Ensure that all technical issues associated with scaling from ProtoDUNE have sufficient resources to converge on decisions that enable the detector to be fully integrated and installed.
- Ensure that the integration and quality control (QC) processes for each consortium are fully developed and reviewed and that the requirements on an ITF are well defined.

TC is responsible for technical quality and schedule and is not responsible for consortia funding or budgets. TC will try to help resolve any issue that it can, but will likely have to push all financial issues to the TB, EB and RC for resolution.

TC maintains a web page<sup>1</sup> with links to project documents. TC maintains repositories of project documents and drawings. These include the work breakdown structure (WBS), schedule, risk register, requirements, milestones, strategy, detector models and drawings that define the DUNE detector.

### 8.1.1 Schedule

A series of tiered milestones are being developed for the DUNE project. The Tier-0 milestones are held by the spokespersons and host laboratory director. Three have been defined and the current milestones and target dates are:

- |  |      |
|--|------|
| 1. Start main cavern excavation                      | 2019 |
| 2. Start detector module 1 installation              | 2022 |
| 3. Start operations of detector module 1–2 with beam | 2026 |

These dates will be revisited at the time of the TDR review. Tier-1 milestones will be held by the technical coordinator and LBNF Project Manager and will be defined in advance of the TDR review. Tier-2 milestones will be held by the consortia.

A high level version of the DUNE milestones from the IMS can be seen in Table 8.1.

TC will maintain the IMS that links all consortium schedules and contains appropriate milestones to monitor progress. The IMS is envisioned to be maintained in MS-Project<sup>2</sup> as it is expected that many consortia will use this tool. It is currently envisioned as three levels of control and notification milestones in addition to the detailed consortium schedules. The highest level contains external milestones, with the second level containing the key milestones for TC to monitor deliverables and

<sup>1</sup>[https://web.fnal.gov/collaboration/DUNE/DUNE%20Project/\\_layouts/15/start.aspx#/](https://web.fnal.gov/collaboration/DUNE/DUNE%20Project/_layouts/15/start.aspx#/).

<sup>2</sup>Microsoft™ Project.



Table 8.1: Overall DUNE Project Tier-1 milestones.

| Milestone  | Date              |
|--|-------------------|
| RRB Approval of Technical Design Review                      | 09/02/2019        |
| Beneficial Occupancy of Integration Test Facility            | 09/01/2021        |
| Construction of steel frame for Cryostat #1 complete         | 12/17/2021        |
| Construction of Mezzanine for Cryostat #1 complete           | 01/17/2022        |
| Begin integration/testing of Detector #1 components at ITF   | 02/01/2022        |
| Beneficial Occupancy of Central Utility Cavern Counting room | 04/16/2022        |
| Construction of steel frame for Cryostat #2 complete         | 07/01/2022        |
| Construction of Mezzanine for Cryostat #2 complete           | 08/01/2022        |
| <b>Beneficial occupancy of Cryostat #1</b>                   | <b>12/23/2022</b> |
| Cryostat #1 ready for TPC installation                       | 05/01/2023        |
| Begin integration/testing of Detector #2 components at ITF   | 11/01/2023        |
| <b>Beneficial occupancy of Cryostat #2</b>                   | <b>03/01/2024</b> |
| Begin closing Temporary Construction Opening for Cryostat #1 | 05/01/2024        |
| Cryostat #2 ready for TPC installation                       | 08/01/2024        |
| Cryostat #1 ready for filling                                | 10/01/2024        |
| Begin closing Temporary Construction Opening for Cryostat #2 | 07/18/2025        |
| <b>Detector #1 ready for operations</b>                      | <b>10/01/2025</b> |
| Cryostat #2 ready for filling                                | 12/05/2025        |
| <b>Detector #2 ready for operations</b>                      | <b>12/18/2026</b> |

installation progress, and the third level containing the inter-consortium links. The schedules will go under change control after agreement with each consortium on the notification milestone dates and the TDR is approved.

In addition to the overall IMS for construction and installation, a schedule of key consortia activity in the period 2018–19 leading up to the TDR has been developed.

To ensure that the DUNE detector remains on schedule, TC will monitor schedule status from each consortium, will organize reviews of schedules and risks as appropriate. As schedule problems arise TC will work with the affected consortium to resolve the problems. If problems cannot be solved, TC will take the issue to the TB and EB.

A monthly report with input from all consortia will be published by TC. This will include updates on consortium technical progress and updates from TC itself.

### 8.1.2 Risk

The successful operation of ProtoDUNE will retire a great many potential risks to DUNE. This includes most risks associated with the technical design, production processes, QA, integration and installation. Residual risks remain relating to design and production modifications associated with scaling to DUNE, mitigations to known installation and performance issues in ProtoDUNE, underground installation at SURF and organizational growth.

The highest technical risks include: development of a system to deliver 600 kV to the DP cathode; general delivery of the required HV; cathode and field cage (FC) discharge to the cryostat membrane; noise levels, particularly for the CE; number of dead channels; lifetime of components surpassing 20 year; QC of all components; verification of improved large electron multiplier (LEM) performance; verification of new cold analog-to-digital converter (ADC) and COLDATA performance; argon purity; electron drift lifetime; photoelectron light yield; incomplete calibration plan; and incomplete connection of design to physics. Other major risks include insufficient funding, optimistic production schedules, incomplete integration, testing and installation plans.

Key risks for TC to manage include the following:

1. Too much scope is unaccounted for by the consortia and falls to TC and common fund.
2. Insufficient organizational systems are put into place to ensure that this complex international mega-science project, including TC, Fermilab as host laboratory, SURF, DOE and all international partners continue to successfully work together to ensure appropriate rules and services are provided to enable success of the project.
3. Inability of TC to obtain sufficient personnel resources so as to ensure that TC can oversee and coordinate all of its project tasks. While the USA has a special responsibility towards TC as host country, it is expected that personnel resources will be directed to TC from each collaborating country. Related to this risk is the fact that consortium deliverables are not

really stand-alone subsystems; they are all parts of a single detector module. This elevates the requirements on coordination between consortia.

The consortia have provided preliminary versions of risk analyses that have been collected on the TC webpage. These are being developed into an overall risk register that will be monitored and maintained by TC in coordination with the consortia.

### 8.1.3 Reviews

TC is responsible for reviewing all stages of detector development and works with each consortium to arrange reviews of the design (preliminary design review (PDR) and final design review (FDR)), production (production readiness review (PRR) and production progress review (PPR)) and operational readiness review (ORR) of their system. These reviews provide input for the TB to evaluate technical decisions. Review reports are tracked by TC and provide guidance as to key issues that will require engineering oversight by the TC engineering team. TC will maintain a calendar of DUNE reviews.

TC works with consortia leaders to review all detector designs, with an expectation for a PDR, followed by a FDR. All major technology decisions will be reviewed prior to down-select. TC may form task forces as necessary for specific issues that need more in-depth review.

Start of production of detector elements can commence only after successful PRRs. Regular production progress reviews will be held once production has commenced. The PRRs will typically include review of the production of *Module 0*, the first such module produced at the facility. TC will work with consortium leaders for all production reviews.

TC is responsible to coordinate technical documents for the LBNC Technical Design Review.

### 8.1.4 Quality Assurance

The LBNF/DUNE QAP outlines the QA requirements for all DUNE consortia and describes how the requirements shall be met. The consortia will be responsible for implementing a quality plan that meet the requirements of the LBNF/DUNE QAP. The consortia implement the plan through the development of individual quality plans, procedures, guides, QC inspection and test requirements and travelers<sup>3</sup> and test reports. In lieu of a consortium-specific quality plan, the consortia may work under the LBNF/DUNE QAP and develop manufacturing and QC plans, procedures and documentation specific to their work scope. The technical coordinator and consortia leaders are responsible for providing the resources needed to conduct the Project successfully, including those required to manage, perform and verify work that affects quality. The DUNE consortia leaders are responsible for identifying adequate resources to complete the work scope and to ensure that their team members are adequately trained and qualified to perform their assigned work.

---

<sup>3</sup>The traveler is a document that details the fabrication and inspection steps and ensures that all steps have been satisfactorily completed.

The consortia work will be documented on travelers and applicable test or inspection reports. Records of the fabrication, inspection and testing will be maintained. When a component has been identified as being in noncompliance to the design, the nonconforming condition shall be documented, evaluated and dispositioned as one of the following: use-as-is (does not meet design but can meet functionality as is), rework (bring into compliance with design), repair (will be brought into meeting functionality but will not meet design) or scrap. For nonconforming equipment or material that is dispositioned as use-as-is or repair, a technical justification shall be provided allowing for the use of the material or equipment and approved by the design authority.

The LBNF/DUNE QAM reports to the LBNF Project Manager and DUNE Technical Coordinator and provides oversight and support to the consortium leaders to ensure a consistent quality program.

1. The QAM will plan reviews as independent assessments to assist the technical coordinator in identifying opportunities for quality and performance-based improvement and to ensure compliance with specified requirements.
2. The QAM is responsible to work with the consortia in developing their QA and QC Plans.
3. The QAM will review consortia QA and QC activity, including production site visits.
4. The QAM will participate in consortia design reviews, conduct PRRs prior to the start of production, conduct PRRs on a regular basis (as described in Section 8.1.3), and perform follow-up visits to consortium facilities prior to shipment of components to ensure all components and documentation are satisfactory.
5. The QAM is responsible for performing assessments at the ITF, the Far Site and the Near Site to ensure the activities performed at these locations are in accordance with the LBNF/DUNE QA Program and applicable procedures, specifications and drawings.

#### 8.1.4.1 Document Control

TC maintains repositories of project documents and drawings in two document management systems. DUNE Project documents will be stored in the DUNE DocDB <sup>4</sup>. DUNE drawings will be stored in electronic document management system (EDMS) <sup>5</sup>. TC will maintain approved versions of QA, QC and testing plans, installation plans, engineering and safety standards in the DUNE DocDB.

Consortia have developed initial interface, risk, schedule and WBS documents that will be put under change control and managed by the TC engineering team along with the consortia involved. These are currently in DocDB and will likely go under change control later in 2018, although they will continue to be developed through the TDR.

---

<sup>4</sup><https://docs.dunescience.org>

<sup>5</sup><https://edms.cern.ch/ui/#!master/navigator/project?P:1637280201:1637280201:subDocs>.

Thresholds for change control are described in the LBNF/DUNE CMP. The control process is further described in Section 8.2.1.

### 8.1.5 ESH

The DUNE ES&H program is described in the LBNF/DUNE IESHP. This plan is maintained by the LBNF/DUNE ES&H Manager, who reports to the LBNF Project Manager and the technical coordinator. The ES&H manager is responsible to work with the consortia in reviewing their hazards and their ES&H plans. The ES&H Manager is responsible to review ES&H at production sites, integration sites and at SURF. It is expected that the ES&H reviews will be conducted as part of the PRR and PPR process described in Section 8.1.3.

A strong ES&H program is essential to successful completion of the LBNF/DUNE Project at Fermilab, collaborating laboratories and universities, the ITF, and SURF. DUNE is committed to ensuring a safe work environment for collaborators at all institutions and to protecting the public from hazards associated with construction and operation of LBNF/DUNE. In addition, all work will be performed in a manner that preserves the quality of the environment and prevents property damage. Accidents and injuries are preventable and it is important that we work together to establish an injury-free workplace.

To achieve the culture and safety performance required for this project, it is essential that DUNE ensure that procedures are established to support the following ES&H policy statements:

- Line managers are responsible for environmental stewardship and personal safety at the DUNE work sites.
- Line managers, supported by the LBNF/DUNE, Fermilab, other collaborating laboratories, and SURF ES&H organizations, will provide consistent guidance and enforcement of the ES&H program that governs the activities of workers at each site where work is being performed.
- Incidents, whether they involve personal injuries or other losses, can be prevented through proper planning. All LBNF/DUNE work is planned.
- Workers are involved in the work planning process and continuous improvement, including the identification of hazards and controls.
- Working safely and in compliance with requirements is vital to a safe work environment. Line managers will enforce disciplinary policies for violations of safety rules.
- Each of us is responsible for our own safety and for that of our co-workers. Together we create a safe work environment.
- A strong program of independent audits, self-assessments and surveillance will be employed to periodically evaluate the effectiveness of the ES&H program.

- Any incidents that result or could have resulted in personal injury or illness, significant damage to buildings or equipment, or impact of the environment, will be investigated to determine corrective actions and lessons that can be applied to prevent recurrence. LBNF/DUNE encourages open reporting of errors and events.

To achieve the culture and safety performance required for this project, it is essential that ES&H be fully integrated into the project and be managed as tightly as quality, cost, and schedule.

## 8.2 Integration Engineering

The major aspects of detector integration focus on the mechanical and electrical connections between each of the detector systems. This includes verification that subassemblies and their interfaces are correct (e.g., APA and SP PDS). A second major area is in the support of the detector modules and their interfaces to the cryostat and cryogenics. A third major area is in assuring that the detector modules can be installed — that the integrated components can be moved into their final configuration. A fourth major area is in the integration of the detector modules with the necessary services provided by the conventional facilities.

### 8.2.1 Configuration Management

The TC engineering team will maintain configuration data in the appropriate format for the management of the detector configuration. The consortia are responsible for providing engineering data for their subsystems to TC. The TC engineering team will work with the LBNF project team to integrate the full detector data into the global LBNF configuration files. Appropriate thresholds for tracking and for change control will be established.

For mechanical design aspects, the TC engineering team will maintain full 3D CAD models of the detector modules. Appropriate level of detail will be specified for each type of model. Each consortium will be responsible for providing CAD models of their detector components to be integrated into overall models. The TC engineering team will work with the LBNF project team to integrate the full detector module models into a global LBNF CAD model which will include cryostats, cryogenics systems, and the conventional facilities. These will include models using varying software packages. The TC engineering team will work directly with the consortium technical leads and their supporting engineering teams to resolve any detector component interference or interface issues with other detector systems, detector infrastructure, and facility infrastructure.

For electrical design aspects, the TC engineering team will maintain high-level interface documents that describe all aspects of required electrical infrastructure and electrical connections. All consortia must document power requirements and rack space requirements. Consortia are responsible for defining any cabling that bridges the design efforts of two or more consortia. This agreed-upon and signed-off interface documentation shall include cable specification, connector specification, connector pinout and any data format, signal levels and timing. All cables, connectors, printed

circuit board components, physical layout and construction will be subject to project review. This is especially true of elements which will be inaccessible during the project lifetime. Consortia shall provide details on LAr temperature acceptance testing and lifetime of components, boards, cables and connectors.

At the time of the release of the TDR, the TC engineering team will work with the consortia to produce formal engineering drawings for all detector components. These drawings are expected to be signed by the consortia technical leads, project engineers, and Technical Coordinator. Starting from that point, the detector modules models and drawings will sit under formal change control as discussed in Section 8.1.4. It is anticipated that designs will undergo further revisions prior to the start of detector construction, but any changes made after the release of the TDR will need to be agreed to by all of the drawing signers and an updated, signed drawing produced. The major areas of configuration management include:

1. 3D model,
2. Interface definitions,
3. Envelope drawings for installation,
4. Drawing management.

TC will put into place processes for configuration management. Configuration management will provide TC and engineering staff the ability to define and control the actual build of the detector at any point in time and to track any changes which may occur over duration of the build as well as the lifetime of the project as described in Section 8.1.4.

For detector elements within a cryostat, configuration management will be frozen once the elements are permanently sealed within the cryostat. However, during the integration and installation process of building the detector modules within the cryostat, changes may need to occur. For detector elements outside the cryostat and accessible, all repairs, replacements, hardware upgrades, system grounding changes, firmware and software changes must be tracked.

Any change will require revision control, configuration identification, change management and release management.

### **Revision Control**

Consortia will be responsible for providing accurate and well documented revision control. Revision control will provide a method of tracking and maintaining the history of changes to a detector element. Each detector element must be clearly identified with a document which includes a revision number and revision history. For mechanical elements, this will be reflected by a drawing number with revision information. For electrical elements, schematics will be used to track revisions. Consortia will be responsible for identifying the revision status of each installed detector element. Revisions are further controlled through maintenance of the documents in DocDB and EDMS.

### **Configuration Identification**

Consortia are responsible for providing unique identifiers or part numbers for each detector element. Plans will be developed on how inventories will be maintained and tracked during the build. Plans will clearly identify any dynamic configuration modes which may be unique to a specific detector element. For example, a printed circuit board may have firmware that affects its performance.

### **Change Management**

TC will provide guidelines for formal change management. During the beginning phase of the project, drawings and interface documents are expected to be signed by the consortium technical leads, project engineers, and technical coordinator. Once this initial design phase is complete, the detector models, drawings, schematics and interface documents will be under formal change control. It is anticipated that designs will undergo further revisions prior to the start of detector construction, but any changes made after the release of the TDR will need to be agreed to by all drawing signers and an updated signed drawing produced.

### **Release Management**

Release management focuses on the delivery of the more dynamic aspects of the project such as firmware and software. Consortia with deliverables that have the potential to affect performance of the detector by changing firmware or software must provide plans on how these revisions will be tracked, tested and released. The modification of any software or firmware after the initial release, must be formally controlled, agreed upon and tracked.

## **8.2.2 Engineering Process and Support**

The TC organization will work with the consortia through its TC engineering team to ensure the proper integration of all detector components. The TC engineering team will document requirements on engineering standards and documentation that the consortia will need to adhere to in the design process for the detector components under their responsibility. Similarly, the project QA and ES&H managers will document QC and safety criteria that the consortia will be required to follow during the construction, installation, and commissioning of their detector components, as discussed in sections 8.1.4 and 8.1.5.

Consortia interfaces with the conventional facilities, cryostats, and cryogenics are managed through the TC organization. The TC engineering team will work with the consortia to understand their interfaces to the facilities and then communicate these globally to the LBNF Project team. For conventional facilities the types of interfaces to be considered are requirements for bringing needed detector components down the shaft and through the underground tunnels to the appropriate detector cavern, overall requirements for power and cooling in the detector caverns, and the requirements on cable connections from the underground area to the surface. Interfaces to the cryostat include the number and sizes of the penetrations on top of the cryostat, required mechanical structures attaching to the cryostat walls for supporting cables and instrumentation, and requirements on the global positioning of the detector modules within the cryostat. Cryogenics system interfaces include requirements on the location of inlet and output ports, requirements on the monitoring of the LAr both inside and outside the cryostat, and grounding and shielding requirements on piping attached to the cryostat.



LBNF will be responsible for the design and construction of the cryostats used to house the detector modules. The consortia are required to provide input on the location and sizes of the needed penetrations at the top of the cryostats. The consortia also need to specify any mechanical structures to be attached to the cryostat walls for supporting cables or instrumentation. The TC engineering team will work with the LBNF cryostat engineering team to understand what attached fixturing is possible and iterate with the consortia as necessary. The consortia will also work with the TC engineering team through the development of the 3D CAD model to understand the overall position of the detector modules within the cryostat and any issues associated with the resulting locations of their detector components.

LBNF will be responsible for the cryogenics systems used to purge, cool, and fill the cryostats. It will also be responsible for the system that continually re-circulates LAr through filtering systems to remove impurities. Any detector requirements on the flow of liquid within the cryostat will be developed by the consortia and transmitted to LBNF through the TC engineering team. Similarly, any requirements on the rate of cool-down or maximum temperature differential across the cryostat during the cool-down process will be specified by the consortia and transmitted to the LBNF team.

The engineering design process is defined by a set of steps taken to fulfill the requirements of the design. By the time of the TDR, all design requirements must be fully defined and proposed designs must be shown to meet these requirements. Based on prior work, some detector elements may be quite advanced in the engineering process, while others may be in earlier stages. Each design process shall closely follow the engineering steps described below.

### **Development of specifications**

Each consortium is responsible for the technical review and approval of the engineering specifications. The documented specifications for all major design elements will include the scope of work, project milestones, relevant codes and standards to be followed, acceptance criteria and specify appropriate internal or external design reviews. Specifications shall be treated as controlled documents and cannot be altered without approval of the TC team. The TC engineering team will participate in and help facilitate all major reviews as described in Section 8.1.3. Special TB reviews will be scheduled for major detector elements.

### **Engineering Risk Analysis**

Each consortium is responsible for identifying and defining the level of risk associated with their deliverables as described in Section 8.1.2. TC will work with the consortia, through its TC engineering team, to document these risks in a risk database and follow them throughout the project until they are realized or can be retired.

### **Specification Review**

The DUNE TC organization and project engineers shall review consortium specifications for overall compliance with the project requirements. Consortia must document all internal reviews and provide that documentation to TC. Additional higher-level reviews may be scheduled by TC as described in Section 8.1.3.

### **System Design**

The system design process includes the production of mechanical drawings, electrical schematics, calculations which verify compliance to engineering standards, firmware, printed circuit board

layout, cabling and connector specification, software plans, and any other aspects that lead to a fully documented functional design. All relevant documentation shall be recorded, with appropriate document number, into the chosen engineering data management system and be available for the review process.

### **Design Review**

The design review process is determined by the complexity and risk associated with the design element. For a simple design element, a consortium may do an internal review. For a more complex or high risk element a formal review will be scheduled. DUNE TC will facilitate the review, bringing in outside experts as needed. In all cases, the result of any reviews must be well documented and captured in the engineering data management system. If recommendations are made, those recommendations will be tracked in a database and the consortia will be expected to provide responses. All results of these engineering reviews will be made available for the subsystem design reviews described in Section 8.1.3.

### **Procurement**

The procurement process will include the documented technical specifications for all procured materials and parts. All procurement technical documents are reviewed for compliance to engineering standards and ES&H concerns. DUNE TC will assist the consortia in working with their procurement staff as needed.

### **Production and assembly**

During the implementation phase of the project, the consortia shall provide the Technical Coordinator with updates on schedule. A test plan will be fully developed which will allow for verification that the initial requirements have been met. This is part of the QA plan that will be documented and followed as described in Section 8.1.4.

### **Testing and Validation**

The testing plan documented in the above step will be followed and results will be well documented in consultation with the QAM. The Technical Coordinator and TC engineering team will be informed as to the results and whether the design meets the specifications. If not, a plan will be formulated to address any shortcomings and presented to the Technical Coordinator.

### **Final Documentation**

Final reports will be generated that describe the as built equipment, lessons learned, safety reports, installation procedures, testing results and operations procedures.

## **8.3 Detector Infrastructure**

TC is responsible for delivering the common infrastructure for the FD. This infrastructure is typically equipment that is used by many groups. This may include: the electronics racks on top of the cryostat with power, cooling, networking and safety systems, cable trays, cryostat crossing tubes, and flanges, detector safety systems and ground monitoring and isolation transformers.

TC is responsible for the systems to support the detectors. For the DP module this may consist of a cable winch system similar to ProtoDUNE-DP. In the case of the SP module the installation group also provides the detector support system (DSS), which supports the detector and is needed to bring equipment into the correct location in the cryostat.

## 8.4 The Integration and Test Facility

DUNE TC is responsible for interfacing with the LBNF logistics team at SURF to coordinate transport of all detector components into the underground areas. Due to the limited availability of surface areas at SURF for component storage, nearby facilities will be required to receive, store and ship materials to the Ross Shaft on an as-needed basis. A team within the TC organization will develop and execute the plan for receiving detector components at a surface facility and transporting them to the Ross Shaft in coordination with the on-site LBNF logistics team. The surface facility will require warehouse space with an associated inventory system, storage facilities, material transport equipment and access to trucking. Basic functions of this facility will be to receive the detector components arriving from different production sites around the world and prepare them for transport into the underground areas, incorporating re-packaging and testing as necessary. As a substantial facility will be required, it can also serve as a location where some detector components are integrated and undergo further testing prior to installation.

The logistics associated with integrating and installing the FDs and their associated infrastructure present a number of challenges. These include the size and complexity of the detector itself, the number of sites around the world that will be fabricating detector and infrastructure components, the necessity for protecting components from dust, vibration and shock during their journey to the deep underground laboratory, and the lack of space on the surface near the Ross Shaft. To help mitigate the associated risks, DUNE plans to establish an ITF somewhere in the vicinity of SURF. This facility and its associated staff will need to provide certain functions and services connected to the DUNE FD integration and installation effort and will have other potential roles that are still under consideration. The areas to which the ITF will and could contribute are the following:

- **Transport buffer:** The ITF needs to provide storage capacity for a minimum one-month buffer of detector components required for the detector installation process in the vicinity of SURF and be able to accept packaging materials returned from the underground laboratory.
- **Longer-term storage:** The ITF needs to provide longer-term storage of detector components that need to be produced in advance of when they are to be installed and for which sufficient storage space does not exist at the production sites.
- **Re-packaging** The ITF needs to have the capability to re-package components arriving from the various production sites into boxes that can be safely transported through the shaft into the underground areas.
- **Component fabrication:** It could be convenient to fabricate some components in the vicinity of SURF at the ITF, taking advantage of undergraduate science and engineering students

from the South Dakota School of Mines and Technology (SDSMT).

- **Component integration:** Integration of detector components received from different production sites that must be done prior to transport underground, such as the installation of photon detectors (PDs) and electronics on the anode plane assemblies, could be done prior to re-packaging at the ITF.
- **Inspection, testing and repair:** In cases where components are re-packaged for transport to the underground area, ITF support for performing tests on these components to ensure that no damage has occurred during shipping is likely desirable. In addition, components integrated at the ITF would require additional testing prior to being re-packaged. The ITF could provide facilities needed to repair some of the damaged components (others would likely need to be returned to their production sites).
- **Collaborator support:** The host institution of the ITF will need to provide support for a significant number of DUNE collaborators involved in the above activities including services such as housing assistance, office space, computing access, and safety training.
- **Outreach:** The host institution of the ITF would be ideally situated for supporting an outreach program to build upon the considerable public interest in the experiment that exists within South Dakota.

The facilities project (LBNF) will provide the cryostats that house the detector modules and the cryogenics systems that support them. Additional large surface facilities in the vicinity of SURF will be required to stage the components of these infrastructure pieces prior to their installation in the underground areas. The requirements for these facilities, in contrast to the ITF, are relatively straight-forward and can likely be met by a commercial warehousing vendor, who would provide suitable storage space, loading and unloading facilities, and a commercial inventory management and control system. It is currently envisioned that operation of the LBNF surface facilities and the DUNE ITF will be independent from one another. However, the inventory systems used at the different facilities will need to ensure proper coordination of all deliveries being made to the SURF site.

A reasonable criterion for the locations of these surface staging facilities is to be within roughly an hour's drive of SURF. Population centers in South Dakota within this radius are Lead, Deadwood, Sturgis, Spearfish, and Rapid City. The LBNF surface facilities, which are not expected to have significant auxiliary functionality, would logically be located as near to the SURF site as possible. In the case of the DUNE ITF, however, locating the facility in Rapid City to take advantage of facilities and resources associated with the South Dakota School of Mines & Technologies (SDSMT) has a number of potential advantages. SDSMT and the local business community in Rapid City have expressed interest in incorporating the DUNE ITF into an overall regional development program.

### 8.4.1 Requirements

The leadership teams associated with the DUNE consortia taking responsibility for the different FD subsystems have provided input to TC on which potential ITF functions and services would be applicable to their subsystems. The consortia have also made preliminary assessments of the facility infrastructure requirements that would be necessary in order for these functions and services to be provided for their subsystems at the ITF. An attempt to capture preliminary, global requirements for the ITF based on the information received from the consortia results in the following:

- Warehousing space on the order of 2800 m<sup>2</sup> (30,000 square feet); driven by potential need to store hundreds of the larger detector components needed to construct the TPCs. The provided space will need to maintain some minimal cleanliness requirements (e.g.; no insects) and be climate-controlled within reasonable temperature and humidity ranges.
- Crane or forklift coverage throughout the warehousing space to access components as needed for further processing or transport to SURF.
- Docking area to load trucks with detector components being transported to SURF and to receive packaging materials returned from the site.
- Smaller clean room areas within the warehousing space to allow for the re-packaging of detector components for transport underground. Re-packaging of larger components will require local crane coverage within the appropriate clean room spaces.
- Dedicated space for racks and cabinets available for dry-air storage and testing of electronics components. Racks and cabinets must be properly connected to the building ground to avoid potential damage from electrostatic discharges.
- Climate-controlled dark room space for the handling and testing PD components.
- Dedicated clean room on order of 1000 m<sup>2</sup> (10,000 square feet) to facilitate integration of electronics and PDs on anode plane assemblies. The integrated anode plane assemblies are tested in cold boxes supported by cryogenics infrastructure. Clean room lighting must be UV-filtered to avoid damaging the PDs. The height of the clean room must accommodate crane coverage needed for movement of the anode plane assemblies in and out of the cold boxes. It will also be necessary to have platforms for installation crews to perform work at heights within different locations in the clean room.
- Access to machine and electronics shops for making simple repairs and fabricating unanticipated tooling.
- Access to shared office space for up to 30 collaborators contributing to the activities taking place at the ITF. Assistance for identifying temporary housing in the vicinity of the ITF for the visiting collaborators.

## 8.4.2 Management

Overall management of the ITF is envisioned to be responsibility of one or more of the collaborating institutions on DUNE. If the ITF is located in Rapid City, SDSMT would be a natural choice due to its physical proximity, connections to the local community and ability to provide access to resources and facilities that would benefit planned ITF activities. Initial discussions with SDSMT representatives have taken place, in which they have expressed a clear interest for hosting the ITF. Additional discussions will be needed to understand the details of the ITF management structure within the context of a more finalized set of requirements for the facility.

## 8.4.3 Inventory System

Effective inventory management will be essential for all aspects of DUNE detector development, construction, installation and operation. While its relevance and importance go beyond the ITF, the ITF is the location at which LBNF, DUNE project management, consortium scientific personnel and SURF operations will interface. We therefore will develop standards and protocols for inventory management as part of the ITF planning. A critical requirement for the project is that the inventory management system for procurement, construction and installation be compatible with future QA, calibration and detector performance database systems. Experience with past large detector projects, notably  $\text{NO}\nu\text{A}$ , has demonstrated that the capability to track component-specific information is extremely valuable throughout installation, testing, commissioning and routine operation. Compatibility between separate inventory management and physics information systems will be maintained for effective operation and analysis of DUNE data.

## 8.4.4 ITF Infrastructure

TC is responsible for providing the common support infrastructure at the ITF. This includes the cranes and forklifts to move equipment in the ITF, any cryostats and cryogenics systems to enable cold tests of consortium-provided components, the cleanrooms and cleanroom equipment to enable work on or testing of consortia components, and UV-filtered lighting as needed. This also includes racks and cable trays.

## 8.5 Installation Coordination and Support

Installation Coordination and Support (also called simply *Installation*) is responsible for coordinating the detector installations, providing detector installation support and providing installation-related infrastructure. The installation group management responsibility is shared by a scientific lead and a technical lead that report to the Technical Coordinator. The group responsible for activities in the underground areas is referred to as the underground installation team (UIT). The

ITF group, which delivers equipment to the Ross Shaft, and the UIT, which receives the equipment underground, need to be in close communication and work closely together.

Underground installation is in general responsible for coordinating and supporting the installation of the detector modules and providing necessary infrastructure for installation of the experiment. While the individual consortia are responsible for the installation of their own detector equipment, it is essential that the detector installation be planned as a whole and that a single group coordinates the installation and adapts the plans throughout the installation process. The UIT has responsibility for overall coordination of the installations. In conjunction with each consortium the UIT makes the installation plan that describes how the detector modules are to be installed. The installation plan is used to define the spaces and infrastructure that will be needed to install them. The installation plan will also be used to define the interfaces between the Installation group and the consortium deliverables.

### 8.5.1 UIT Infrastructure

The installation scope includes the infrastructure needed to install the FD such as the cleanroom, a small machine shop, special cranes, scissor lifts, and access equipment. Additional equipment required for installation includes: rigging equipment, hand tools, diagnostic equipment (including oscilloscopes, network analyzers, and leak detectors), local storage with some critical supplies and some personal protective equipment (PPE). The UIT will also provide trained personnel to operate the installation infrastructure. The consortia will provide the detector elements and custom tooling and fixtures as required to install their detector components.

### 8.5.2 Underground Detector Installation

For the detector modules to be installed in safe and efficient manner, the efforts of the individual consortia must be coordinated such that the installation is planned as a coherent process. The interfaces between the individual components must be understood and the spaces required for the installation process planned and documented. The installation planning must take into account the plans and scope of the LBNF effort and the individual plans of the nine consortia. By working with the LBNF team and the members of the consortia responsible for building and installing their components, a joint installation plan and schedule, taking into account all activities and needs of all stakeholders, can be developed. Although the organization of the installation effort is still evolving, an installation coordinator will be the equivalent of a scientific lead for this effort.

One of the primary early responsibilities of the UIT is to develop and maintain the DUNE installation plan and the installation schedule. This installation plan describes the installation process in sufficient detail to demonstrate how all the individual consortium installation plans mesh and it gives an overview of the installation process. The installation plan is used by the UIT to define the underground infrastructure needed for detector installation and the interfaces it has with respect to the consortia. The UIT is responsible for reviewing and approving the consortium installation plans. Approved installation plans, engineering design notes, signed final drawings, and safety

documentation and procedures are all prerequisites for the PRR. Approved procedures, safety approval, and proper training are all required before the UIT performs work. During the installation phase the installation leadership coordinates the DUNE installation effort and adapts the schedule as needed. The installation coordinator, together with management, will also resolve issues when problems occur.

The installation infrastructure to be provided by the UIT includes: the underground ISO 8 (or class 100,000) clean room used for the installation; cranes and hoists (if they are not delivered by LBNF); and scissor lifts, aerial lifts, and the common work platforms outside the cryostat. The UIT will have responsibility for operating this equipment and assisting the consortia with activities related to rigging, material transport, and logistics. Each consortium is responsible for the installation of their own equipment, so the responsibility of the installation group is limited, but the material handling scope is substantial. To support the installation process, an installation floor manager will lead a trained crew with the main responsibility of transporting the equipment to the necessary location and operating the cranes, hoists, and other common equipment needed for the installation. It is expected that the installation crew will work with the teams from the various consortia but will mainly act in a supporting function. The UIT floor manager will be responsible for supervising the UIT crew, but the ultimate responsibility for all detector components remains with the consortia even while the underground team is rigging or transporting these components. This will be critical in the case where any parts are damaged during transport or installation, as the consortia need to judge the necessary actions. For this reason, a representative or point of contact (POC) from the consortia must be present when any work is performed on their equipment. The consortium is responsible for certifying that each installation step is properly performed.

The UIT acts as the primary point of contact with LBNF and SURF from the time the components reach the Ross headframe until the equipment reaches the experimental cavern. If something goes wrong, SURF calls the UIT leader who then contacts the responsible party. The consortia are responsible for delivering to the UIT all approved procedures and specialized tooling required for transport. The UIT leader acts as a point of contact if the LBNF or SURF team has questions or difficulties with the underground transport. The UIT receives the materials from LBNF and SURF at the entrance to the DUNE excavations. The UIT then delivers the equipment to the required underground location.

In an effort to get an early estimate of the equipment required to install the detectors the UIT has developed a preliminary installation plan that outlines the installation process. At present the installation plan consists of a 3D model of the cryostat in the excavations. The SP module elements are inserted in the model and a proposal for how they are transported, assembled, and inserted into the cryostat has been conceptually developed and expressed in a series of images some of which are shown in Figures 8.6 and 8.7. Conceptual designs of the infrastructure needed to support the transport and assembly are also included in the model. See Figures 8.8 and 8.9. With this as a tool, the proposed installation sequence can be iterated with the consortia to converge on a baseline installation plan. A similar process will be followed for the DP module once the base configuration for the single-phase (SP) installation is agreed upon. The UIT has focused initially on the SP module as the SP components are larger and the installation process more complex.

In the current installation plan, DUNE will take ownership of the different underground areas at different times. The surface data room and the underground room in the CUC are available



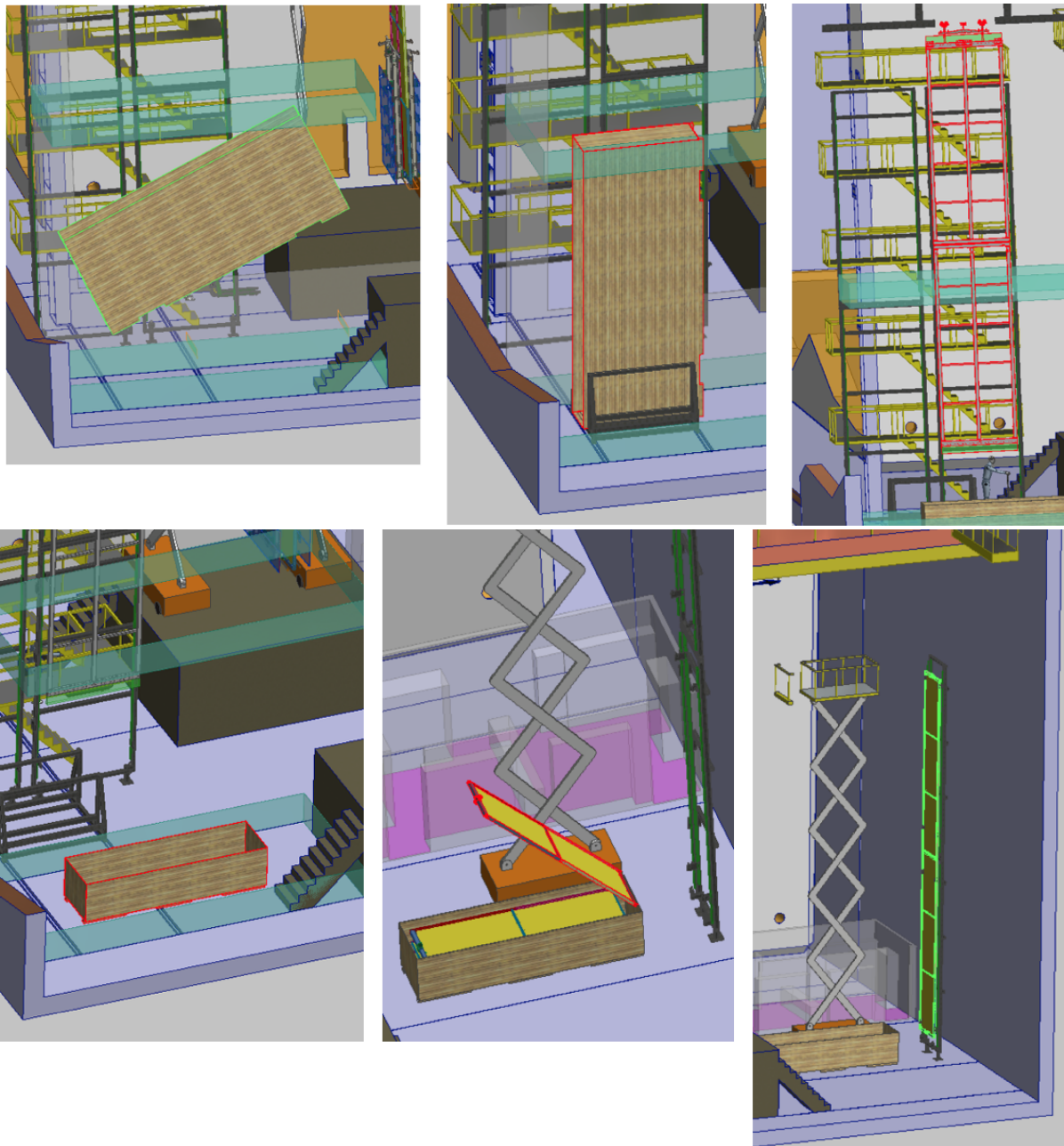


Figure 8.6: Top row from left: crated APA rotating to vertical position; crated vertical APA placed in cart; APA panels moved to fixture using the under-bridge crane. Bottom row: series showing CPA panels uncrated and moved to fixture.

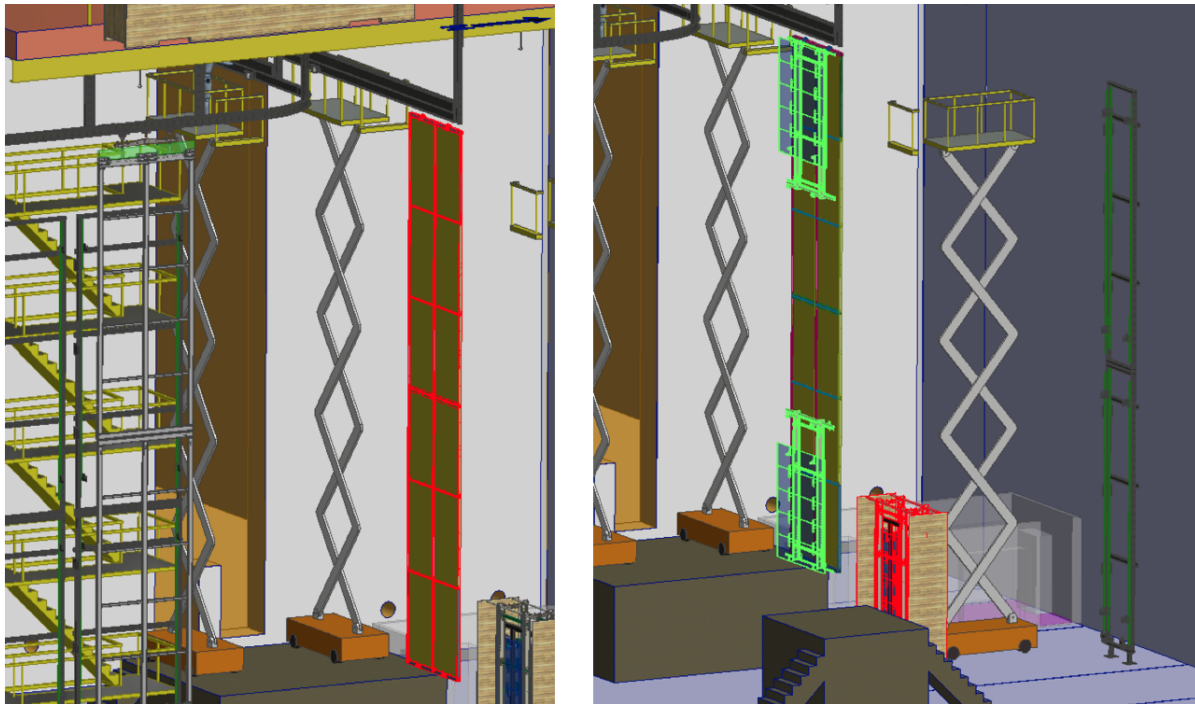


Figure 8.7: On the left, the assembled CPA panel is placed onto the north TCO beam. On the right, the (green) FC panels (already lowered into SAS and moved into the clean room) are installed as the CPA array hangs under the TCO beam.

significantly before the collaboration has access to the cryostats; the optical fibers between the surface and underground will be in place even earlier. This will allow a DAQ prototype to be developed and tested early. The installation of the DAQ hardware can also be finished before the start of detector installation if desired, so the DAQ will not be on the critical path. When the collaboration receives access to Cryostat 1 the steel work for Cryostat 2 will be finished and the work on installing the membrane will have started. Excavation will be complete. For planning purposes it is assumed that the first detector module will be SP and the second dual-phase (DP). The first step in the SP installation is to install the cryogenics piping and the DSS. As this piping will require welding and grinding, it is a dirty process and must be complete before the area can be used as a clean room. When this is complete the cryostat can be cleaned and the false floor re-installed. The clean infrastructure for installing the detector module, including the clean room, work platforms, scaffolding, the fixturing to hold the detector elements during assembly, and all the lifts need to be set up. Once the infrastructure is in place and the area is clean, the installation of the main elements can start. The general layout of the installation area showing the necessary space and equipment is shown in Figure 8.6.

The SP module is installed by first installing the west endwall or endwall 1 (see Figure 8.10).

The anode plane assemblies and cathode plane assemblies with top and bottom FC panels are installed next. The plan is to install six anode plane assemblies and four cathode plane assemblies per week, which is enough to complete one of the 25 rows every week. Additional time is built into the schedule to take into account that the installation will be slower at the beginning and some re-work may be needed. By building west-to-east, complete rows can be finished and tested before

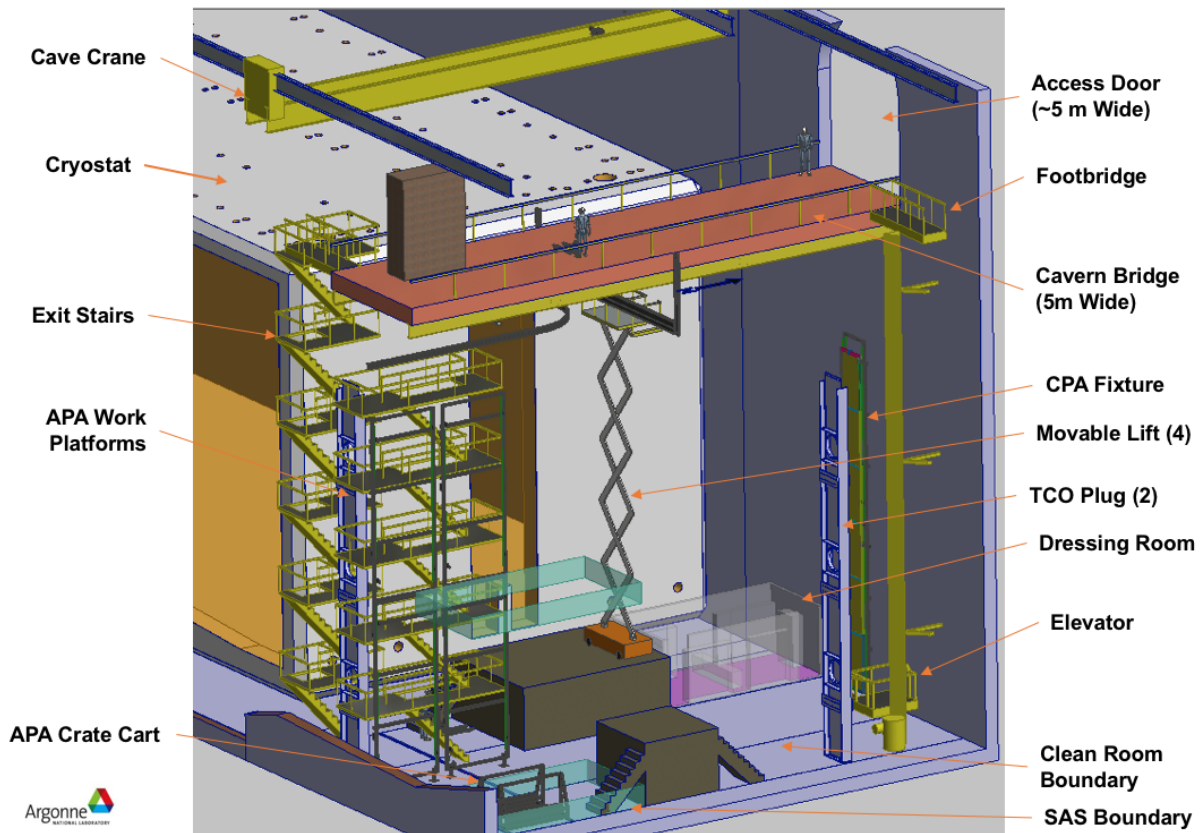


Figure 8.8: 3D model of the underground area showing the infrastructure to install the SP module in cryostat 1. The most significant features are presented including the APA and CPA assembly areas, the region around the TCO for materials entering the cryostat, the changing room, the region for the materials air lock, (SAS), and the means of egress.

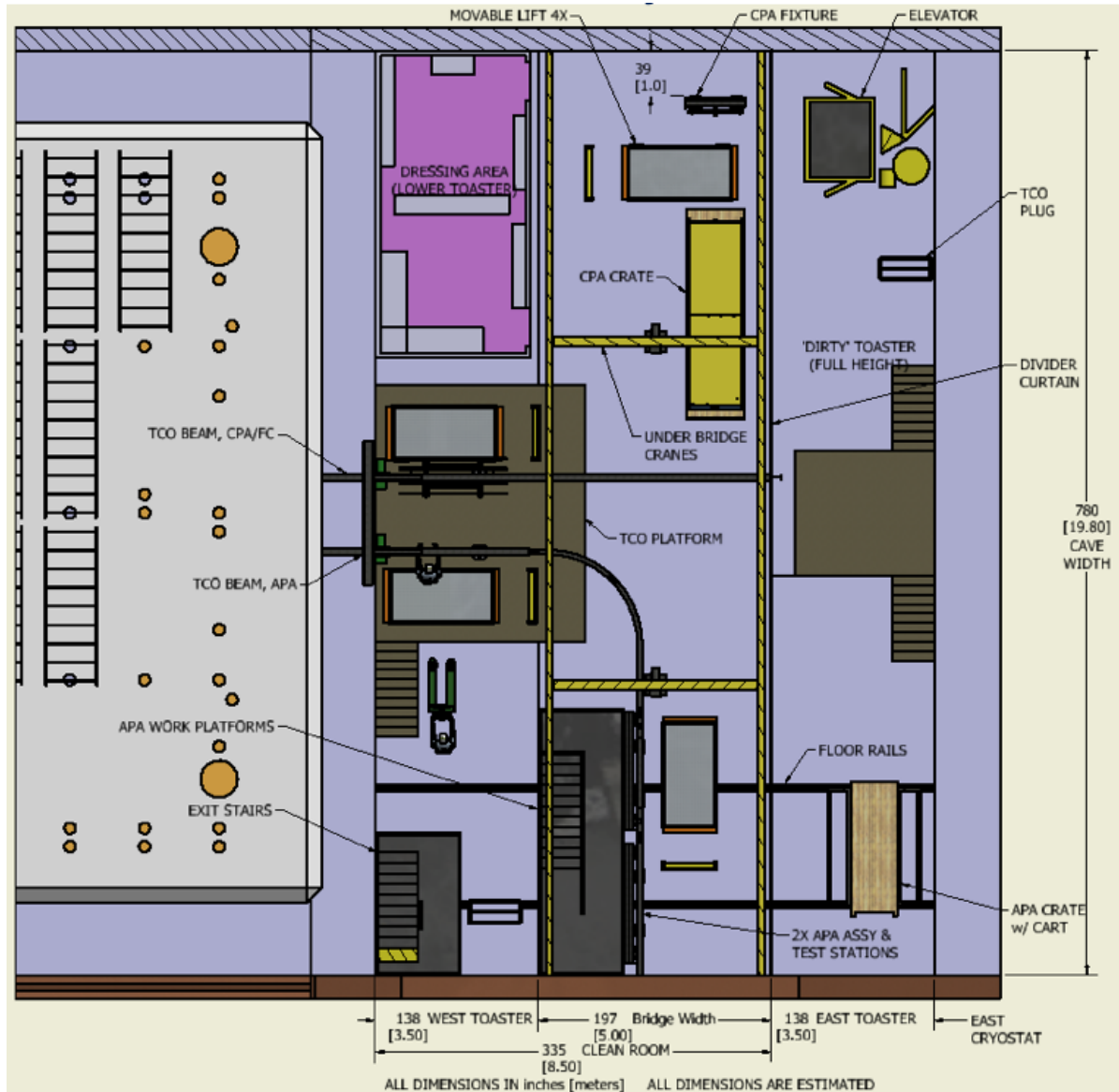


Figure 8.9: Section view of the 3D model showing layout, looking down on the installation area from below the bridge. Areas shown, left to right, are the cryostat and TCO, the platform in front of the TCO, the dressing area, the APA and CPA assembly area (directly under the bridge), and the stairs and elevator. The lower right corner of the region is used as the materials air lock.

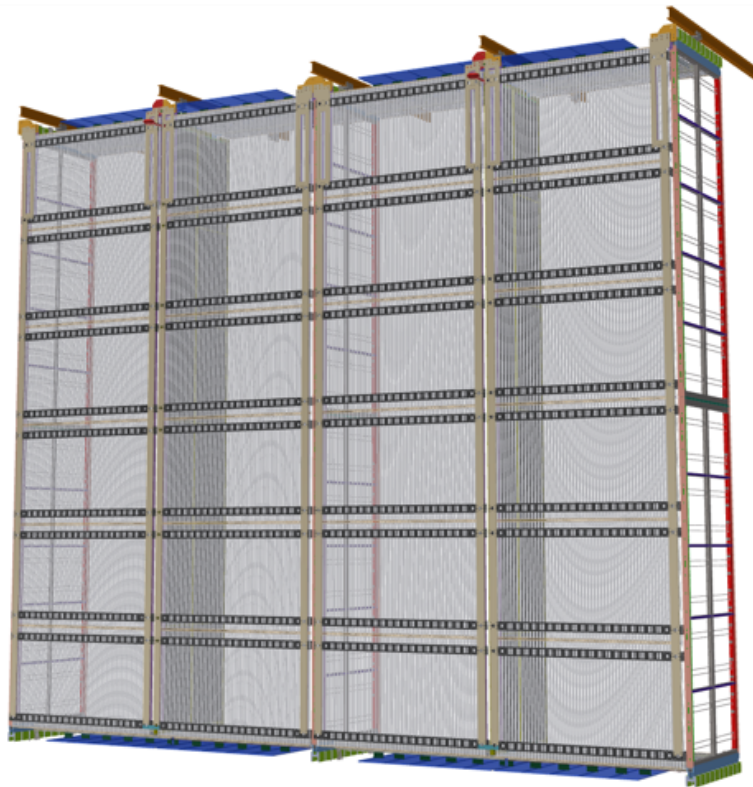


Figure 8.10: End view of SP module with endwall FC in place, with one row of anode plane assemblies and cathode plane assemblies.

moving to the next row. This reduces the risk of finding a fault after final FC deployment and cabling, which would require dismantling part of the detector module. Some of the steps needed to install the APA and CPA modules outside the cryostat are also shown in Figure 8.6. The middle three panels show how the APA needs to be handled in order to rotate it and mount it to the assembly frame. After two anode plane assemblies are mounted on top of each other, the cabling for the lower anode plane assemblies, and the CE and PD cables can be installed. The lower three panels show how the 2m CPA sub-panels are removed from the transport crates and assembled on a holding frame. Once the CPA module is assembled the FC units can be mounted. Finally, once the anode plane assemblies and cathode plane assemblies are installed, the endwall 2 can be installed. A high-level summary of the schedule is shown in Figure 8.11.

As is seen in the installation schedule the second cryostat becomes available four months before the first detector module installation is complete. In this period, installation work for both detector modules proceeds in parallel. Like the SP module, the first step is the installation of the cryogenics piping, followed by a thorough cleaning and installation of the false floor. While this piping is being installed, the DP chimneys for the electronics along with the PDS and CRP instrumentation feedthroughs can also be installed. Since the chimneys are installed into the roof of the cryostat, this work is performed well away from the final installation work on the first detector module so there should be no conflicts. Once the first detector module is installed work on setting up the second detector module's installation infrastructure can begin. This work includes moving the cranes and work platforms along with moving the walls of the clean room so that the second cryostat is clean. The air filtration to the cryostat is also moved to the second cryostat. Since



much of the work for the DP installation will be performed inside the cryostat, in principle, outside the cryostat a clean room area smaller than that for the SP module would suffice. However, for planning purposes, it will not be completely clear what type of detector module will be installed in the second cryostat until fairly late. Therefore the UIT will plan to provide a sufficiently large area outside the cryostat to accommodate either detector technology. The much smaller clean room for a DP module could be installed just outside the TCO. The installation process inside the DP module will proceed east-to-west. At the start of the TPC installation the first four CRPs – comprising the first row – will be installed. The left panel in Figure 8.12 shows two CRPs being installed near the roof of the cryostat and the right panel shows one of the CRPs in a transport box being moved into the cryostat. Once the first CRP row is installed and tested, the first endwall FC can be installed. In general rows of CRPs will be installed, followed by rows of FC modules, followed by the cathode installation at the bottom of the detector module, followed by PDs under the cathode plane. At the end of the installation, the second endwall FC is installed and a final testing period for the full detector module is foreseen. The DP module installation sequence is shown in green in Figure 8.11.

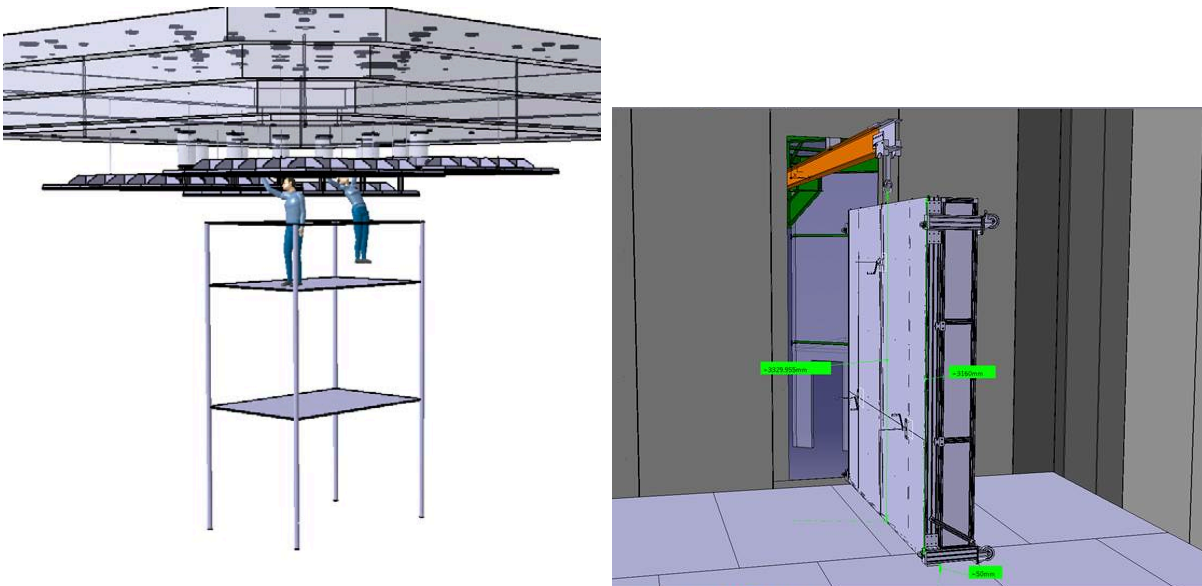


Figure 8.12: Left: Image of the DP CRPs being installed in the DP module, showing the connection from the CRP to the electronics readout chimney. Right: Image of the CRP being inserted into the cryostat using a transport beam. The DP FC modules will be inserted in a similar fashion.

Prior to the TDR, mutually agreed upon installation plans must be approved. These will set the schedule for the installation and will determine the planning for staffing and budget. Having good estimates for the time needed and having enough experience to ensure that the interfaces are understood and the procedures are complete is important for accurate planning. The experience at ProtoDUNE will be very important as the ProtoDUNE installation establishes the procedures for handling all the detector elements and in many cases gives accurate estimates for the time needed. However, in the case of the SP module, many of these procedures need to be revised or newly developed. For example, the SP module will be twice as high as ProtoDUNE-SP, so two anode plane assemblies need to be assembled together and a totally different cabling scheme is needed. Testing the cabling must be done prior to the TDR in order to ensure the design is viable. The DP will also need to develop installation procedures as the DP module will have a significantly

different FC and cathode plane.

By definition, the installation is on the critical path, making it vital that the work be performed efficiently and in a manner that has low risk. In order to achieve this, a prototype of the installation equipment for the SP module will be constructed at Ash River (the  $\text{NO}\nu\text{A}$  neutrino experiment FD site in Ash River, Minnesota, USA), and the installation process tested with dummy detector elements. It is expected that the setup will be available at the time of the TDR, but any lessons learned will need to be implemented and tested after this. In the period just prior to the start of installation, the Ash River setup will be used as a training ground for the UIT.

### 8.5.3 Preparation for Operations

After the detector modules are installed in the cryostats there remains a lot of work before they can be operated. First the TCO must be closed. This requires bringing back the cryostat manufacturer. First the missing panel with the steel beams and steel panel are installed to complete the cryostat's outer structural hull. Then the remaining foam blocks and membrane panels are installed from the inside using the roof access holes to enter the cryostat.

In parallel, the LAr pumps are installed at the ends of the cryostat and final connections are made to the recirculation plant. Once the pumps are installed, the cryostat is closed, and everything is leak tested, the cryogenics plant can be brought into operation. First the air inside the cryostat is purged by injecting pure argon gas at the bottom at a rate such that the cryostat volume is filled uniformly but faster than the diffusion rate. This produces a column of argon gas that rises through the volume and sweeps out the air. This process is referred to as the *piston purge*. When the piston purge is complete the cool-down of the detector module can begin. Misting nozzles inject a liquid-gas mix into the cryostat that cools the detector components at a controlled rate.

Once the detector is cold the filling process can begin. Gaseous argon stored at the surface at SURF is brought down the shaft and is re-condensed underground. The LAr then flows through filters to remove any  $\text{H}_2\text{O}$  or  $\text{O}_2$  and flows into the cryostat. Given the very large volume of the cryostats and the limited cooling power for re-condensing, it is expected to take 12 months to fill the first detector module and 14 months to fill the second. During this time the detector readout electronics will be on monitoring the status of the detector. Once the detector module is full, the drift high voltage can be carefully ramped up and data taking can begin.



# Glossary

**35 ton prototype** The 35 ton prototype cryostat and single-phase (SP) detector built at Fermilab before the ProtoDUNE detectors. ix, 139, 173, 176–178, 180, 187, 189, 191

**analog-to-digital converter (ADC)** A sampling of a voltage resulting in a discrete integer count corresponding in some way to the input. x, 10, 31, 44, 45, 47, 50, 51, 53–55, 57–59, 64, 65, 100, 222

**as low as reasonably achievable (ALARA)** Typically used with regard management of radiation exposure but may be used more generally. It means making every reasonable effort to maintain e.g., exposures, to as far below the limits as practical, consistent with the purpose for that the activity is undertaken. 75

**advanced mezzanine card (AMC)** Holds digitizing electronics and lives in Micro Telecommunications Computing Architecture ( $\mu$ TCA) crates. vii, 9, 10, 42, 45–48, 53–55, 59–61, 63, 68, 69, 71, 72, 155

**anode plane assembly (APA)** A unit of the SP detector module containing the elements sensitive to ionization in the LAr. It contains two faces each of three planes of wires, and interfaces to the cold electronics and photon detection system. 133, 139, 141, 143, 147, 154, 160, 172, 173, 180, 181, 189, 191, 192, 199, 203, 204, 207, 214, 226, 232, 233, 237–241, 243, 249

**artDAQ** A general-purpose Fermilab data acquisition framework for distributed data combination and processing. It is designed to exploit the parallelism that is possible with modern multi-core and networked computers. 147, 148

**ASIC** application-specific integrated circuit. vii, viii, 6, 9, 10, 41, 43, 46–51, 55, 57, 58, 62, 64, 65, 67

**Advanced Telecommunications Computing Architecture (ATCA)** An advanced computer architecture specification developed for the telecommunications, military, and aerospace industries that incorporates the latest trends high-speed interconnect technologies, next-generation processors, and improved reliability, availability and serviceability. 58

**Bump On Wire (BOW)** A working name for the front-end readout computing elements used in the nominal DAQ design to interface the DP crates to the DAQ front-end computers. 143,

145, 146

**CATIROC** charge and time integrated readout chip. viii, x, 47, 55, 57–59, 65

**cold electronics (CE)** Refers to readout electronics that operate at cryogenic temperatures. 134, 139, 214, 222, 241

**computational fluid dynamics (CFD)** High performance computer-assisted modeling of fluid dynamical systems. 166, 173, 175, 179

**conventional facilities (CF)** Pertaining to construction and operation of buildings or caverns and conventional infrastructure. 160

**cryogenic instrumentation and slow controls (CISC)** A DUNE consortium responsible for the cryogenic instrumentation and slow controls components. ix, x, 12, 34, 39, 124, 156, 157, 160, 166–171, 191, 195–197, 200, 201, 210–214

**CMOS** Complementary metal-oxide-semiconductor. 9, 191

**CMP** configuration management plan. 225

**Cluster On Board (COB)** An ATCA motherboard housing four RCEs. 158, 252

**COLDATA** a 64-channel control and communications ASIC. 222

**common fund** The shared resources of the collaboration. 219, 222

**cathode plane assembly (CPA)** The component of the SP detector module that provides the drift HV cathode. ix, 189, 191, 192, 237–241

**charge parity (CP)** Product of charge and parity transformations. 1

**charge readout (CRO)** The system for detecting ionization charge distributions in a DP detector module. vii, 41–46, 48, 53, 57, 59, 64, 65, 69, 72, 133, 139, 141, 143–147, 154–156

**charge-readout plane (CRP)** In the DP technology, a collection of electrodes in a planar arrangement placed at a particular voltage relative to some applied E field such that drifting electrons may be collected and their number and time may be measured. ii, vii, x, 2, 4–10, 12, 13, 15–21, 23, 24, 26–28, 31–39, 41–44, 46–48, 50, 51, 53, 64, 65, 68, 70, 73, 74, 76, 78, 91, 168–172, 186–189, 191, 192, 197, 199, 214, 241, 243

**central utility cavern (CUC)** The central underground cavern containing utilities such as central cryogenics and other systems, and the underground data center and control room. 66, 141, 156, 157, 159–161, 163, 164, 201, 218, 236

**DAQ primary buffer (primary buffer)** The portion of the DAQ front-end fragment that accepts full data stream from the corresponding detector unit and retains it sufficiently long for it

to be available to produce a data fragment. 141, 143, 147, 148, 153, 247, 249

**DAQ data receiver (DDR)** The portion of the DAQ front-end fragment that accepts data from the DAQ front-end readout (FER), emits trigger candidates produced from the input trigger primitives, and forwards the full data stream to the DAQ primary buffer (primary buffer). 141, 143, 249

**data selector** The portion of the DAQ front-end fragment that accepts trigger commands and returns the corresponding data fragment. 141, 143, 147, 249

**DAQ front-end readout (FER)** The portion of a DAQ front-end fragment that accepts data from the detector electronics and provides it to the front-end computer (FEC). In the nominal design it is also responsible for generating channel level trigger primitives. 137, 138, 143, 145, 147–150, 152, 247, 249

**DAQ front-end fragment** The portion of one DAQ partition relating to a single FEC and corresponding to an integral number of detector units. See also data fragment. 134–137, 139, 142, 143, 145–149, 151, 154, 246, 247

**out-of-band trigger command dispatcher (OOB dispatcher)** This component is responsible for dispatching a supernova neutrino burst (SNB) dump command to all FERs in the detector module. 137, 141, 148

**DAQ partition** A cohesive and coherent collection of DAQ hardware and software working together to trigger and read out some portion of one detector module; it consists of an integral number of DAQ front-end fragments. Multiple DAQ partitions may operate simultaneously, but each instance operates independently. 133–137, 143, 144, 149, 247, 249

**data acquisition (DAQ)** The data acquisition system accepts data from the detector FE electronics, buffers the data, performs a trigger decision, builds events from the selected data and delivers the result to the offline secondary DAQ buffer. viii, x, 6, 7, 10, 11, 29, 43, 47, 53, 55, 59–61, 64–66, 68, 69, 108, 110, 115, 124, 126, 132–139, 141–145, 147–150, 153–165, 169, 178, 179, 185, 197–199, 201, 206, 212, 214, 218, 238, 248

**data fragment** A block of data read out from a single DAQ front-end fragment that span a contiguous period of time as requested by a trigger command. 137, 143, 147, 150, 155, 247

**detector module** The entire DUNE far detector is segmented into four modules, each with a nominal 10 kt fiducial mass. 1, 4, 9, 10, 12, 98, 107, 123, 127, 132–134, 137–139, 142–144, 146, 147, 149–156, 158, 161, 162, 166, 169, 173, 175, 179, 182, 185, 186, 188, 189, 194, 200, 202, 204, 214, 218, 220, 223, 226–229, 232, 235, 238, 241, 243, 244, 247, 248, 252–254

**detector unit** A subdetector may be partitioned into a number of similar parts. For example the single-phase TPC subdetector is made up of APA units. 133, 137, 142, 143, 149–151, 154, 246, 247, 249, 251, 255

**secondary DAQ buffer** A secondary DAQ buffer holds a small subset of the full rate as selected

by a trigger command. This buffer also marks the interface with the DUNE Offline. 137, 138, 143, 146, 147, 247

**DP module** dual-phase detector module. vii–x, 1, 4–7, 9–11, 16, 22, 26–29, 41–43, 45–48, 50, 51, 53, 55, 60, 61, 65, 67, 69, 70, 73, 74, 78, 83, 85, 91, 93–95, 98–101, 103, 105, 106, 109–112, 115, 117, 119, 121, 123, 124, 128–131, 140, 141, 146, 164, 171, 175, 176, 181, 186, 205, 214, 231, 236, 243

**dual-phase (DP)** Distinguishes one of the DUNE far detector technologies by the fact that it operates using argon in both gas and liquid phases. vii, 1, 41–43, 64, 93, 94, 97, 133, 143, 146, 147, 149, 150, 154, 155, 238, 241, 243

**data quality monitoring (DQM)** Analysis of the raw data to monitor the integrity of the data and the performance of the detectors and their electronics. This type of monitoring may be performed in real time, within the data acquisition (DAQ) system, or in later stages of processing, using disk files as input. 156

**detector support system (DSS)** The system used to support the SP detector within the cryostat. 181, 183, 205, 231, 238

**DUNE** Deep Underground Neutrino Experiment. xi, 214, 215, 217, 218, 220–226, 229–236

**event builder (EB)** A software agent servicing one detector module by executing trigger commands by reading out the requested data. 137, 138, 141, 143, 147, 148

**electronic document management system (EDMS)** A computerized system used at CERN by which documents are managed. 224, 227

**ES&H** Environment, Safety and Health. 217, 225, 226, 228, 230

**external trigger logic (ETL)** Trigger processing that consumes detector module level trigger notification information and other global sources of trigger input and emits trigger command information back to the module trigger logics (MTLs). 137, 149–152, 251, 254

**endwall field cage (endwall FC)** The vertical portions of the SP FC near the wall. ix, 180, 181, 241, 243

**external trigger candidate** Information provided to the MTL about events external to a detector module so that it may be considered in forming trigger commands. 150, 151, 251

**field cage (FC)** The component of a LArTPC that contains and shapes the applied E field. viii, ix, 1, 4–7, 10, 11, 73–76, 78–80, 82–86, 91–96, 101, 105, 106, 116, 119, 121, 126, 131, 173, 189, 191, 192, 204, 222, 238, 241, 243, 244

**final design review (FDR)** A project management device by which a final design is reviewed. 223

**far detector (FD)** Refers to the 40 kt fiducial mass DUNE detector to be installed at the far site

at SURF in Lead, SD, to be composed of four 10kt modules. ix, x, 64, 94, 132–136, 138, 152, 157, 158, 163, 164, 173, 175, 176, 179, 200, 214–217, 230, 231, 233, 235, 244

**front-end computer (FEC)** The portion of one DAQ partition that hosts the DAQ data receiver (DDR), primary buffer and data selector. It is connected to the FER via fiber optic. Each detector unit of a certain granularity, such as two SP anode plane assemblies (APAs), has one front-end computer that receives data from the readout hardware, hosts the primary DAQ memory buffer for that data, emits trigger candidates derived from that data, and satisfies requests for producing subsets of that data for egress. 134, 137–139, 142, 143, 145–151, 158, 247

**Front-End Link eXchange (FELIX)** A high-throughput interface between front-end and trigger electronics and the standard PCIe computer bus. 145, 147, 158, 161

**front-end (FE)** The front-end refers a point that is “upstream” of the data flow for a particular subsystem. For example the front-end electronics is where the cold electronics meet the sense wires of the TPC and the front-end DAQ is where the DAQ meets the output of the electronics. vii, viii, 4–6, 8–10, 12, 13, 29, 39, 41–53, 55, 62–65, 67, 68, 70, 72, 99, 108–110, 123, 127, 134–136, 138, 141, 142, 144, 149, 154, 155, 158, 169, 178, 179, 196, 197, 202, 203, 254

**field programmable gate array (FPGA)** An integrated circuit technology that allows the hardware to be reconfigured to execute different algorithms after its manufacture and deployment. 53, 55, 57, 58, 158, 252

**GEometry ANd Tracking, version 4 (Geant4)** A software toolkit for the simulation of the passage of particles through matter using Monte Carlo methods. 115, 119, 122

**Generates Events for Neutrino Interaction Experiments (GENIE)** Software providing an object-oriented neutrino interaction simulation resulting in kinematics of the products of the interaction. 122

**ground grid** An electrode that is held to be electrically neutral relative to Earth ground voltage ???. 81, 82, 86, 90, 92

**ground plane (GP)** An electrode that is held to be electrically neutral relative to Earth ground voltage. 76, 93, 96, 173, 183, 185, 189, 203, 204

**high-level trigger (HLT)** A source of triggering at the module level. 149, 150, 152

**HVDB** dual-phase HV divider board. viii, 84–86, 88, 91

**high voltage (HV)** Generally describes a voltage applied to drive the motion of free electrons through some media. vii, x, 6–13, 16–18, 21, 22, 28–30, 34–39, 48, 50, 51, 70, 73–76, 78–80, 83–86, 88, 91–97, 99–101, 103, 104, 107, 108, 124, 126, 134, 169, 171, 179, 185, 186, 188–192, 196, 197, 199–203, 205, 211, 214, 222

- IESHP** integrated environmental, safety and health plan. 225
- integrated master schedule (IMS)** A project management device consisting of linked tasks and milestones. 219, 220, 222
- integration and test facility (ITF)** A facility where various detector components will be tested prior to installation. 32, 93, 124–128, 164, 207, 214, 220, 224, 225, 231–235
- liquid argon time-projection chamber (LARTPC)** A class of detector technology that forms the basis for the DUNE far detector modules. It typically entails observation of ionization activity by electrical signals and of scintillation by optical signals. 48, 73, 132
- liquid argon (LAR)** The liquid phase of argon. ix, 41, 79, 166, 168, 170–176, 187–189
- LEM-anode Sandwich (LAS)** In the DP technology, a large electron multiplier (LEM) and its corresponding anode are mounted together in a module called a LEM-anode sandwich. 15–17
- long-baseline (LBL)** Refers to the distance between the neutrino source and the far detector. It can also refer to the distance between the near and far detectors. The “long” designation is an approximate and relative distinction. For DUNE, this distance (between Fermilab and SURF) is approximately 1300 km. 133
- Long-Baseline Neutrino Facility (LBNF)** The organizational entity responsible for developing the neutrino beam, the cryostats and cryogenics systems, and the conventional facilities for DUNE. 215, 217, 218, 220, 223–226, 228, 229, 231, 232, 234–236
- LED** Light-emitting diode. ix, 34, 108, 111, 114, 127, 193, 194, 210
- large electron multiplier (LEM)** A micro-pattern detector suitable for use in ultra-pure argon vapor; LEMs consist of copper-clad PCB boards with sub-millimeter-size holes through which electrons undergo amplification. vii, x, 2, 6–9, 12–24, 27–37, 39, 50, 98, 114, 116, 119, 120, 168, 169, 171, 172, 186, 187, 196, 197, 222, 250
- light readout (LRO)** The system for detecting scintillation photons in a DP detector module. vii, viii, 41–48, 55, 56, 59, 63, 65, 69, 72, 133, 143–147, 155
- LV** low voltage. 10, 13, 169, 179
- MicroTCA Carrier Hub (MCH)** An network switching device. 10, 47, 55, 59, 60, 63, 66, 69, 70
- Monte Carlo (MC)** Refers to a method of numerical integration that entails the statistical sampling of the integrand function. Forms the basis for some types of detector and physics simulations. 43, 120, 129, 130
- minimum ionizing particle (MIP)** Refers to a momentum traversing some medium such that the particle is losing near the minimum amount of energy per distance traversed. 9, 43, 44, 48, 51, 115

- module trigger logic (MTL)** Trigger processing that consumes detector unit level trigger command information and emits trigger commands. It provides the external trigger logic (ETL) with trigger notifications and receives back any external trigger candidates. 138, 141, 143, 144, 146–152, 248, 254
- near detector (ND)** Refers to the detector(s) installed close to the neutrino source at Fermilab. 214, 215
- network interface controller (NIC)** Hardware for controlling the interface to a communication network. Typically, one that obeys the Ethernet protocol. 145
- online monitoring (OM)** Processes that run inside the DAQ on data “in flight,” specifically before landing on the offline disk buffer, and that provide feedback on the operation of the DAQ itself and the general health of the data it is marshalling. 141, 156
- operational readiness review (ORR)** A project management device by which the operational readiness is reviewed. 223
- ProtoDUNE-DP** The DP ProtoDUNE detector. vii, viii, 6, 10–12, 16, 19, 20, 22, 26–30, 32–34, 37, 39, 41, 46–48, 51, 55, 59, 61, 63, 71–73, 78, 79, 81–83, 85, 86, 89, 91, 93–95, 97–100, 102, 103, 105–109, 111–118, 121–123, 129–131, 145, 146, 167, 170, 175, 176, 231
- preliminary design review (PDR)** A project management device by which an early design is reviewed. 223
- ProtoDUNE-SP** The SP ProtoDUNE detector. 78, 79, 96, 158, 170, 176, 180, 181, 183, 185, 207, 243
- photon detection system (PDS)** The detector subsystem sensitive to light produced in the LAr. x, 7, 11, 41, 42, 65, 69, 70, 74, 76, 91, 97, 98, 100–102, 105, 113, 114, 122–126, 128–130, 132, 137, 169, 171, 179, 193, 196, 197, 201, 214, 226, 241
- photon detector (PD)** Refers to the detector elements involved in measurement of number and arrival times of optical photons produced in a detector module. x, 1, 44, 64, 70, 81, 82, 91, 96, 97, 99, 102, 103, 115, 116, 119–122, 124, 125, 128–130, 134, 142, 199, 201, 232, 233, 241, 243
- photomultiplier tube (PMT)** A device that makes use of the photoelectric effect to produce an electrical signal from the arrival of optical photons. viii, 2, 4–6, 8–11, 13, 41, 42, 44, 47, 55, 57, 64, 65, 67–69, 92, 97–112, 114–129, 131, 169
- parts per billion (ppb)** A number equal to  $10^{-9}$ . 175
- production progress review (PPR)** A project management device by which the progress of production is reviewed. 223–225
- parts per trillion (ppt)** A number equal to  $10^{-12}$ . 175

- ProtoDUNE** Either of the two DUNE prototype detectors constructed at CERN and operated in a CERN test beam (expected fall 2018). One prototype implements SP and the other DP technology. 132, 147, 164, 167, 168, 170, 173, 179, 191, 212, 220, 222, 243, 245
- production readiness review (PRR)** A project management device by which the production readiness is reviewed. 223–225, 236
- QAM** quality assurance manager. 224, 230
- QAP** quality assurance plan. 223
- quality assurance (QA)** The process by which quality is maintained so as to preserve high availability and precise function. 17, 27, 28, 63, 88, 89, 158–160, 210, 217, 222–224, 228, 230, 234
- quality control (QC)** A system of maintaining quality through testing products against a specification. 26–28, 89, 90, 92, 95, 97, 126, 127, 130, 131, 158–160, 206–210, 220, 222–224, 228
- DAQ event block** The unit of data output by the DAQ. It contains trigger and detector data spanning a unique, contiguous time period and a subset of the detector channels.. 137, 143, 147, 149
- reconfigurable computing element (RCE)** Data processor located outside of the cryostat on a Cluster On Board (COB) which contains field programmable gate array (FPGA), RAM and SSD resources, responsible for buffering data, producing trigger primitives, responding to triggered requests for data and sinking SNB dumps. 143, 161
- run control (RC)** The system for configuring, starting and terminating the DAQ. 151
- readout window** A fixed, atomic and continuous period of time over which data from a detector module, in whole or in part, is recorded. This period may differ based on the trigger that initiated the readout. 150, 152
- ROI** region of interest. 12
- RTD** Cryostat level and temperature monitoring devices. 185
- S/N** signal-to-noise (ratio). 1, 2, 7–11, 44, 99, 218
- SAS** A pass-through chamber used to ensure safe transfer of materials, avoiding contamination in both directions. 238, 239
- SBN** Short-Baseline Neutrino program (at Fermilab). 138
- signal feedthrough chimney (SFT chimney)** In the DP technology, a volume above the cryostat penetration used for a signal feedthrough. vii, viii, 5–7, 9, 10, 35, 38, 39, 42, 44, 46–49,



51–53, 60, 62–70

**signal feedthrough (SFT)** A cryostat penetration allowing for the passage of cables or other extended parts. viii, 51, 52, 65, 68, 72

**silicon photomultiplier (SiPM)** A solid-state avalanche photodiode sensitive to single photoelectron signals. 111

**spill location system (SLS)** A system residing at the DUNE far detector site that provides information, possibly predictive, indicating periods of time when neutrinos are being produced by the Fermilab Main Injector beam spills. 152, 153

**supernova neutrino burst (SNB)** A prompt increase in the flux of low-energy neutrinos emitted in the first few seconds of a core-collapse supernova. It can also refer to a trigger command type that may be due to an SNB, or detector conditions that mimic its interaction signature. 11, 12, 66, 97, 98, 101, 102, 113, 121–123, 132–138, 140, 142–152, 157, 179, 247, 252

**SuperNova Early Warning System (SNEWS)** A global supernova neutrino burst trigger formed by a coincidence of SNB triggers collected from participating experiments. 149, 151, 157

**SP module** single-phase detector module. ix, x, 1, 78, 94, 96, 106, 119, 139, 140, 148, 150, 158, 160, 164, 171, 172, 175, 176, 180, 181, 214, 231, 236, 238, 239, 241, 243, 244

**single-phase (SP)** Distinguishes one of the DUNE far detector technologies by the fact that it operates using argon in its liquid phase only . 133, 143, 146–150, 154, 236, 238, 245

**solid-state disk (SSD)** Any storage device that may provide sufficient write throughput to receive, both collectively and distributed, the sustained full rate of data from a detector module for many seconds. 138, 143, 145, 148, 149

**subdetector** A detector unit of granularity less than one detector module such as the TPC of either a SP or DP module. 142, 247

**SWC** Software & Computing. 201

**temporary construction opening (TCO)** An opening in the side of a cryostat through which detector elements are brought into the cryostat; utilized during construction and installation. 38, 72, 92, 218, 238–240, 243, 244

**technical coordination (TC)** A dedicated DUNE project effort responsible for assuring proper interfaces between the collaboration consortia. ix, 159, 214, 215, 217–220, 222–224, 226–231, 233, 234

**technical design report (TDR)** A formal project document that describes the experiment at a technical level. x, 72, 94, 115, 121, 130, 131, 164, 214, 220, 222, 224, 227–229, 243, 244, 254

**tetra-phenyl butadiene (TPB)** A type of wavelength shifting material. 11, 42, 99, 101, 103, 105,

106, 114, 121, 125, 127–129, 131, 190

**time projection chamber (TPC)** The portion of each DUNE detector module that records ionization electrons after they drift away from a cathode through the LAr, and also through gaseous argon in a DP module. The activity is recorded by digitizing the waveforms of current induced on the anode as the distribution of ionization charge passes by or is collected on the electrode. 73, 132, 174, 205

**interim design report (IDR)** An intermediate milestone on the path to a full technical design report (TDR). 72, 164

**trigger candidate** Summary information derived from the full data stream and representing a contribution toward forming a trigger decision. 137, 143–147, 149–152, 254

**trigger command** Information derived from one or more trigger candidates that directs elements of the detector module to read out a portion of the data stream. 137, 143, 147–152, 247, 248, 251, 254

**trigger decision** The process by which trigger candidates are converted into trigger commands. 137, 139, 142, 145, 153, 154, 247, 254

**trigger notification** Information provided by MTL to ETL about trigger decision its processing. 248, 251

**trigger primitive** Information derived by the DAQ front-end (FE) hardware that describes a region of space (e.g., one or several neighboring channels) and time (e.g., a contiguous set of ADC sample ticks) associated with some activity. 134, 137, 141, 143, 145–149, 151, 247

**user datagram protocol (UDP)** A simple, connectionless Internet protocol that supports data integrity checksums, requires no handshaking, and does not guarantee packet delivery. 66, 145, 155

**underground installation team (UIT)** An organizational unit responsible for installation in the underground area at the SURF site. 68, 234–236, 243, 244

**Micro Telecommunications Computing Architecture ( $\mu$ TCA)** The computer architecture specification followed by the crates that house charge and light readout electronics in the dual-phase module. 9–13, 42, 43, 45–48, 51, 55, 58–61, 63–70, 72, 110, 123, 146, 155, 169, 245, 255

**VUV** vacuum ultra-violet. 105, 114

**WA105 DP demonstrator** The  $3 \times 1 \times 1 \text{ m}^3$  WA105 dual-phase prototype detector at CERN. vii, viii, 27, 41, 50, 51, 53, 60, 61, 65, 70, 71, 77, 100, 104, 106, 108–111, 114, 120, 123, 170, 186, 188, 191

**work breakdown structure (WBS)** An organizational project management tool by which the

tasks to be performed are partitioned in a hierarchical manner. 71, 130, 220, 224

**warm interface board (WIB)** Digital electronics situated just outside the SP cryostat that receives digital data from the FEMBs over cold copper connections and sends it to the RCE FE readout hardware. 133, 160, 161

**wavelength shifting (WLS)** A material or process by which incident photons are absorbed by a material and photons are emitted at a different, typically longer, wavelength. 106

**WR grandmaster** White Rabbit grandmaster. 10, 55, 61, 65, 66, 69

**White Rabbit  $\mu$ TCA Carrier Hub (WR-MCH)** add def. 10, 43, 45–48, 55, 61, 63, 66, 69

**White Rabbit (WR)** A component of the timing system that forwards clock signal and time-of-day reference data to the master timing unit. viii, 10, 43, 45, 47, 55, 60, 61, 63, 66, 68, 72, 110, 152

**zero-suppression (ZS)** Used to delete some portion of a data stream that does not significantly deviate from zero or intrinsic noise levels. It may be applied at different granularity from per-channel to per detector unit. 150

# References

- [1] DOE Office of High Energy Physics, “Mission Need Statement for a Long-Baseline Neutrino Experiment (LBNE),” tech. rep., DOE, 2009. LBNE-doc-6259.
- [2] L. Agostino *et al.*, “LBNO-DEMO: Large-scale neutrino detector demonstrators for phased performance assessment in view of a long-baseline oscillation experiment, The LBNO-DEMO - WA105 - Collaboration.” CERN-SPSC-2014-013; SPSC-TDR-004, 2014.
- [3] S. Blin, S. Callier, S. Conforti Di Lorenzo, F. Dulucq, C. De La Taille, G. Martin-Chassard, and N. Seguin-Moreau, “Performance of CATIROC: ASIC for smart readout of large photomultiplier arrays,” *Journal of Instrumentation* **12** (Mar., 2017) C03041.
- [4] “Om3 fibers.” <http://shop.fiber24.net/index.php/en/F0-Patch-Cable-OM3-Multi-mode-50-125-m-Duplex-LC-PC-LC-PC/c-OM3-DUPLEX-1T01/a-F0PC-F2-03-DX-LCU-LCU>.
- [5] “Nat-mch.” <http://www.nateurope.com/products/NAT-MCH.html>.
- [6] “Technical Design Report for large-scale neutrino detectors prototyping and phased performance assessment in view of a long-baseline oscillation experiment,” tech. rep., 2014. <http://cds.cern.ch/record/1692375/files/arXiv%3A1409.4405.pdf?version=2>.
- [7] **DUNE** Collaboration, C. Cuesta, “Photon detection system for ProtoDUNE dual phase,” *JINST* **12** no. 12, (2017) C12048, arXiv:1711.08307 [physics.ins-det].
- [8] T. Heindl *et al.*, “The scintillation of liquid argon,” *EPL (Europhysics Letters)* **91** no. 6, (2010) 62002. <http://stacks.iop.org/0295-5075/91/i=6/a=62002>.
- [9] [http://www.hamamatsu.com/resources/pdf/etd/LARGE\\_AREA\\_PMT\\_TPMH1286E.pdf](http://www.hamamatsu.com/resources/pdf/etd/LARGE_AREA_PMT_TPMH1286E.pdf).
- [10] R. Francini *et al.*, “Vuv-vis optical characterization of tetraphenyl-butadiene films on glass and specular reflector substrates from room to liquid argon temperature,” *Journal of Instrumentation* **8** no. 09, (2013) P09006. <http://stacks.iop.org/1748-0221/8/i=09/a=P09006>.
- [11] J. Asaadi *et al.*, “Tetraphenyl butadiene emanation and bulk fluorescence from wavelength

- shifting coatings in liquid argon,” <https://arxiv.org/pdf/1804.00011.pdf>.
- [12] R. Acciarri *et al.*, “Design and construction of the microboone detector,” *Journal of Instrumentation* **12** no. 02, (2017) P02017.  
<http://stacks.iop.org/1748-0221/12/i=02/a=P02017>.
- [13] **MiniCLEAN** Collaboration, A. Hime, “The MiniCLEAN Dark Matter Experiment,” in *Particles and fields. Proceedings, Meeting of the Division of the American Physical Society, DPF 2011, Providence, USA, August 9-13, 2011*. 2011. arXiv:1110.1005 [physics.ins-det].  
<https://inspirehep.net/record/930736/files/arXiv:1110.1005.pdf>.
- [14] **ICARUS** Collaboration, F. Varanini, “ICARUS detector: present and future,” *EPJ Web Conf.* **164** (2017) 07017.
- [15] <http://www.et-enterprises.com/>.
- [16] [http://www.hzcpotonics.com/en\\_index.html](http://www.hzcpotonics.com/en_index.html).
- [17] **ArDM** Collaboration, V. Boccone, “Development and test in liquid argon of the light readout system for the ArDM experiment,” *AIP Conf. Proc.* **1182** (2009) 280–283.
- [18] **WA105** Collaboration, L. Zambelli and S. Murphy, “WA105: A large demonstrator of a liquid argon dual phase TPC,” *J. Phys. Conf. Ser.* **888** no. 1, (2017) 012202.
- [19] <https://www.picmg.org/openstandards/microtca/>.
- [20] C. M. B. Monteiro *et al.*, “Secondary scintillation yield from GEM and THGEM gaseous electron multipliers for direct dark matter search,” *Phys. Lett.* **714** (2012) 18.
- [21] S. Agostinelli *et al.*, “Geant4 - a simulation toolkit,” *Nuclear Instruments and Methods in Physics Research Section A: Accelerators, Spectrometers, Detectors and Associated Equipment* **506** no. 3, (2003) 250 – 303.  
<http://www.sciencedirect.com/science/article/pii/S0168900203013688>.
- [22] R. Brun and F. Rademakers, “Root - an object oriented data analysis framework,” *Nucl. Inst. And Meth. in Phys. Res. A* **389** (1997) .
- [23] <http://sbn-nd.fnal.gov/>.
- [24] Duchesneau, D. and Autiero, D. and Gil-Botella, I. and Hasegawa, T., “DUNE FD Interface Document: DP TPC Electronics to DP Photon Detector,” tech. rep., 2018.  
<http://docs.dunescience.org/cgi-bin/ShowDocument?docid=6772&version=1>.
- [25] Duchesneau, D. and Gil-Botella, I. and Pietropaolo, F. and Yu, B., “DUNE FD Interface Document: DP Photon Detector to Joint HV,” tech. rep., 2018.  
<http://docs.dunescience.org/cgi-bin/ShowDocument?docid=6799&version=2>.

- [26] Karagiorgi, G. and Newbold, D. and Segreto, E. and Warner, D., “DUNE FD Interface Document: DP Photon Detector to Joint DAQ,” tech. rep., 2018.  
<http://docs.dunescience.org/cgi-bin/ShowDocument?docid=6802&version=1>.
- [27] D. Duchesneau, I. Gil-Botella, , S. Gollapinni, and A. Villanueva, “DUNE FD Interface Document: DP Photon Detector to Joint CISC,”  
<http://docs.dunescience.org/cgi-bin/ShowDocument?docid=6781&version=1>.
- [28] Duchesneau, D. and Gil-Botella, I. and Worcester, E. and Patterson, R., “DUNE FD Interface Document: DUNE Physics to DP Photon Detector,” tech. rep., 2018.  
<http://docs.dunescience.org/cgi-bin/ShowDocument?docid=7087&version=1>.
- [29] Duchesneau, D. and Gil-Botella, I. and Norman, A. and Schellman, H., “DUNE FD Interface Document: Software and Computing to DP Photon Detector,” tech. rep., 2018.  
<http://docs.dunescience.org/cgi-bin/ShowDocument?docid=7114&version=1>.
- [30] Duchesneau, D. and Gil-Botella, I. and Gollapinni, S. and Mann, K., “DUNE FD Interface Document: Calibration to DP Photon Detector,” tech. rep., 2018.  
<http://docs.dunescience.org/cgi-bin/ShowDocument?docid=7060&version=1>.
- [31] Duchesneau, D. and Gil-Botella, I. and James, E. and Kettell, S. and Marshak, M., “DUNE FD Interface Document: Integration Facility to DP Photon Detector,” tech. rep., 2018.  
<http://docs.dunescience.org/cgi-bin/ShowDocument?docid=7033&version=1>.
- [32] Duchesneau, D. and Feyzi, F. and Gil-Botella, I. and James, E. and Shaw, T., “DUNE FD Interface Document: Facility Interfaces to DP Photon Detector,” tech. rep., 2018.  
<http://docs.dunescience.org/cgi-bin/ShowDocument?docid=6979&version=1>.
- [33] Duchesneau, D. and Gil-Botella, I. and James, E. and Kettell, S. and Stewart, J., “DUNE FD Interface Document: Installation Interfaces to DP Photon Detector,” tech. rep., 2018.  
<http://docs.dunescience.org/cgi-bin/ShowDocument?docid=7006&version=1>.
- [34] The DUNE Collaboration, “CDR Volume 4: The DUNE Detectors at LBNF,” tech. rep., 2015. <https://arxiv.org/abs/1601.02984>.
- [35] James, E. and Kettell, S., “DUNE Project WBS for the Far Detector,” tech. rep., 2018.  
<http://docs.dunescience.org/cgi-bin/ShowDocument?docid=5594&version=9>.
- [36] Autiero, D. and Hasegawa, T. and Karagiorgi, G. and Newbold, D., “DUNE FD Interface Document: DP TPC Electronics to Joint DAQ,” tech. rep., 2018.  
<http://docs.dunescience.org/cgi-bin/ShowDocument?docid=6778&version=1>.
- [37] G. Karagiorgi, D. Newbold, A. Norman, and H. Schellman, “DUNE FD Interface Document: Software and Computing to Joint DAQ,” tech. rep., Columbia, Bristol, Fermilab, and Oregon State, 2018. <http://docs.dunescience.org/cgi-bin/ShowDocument?docid=7123>.
- [38] P. Antonioli *et al.*, “SNEWS: The SuperNova Early Warning System,” *New J. Phys.* **6**

- (2004) 114, arXiv:astro-ph/0406214.
- [39] **GROND, SALT Group, OzGrav, DFN, INTEGRAL, Virgo, Insight-Hxmt, MAXI Team, Fermi-LAT, J-GEM, RATIR, IceCube, CAASTRO, LWA, ePESSTO, GRAWITA, RIMAS, SKA South Africa/MeerKAT, H.E.S.S., 1M2H Team, IKI-GW Follow-up, Fermi GBM, Pi of Sky, DWF (Deeper Wider Faster Program), Dark Energy Survey, MASTER, AstroSat Cadmium Zinc Telluride Imager Team, Swift, Pierre Auger, ASKAP, VINROUGE, JAGWAR, Chandra Team at McGill University, TTU-NRAO, GROWTH, AGILE Team, MWA, ATCA, AST3, TOROS, Pan-STARRS, NuSTAR, ATLAS Telescopes, BOOTES, CaltechNRAO, LIGO Scientific, High Time Resolution Universe Survey, Nordic Optical Telescope, Las Cumbres Observatory Group, TZAC Consortium, LOFAR, IPN, DLT40, Texas Tech University, HAWC, ANTARES, KU, Dark Energy Camera GW-EM, CALET, Euro VLBI Team, ALMA Collaboration, B. P. Abbott *et al.*, “Multi-messenger Observations of a Binary Neutron Star Merger,” *Astrophys. J.* **848** no. 2, (2017) L12, arXiv:1710.05833 [astro-ph.HE].**
- [40] **DUNE Collaboration**, “DUNE Far Detector Task Force Final Report,” tech. rep., 2017. DUNE-doc-3384-v6, <http://docs.dunescience.org/cgi-bin/ShowDocument?docid=3384>.
- [41] G. J. Michna *et al.*, “CFD Analysis of Fluid, Heat, and Impurity Flows in DUNE FAR Detector to Address Additional Design Considerations,” tech. rep., South Dakota State University, 2017. <http://docs.dunescience.org/cgi-bin/ShowDocument?docid=5915>.
- [42] Strons, Ph., and Bailey, J. L., “Flow visualization methods for field test verification of CFD analysis of an open gloveport,” 2017. <https://www.osti.gov/pages/servlets/purl/1402050>.
- [43] W. Walkowiak, “Drift velocity of free electrons in liquid argon,” *Nucl. Instrum. Meth.* **A449** (2000) 288–294.
- [44] M. Adamowski *et al.*, “The Liquid Argon Purity Demonstrator,” *JINST* **9** (2014) P07005, arXiv:1403.7236 [physics.ins-det].
- [45] **WA105 Collaboration**, S. Murphy, “Status of the WA105-3x1x1 m<sup>3</sup> dual phase prototype,” tech. rep., 2017. <https://indico.fnal.gov/event/12345/session/1/contribution/5/material/slides/0.pdf>.
- [46] Delaquis, S. C. and Gornea, R. and Janos, S. and Lüthi, M. and Rudolf von Rohr, C. and Schenk, M. and Vuilleumier, J. -L., “Development of a camera casing suited for cryogenic and vacuum applications,” *JINST* **8** (2013) T12001, arXiv:1310.6601 [physics.ins-det].
- [47] Auger, M. and Blatter, A. and Ereditato, A. and Goeldi, D. and Janos, S. and Kreslo, I. and Lüthi, M. and Rudolf von Rohr, C. and Strauss, T. and Weber, M. S., “On the Electric Breakdown in Liquid Argon at Centimeter Scale,” *JINST* **11** no. 03, (2016) P03017, arXiv:1512.05968 [physics.ins-det].

- [48] T. I. Banks *et al.*, “A compact ultra-clean system for deploying radioactive sources inside the KamLAND detector,” *Nucl. Instrum. Meth.* **A769** (2015) 88–96, arXiv:1407.0413 [physics.ins-det].
- [49] N. McConkey, N. Spooner, M. Thiesse, M. Wallbank, and T. K. Warburton, “Cryogenic CMOS Cameras for High Voltage Monitoring in Liquid Argon,” *JINST* **12** no. 03, (2017) P03014, arXiv:1612.06124 [physics.ins-det].
- [50] E. Valencia-Rodriguez and M. Kordosky, “Cameras and lighting: experience,” tech. rep., 2018. <https://indico.fnal.gov/event/14581/session/7/contribution/60/material/slides/0.pdf>.
- [51] J. Carron, A. Philippon, L. S. How, A. Delbergue, S. Hassanzadeh, D. Cillierre, P. Danto, and M. Boutillier, “Cryogenic characterization of LEDs for space application,” *Proc. SPIE, Sixteenth International Conference on Solid State Lighting and LED-based Illumination Systems* **10378** (2017) 20.
- [52] A. C. Villanueva *et al.*, “DUNE FD Interface Document: SP TPC Electronics to Joint CISC,”. <http://docs.dunescience.org/cgi-bin/ShowDocument?docid=6745&version=2>.
- [53] S. Gollapinni *et al.*, “DUNE FD Interface Document: Installation Interfaces to Joint CISC,”. <http://docs.dunescience.org/cgi-bin/ShowDocument?docid=7018&version=1>.
- [54] A. C. Villanueva *et al.*, “DUNE FD Interface Document: High Voltage to CISC,”. <http://docs.dunescience.org/cgi-bin/ShowDocument?docid=6787&version=1>.
- [55] A. C. Villanueva *et al.*, “DUNE FD Interface Document: SP Photon Detector to Joint CISC,”. <http://docs.dunescience.org/cgi-bin/ShowDocument?docid=6730&version=1>.
- [56] A. C. Villanueva *et al.*, “DUNE FD Interface Document: DAQ to CISC,”. <http://docs.dunescience.org/cgi-bin/ShowDocument?docid=6790&version=1>.
- [57] S. Gollapinni *et al.*, “DUNE FD Interface Document: Software and Computing to Joint CISC,”. <http://docs.dunescience.org/cgi-bin/ShowDocument?docid=7126&version=1>.
- [58] S. Gollapinni *et al.*, “DUNE FD Interface Document: Calibration to Joint CISC,”. <http://docs.dunescience.org/cgi-bin/ShowDocument?docid=7072&version=1>.
- [59] S. Gollapinni *et al.*, “DUNE FD Interface Document: DUNE Physics to Joint CISC,”. <http://docs.dunescience.org/cgi-bin/ShowDocument?docid=7099&version=1>.
- [60] F. Feyzi *et al.*, “DUNE FD Interface Document: Facility Interfaces to Joint CISC,”. <http://docs.dunescience.org/cgi-bin/ShowDocument?docid=6991>.
- [61] S. Gollapinni *et al.*, “DUNE FD Interface Document: Integration Facility to Joint CISC,”. <http://docs.dunescience.org/cgi-bin/ShowDocument?docid=7045&version=1>.